MULTIDISCIPLINARY CENTER FOR EARTHQUAKE ENGINEERING RESEARCH
A National Center of Excellence in Advanced Technology Applications

ISSN 1520-295X

Experimental Investigation of the Dynamic Response of Two Bridges Before and After Retrofitting with Elastomeric Bearings

by

D.A. Wendichansky, S.S. Chen and J.B. Mander
University at Buffalo, State University of New York
Department of Civil, Structural and Environmental Engineering
Ketter Hall
Buffalo, New York 14260

Technical Report MCEER-98-0012

October 2, 1998

This research was conducted at the University at Buffalo, State University of New York and was supported by the Federal Highway Administration under contract number DTFH61-92-C-00106.

NOTICE

This report was prepared by the University at Buffalo, State University of New York as a result of research sponsored by the Multidisciplinary Center for Earthquake Engineering Research (MCEER) through a contract from the Federal Highway Administration. Neither MCEER, associates of MCEER, its sponsors, the University at Buffalo, State University of New York, nor any person acting on their behalf:

a. makes any warranty, express or implied, with respect to the use of any information, apparatus, method, or process disclosed in this report or that such use may not infringe upon privately owned rights; or

b. assumes any liabilities of whatsoever kind with respect to the use of, or the damage resulting from the use of, any information, apparatus, method, or process disclosed in this report.

Any opinions, findings, and conclusions or recommendations expressed in this publication are those of the author(s) and do not necessarily reflect the views of MCEER or the Federal Highway Administration.

MULTIDISCIPLINARY CENTER FOR EARTHQUAKE ENGINEERING RESEARCH
A National Center of Excellence in Advanced Technology Applications

Experimental Investigation of the Dynamic Response of Two Bridges Before and After Retrofitting with Elastomeric Bearings

by

D.A. Wendichansky[1], S.S. Chen[2] and J.B. Mander[2]

Publication Date: October 2, 1998
Submittal Date: May 26, 1996

Technical Report MCEER-98-0012

Task Number 106-F-4.3.1 (a)

FHWA Contract Number DTFH61-92-C-00106

1 Assistant Professor, Civil Engineering Department, University of Puerto Rico, Mayaguez; former Graduate Research Assistant, Department of Civil, Structural and Environmental Engineering, University at Buffalo, State University of New York
2 Associate Professor, Department of Civil, Structural and Environmental Engineering, University at Buffalo, State University of New York

MULTIDISCIPLINARY CENTER FOR EARTHQUAKE ENGINEERING RESEARCH
University at Buffalo, State University of New York
Red Jacket Quadrangle, Buffalo, NY 14261

Preface

The Multidisciplinary Center for Earthquake Engineering Research (MCEER) is a national center of excellence in advanced technology applications that is dedicated to the reduction of earthquake losses nationwide. Headquartered at the University at Buffalo, State University of New York, the Center was originally established by the National Science Foundation in 1986, as the National Center for Earthquake Engineering Research (NCEER).

Comprising a consortium of researchers from numerous disciplines and institutions throughout the United States, the Center's mission is to reduce earthquake losses through research and the application of advanced technologies that improve engineering, pre-earthquake planning and post-earthquake recovery strategies. Toward this end, the Center coordinates a nationwide program of multidisciplinary team research, education and outreach activities.

MCEER's research is conducted under the sponsorship of two major federal agencies, the National Science Foundation (NSF) and the Federal Highway Administration (FHWA), and the State of New York. Significant support is also derived from the Federal Emergency Management Agency (FEMA), other state governments, academic institutions, foreign governments and private industry.

The Center's FHWA-sponsored Highway Project develops retrofit and evaluation methodologies for existing bridges and other highway structures (including tunnels, retaining structures, slopes, culverts, and pavements), and improved seismic design criteria and procedures for bridges and other highway structures. Specifically, tasks are being conducted to:

- assess the vulnerability of highway systems, structures and components;
- develop concepts for retrofitting vulnerable highway structures and components;
- develop improved design and analysis methodologies for bridges, tunnels, and retaining structures, which include consideration of soil-structure interaction mechanisms and their influence on structural response;
- review and recommend improved seismic design and performance criteria for new highway systems and structures.

Highway Project research focuses on two distinct areas: the development of improved design criteria and philosophies for new or future highway construction, and the development of improved analysis and retrofitting methodologies for existing highway systems and structures. The research discussed in this report is a result of work conducted under the existing highway structures project, and was performed within Task 106-F-4.3.1 (a), "Field Testing of a Seismically Isolated Bridge" of that project as shown in the flowchart on the following page.

The overall objective of this task was to measure and assess the in-situ dynamic behavior and performance of a typical slab-on-girder bridge. Two bridges were subjected to transverse quick-release testing, which simulated transverse seismic loading. This report presents the results of a study of these two bridges before and after replacement of the original steel bearings; one with ordinary neoprene elastomeric bearings, and the other with laminated rubber seismic isolation

bearings. Test results indicate that steel bearings have considerable intrinsic strength and are able to withstand strong ground motions, primarily due to the frictional resistance of the bearings. The use of seismic isolation bearings, for these specific bridges, resulted in marginal performance improvement.

SEISMIC VULNERABILITY OF EXISTING HIGHWAY CONSTRUCTION
FHWA Contract DTFH61-92-C-00106

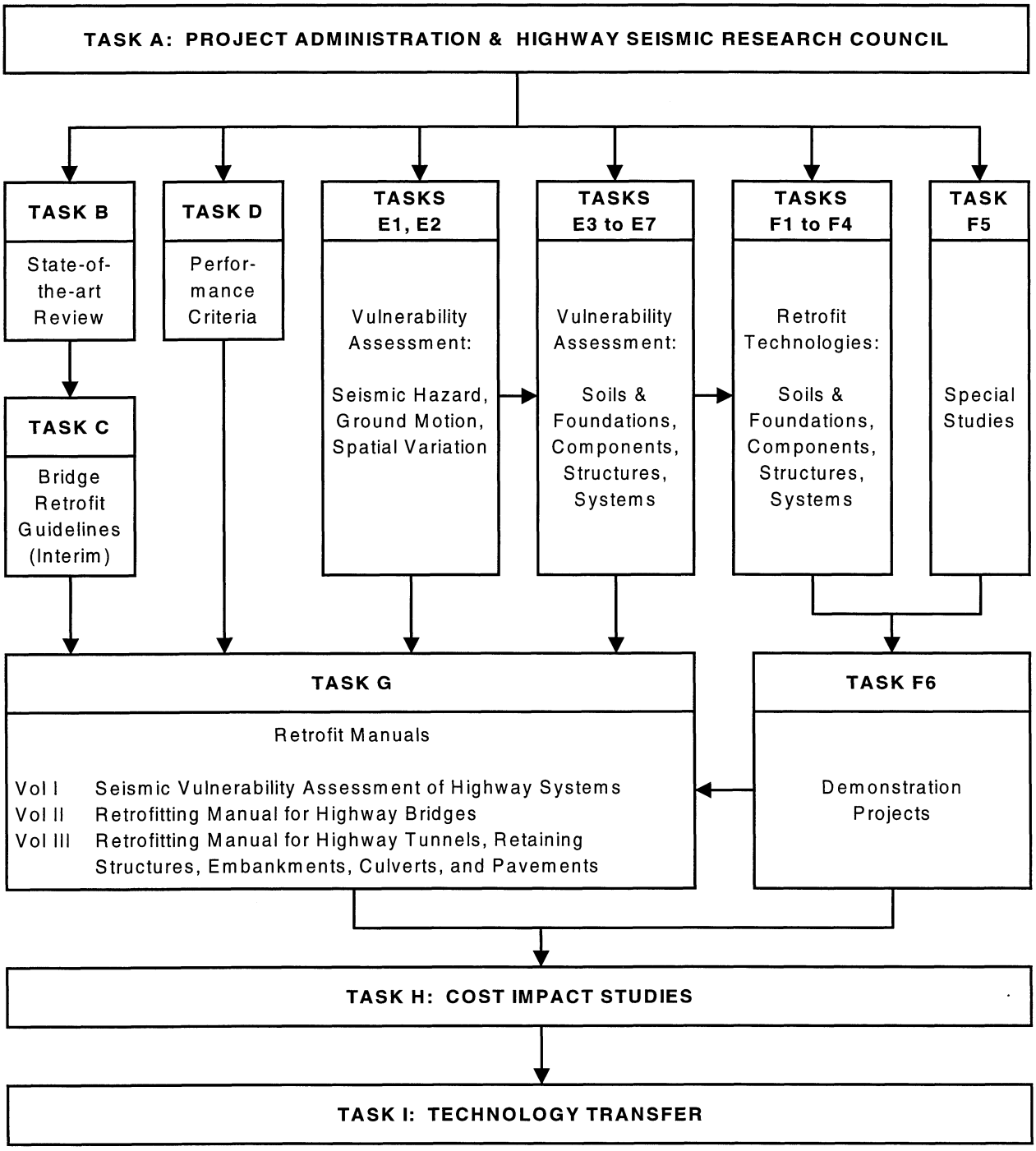

ABSTRACT

This study presents an investigation of the lateral dynamic response behavior of two highway bridges before and after the replacement of the original steel bearings. The bearings on the Northbound bridge were replaced with ordinary neoprene elastomeric bearings, while for the Southbound bridge, laminated rubber seismic isolation bearings were used. The study is in two parts: an experimental field investigation under quick release (snap-back) testing, and an analytical modeling study to investigate seismic performance of the bridges with different support conditions.

Several quick release testing methodologies were explored including: oil pressure release, breakable fuse-bars, and a mechanical fuse. It was shown that the oil release system acts as a large viscous damper, the breakable fuse-bars are satisfactory for only one large force jacking location, and the mechanical fuse being the most versatile is capable of providing near instantaneous release at several locations via solenoid values. With the latter two loading systems, deck accelerations of up to 0.43 g were attained. A hybrid frequency domain/time-domain system identification methodology was developed to separate non-linear and linear portions of the experimental vibration time histories, thus enabling mode shapes and frequencies to be identified. Experimental observations showed that for the Southbound and Northbound bridges, the respective first transverse natural frequencies prior to rehabilitation (steel bearing seats) were 5.5 Hz and 5.8 Hz; after rehabilitation with elastomeric bearings these frequencies reduced to 1.08 Hz and 1.8 Hz.. Several sources of non-linear material behavior were identified, the most pronounced being the soil-structure interaction and elastomeric bearing behavior.

The analytical portion of the study focused on the development of non-linear structural models that could reproduce the experimentally observed displacement time histories. Once validated, the models were then used to predict the transient-seismic performance of the bridges with different bearing conditions under a variety of strong ground

motions. Results of this study showed that bridges with steel bearings have considerable intrinsic strength and are able to withstand quite strong ground motions —— primarily due to frictional resistance of the bearings. If existing steel bearings are rehabilitated with engineered isolation bearings, the seismic performance may improve marginally. However, these replacement bearings may have difficulty coping with the displacement demands imposed by long period near-fault pulse-like ground motions. Adding supplemental shock absorbing dampers may help to improve performance under these adverse near-field effects.

ACKNOWLEDGMENTS

This research was undertaken in the Department of Civil Engineering at the State University of New at Buffalo. Financial support is gratefully acknowledged from the National Center for Earthquake Engineering Research under a contract for the FHWA on the Seismic Vulnerability of Existing Highway Construction (Contract 106).

The generosity of Professor Bruce Douglas of the University of Nevada is acknowledged. He for provided the jacks and quick-release mechanisms used in the first portion of the field work. Watson, Bowman and Acme are thanked for providing the expansion joint material for testing. The NYSDOT is also thanked for making available the drawings and general information on the bridges. Union Concrete Construction Corp. is acknowledged along with NYSDOT for help with site access and field coordination, including providing traffic control during the field tests.

Assistance provided by technicians Messrs Cizdziel, Patarroyo, Pitman, Walch, Kuhl and Majewski of the Department of Civil Engineering Seismic Research Laboratory and the graduate students Messrs G. Pekcan, J-H Kim, D-K Kim, and C-T Cheng, M. Tracey, P. Dreyer, D. MacEwan, S. Bhadra and L. Zhang is gratefully acknowledged.

TABLE OF CONTENTS

LIST OF ILLUSTRATIONS

LIST OF TABLES

SECTION 1
INTRODUCTION

1.1 BACKGROUND

Dynamic field tests have been carried out on bridges for several decades. Many of the early tests were conducted as part of safety inspections and were done using the limited technology available at the time. In the 1970's, an important event occurred which marked a turning point in the development of research and design on the seismic response of highway structures.

The 1971 San Fernando earthquake dramatically revealed the vulnerability of highway bridges to large earthquakes. In earthquakes prior to the San Fernando event, only limited damage was observed in bridges. According to Penzien et al. (1972), the damage to bridges prior to the 1971 San Fernando earthquake had been caused by settlements and overturning of substructures, displacement of supports, anchor bolt breakage and settlement of approach fills and wingwall damage. From 1933 to 1971, eleven separate earthquakes occurred in California ranging in Richter magnitude from 5.4 to 7.7 and affected some 1000 bridges. None of these bridges, however, were close to the area of intense shaking, as they were during the 1971 San Fernando earthquake. Several publications addressed different problems observed during this earthquake (Jennings, 1971; Wood, 1971; Elliott, 1973; Fung, 1971).

After the 1971 San Fernando earthquake, a call was issued to review of the predominant linear elastic design philosophy. Ductile ultimate strength design was introduced into codes, and the profession quickly realized that this was an essential alternative to the linear elastic analysis and design method. Under the ductile ultimate strength design philosophy, plastic hinges are designed to form in some structural members of a bridge under severe seismic loads. Collapse of the structure must be avoided by detailing for ductility. It must be accepted by the designers and owning agencies, however, that for moderate to severe earthquakes, damage is not only expected but will indeed occur. Thus, the ability of the structure to function after the earthquake

is unknown. It is to address this potential lack of post-earthquake serviceability that research into seismic isolation and mechanical energy dissipation techniques began.

The seismic isolation concept is based on two simple principles: to shift the natural period of the structure out of the region of dominant earthquake energy; and to increase the damping which is equivalent to increasing the capacity for energy dissipation in the structure.

If these two objectives can be accomplished, the structure will remain intact and undamaged after a major earthquake. The application and acceptance of the seismic isolation design philosophy has been somewhat slow in North America, and many questions have been posed concerning the behavior of the structure under the elements used to isolate it. Until now, most work in seismic isolation has been done in the laboratory on the isolator alone (Tyler 1984) or scale bridge models (Kelly, 1986; Tsopelas, 1994). However, in situ conditions may differ from those in the laboratory and field verification of the entire structural system is needed.

1.2 Previous Full-Scale Experimental Investigations

Full scale tests of bridges have gained interest during the last 20 years. Improvements in data acquisition technology and the application of system identification concepts (Douglas, 1982) have contributed to make this kind of test an important source of information. The main pursuit in these full scale tests is a better understanding of the behavior of the bridges under in situ conditions for both service live loads and loads that resemble unusual overload conditions. In order to investigate techniques for the assessment and integrity monitoring of the experimental results, in most cases it is desirable to also construct reliable mathematical structural models that can predict the behavior of the structure under different dynamic loading conditions.

According to Salawu (1995), the classification of experimental testing technique is related to the degree of control over the input excitation. Dynamic testing methods without any input control are classified as *ambient* vibration testing. *Forced* vibration testing incorporates those methods where the vibration is artificially induced. In the first group, traffic and wind serve

as the major source of excitation for the vertical and transverse directions, respectively. Most of the work done using the ambient vibration as the input excitation can produce reliable dynamic models provided linear elastic small-strain behavior is expected. However, for regular (non-cable suspended or truss) bridges, wind loading or traffic is insufficient to provide information about the transverse modes and frequencies, particularly if some soil-structure interaction is to be expected and non-linear soil behavior is encountered.

In *forced* vibration tests, there are several alternatives: eccentric rotating mass vibrators; hydraulic vibrators; impact hammers; and others. Each alternative has advantages and disadvantages, and the use of one or the other depends on the expected results and the characteristics of the bridge in question.

Several works have used the vibration produced by traffic or wind to extract the dynamic characteristics of the bridges. Gates (1982) reported the results of tests performed on 57 bridges in an effort to improve the dynamic modeling of such structures. Buckland (1979) studied the Lions Gate suspension bridge in Vancouver. His study showed a discrepancy of some 45% with the prediction of frequencies. The author explains in his paper that the discrepancy could be attributed to measurement errors, dynamic coupling of torsional and horizontal motion, stiffness changes and others, and warned about the reliability of the results of small vibration tests. Abdel-Ghaffar (1978) developed a structural measuring technique using vehicular traffic-induced vibrations for full scale testing of the Vincent-Thomas Suspension Bridge. The results of this test showed the reliability of this technique by comparing the experimental and analytical results.

Quick-release and impact tests, according to Salawu's (1995) classification are *forced* vibration tests. They should strictly be considered as a special category of testing to differentiate them from continuous forced vibration tests.

Douglas (1976, 1990) has been one of the most active researchers in the area of forced dynamics excitation of full scale bridges. He and his co-workers have tested bridges with different characteristics and worked on the parameter identification of bridges under earthquake

loading. Aktan (1992) has used an impact technique as a source of excitation to test full scale bridges. It is maintained that this technique is a good alternative for the integrity monitoring and diagnostics of bridges. A study of the behavior of bridges under both static and dynamic loading was done by Eberhard (1992). He found that for structural deficits up to 0.15 percent, a large amount of stiffness and strength can be attributed to the resistance of the soil at the abutments and the soil surrounding the columns at the intermediate piers. He also found that despite the deficiencies of the piers in this test, they were able to resist forces of approximately 40% of the weight of the bridge at a drift of 3%. Buckle (1986, 1990, 1993) has also worked for some time in this area. His work includes full scale tests and shaking table studies of bridges in conjunction with Kelly. Kelly and Buckle (1981, 1986) have been the chief proponents of base isolation in the US. Recently, Constantinou (1993) and his coworkers have been using different base isolation devices to protect the structure or reduce the structural impact of the forces produced by an earthquake.

There are several analytical concerns or issues which should accompany any experimental study. Chen (1975) has studied the effect of the soil structure interaction in the earthquake response of bridges. Cofer (1994) identified general foundation models which are suitable for modeling soil-structure interaction in seismic bridge analysis. He modified the NEABS (Penzien, 1981) program to account for this effect and, based on his studies, concluded that accounting for soil-structure interaction in foundation models can produce an important change in the bridge response especially when compared to that of the fixed-base model. Maragakis (1985) studied the interaction of the slab with the abutment during an earthquake and proposed a simple analytical model for skew bridges. McCallen (1994) developed a very sophisticated model that included the structure and the soil. The sensitivity of bridge response to various parameters such as deck skew, embankment soil stiffness and soil mass, stick model, modal damping values, and soil non-linearity were investigated. The ability of the model to accurately represent the seismic response of the bridge was discussed.

Wilson (1984) studied the behavior of the San Juan Bautista bridge after the earthquake of Coyote Lake and proposed equations for the computation of the stiffness of non-skewed

monolithic abutments. Imbsen (1986) studied bridge energy absorption during an earthquake. He also studied and modeled the behavior of expansion joints, hinges, and bearings supports.

1.3 Previous System Identification Investigations

Reliable mathematical models can be constructed which represent a test structure if certain parameters that govern the behavior of the structure in the area in question are extracted. The technique used to extract these parameters is generally referred to as system identification and has been used widely in aerospace and mechanical structures. The application of such techniques in civil and structural engineering is less common. Trifunac (1970) used the technique to obtain modes and frequencies of a twenty two story steel frame; Somaprasad (1991) identified the dynamic properties of a 27 story reinforced concrete flat plate building, and DiJulio (1974) analyzed the torsional response of a high-rise building. The researchers previously noted have used existing system identification techniques. Beck (1978) proposed a new system identification approach, specifically for civil engineering structures. His technique is based on a time domain approach and is especially suitable for earthquake records. McVerry (1979) proposed a new approach based on a frequency domain approach. Both Beck and McVerry compared the proposed system identification techniques with the results obtained from structures subject to earthquakes. Douglas (1982) has described a system identification technique and applied it to bridge analysis. Richardson (1988) proposed a system identification methodology for structures which are tested using the snap back technique. His approach was based on curve fitting of the experimental results in the frequency domain, and one of the main objectives of this work was to address the problem of the closely spaced modes.

Only a limited number of full-scale tests conducted in the past were performed on bridges with highly damped non-linear isolation devices (Lam, 1990; Kakinuma, 1994; Hasegawa, 1994). There is a lack of information in this area which needs to be addressed. There is also practically no information regarding bridges tested before and after retrofitting with seismic isolation devices. This last point raises the question of how effective the isolation system will be for a specific bridges and the extent of new isolation bearing seats will change the behavior

of the bridge as compared with conventional steel bearing supports. Full scale experiments under these two different conditions can help to answer these questions and are the focus of the investigation reported herein.

1.4 Focus of the Present Study

This research presents the results of a series of experiments on two slab-on-girder bridges that are illustrated in figure 1-1 and of companion analytical studies. These bridges were retrofitted with two different kinds of elastomeric bearings and were tested before and after the retrofitting.

The purpose of this research is therefore to investigate and characterize the behavior of two similar slab-on-girder bridges under large-amplitude transverse quick-release (free vibration) excitation, both before and after their existing steel bearings were replaced with seismic isolation bearings.

Specific objectives to be achieved in order to accomplish this purpose are as follows:

1. devise and construct a tension-loaded quick-release apparatus suitable for the subject bridges,
2. develop the means by which the fundamental dynamic characteristics of the subject bridges can be identified from the quick-release experimental data,
3. devise analytical models which enable suitably accurate predictions of observed behavior of the subject bridges, both before and after the bearing retrofit.

1.5 IMPORTANCE OF THIS RESEARCH

It is considered important to identify what material is particularly new in this work and makes a unique contribution to the art and science of seismic bridge engineering.

FIGURE 1-1 Typical View of the Bridges Over Cazenovia Creek

During the last 25 years there have been several full scale bridge tests as described in Section 1.2. Several other bridges have been studied using real earthquake records. However, there is lack of information about bridges that were tested before and after the initial steel bearings were replaced by elastomeric bearings. There is also a lack of information concerning full scale bridge tests, particularly where companion studies on component material provide a wealth of information on the bearing performance, as well as expected soil-structure interaction effects (Mander et al. 1996, Kim et al. 1996, and Douglas et al. 1994). Thus, it is considered that the experimental information provided herein is by itself a valuable contribution to the understanding of bridge behavior.

The construction of a reliable quick release snap-back experimental setup necessary to perform the test, and the inherent problems and solutions adopted during its implementation provide another source of valuable information that can be used by other researchers. In this study, a new tension snap back system is proposed and the problems observed with the use of hydraulic systems to release the forces is addressed. A quick-release mechanism that can release simultaneously more than one loading point was developed for this project and is described herein.

The data reduction of experimental results for any large, full scale series of dynamic tests is a complex problem. The identification of the dynamic characteristics of any structure can be done if an appropriate approach is used. The approach used herein is a coupled frequency domain-time domain hybrid solution. It is demonstrated that such a solution is simple to formulate and can be implemented without requiring special software. Such a straightforward approach should appeal to practicing engineers as well as researchers.

A full scale test is conducted not only to provide information that later will be part of a data base but also to serve as the benchmark for comparative analytical studies. In this project, different models with varying degrees of complexity are implemented and compared. It was demonstrated that for the kind of slab-on-girder class of bridge investigated it is possible to construct reliable models by using only the basic concepts of mechanics and dynamics.

SECTION 2
DESCRIPTION OF BRIDGES STUDIED AND EXPERIMENTS PERFORMED

2.1 INTRODUCTION

This section describes the characteristics of the bridges investigated, the loading setup constructed for the experiment and the location of the instruments used during testing. It also briefly describes the problems encountered during the experiments and the solutions adopted. Additionally, each bridge is identified by its position relative to the other as either the Northbound bridge or the Southbound bridge. As both bridge structures are quite similar, unless otherwise stated, the information and figures presented are for the Southbound bridge structure.

2.2 DESCRIPTION OF THE BRIDGES INVESTIGATED

During the period 1993/94, a portion of the Route 400 highway which is located near the town of East Aurora in New York State was reconstructed and its bridges rehabilitated. Of the several bridges along this route both the Northbound and Southbound bridges over Cazenovia Creek were subjected to quick-release tests. Both bridges are typical three span slab on girder bridges with a small skew angle of 9.7° for the Southbound and 11.5° for the Northbound. Both bridges were designed in 1967 and constructed by the end of that decade. Figure 2-1 presents a plan and elevation view of both bridges, as well as detailed information on the bearing seats before and after retrofitting. Figure 2-2a presents a transverse section of the bridge and figure 2-2b a column detail of the bents. The geometric dimensions and elevations were extracted from a set of as-built drawings of the bridges provided by the New York State Department of Transportation (NYSDOT) for the present study.

Southbound Bridge: This bridge consists of the two principal traffic lanes plus one additional on-ramp lane on the right hand side of the bridge giving a total width of 14.78 m and 61.24 m in length. The superstructure consists of a 230 mm concrete deck cast compositely on seven W36 × 150 steel girders. The seven steel girders are laterally supported by cross

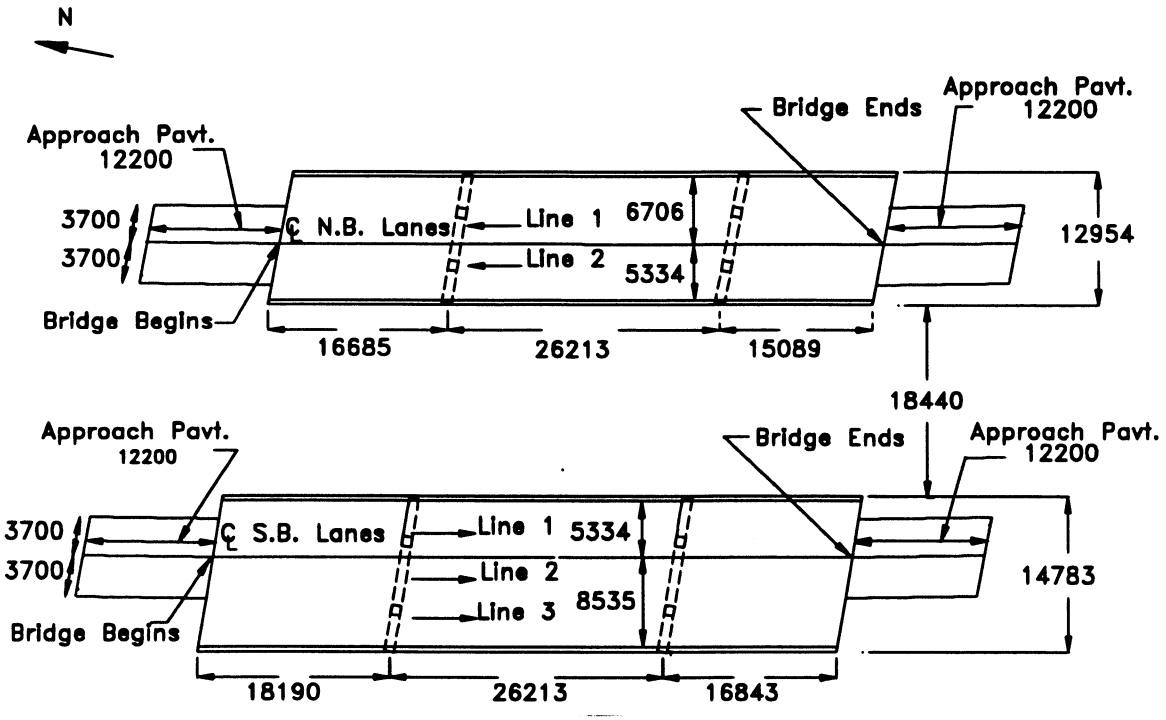

(a) Plan View

	BEARING TYPE		
	PRE-RETROFIT	POST-RETROFIT	
	S. BOUND & N. BOUND	S. BOUND	N. BOUND
N. ABUT.	LOW STL. EXP.	LEAD CORE ELAST.	STD. ELAST.
PIER #1	HIGH STL. FIXED	STD. ELAST.	STD. ELAST.
PIER #2	HIGH STL. EXP.	STD. ELAST.	STD. ELAST.
S. ABUT.	LOW STL. EXP.	LEAD CORE ELAST.	STD. ELAST.

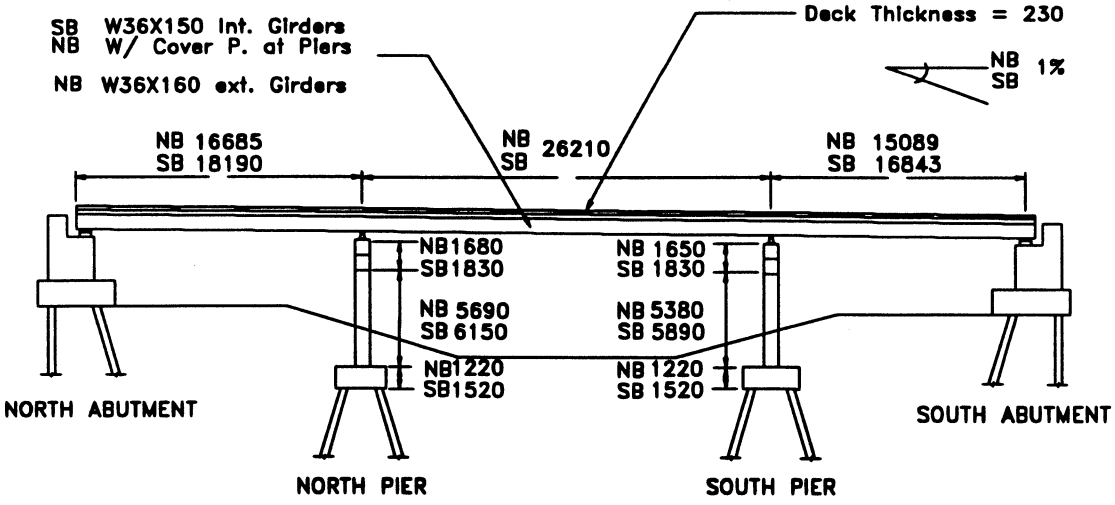

(b) Longitudinal View

(All Dimmensions in mm)

FIGURE 2-1 Plan and Longitudinal View of the Bridges Over Cazenovia Creek

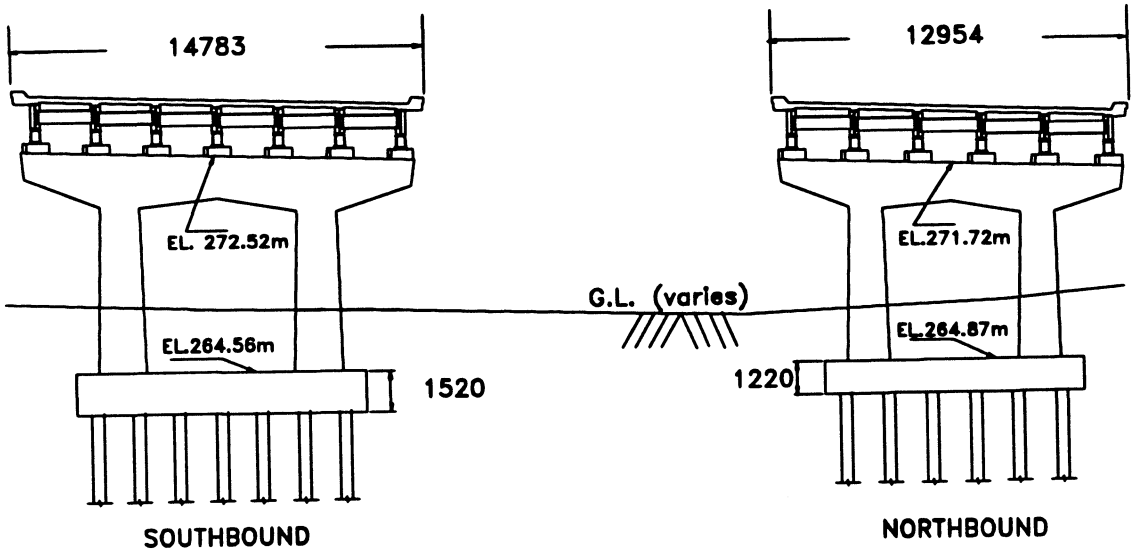

(a) Bridge Cross Sections

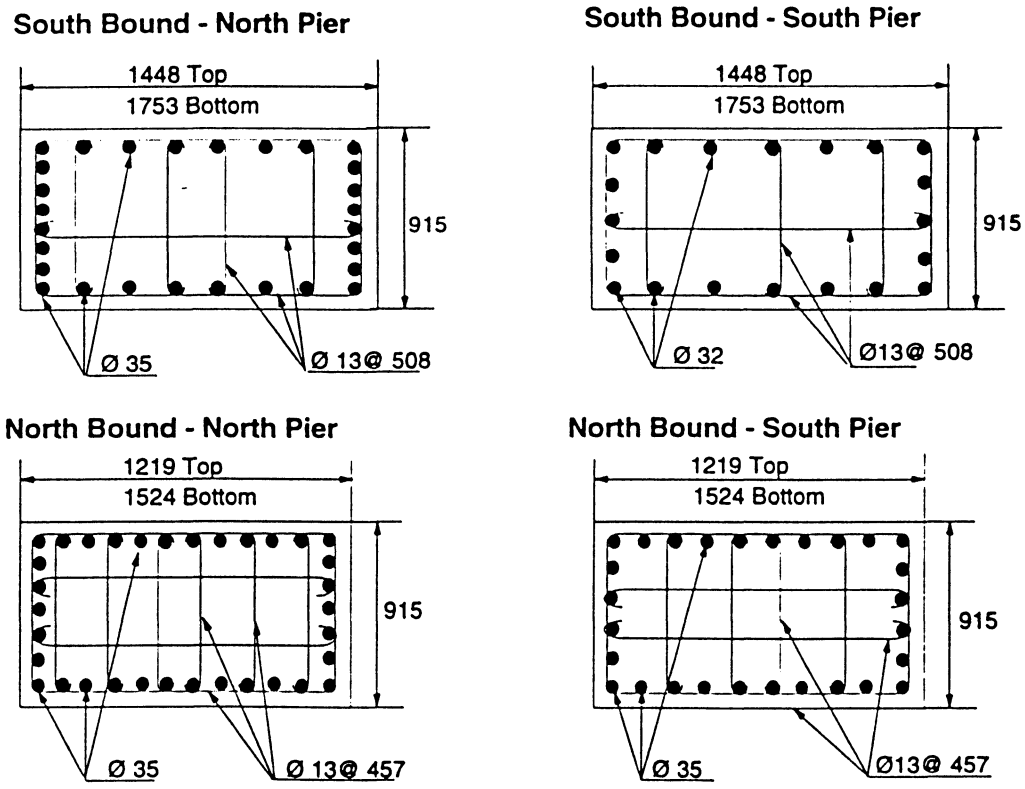

(b) Column Details

(All Dimmensions in mm)

FIGURE 2-2 Bridge Cross Sections and Column Details

diaphragms that consist of channel sections bolted to vertical connection plates welded to the principal girders' webs. The diaphragms exist at abutments, pier supports, third points in the end spans and quarter points in the center span. Typical pier and abutment diaphragms are shown in figure 2-3 and 2-4, respectively. The piers are of reinforced concrete with tapered rectangular columns as shown in figure 2-3.

In the longitudinal direction, the elevation of the bridge is higher at the North abutment than at the south abutment; the average vertical grade in the longitudinal direction is around 1% and 3% in the transverse direction.

Figure 2-5 shows the original bearings used in the Southbound bridge. Low expansion bearings were located at both abutments and high expansion (rocker) bearings at the south pier. High fixed bearings were used on the north pier bent. Figures 2-6a and 2-6b show the pier bent foundation which consists of a rectangular concrete pile cap and 14 10BP42 steel bearing piles. The length, width and depth of the pile cap are 10.37 m, 3.2 m and 1.52 m, respectively. The two rows of steel piles run the length of the pile cap (transverse to the axis of the bridge) and each row has seven piles. Each pile is embedded 300 mm into the concrete pile cap bottom and spaced at 1.58 m and 2.6 m along the longitudinal and the transverse directions of the pile cap, respectively. The battered steel piles are approximately 16.5 m in length and have a slope of one to four in the vertical direction.

A typical view of the bridge foundation is illustrated in figures 2-6 and 2-7. A marked difference in the amount of soil over the pile cap was observed between the North and South piers; the amount of soil averaging the North and South pier caps being 3.4 and 0.9 m, respectively. At the abutments the soil consists of nine layers, seven of which are below the pile cap, one of which is around the pile cap, and the uppermost layer is above the pile cap.

The abutment foundation consists of a concrete pile cap and 22 10BP42 steel piles. The concrete pile cap is 2.44 m wide and 1.22 m deep. The steel bearing piles are embedded 305 mm into the bottom of the pile cap. The steel piles around the outside of the pile cap are

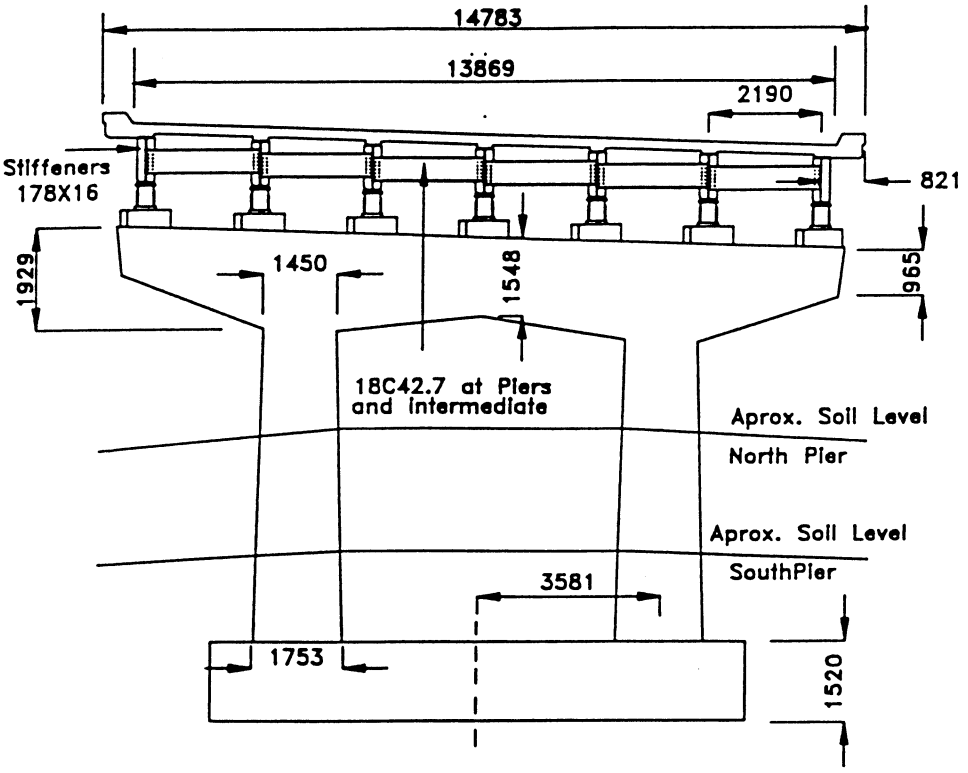

(a) South Bound Bridge

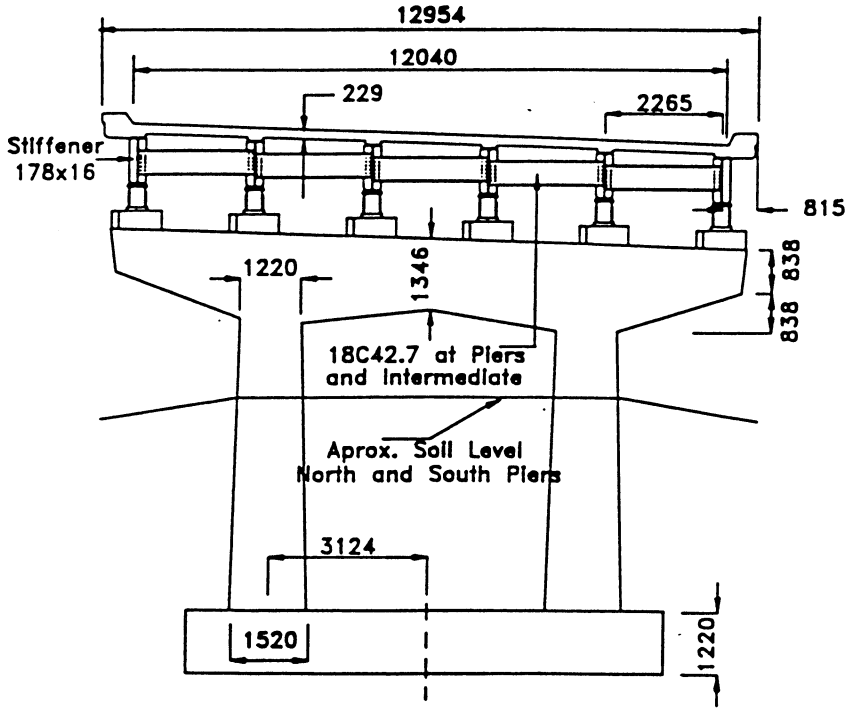

(b) North Bound Bridge

(All Dimmensions in mm)

FIGURE 2-3 Pier Bent Dimensions of the Bridges Over the Cazenovia Creek

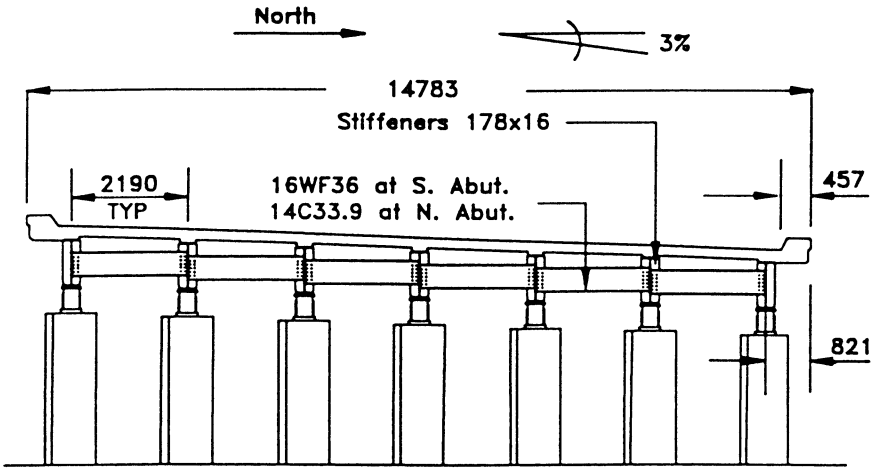

(a) South Bound Bridge

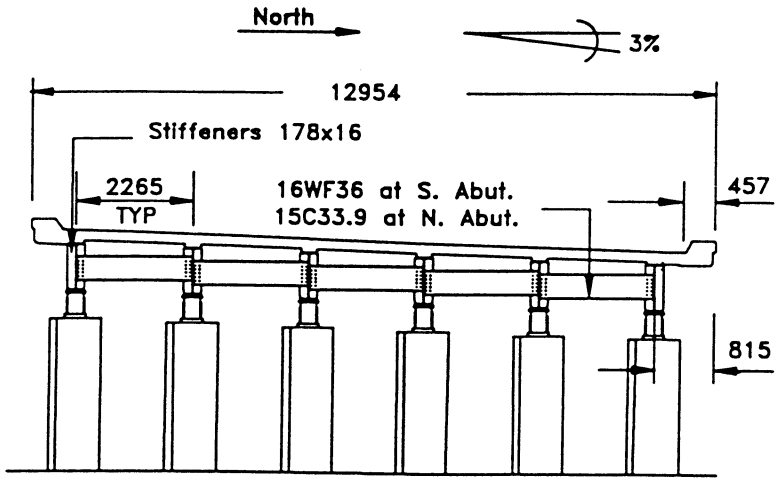

(b) North Bound Bridge

(All Dimmensions in mm)

FIGURE 2-4 Abutment Dimensions of the Bridges Over the Cazenovia Creek

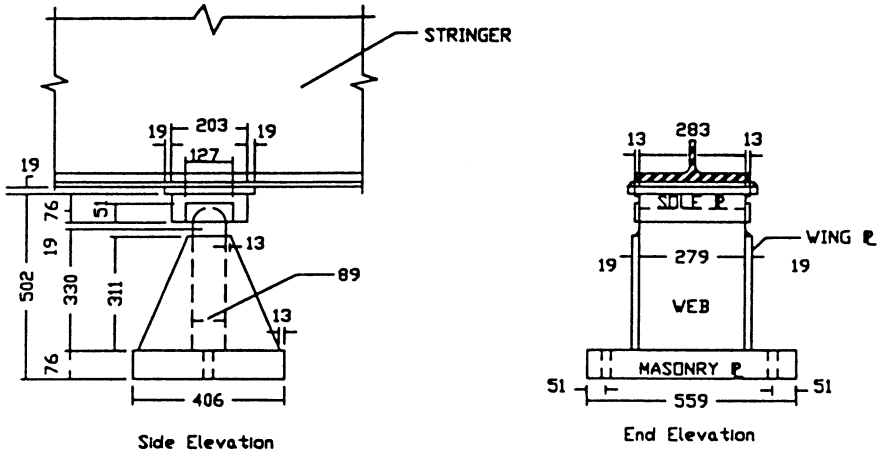

FIXED BEARINGS AT PIER

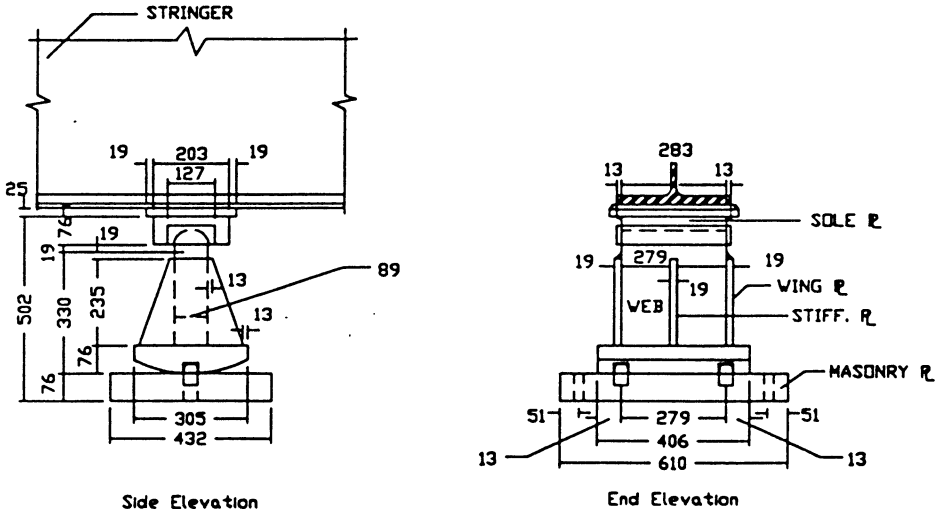

EXPANSION BEARINGS AT PIER

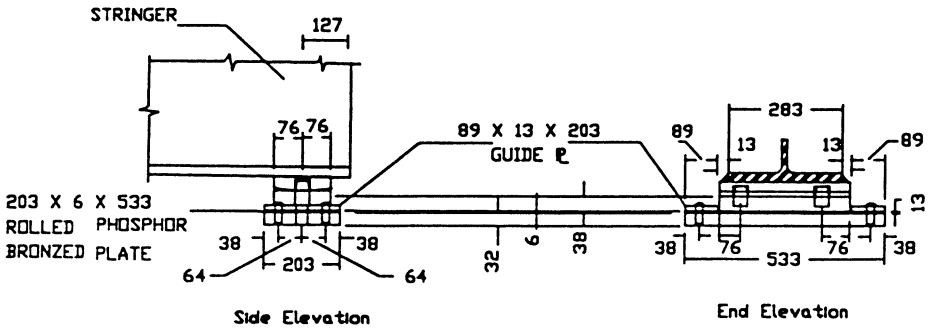

EXPANSION BEARINGS AT ABUTMENTS

(All Dimmensions in mm)

FIGURE 2-5 Steel Bearings Characteristics

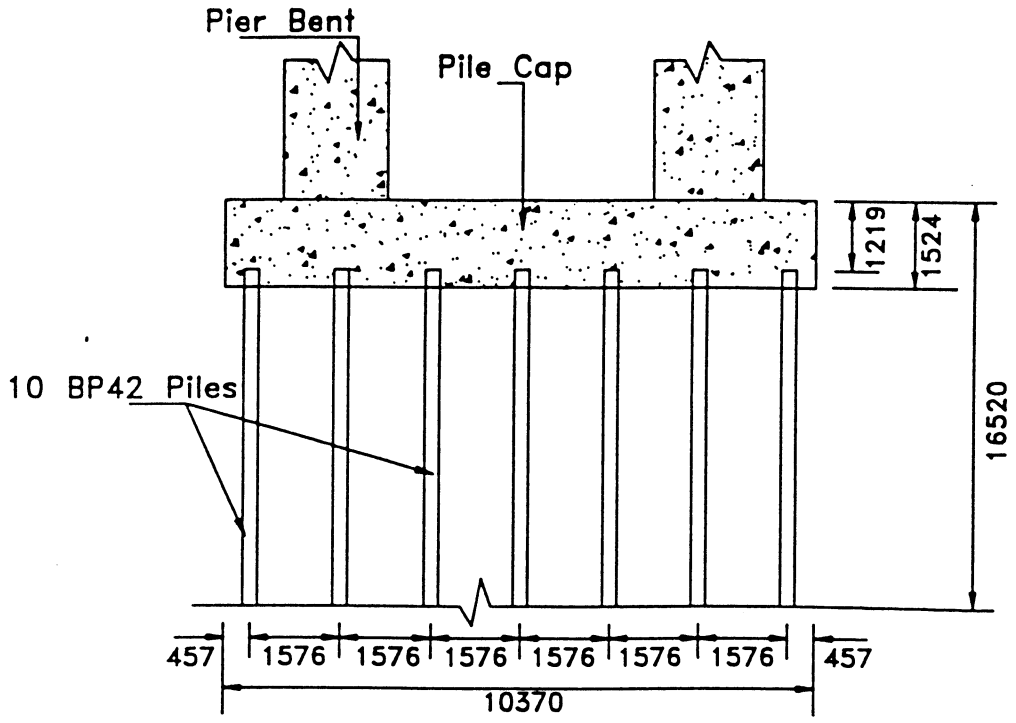

(a) Longitudinal Section

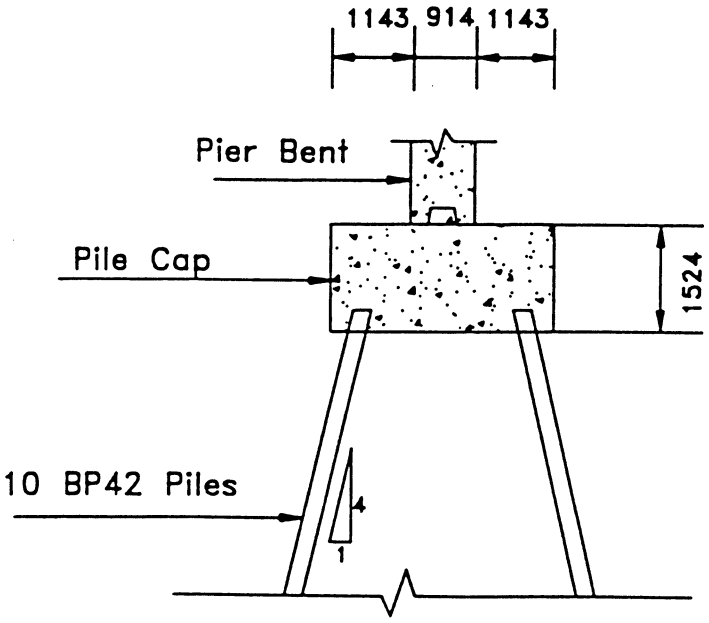

(b) Cross Section

(All Dimmensions in mm)

FIGURE 2-6 Pier Bent Foundation

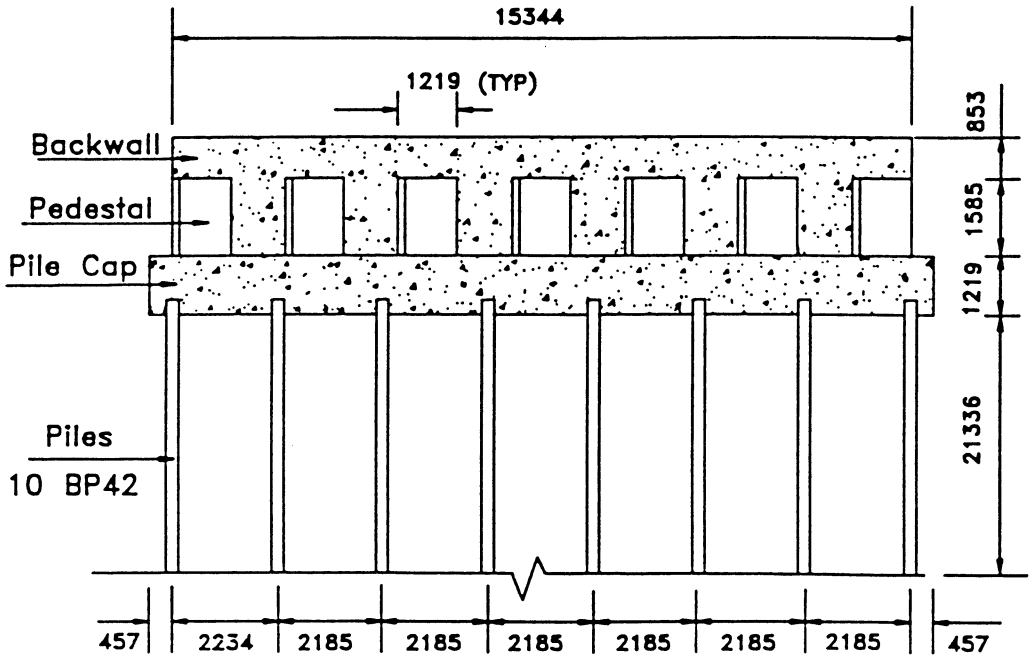

(a) Longitudinal Section

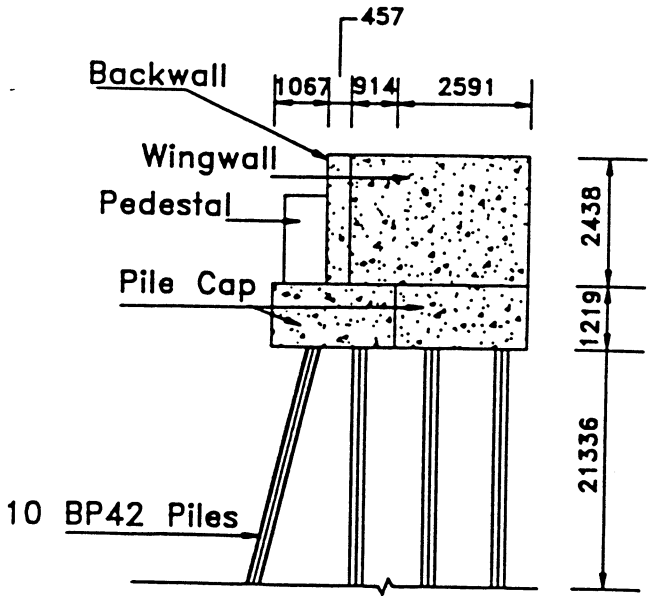

(b) Cross Section

(All Dimmensions in mm)

FIGURE 2-7 Abutment Foundation

battered. They are approximately 21 m in length, having a batter slope of 1:4 in vertical direction.

Soil layering at the abutments consists of thirteen layers, eleven of them below the pile cap, one surrounding the pile cap, and the upper layer above the pile cap. The upper layer consists of soil around the wingwall and backfill of the backwall of the abutments. There is no soil at the front of the abutment.

Figure 2-8 shows one of the soil profiles provided by the NYSDOT (1964). A detailed study of the modeling of the abutments and the pier bents foundation system for this bridge is investigated in companion research by Douglas et al. (1994).

Northbound Bridge: This bridge is quite similar to the Southbound structure. The principal difference is in the bridges' width, the Northbound having only two lanes with the concrete deck seated on six steel girders. The bridge has a total width of 12.95 m and 57.98 m of length. The superstructure is similar to the Southbound structure and consists of a 230 mm concrete deck cast compositely on six W36$\times$150 steel girders. Diaphragms are located in a similar fashion to the Southbound structure. Bridge dimensions are given in figures 2-1 to 2-4.

Foundation differences lie only in the dimensions of the pile cap and the number of piles. A rectangular concrete pile cap with length, width and depth of 9.30 m, 3.12 m and 1.2 m, respectively and a total of 12 10BP42 steel bearings piles divided in two rows of 6 piles each, constitute the foundation of the pier bent. The steel piles are embedded 300 mm at the pile cap bottom and spaced at 1.68 m and 2.21 m along the longitudinal and the transverse directions of the pile cap, respectively. The battered steel piles are approximately 16 m in length and have a slope of one to four in the vertical direction.

The abutment foundation consists of a concrete pile cap and 20 10BP42 steel piles. The concrete pile cap is 2.29 m wide and 1.22 m deep. The steel bearing piles are embedded 300

STATE OF NEW YORK
DEPARTMENT OF PUBLIC WORKS
BUREAU OF SOIL MECHANICS
SUBSURFACE EXPLORATION LOG
(CONTRACT)

DISTRICT NO. 5
COUNTY Erie
B.S.M. PROJ. NO. 5-517
CONTRACT SM 232
PROJECT Aurora Expy. Maple Road to Emery Road
QUAD. LOCATION
SOIL SERIES

HOLE NO. C-44
LINE & STA. 3806+34
OFFSET 105' R

DATE, START 2-5-66
DATE, FINISH 2-10-66
SURF. ELEV. 878.90'
DEPTH TO WATER As Noted
(ALSO DESCRIBE UNDER "REMARKS")

CASING O.D. 2.5" I.D. 2.0"
SAMPLER O.D. 2.0" I.D. 1.5"
WEIGHT OF HAMMER 300#
INSIDE LENGTH OF SAMPLER 24"
HAMMER FALL CASING 18" SAMPLER 18"

DEPTH BELOW SURFACE	BLOWS ON CASING	SAMPLE NO	BLOWS ON SAMPLER 0/6	6/12	12/18	18/24	CROSS SECTION	MOISTURE	COLOR	FIELD DESCRIPTION OF SOIL AND ROCK	REMARKS
0	3									0'-4'	
	3	1	1	1				M	Br	SILT, tr. fine sand	Soft
	4				2						Elevation 874.90'
	5										
5	4									4'-8'	
	8	2	1	1				M	Br	SILT, some fine Sand	Very Soft
	5				1						Elevation 870.90'
	4										
	8									8'-16.5'	
10	10										
	8	3	2	1				M	Gr	SILT, some fine Sand, tr. clay, tr. weathered shale fragments	Very Soft
	8				1						
	4										
	3										
15	5										
	21	4									
	20	4A	1	2				M	Gr	16.5'	Elevation 862.40'
	17									VANE TEST 4-A	16.5'-20' Soft
	16	4B	2	2				M	Gr	VANE TEST 4-B	
	17									SILT, some fine Sand	Elevation 858.90'
20	13	5	1	1							
	13				1			M	Gr	20'28'	
	15									SILT, some fine Sand, tr. clay	Very Soft to Soft
	21										
	20										
25	18	6	2	2							
	18				2			M	Gr		Elevation 850.90'
	18										
	15									28'-32'	
	15									SILT, some fine Sand, tr. gravel, tr. shale fragments	Firm
30	17	7	1	2				M	Gr		Elevation 846.90'
	38				8						
	64									32'-48'	
	29										
	83									Fine to coarse SAND some Silt, tr. gravel, tr. weathered shale fragments	Very Compact
35	104	8	31	49				M	Gr		
	141				15						
	240										
	575										
	596										
40	526	9	69	154							
	562				168			M	Gr		
	590										
	625										
	666										
45	544	10	78	186							
	621				211			M	Gr		
	700										Elevation 830.90'
	860									48'-58'	
50	849										

ALL CONDITIONS, MATERIALS, AND LAYERS ENCOUNTERED MUST BE DESCRIBED IN ACCORDANCE WITH CONTRACT SPECIFICATIONS. ALL WATER LEVEL OBSERVATIONS MUST BE DESCRIBED IN DETAIL UNDER "REMARKS".

THE SUBSURFACE INFORMATION SHOWN HEREON WAS OBTAINED FOR STATE DESIGN AND ESTIMATE PURPOSES. IT IS MADE AVAILABLE TO BIDDERS ONLY THAT THEY MAY HAVE ACCESS TO IDENTICAL INFORMATION AVAILABLE TO THE STATE. IT IS PRESENTED IN GOOD FAITH, BUT IS NOT INTENDED AS A SUBSTITUTE FOR INVESTIGATIONS, INTERPRETATION OR JUDGMENT OF THE BIDDER.

DRILLING CONTRACTOR Empire Soils Invest.
CONTR. SOILS TECH. W. Leaver
D.P.W. INSPECTOR P. Carderella
DISTRICT SOILS ENGR. P. Nowadly

SHEET 1 OF 2. HOLE NO. C-44

FIGURE 2-8 Typical Soil Profile

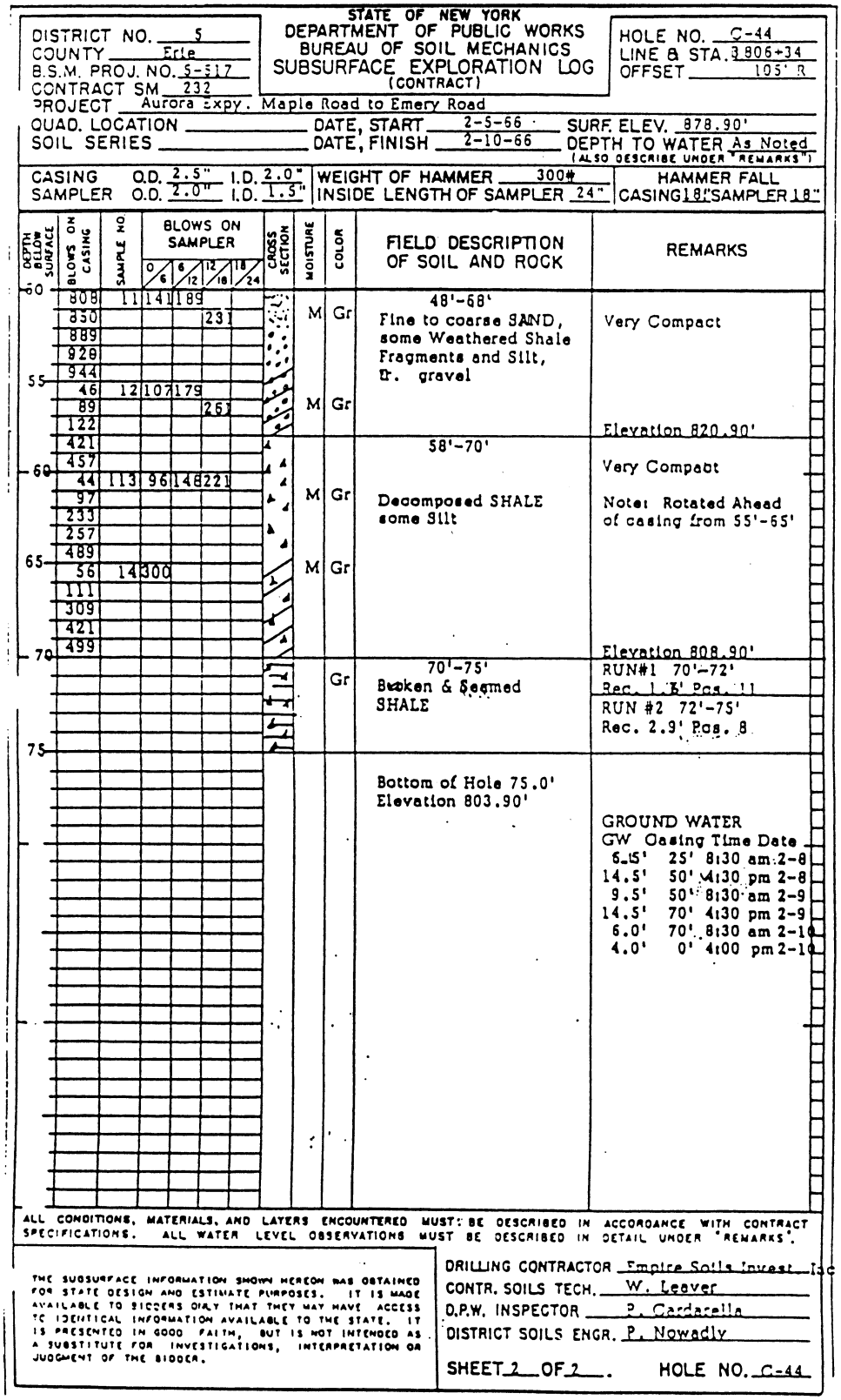

STATE OF NEW YORK
DEPARTMENT OF PUBLIC WORKS
BUREAU OF SOIL MECHANICS
SUBSURFACE EXPLORATION LOG
(CONTRACT)

DISTRICT NO. 5
COUNTY Erie
B.S.M. PROJ. NO. 5-517
CONTRACT SM 232
PROJECT Aurora Expy. Maple Road to Emery Road
QUAD. LOCATION
SOIL SERIES

HOLE NO. C-44
LINE & STA. 9806+34
OFFSET 105' R
DATE, START 2-5-66
DATE, FINISH 2-10-66
SURF. ELEV. 878.90'
DEPTH TO WATER As Noted
(ALSO DESCRIBE UNDER "REMARKS")

CASING O.D. 2.5" I.D. 2.0"
SAMPLER O.D. 2.0" I.D. 1.5"
WEIGHT OF HAMMER 300#
INSIDE LENGTH OF SAMPLER 24"
HAMMER FALL CASING 18" SAMPLER 18"

DEPTH BELOW SURFACE	BLOWS ON CASING	SAMPLE NO	BLOWS ON SAMPLER (0/6 6/12 12/18 18/24)	CROSS SECTION	MOISTURE	COLOR	FIELD DESCRIPTION OF SOIL AND ROCK	REMARKS
50	808	11	14 18 9					
	830		23		M	Gr	48'-68'	
	889						Fine to coarse SAND, some Weathered Shale Fragments and Silt, tr. gravel	Very Compact
	928							
	944							
55	46	12	10 7 17 9					
	89		26		M	Gr		
	122							
	421							Elevation 820.90'
	457						58'-70'	
60	44	113	9 6 14 8 22 1					Very Compact
	97				M	Gr	Decomposed SHALE some Silt	Note: Rotated Ahead of casing from 55'-65'
	233							
	257							
	489							
65	56	14	30 0		M	Gr		
	111							
	309							
	421							
	499							Elevation 808.90'
70							70'-75'	
						Gr	Broken & Seamed SHALE	RUN#1 70'-72' Rec. 1.5' Pos. 11
								RUN #2 72'-75' Rec. 2.9' Pos. 8
75							Bottom of Hole 75.0' Elevation 803.90'	

GROUND WATER

GW	Casing	Time	Date
6.5'	25'	8:30 am	2-8
14.5'	50'	4:30 pm	2-8
9.5'	50'	8:30 am	2-9
14.5'	70'	4:30 pm	2-9
6.0'	70'	8:30 am	2-10
4.0'	0'	4:00 pm	2-10

ALL CONDITIONS, MATERIALS, AND LAYERS ENCOUNTERED MUST BE DESCRIBED IN ACCORDANCE WITH CONTRACT SPECIFICATIONS. ALL WATER LEVEL OBSERVATIONS MUST BE DESCRIBED IN DETAIL UNDER "REMARKS".

THE SUBSURFACE INFORMATION SHOWN HEREON WAS OBTAINED FOR STATE DESIGN AND ESTIMATE PURPOSES. IT IS MADE AVAILABLE TO BIDDERS ONLY THAT THEY MAY HAVE ACCESS TO IDENTICAL INFORMATION AVAILABLE TO THE STATE. IT IS PRESENTED IN GOOD FAITH, BUT IS NOT INTENDED AS A SUBSTITUTE FOR INVESTIGATIONS, INTERPRETATION OR JUDGMENT OF THE BIDDER.

DRILLING CONTRACTOR Empire Soils Invest Inc
CONTR. SOILS TECH. W. Leaver
D.P.W. INSPECTOR P. Cardarella
DISTRICT SOILS ENGR. P. Nowadly

SHEET 2 OF 2. HOLE NO. C-44

FIGURE 2-8 (Continuation)

mm into the bottom of the pile cap. The steel piles around outside of the pile cap are battered. They are approximately 21 m in length and have a slope of one to four in the vertical direction.

No information was provided as to the soil condition of the Northbound bridge. However, due to the proximity of this bridge with the Southbound (around 18 m) it was assumed for this project that the soil properties and number of layers are similar to the Southbound bridge. The only major difference in the soil conditions compared to the Southbound was that in the Northbound bridge the level of the ground under both piers came within 1.52 m of the cap beam, which left the columns mostly buried in soil.

2.3 Modification During the Retrofitting Process

Prior to bearing replacement, decks were rehabilitated and approach slabs replaced. Subsequently, during the period between October 1993 and June 1994, the existing steel bearings were replaced with new, laminated elastomeric bearings. To accommodate the new bearings, the existing reinforced concrete pedestal beneath each steel bearing over the pier caps was removed down to the top of the cap beam, and replaced having a new pedestal with an enlarged transverse cross-section.

At each of the abutments the empty space between the pedestals illustrated in figure 2-9a, which were initially protruding from the wall, was filled with concrete. These modifications were performed in both the Northbound and Southbound bridges. To install the new bearings, the contractor jacked up each girder (one at a time), removed the old steel bearing and seated the new elastomeric bearing (figure 2-9b), and then moved onto the next bearing to be replaced. This process was repeated on alternate girders. Figure 2-10a illustrates a bearing before it was installed, and figure 2-10b shows the installation procedure.

At the abutments of the Southbound bridge, the steel bearings were replaced by laminated lead-rubber bearings. Laminated rubber bearings (without the lead core) were used over the piers. Figure 2-11 shows one of the lead-rubber bearings used at the abutment, and figure 2-12

(a) Abutment

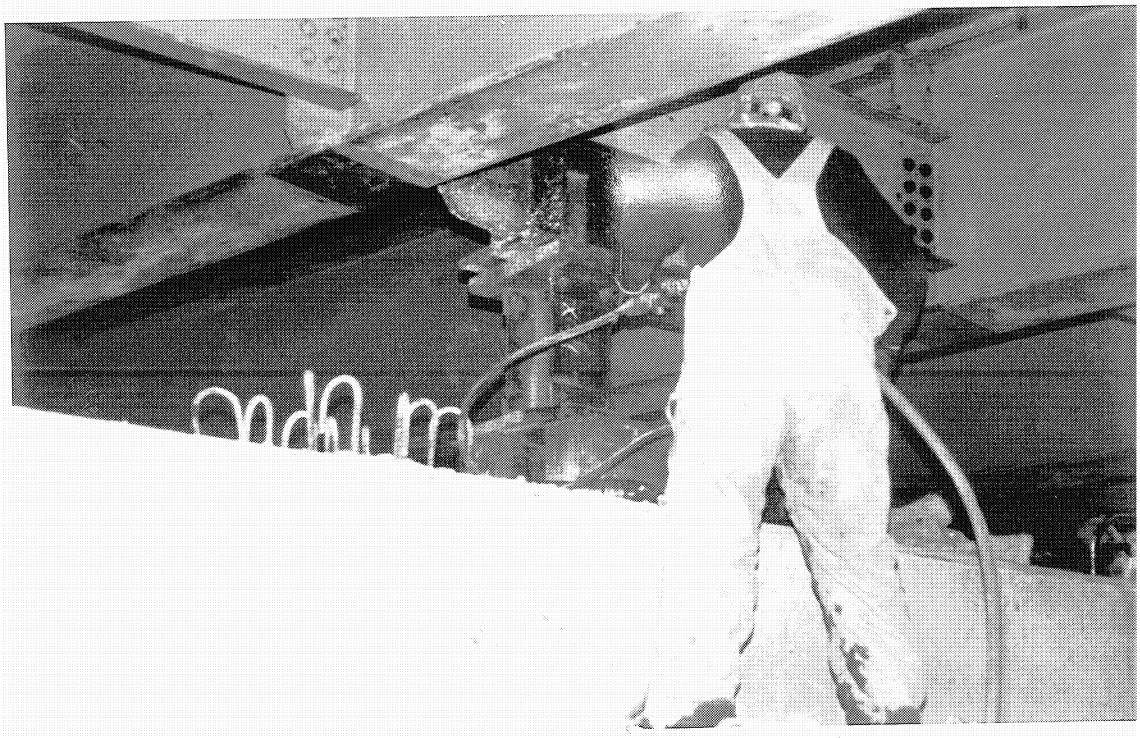

(b) Pier

FIGURE 2-9 General View of the Bearing Installation Procedure

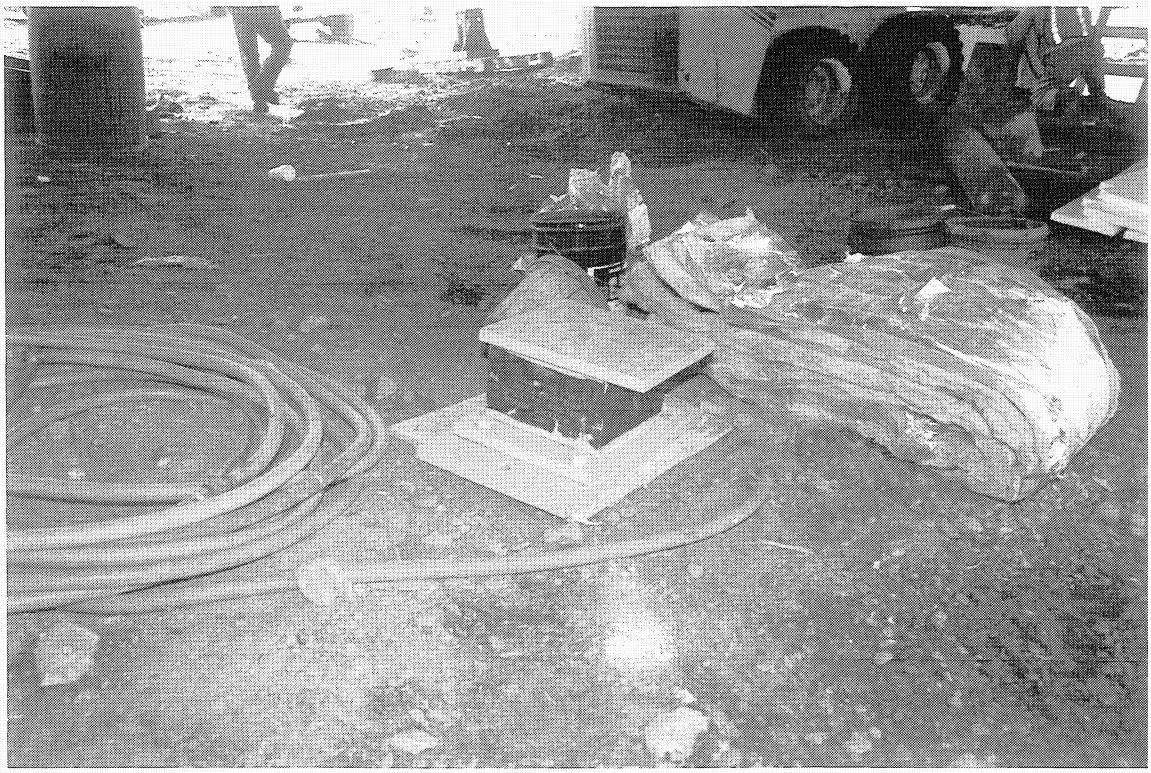

(a) Lead Rubber Bearing Ready to be Installed

(b) Bearing Installation Procedure at the Abutment

FIGURE 2-10 Bearing Installation Procedure

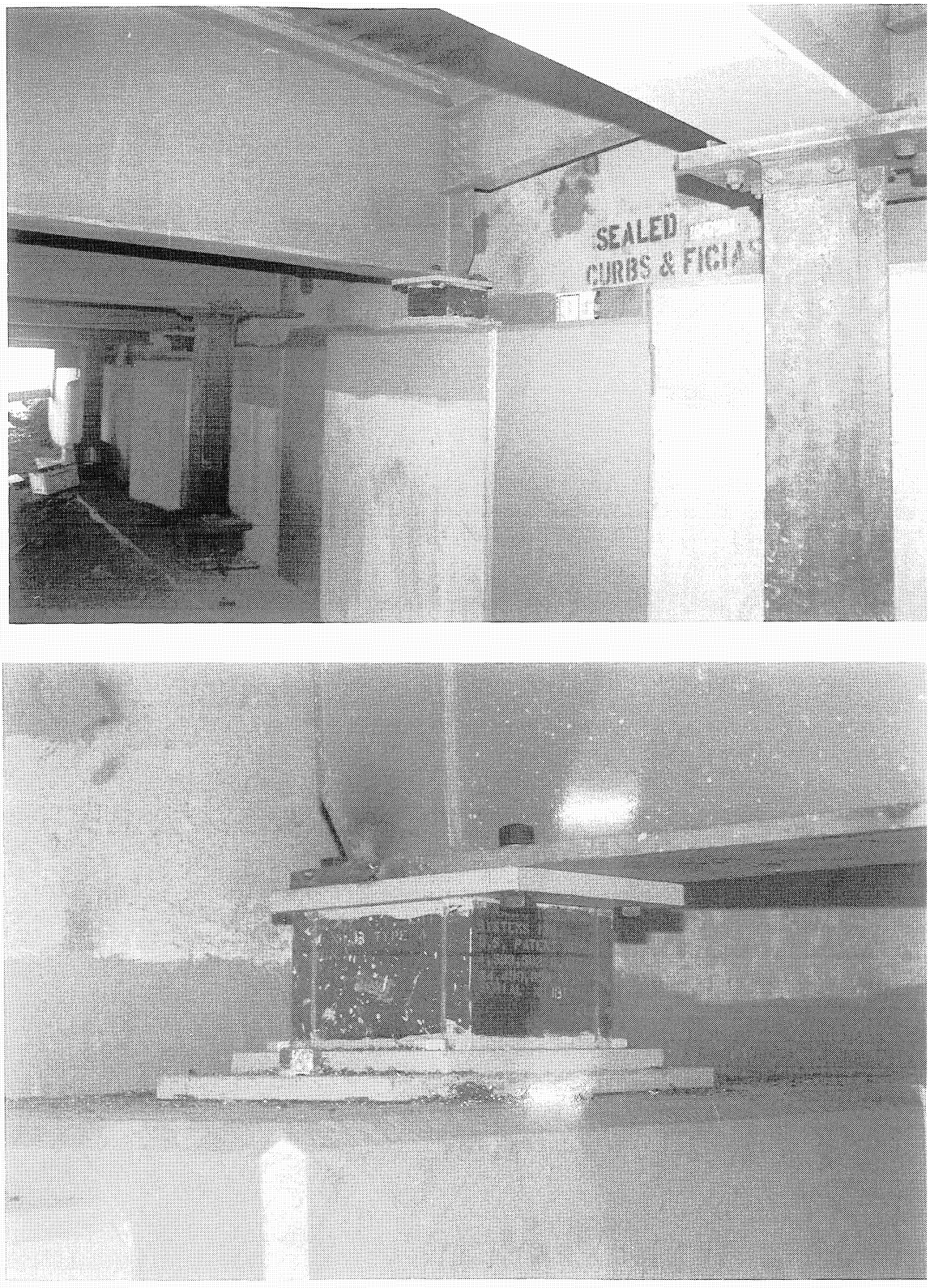

FIGURE 2-11 Laminated Lead Core Bearings

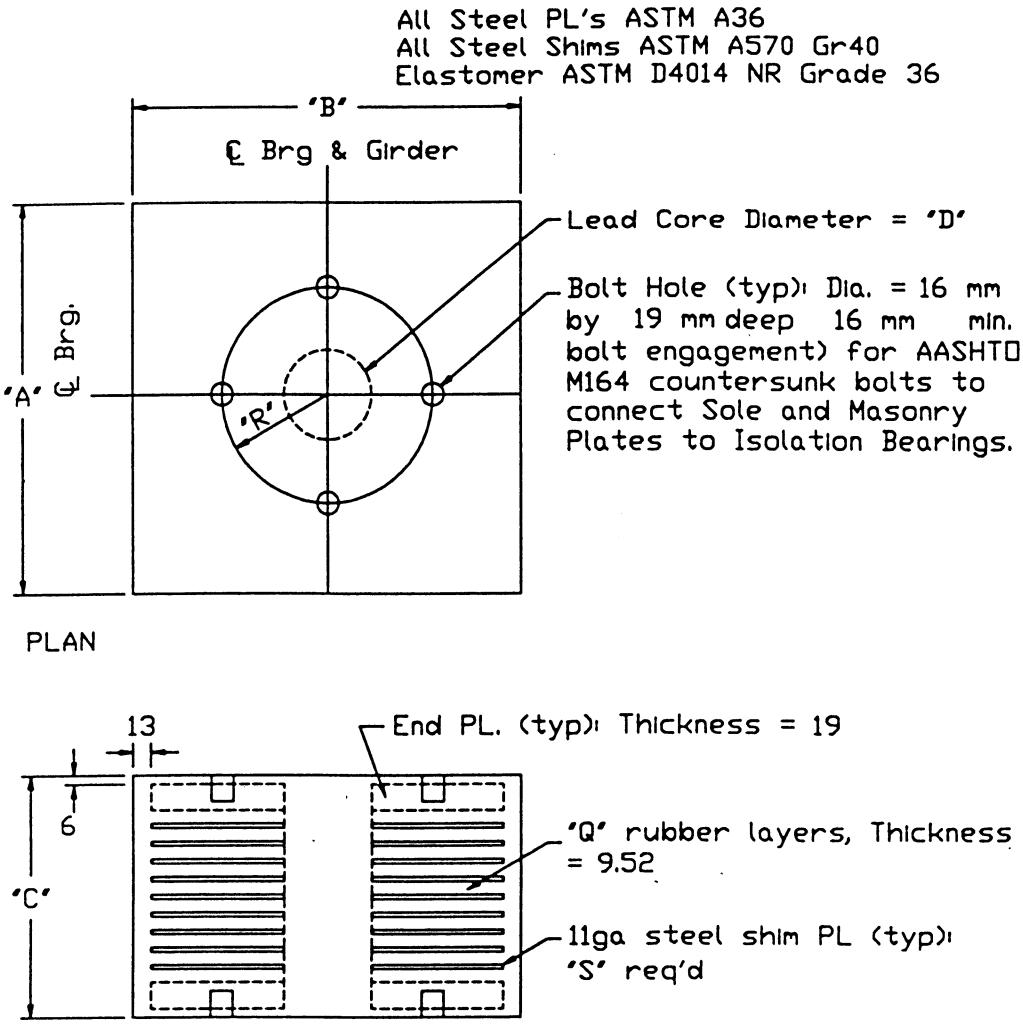

Dimension	E.L.C.	E.
A	280	330
B	280	330
C	175	225
D	64	0
Q	10	14
R	76	114
S	9	13

NOTEı E.L.C. = Elastomeric Lead Core Bearing Used at Abutments
E. = Elastomeric Bearing Used at Piers

FIGURE 2-12 Bearings for Southbound Bridge

describes the geometric characteristics of both types of bearings used in the Southbound bridge. An exhaustive series of laboratory tests on identical bearings from the same manufacturing lots as the bearings installed in the Southbound and Northbound bridges was conducted by Kim et al. (1996). Figure 2-13 shows the load-displacement plots for both the lead-rubber and the ordinary laminated rubber bearings. Table 2-1 summarizes the stiffness and strength parameters of the bearings obtained from the laboratory tests (Mander et al., 1996).

Figure 2-14a shows one of the fixed bearings used to retrofit the north abutment of the Northbound bridge and figure 2-14b illustrates the bearing used in the south abutment. Figure 2-15 describes the characteristics of the bearings used to retrofit the Northbound bridge. In this bridge four different kinds of laminated neoprene bearings were used. All of the bearings in a line of support on a given pier or abutment are similar, but they vary from those installed in another pier or abutment. The north abutment and north pier bearings are stiffer than the south pier and south abutment bearings. Figure 2-16 presents the load-displacement plots obtained from companion laboratory tests by Kim et al. (1996) for these bearings. Essentially linear elastic behavior may be observed, with a minor amount of hysteretic response that provides some effective damping. Table 2-2 presents the stiffness and strength properties reported by Kim et al. (1996). These values are used later in this study for performing dynamic analyses.

2.4 Test Setup

Due to the clear distance between the two bridges (18.4 m), it was decided to construct a tension-based quick release loading scheme using high-strength 32 mm dia high alloy high strength (Dywidag™) prestressing threadbars (ultimate tensile strength = 1100 *MPa*). Figures 2-17, 2-18 and 2-19 illustrate the technique used for this project. The tension bars straddle the near column of the anchor pier and pass through holes cored into both curbs of the tested bridge, being anchored on the far side of the test structure. Figure 2-20a shows the anchor detail, and figure 2-20b shows the jack loading system. One of these setups was installed in each pier bent of the comparison bridge structure which was used as a reaction frame. Releasing the load in both piers or in one pier at a time was intended to excite symmetric and asymmetric modes of vibration.

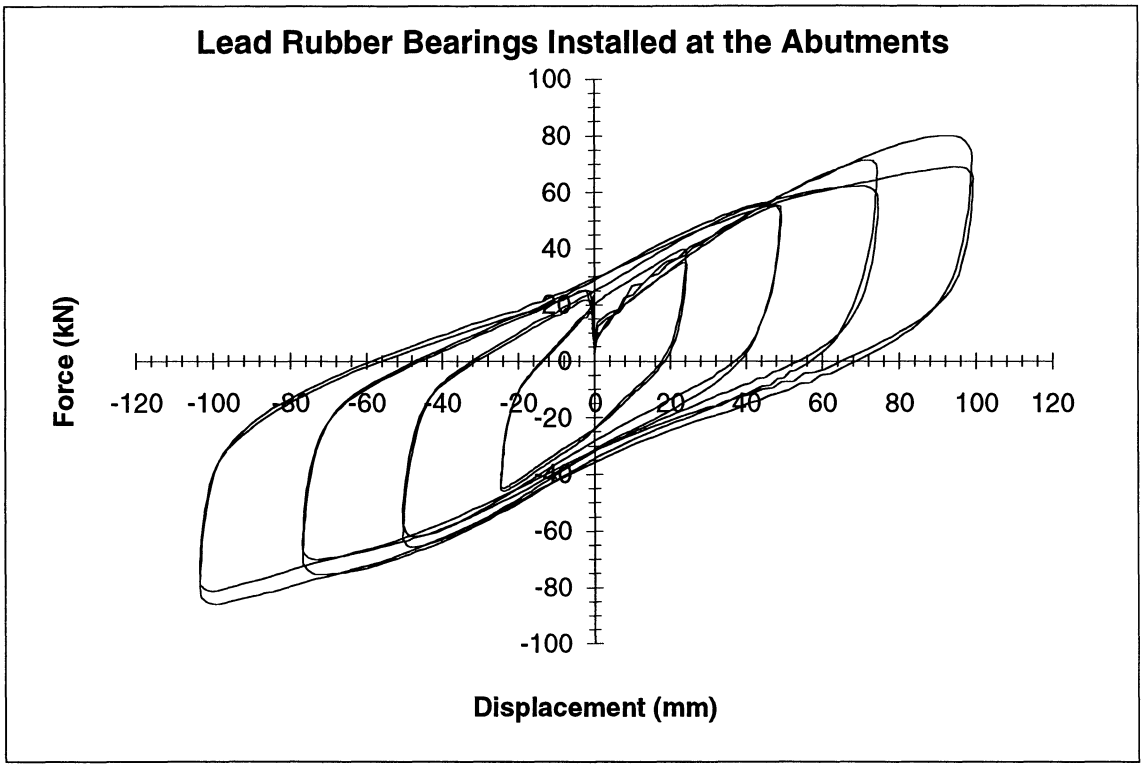

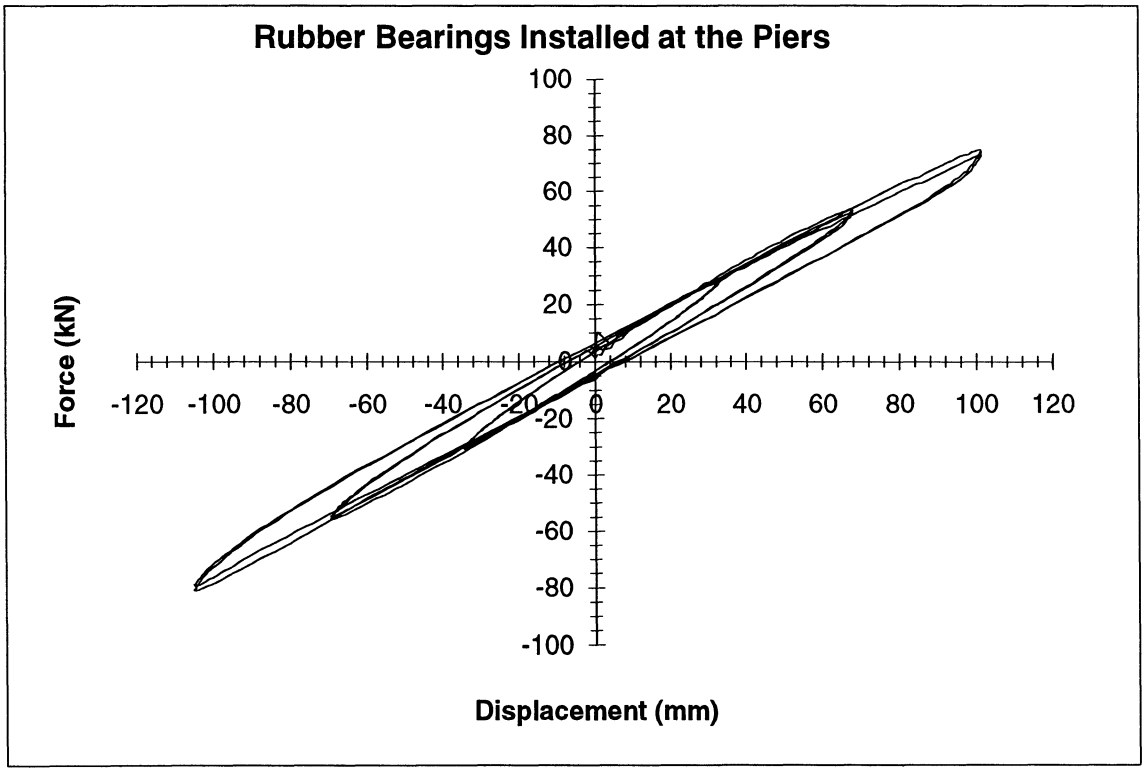

FIGURE 2-13 Isolators Load vs Displacement Curve - Southbound Bridge

TABLE 2-1 Southbound Bridge - Bearings Properties by (Kim et al. 1996)

Post-Retrofitted Bridge

Axial Stiffness

Location	Stiffness	Modulus
	(kN/m)	(MPa)
North Abutment	140101	221
North Pier	175125	248
South Pier	175125	248
South Abutment	140100	221

Rotational Stiffness

Location	Stiffness
	(kN-m/rad)
North Abutment	311
North Pier	497
South Pier	497
South Abutment	311

North Abutment

Shear Strain	Fu	K1	K2	G	Qd
(%)	(kN)	(kN/m)	(kN/m)	(MPa)	(kN)
25	43.15	10508	701	1.03	28.91
50	60.54	10508	683	1.03	31.14
75	73.13	10508	665	1.03	31.14
100	82.78	10508	630	0.97	31.14

North Pier

Shear Strain	Shear Force	Stiffness	Shear Mod.
(%)	(kN)	(kN/m)	(MPa)
25	29.76	874	1.24
50	53.91	783	1.10
75	76.73	743	1.03
100			

South Pier

Shear Strain	Shear Force	Stiffness	Shear Mod.
(%)	(kN)	(kN/m)	(MPa)
25	29.76	874	1.24
50	53.91	783	1.10
75	76.73	743	1.03
100			

South Abutment

Shear Strain	Fu	K1	K2	G	Qd
(%)	(kN)	(kN/m)	(kN/m)	(MPa)	(kN)
25	43.15	10508	701	1.03	28.91
50	60.54	10508	683	1.03	31.14
75	73.13	10508	665	1.03	31.14
100	82.78	10508	630	0.97	31.14

Notes:

Fu= Maximum shear force at the maximum shear strain

K1= Initial stiffness

K2= Post-yielding stiffness

G= Shear modulus

Qd= Force across a Coulomb slider yields

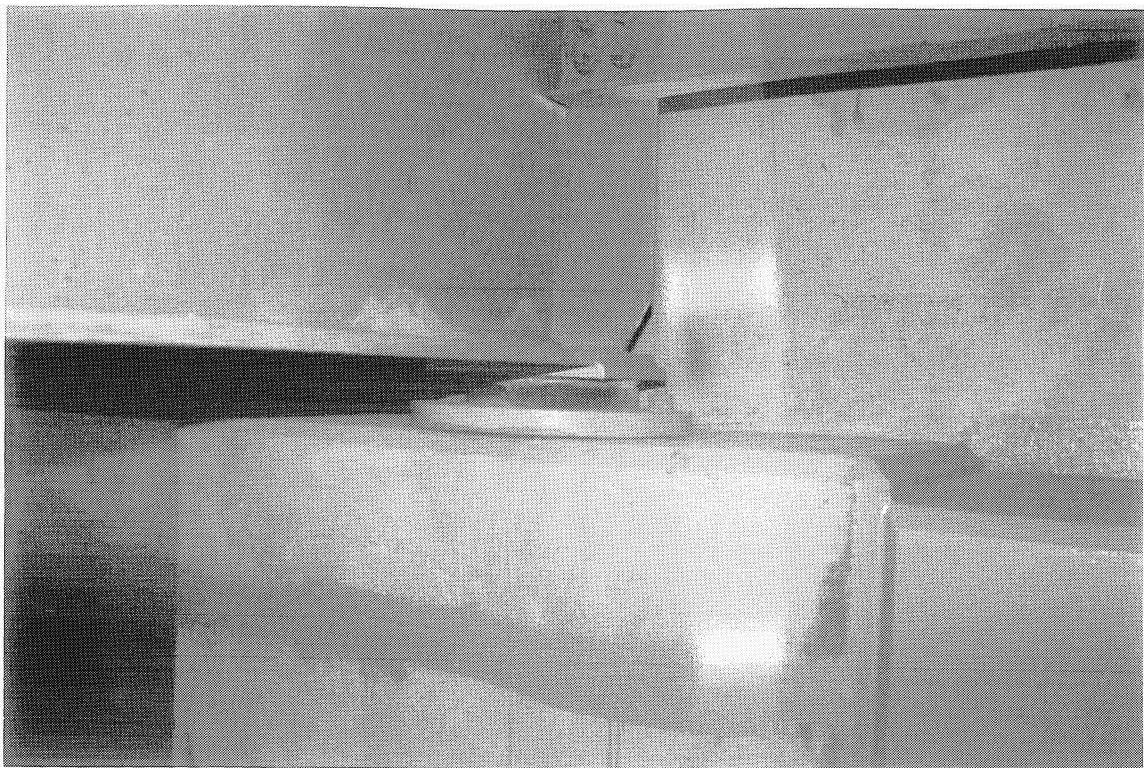

(a) Fixed Bearing at the North Abutment

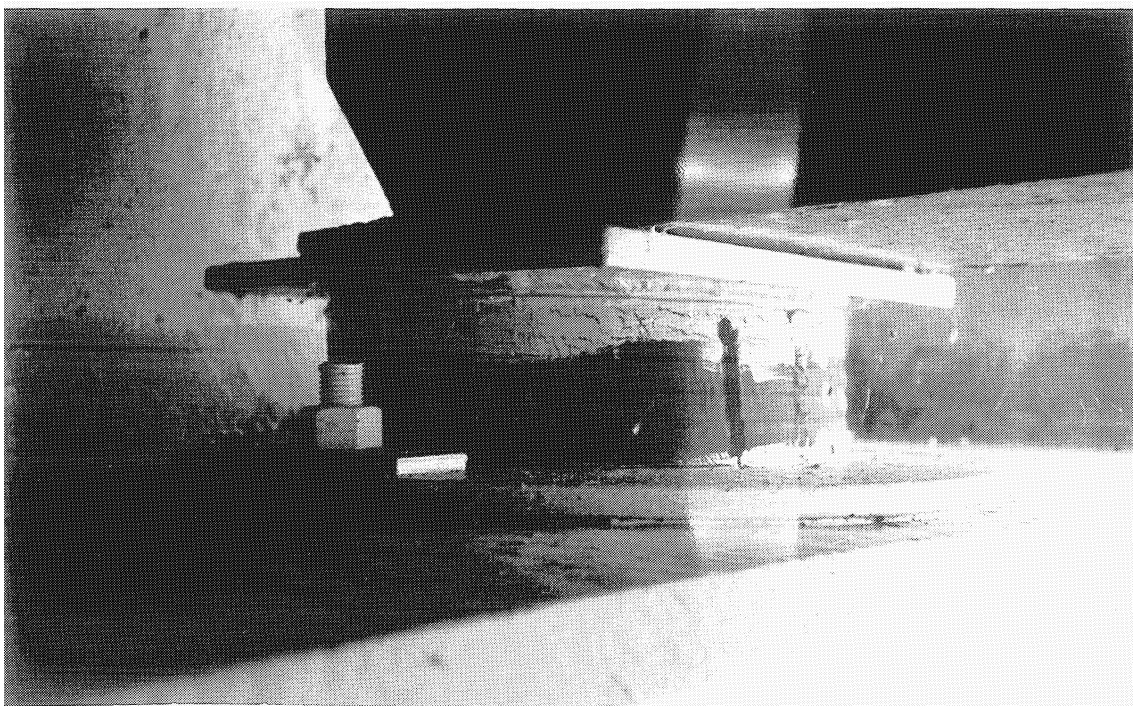

(b) Expansion Bearing at the South Abutment

FIGURE 2-14 Northbound Bridge Bearings

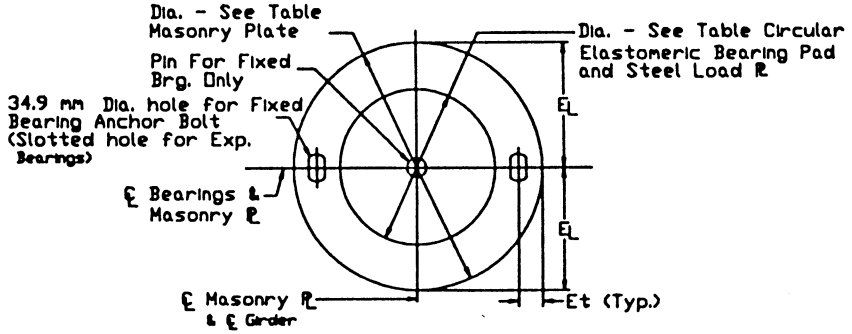

TYPICAL CIRCULAR BEARING AND CIRCULAR MASONRY PLATE (PLAN)

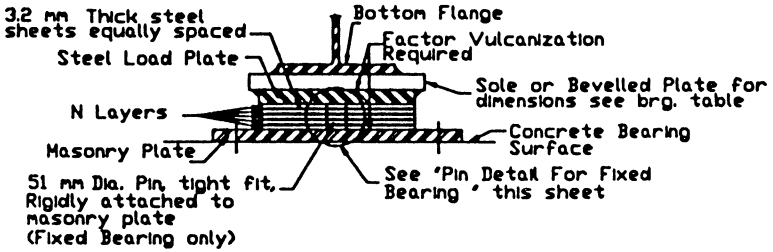

STEEL LAMINATED WITH LOAD PLATES

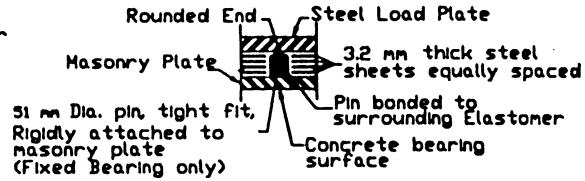

PIN DETAIL FOR FIXED BEARINGS

LOCATION		SHAPE FACTOR	LOAD PLATE		ELASTOMER LAYERS			MASONRY PLATE				SOLE PLATE			
			Dia.	Thick.	Dia.	Thick.	N. Layer	Dia.	Thick.	Et	EL	Ls	Ws	T1	T2
NORTH ABUT.	FIX.	8.0	305	19	305	9.5	3	508	41	51	254	330	330	22	19
PIER 1	EXP.	10.7	406	38	406	9.5	3	648	51	60	324	457	457	43	38
PIER 2	EXP.	9.14	406	38	406	11	5	648	32	60	324	457	457	43	38
SOUTH ABUT.	EXP.	7	356	16	356	13	6	559	16	51	279	381	381	20	16

FIGURE 2-15 Bearing Description for Northbound Bridge

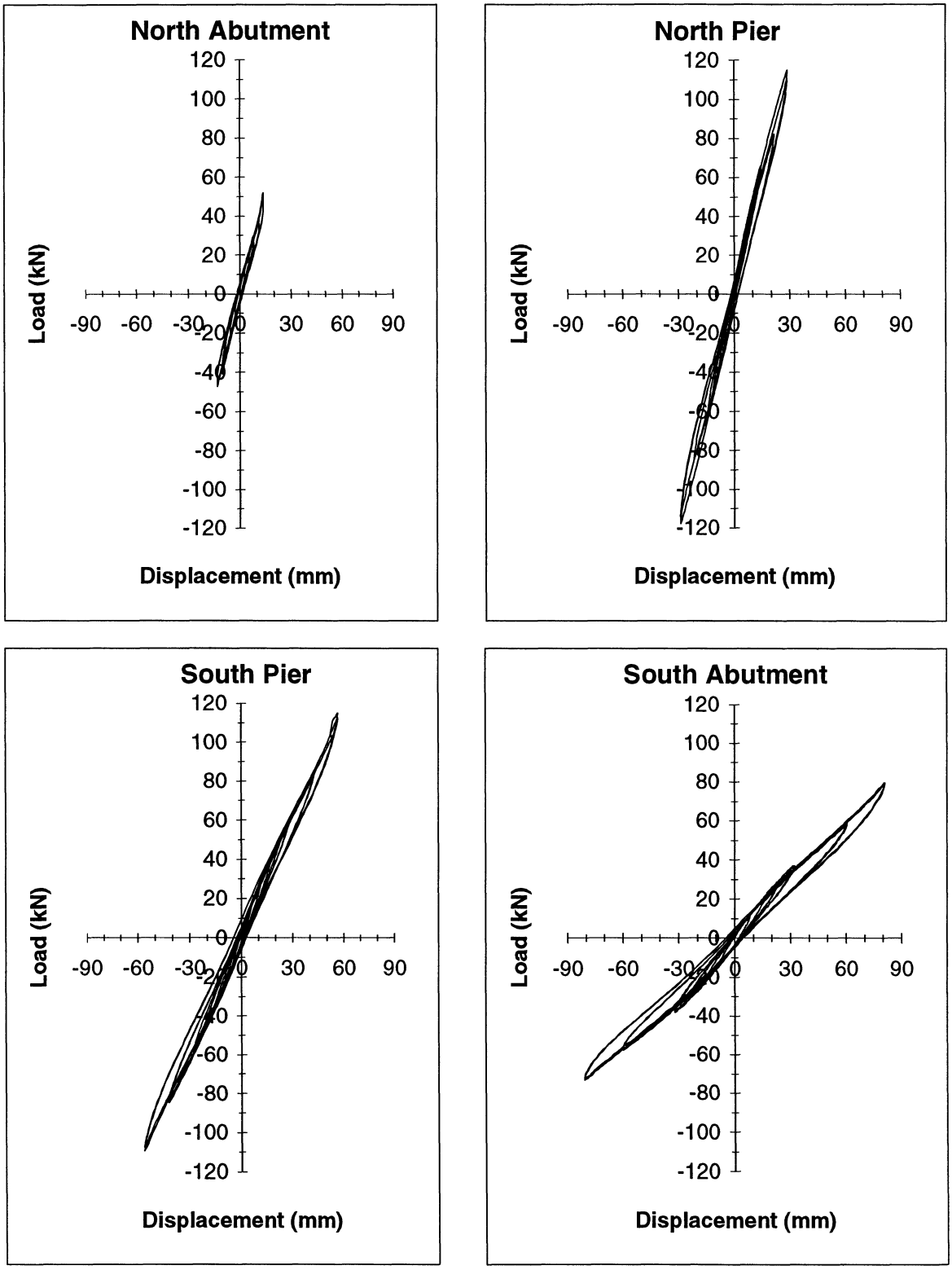

FIGURE 2-16 Load vs Displacement Post-Retrofitted Northbound Bearings

TABLE 2-2 Northbound Bridge - Bearings Properties by (Kim et al. 1996)

Post-Retrofitted Bridge

Axial Stiffness

Location	Stiffness	Modulus
	(kN/m)	(MPa)
North Abutment	1593654	621
North Pier	1681200	345
South Pier	656719	296
South Abutment	350250	276

Rotational Stiffness

Location	Stiffness
	(kN-m/rad)
North Abutment	5796
North Pier	17558
South Pier	8327
South Abutment	2576

North Abutment

Shear Strain	Shear Force	Stiffness	Shear Mod.
(%)	(kN)	(kN/m)	(MPa)
10	12.01	4273	1.65
20	21.44	3851	1.52
30	30.91	3669	1.45
40	40.26	3695	1.45
50	49.73	3679	1.45
75			
100			

North Pier

Shear Strain	Shear Force	Stiffness	Shear Mod.
(%)	(kN)	(kN/m)	(MPa)
10	17.39	6068	1.31
20	30.65	5331	1.17
30	43.06	4970	1.10
40	54.18	4658	1.03
50	64.45	4443	0.97
75	83.63	3837	0.83
100	116.45	4017	0.90

South Pier

Shear Strain	Shear Force	Stiffness	Shear Mod.
(%)	(kN)	(kN/m)	(MPa)
10	15.61	2748	1.17
20	28.11	2473	1.03
30	39.54	2305	0.97
40	49.69	2187	0.97
50	59.61	2107	0.90
75	84.52	1982	0.83
100	112.27	1981	0.83

South Abutment

Shear Strain	Shear Force	Stiffness	Shear Mod.
(%)	(kN)	(kN/m)	(MPa)
10	12.41	1529	1.17
20	21.71	1352	1.03
30	30.25	1252	0.97
40	37.72	1170	0.90
50	44.97	1117	0.83
75	58.40	967	0.76
100	76.51	944	0.76

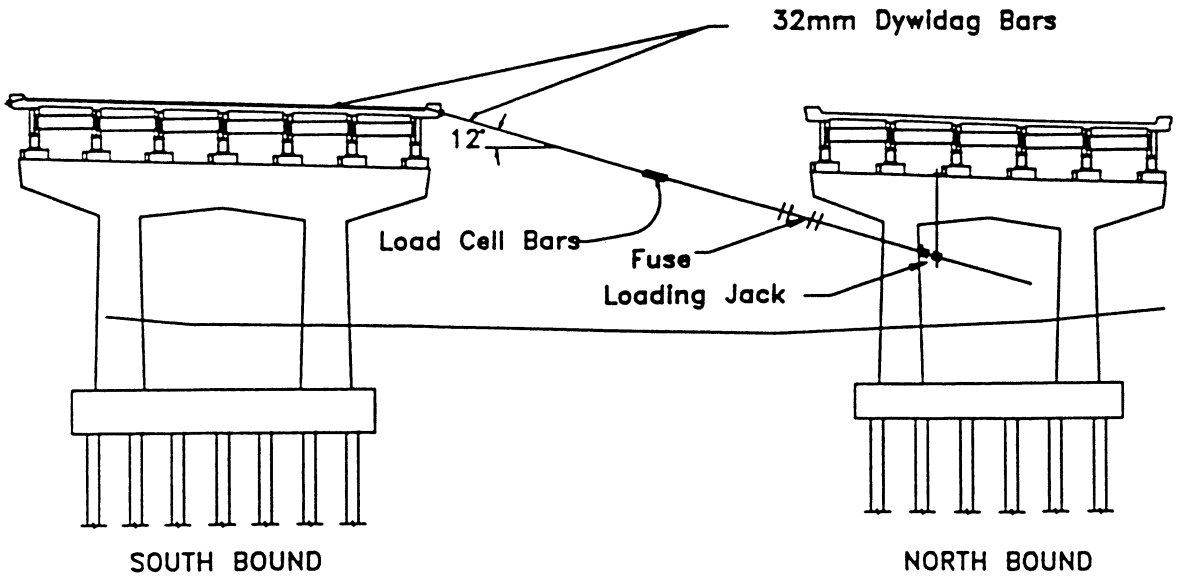

(a) Cross Section

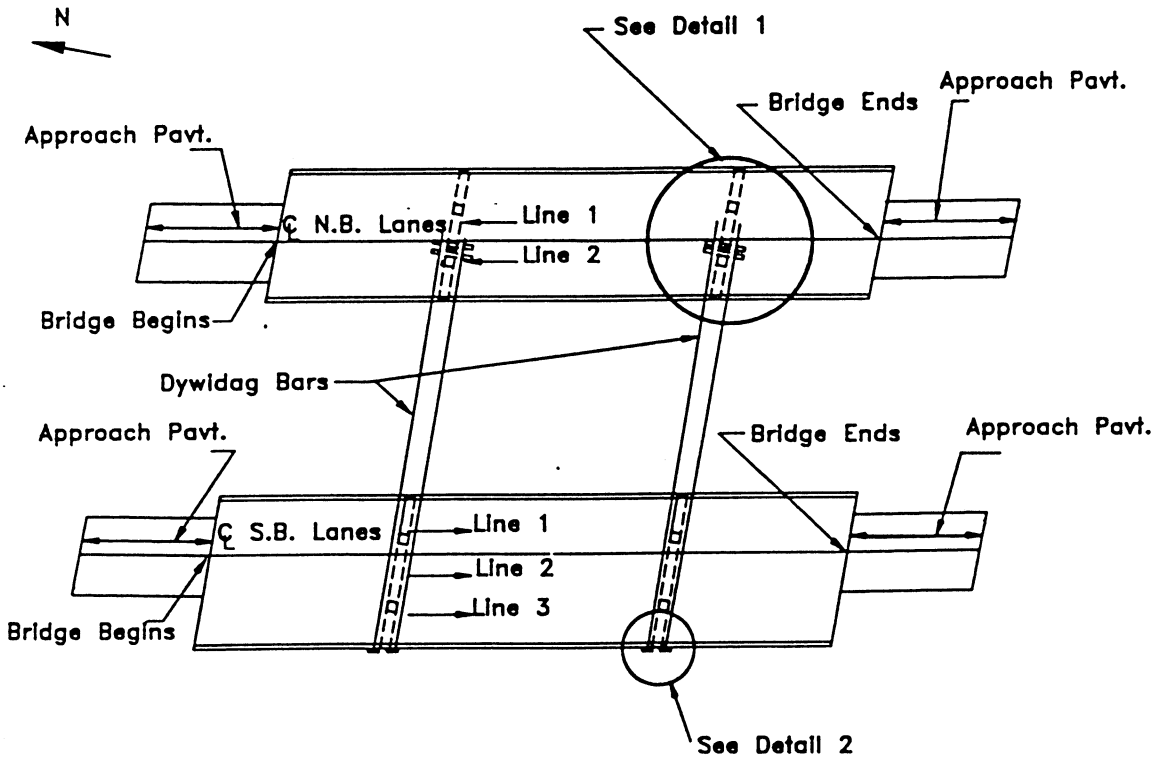

(b) Plan View

(All Dimmensions in mm)

FIGURE 2-17 Longitudinal and Plan View of the Tension Loading System

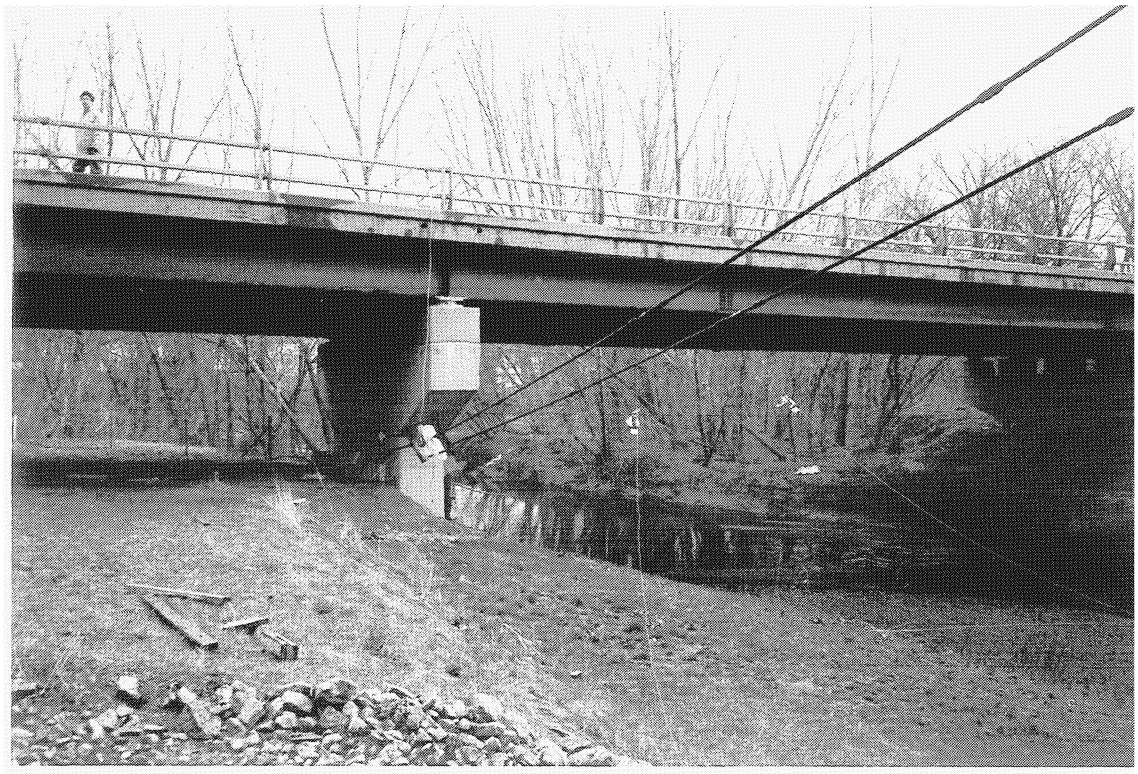

View of the Anchor Pier

Deck View of the Loading System

FIGURE 2-18 Tension Loading System

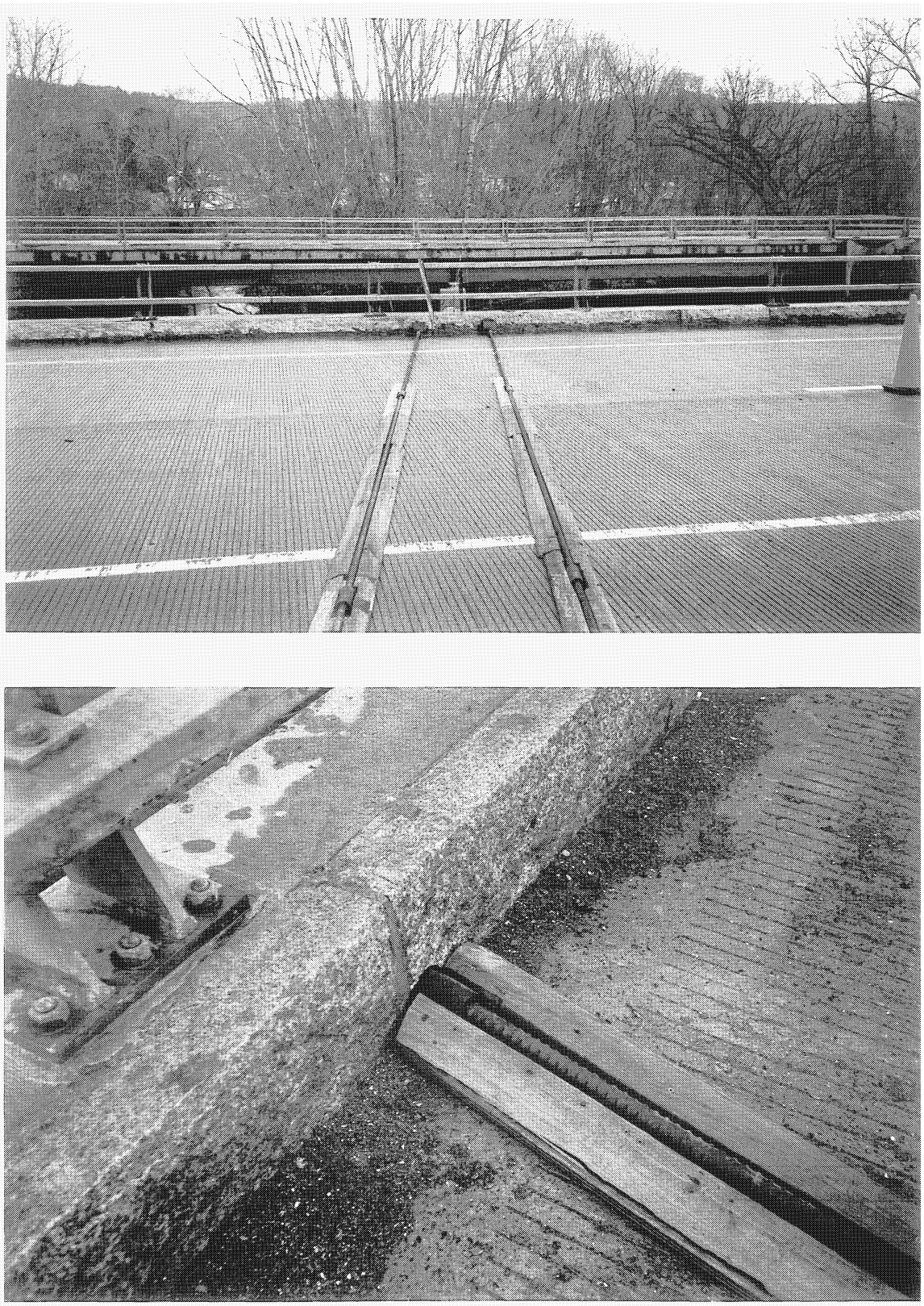

FIGURE 2-19 Overview of the Tension Loading System at the Deck Level

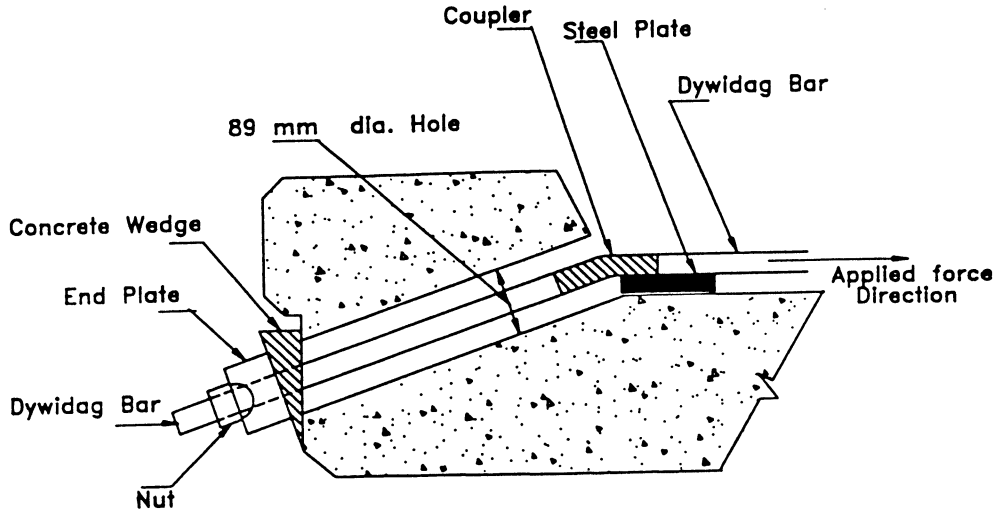

(a) Detail #1

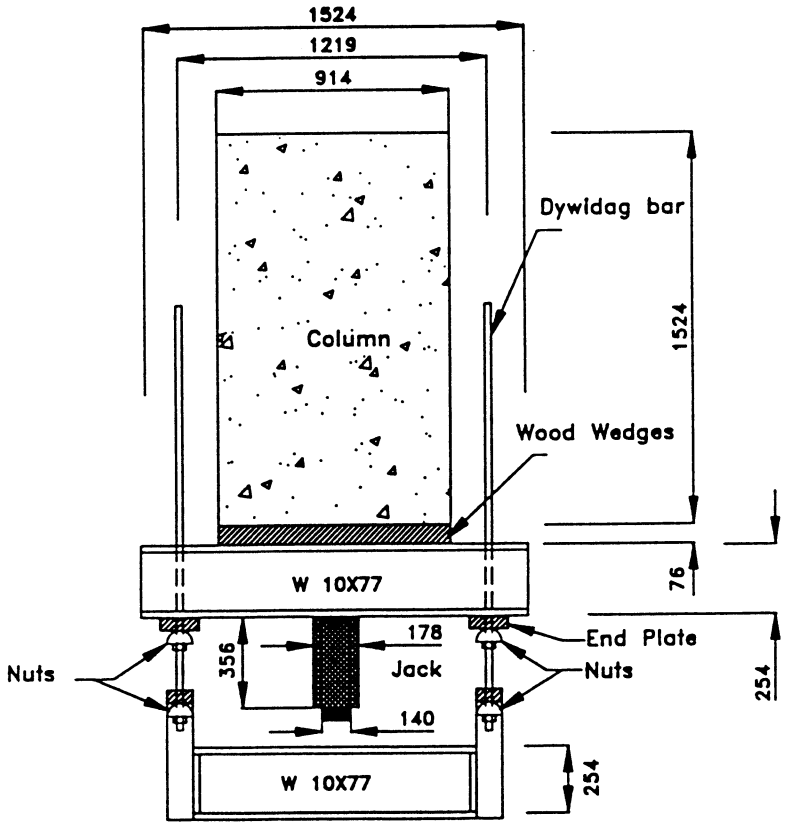

Detail #2

(All Dimmensions in mm)

FIGURE 2-20 Tension Loading System Details

Between the two parallel beams, a hydraulic jack with capacity of 890 kN as illustrated in figure 2-21 was used to apply the tensile load between the two bridges.

Roughly midway between the two bridges the tension bars were strain gauged to act as a load cell unit. Four strain gauges were installed to enable full bridge wiring.

Two different quick-release systems were used during the tests of the bridges. The first was a quick release system that suddenly dropped the hydraulic pressure and damped the hydraulic fluid into a reservoir. This same system has been used previously in quick release compressive strut systems developed by Buckle and Douglas (1986). This system consists of a jack with two ports, one to pump oil into the cylinder and other to quickly release the pressure, returning the oil to the reservoir in the pump. A quick-release valve was connected in series with the return line and remained closed during the loading process. The quick release valves of each jack were connected to the same trigger system in a such a way that both were opened simultaneously, producing the simultaneous release of the structure over both piers.

The release system described above was initially used on both bridges prior to bearing replacement. Unfortunately, it did not work particularly well. Due to the tension bar elongation and very high stiffness of the bridges when seated on their steel bearings, the pressure release was not quick enough to permit free vibration response in the first quarter cycle of loading. Due to the distance between both bridges (18.4 m clear) and the deformations of the loading system during the loading process, the displacement of the piston was between 100 mm and 150 mm at the moment of the release. The total time to evacuate the cylinder is governed by several parameters, but one of the most important is the size of the orifice. The diameter of the orifice is related to two other parameters – the structural integrity of the jack under the maximal pressure (69 MPa), and the force necessary to open a valve instantaneously. In this jack the size of the return port was 12.7 mm. Due to size of this orifice and the great amount of oil inside the cylinder at the moment of the release, the jacks consequently acted as a viscous damper during the first half cycle of the free vibration response. This effect substantially reduced the initial peak accelerations.

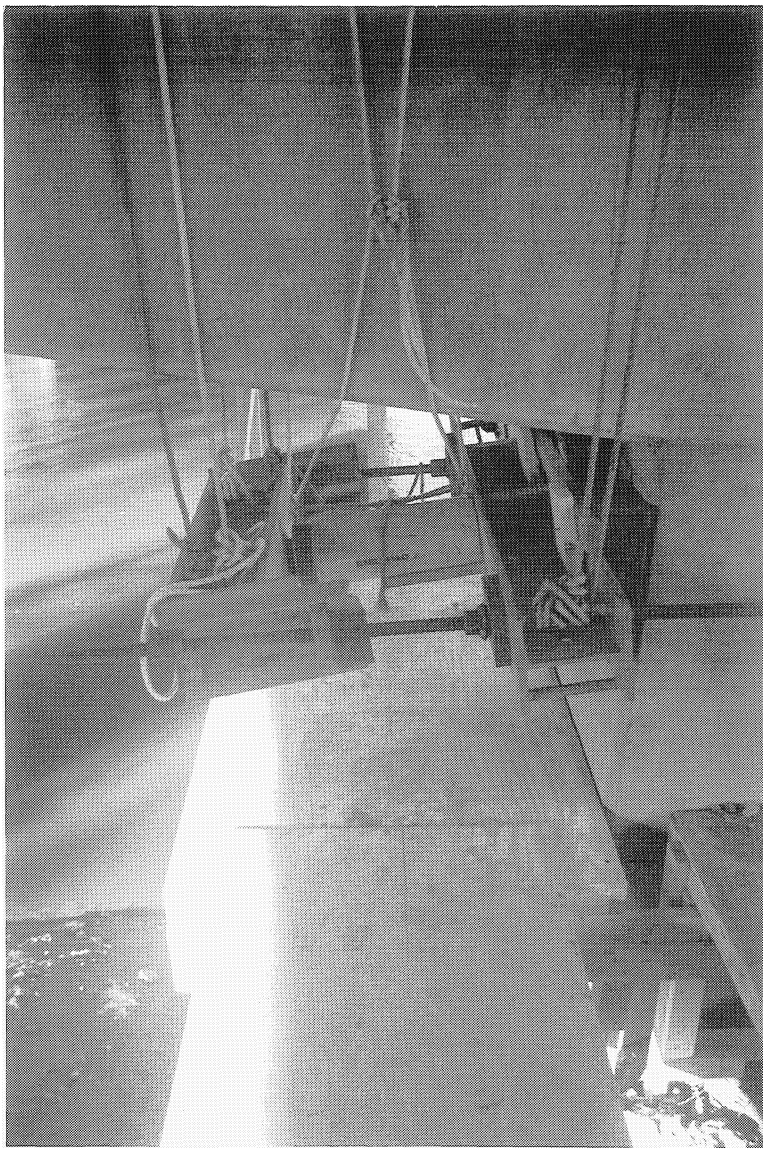

FIGURE 2-21 General View of the Loading Arrangement

In order to solve this problem later tests on the bridges seated on steel bearings used a snap-back "fuse bar" system in series with one of the loading bars. This fuse bar was fabricated by machining down the cross section of a replaceable section of the threadbars used in the tension system. The final cross-sectional area of this fuse bar was fabricated based on the expected ultimate load. Two bars were made from the same threadbar; the first one was tested in the laboratory to obtain the maximum load and the breaking load; the second was pre-strained beyond the strain of maximum stress and then deployed and loaded to tensile fracture in the field. This pre-strain of the fuse bar gave an accurate indication of the expected breaking load. The snap-back fuse bar release system worked well in the field. The major limitation, however, was that only one pier could be released due to the extreme difficulty of synchronizing the failure of two fuse bars. This was later remedied for some of the post-retrofit bridge tests.

For the post-retrofitted bridge tests, efforts were made to reduce the time delay observed in the release system in the pre-retrofit test series. As explained above, the initial release system did not work quickly enough in the pre-retrofitted bridges and the jacks acted as dampers on the initial quarter cycle. The results of several low level pre-tests showed that the same problem observed in the pre-retrofitted bridges continued. In order to solve the problem, a mechanical fuse was designed, constructed and deployed. Illustrated in figure 2-22 the mechanical system solved most of problems observed in the previous oil release alternative. As the quick-release system is electrically triggered, it is possible to enable the simultaneous release of more than one fuse.

Figure 2-23a compares the time history of the unloading portion of the pre-retrofitted test on the Northbound bridge using the oil-jack release system and the unloading time history of the post-retrofitted test using the mechanical fuse with a similar load. It is clearly evident that there is a marked difference in the release time between the two systems. Figure 2-23b compares for the same kind of one pier test the fuse bar release system used in the pre-retrofitted Southbound bridge and two tests performed over the post-retrofitted bridge, one using the mechanical fuse and the other using the fuse bar system. From the graph it can be inferred that both kinds of release systems produce similar near-instantaneous release times.

FIGURE 2-22 Mechanical Fuse

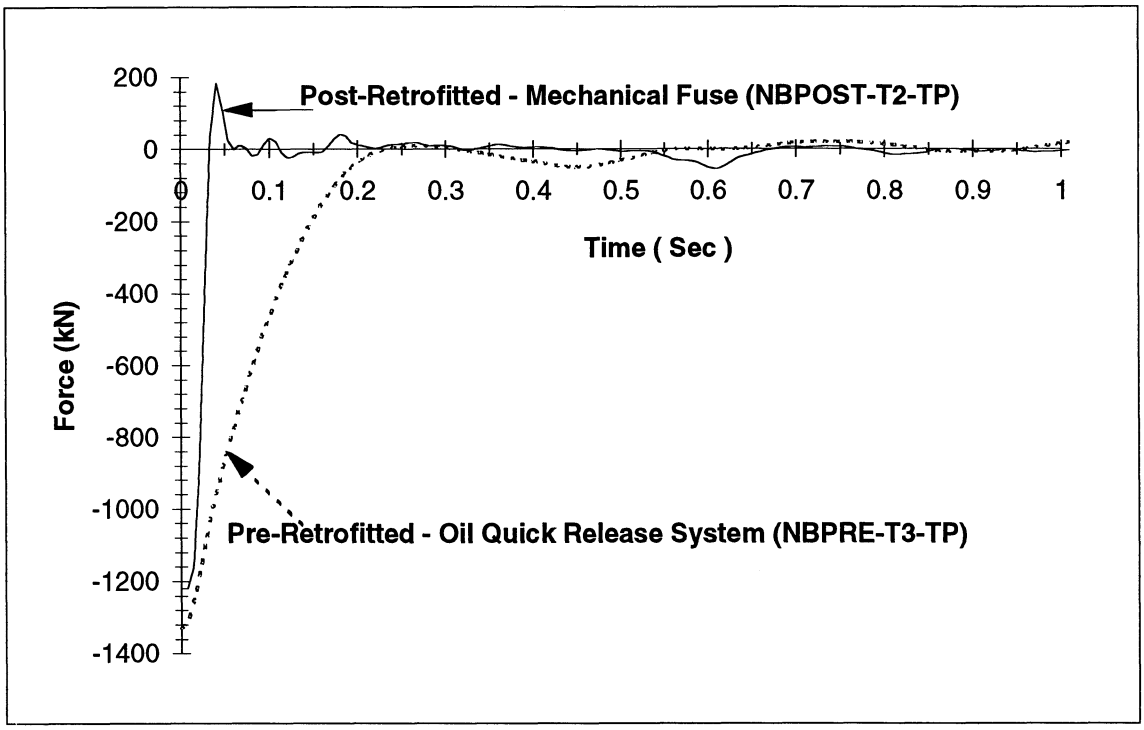

Northbound Bridge

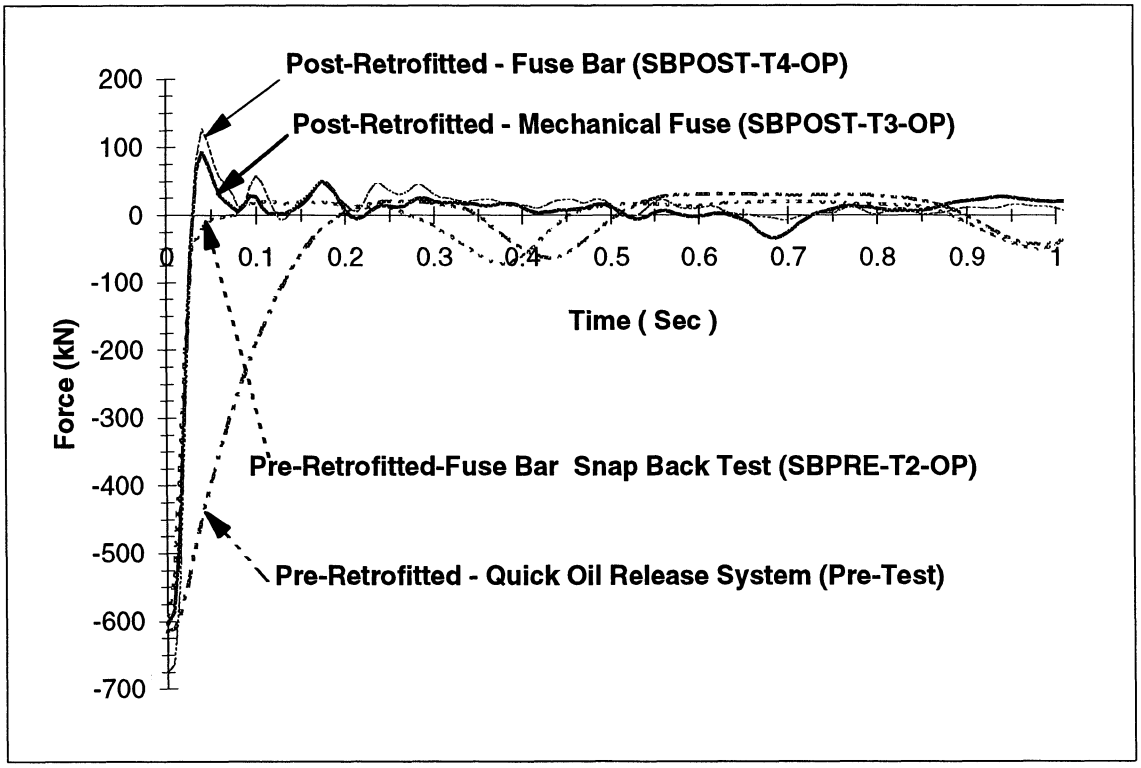

Southbound Bridge

FIGURE 2-23 Load Time History for Different Release Systems

During the pre-test performed on the post-retrofitted bridge using the jack-oil system it was observed that the bridge did not return quite to its original position after the vibration ceased. In all cases the off-set displacements were in the direction of the applied loads. This situation was a concern since the gap between the deck and the wingwall of the abutments is only 51 mm. In order to re-center the bridge after each test and avoid an accumulated displacement, a special set-up was constructed at the top of the piers in order to re-center the bridge after each test. Fortunately due to the higher accelerations observed with the use of the new release system this off-set was substantially reduced and the re-centering system was not used after all.

As discussed for the pre-retrofitted bridge testing, the 32 m long high-strength threadbars that formed part of the tension system used for this project suffered an elongation of some 75 mm. This added to the natural "bedding-in" deformations of the other components of the setup (wood wedges, concrete wedges, loading beams, etc.) and the expected displacement of approximately 51 mm of the bridge under the new bearings exceeded the 153 mm stroke capability of the jacks used in the first series of tests. Therefore, two new jacks with a capacity of 890 kN (200 kips) and 1335 kN (300 kips), with stroke capabilities of 254 mm (10 in.) and 330 mm (13 in.) were installed in the north pier and south pier, respectively. To reduce the elongation of the high-strength threadbars, it was decided to post-tension the bars located over the deck during the test. In order to accomplish this, a new anchor system which is shown in figure 2-24 was installed in the interior face of the curb which is on the side of the pulling system. Before any test was conducted the bridge deck was prestressed with a load close to the maximum jacking load level. In this manner, the effective length of thread bar that elongated was reduced by an amount equal to the width of the bridge deck.

2.5 INSTRUMENTATION

During the month of July 1993 a series of pre-tests was performed on the pre-retrofitted Northbound bridge. With the experience gained from these tests, the location of the instruments

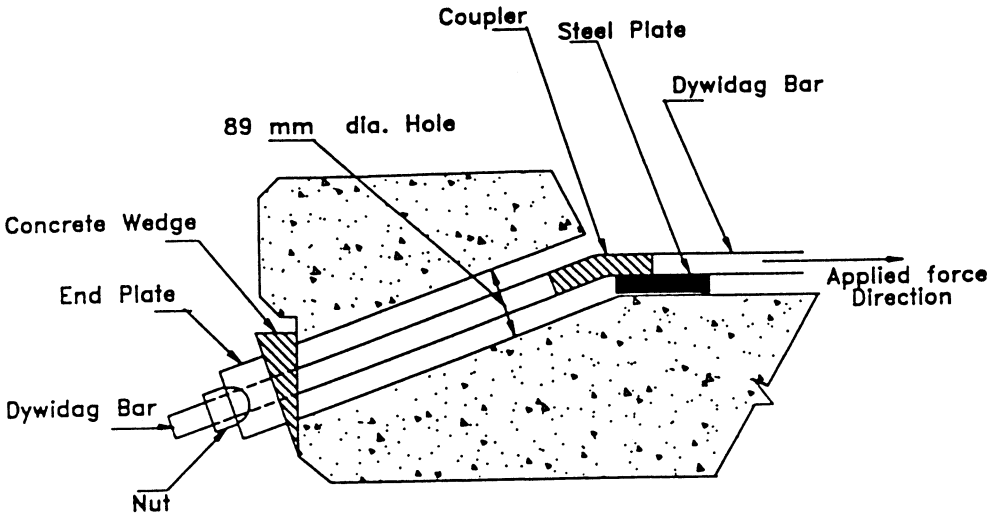

Exterior Curb

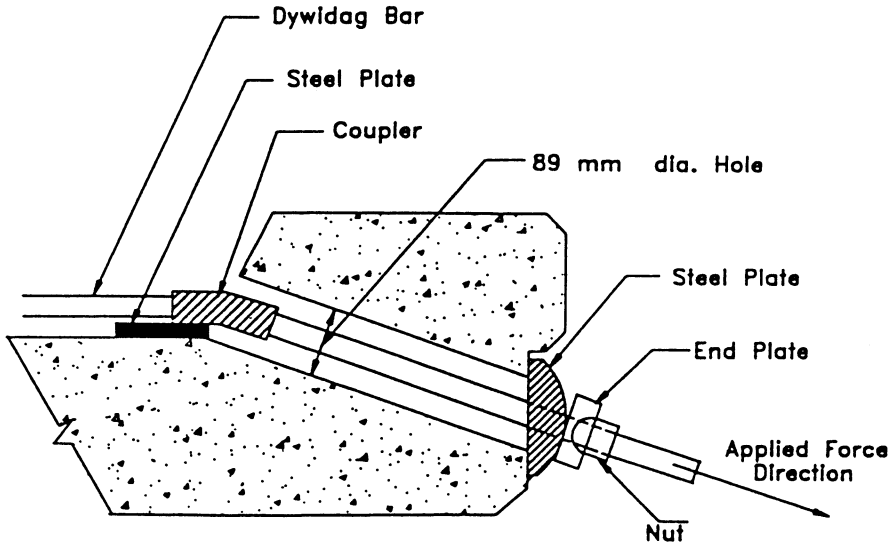

Interior Curb

FIGURE 2-24 Curb Details - Post-Retrofitted Bridges

as optimized in such a way that it was possible to obtain the most reliable representation of the bridge behavior. After this configuration was determined most of the instruments were installed in the same position during the entire project except for the addition of several accelerometers in the transverse direction on the post-retrofitted bridges. Following the configuration adopted for the Northbound structure and using the results of a series of pre-tests, it was decided that with minor changes the location of instruments in the Southbound bridge would follow the same pattern as that adopted for the Northbound bridge.

Three different kinds of measurements were taken during the tests; acceleration, displacement and load, the latter from the strain-gauged load cell bars. Each were recorded using a PC-based data acquisition system. This consisted of two 486 DX2 PC computers, each with four A/D boards. All boards were eight channels, the level of resolution being either 16 or 12 bit. Accelerometers and load cell bars were connected to the 16 bit board while the displacements transducers (linear potentiometers) to the 12 bit boards. Prior to the test and using analytical predictions, it was established that a sampling rate of 140 Hz was sufficient to avoid aliasing problems. The computer data analysis computer software LABTECH NOTEBOOK (1993) was used to manage the experiments, while post-test analysis was carried out using the software DADISP (1993).

Although 32 channels were available for each computer, only 30 channels could be used due to local bus limitations. One channel was used in common to synchronize the data; thus 58 channels were available for data acquisition purposes.

Due to the low signal output of certain instruments, signal conditioners were used to filter high frequency noise and amplify voltages. These were installed in series with these instruments. The conditioners used were Micro-Measurements™ type 2310 which have capability to select the desired gain and level of filtering. Based on analytical predictions and the ambient vibration tests, a 25 Hz low pass filter was selected for these tests. Shielded cables were used for all of the instruments in order to reduce the noise associated with the use of long cables. In order to detect any possible delay or differences between the computers, the accelerometer

located in the center of the middle span (A4) reading in the transverse direction was connected to both computers. Comparing the time history of this instrument, small delays observed could be corrected for.

Figure 2-25 shows the accelerometers (represented by the letter "A") installed at the top of the girders 25 mm under the bottom of the deck of the Southbound bridge, and figures 2-26 and 2-27 show the location of the accelerometers in the piers and abutments respectively. Table 2-3 summarizes the location and direction of the instruments for the tests. The accelerometers used for this project were ENDEVCO type 2262-25 with a response of $\pm$25g at 0-100 Hz. All of them were mounted on a magnetic support and attached to the metal portions of the bridge.

Figures 2-28 and 2-29 show the potentiometers (represented by the letter "P") at the piers and abutments of the Southbound bridge. A given potentiometer was selected to provide enough resolution for its expected displacements. Table 2-4 summarizes the location and type of the potentiometers used.

The data acquisition, signal conditioners and instrument location used for the post-retrofitted bridges were the same as those used for the pre-retrofitted bridges. The accelerometer located in the center of the bridge in the transverse direction (A4) was common to the two computers to enable synchronization of the data sets. The sampling rate of the data acquisition was increased to 150 Hz and the potentiometers used for the pre-retrofitted bridges were replaced by the same kind of potentiometers but with the ability to read the larger expected displacement of $\pm$50 mm. Tables 2-5 and 2-6 show the active instruments for each test performed in the Northbound and Southbound bridges, respectively.

2.6 Experimental Procedures

Two different kinds of tests were performed during this project, ambient vibration tests and quick-release tests. The ambient vibration tests were performed prior to the quick-release tests. For the ambient vibration tests, the accelerometers in the superstructure were installed in the same location as for the quick-release tests but reading in the vertical direction. No

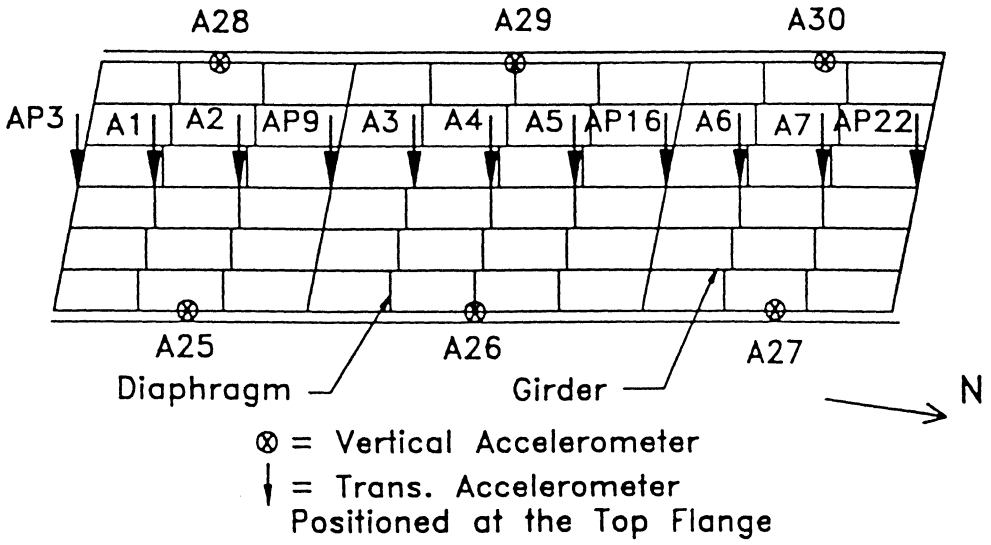

(a)

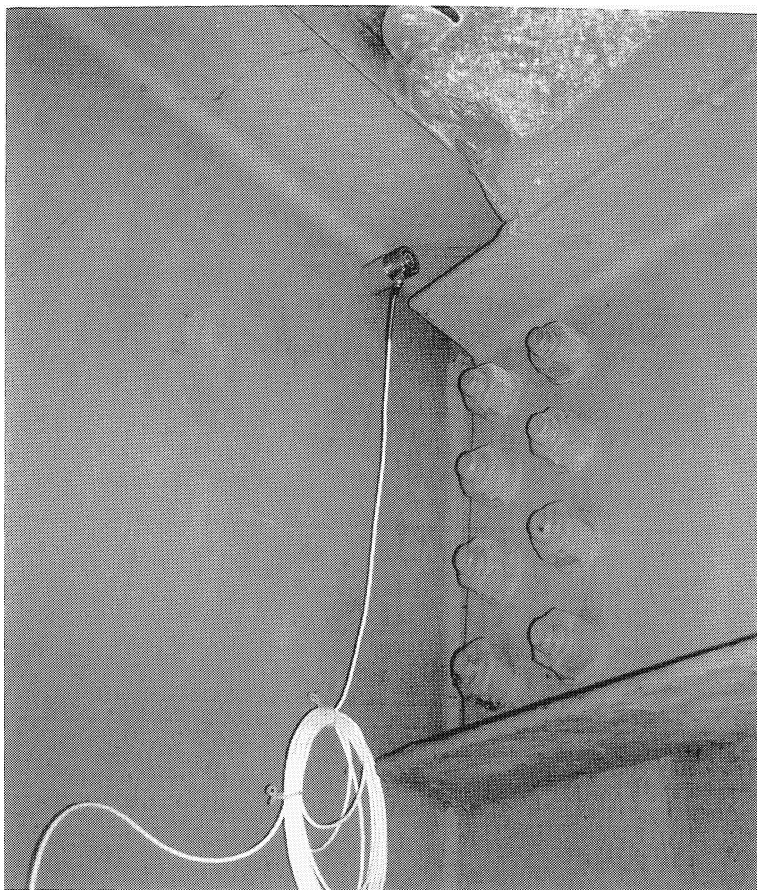

(b)

FIGURE 2-25 Accelerometer Locations at the Deck

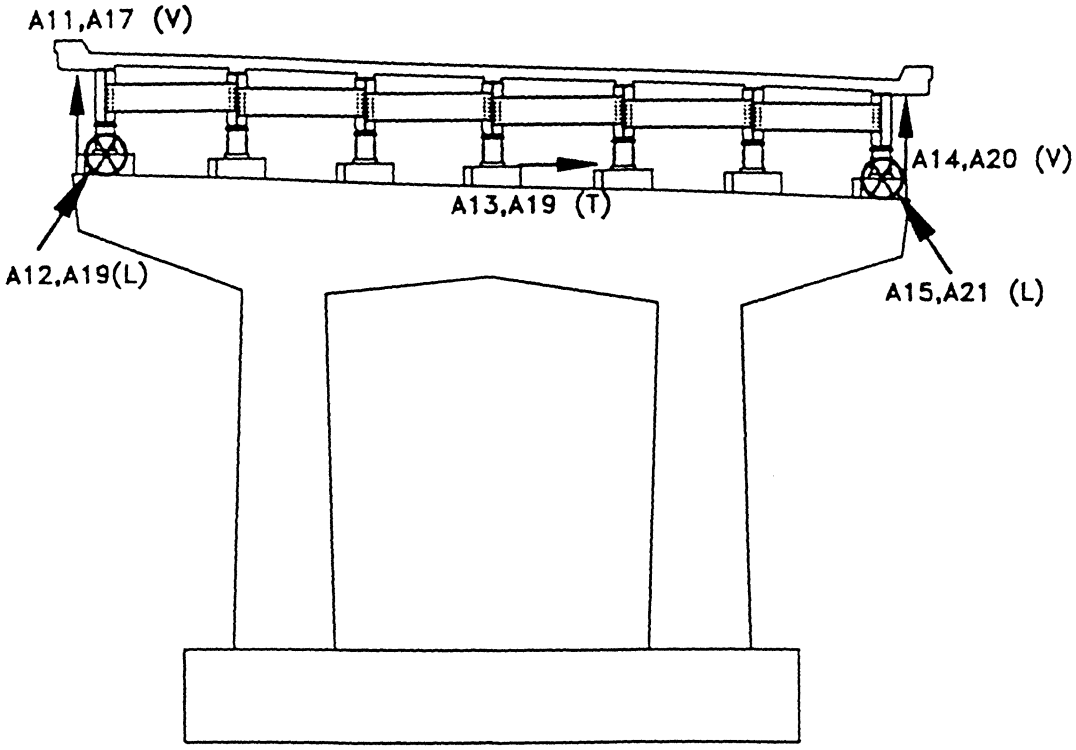

⊗ = Longitudinal Accelerometers
A11,12,13,14,15 = North Pier Accelerometers
A17,18,19,20,21 = South Pier – Accelerometers
L = Longitudrinal Direction of the Bridge
T = Transverse Direction of the Bridge
V = Vertical Direction of the Bridge

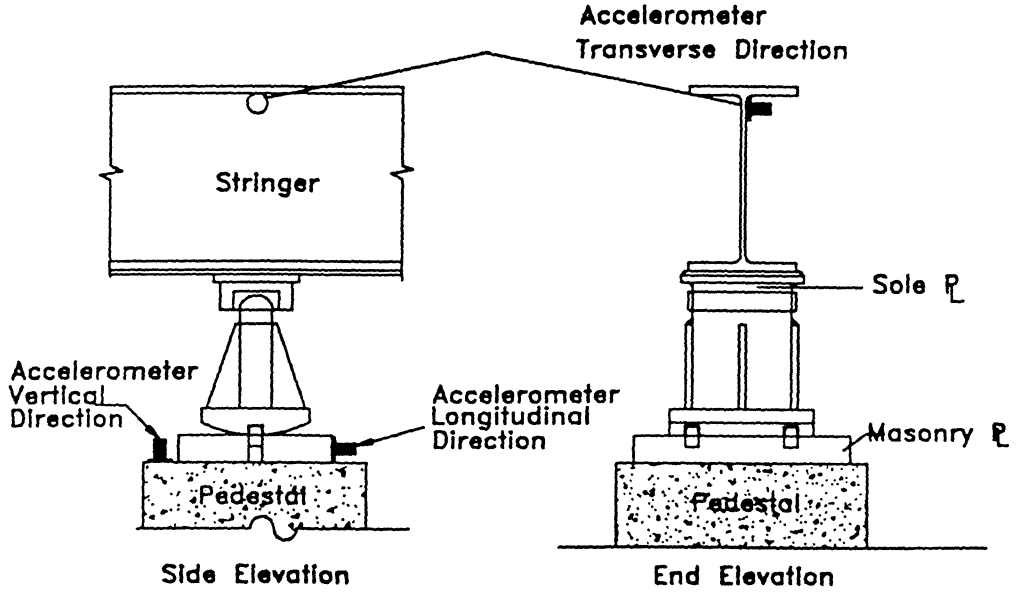

FIGURE 2-26 Accelerometer Locations at the Piers

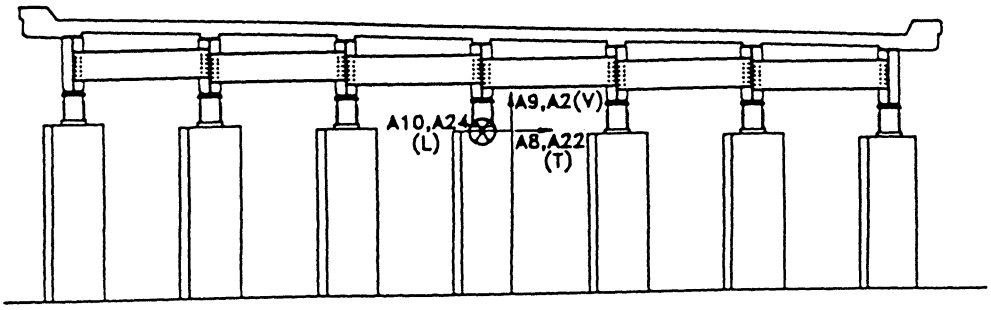

⊗ = Longitudinal Accelerometers
A8,9,10 = North Abutment
A22,23,24 = South Abutment
L = Longitudinal Direction of the Bridge
T = Transverse Direction of the Bridge
V = Vertical Direction of the Bridge

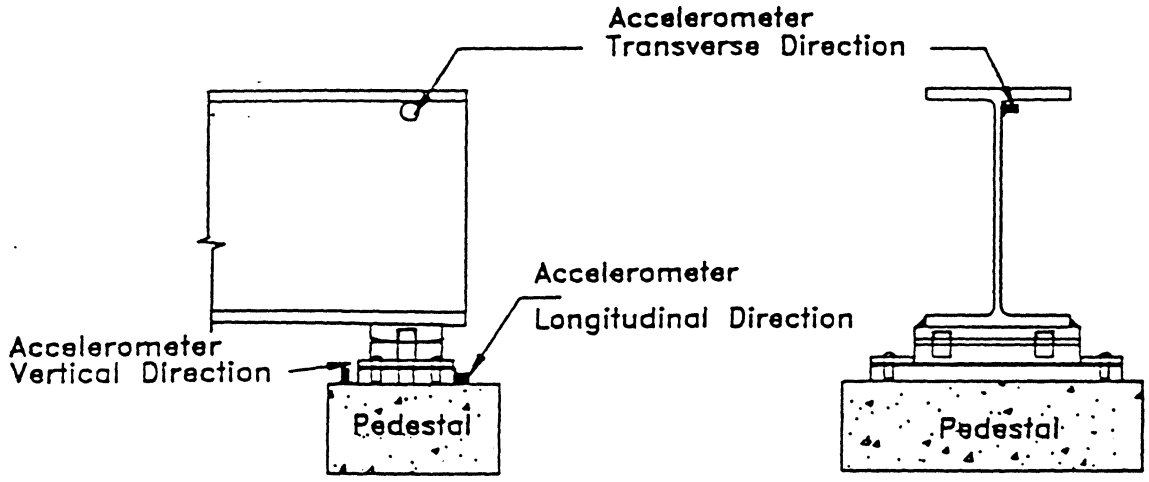

Expansion Bearings at Abutments

FIGURE 2-27 Accelerometer Locations at the Abutments

TABLE 2-3 Accelerometer Locations-Pre-Retrofitted Bridges

Southbound Bridge			Northbound Bridge		
Accel.	**Location**	**Direction**	**Accel.**	**Location**	**Direction**
*AP3	Deck	Transverse	* *AP3	Deck	Transverse
A1	Deck	Transverse	A1	Deck	Transverse
A2	Deck	Transverse	A2	Deck	Transverse
A3	Deck	Transverse	A3	Deck	Transverse
*AP9	Deck	Transverse	* *AP9	Deck	Transverse
A4	Deck	Transverse	A4	Deck	Transverse
A5	Deck	Transverse	A5	Deck	Transverse
A6	Deck	Transverse	A6	Deck	Transverse
A7	Deck	Transverse	A7	Deck	Transverse
A8	North Abutment	Transverse	A8	North Abutment	Transverse
A13	North Pier	Transverse	A13	North Pier	Transverse
A19	South Pier	Transverse	A19	South Pier	Transverse
A22	South Abutment	Transverse	A22	South Abutment	Transverse
A9	North Abutment	Vertical	A9	North Abutment	Vertical
A11	North Pier	Vertical	A11	North Pier	Vertical
A14	North Pier	Vertical	A14	North Pier	Vertical
A17	South Pier	Vertical	A17	South Pier	Vertical
A20	South Pier	Vertical	A20	South Pier	Vertical
A23	South Abutment	Vertical	A23	South Abutment	Vertical
A25	Deck	Vertical	A25	Deck	Vertical
A26	Deck	Vertical	A26	Deck	Vertical
A27	Deck	Vertical	A27	Deck	Vertical
A28	Deck	Vertical	A28	Deck	Vertical
A29	Deck	Vertical	A29	Deck	Vertical
A30	Deck	Vertical	A30	Deck	Vertical
A10	North Abutment	Longitudinal	A10	North Abutment	Longitudinal
A12	North Pier	Longitudinal	A12	North Pier	Longitudinal
A15	North Pier	Longitudinal	A15	North Pier	Longitudinal
A18	South Pier	Longitudinal	A18	South Pier	Longitudinal
A21	South Pier	Longitudinal	A21	South Pier	Longitudinal
A24	South Abutment	Longitudinal	A24	South Abutment	Longitudinal

AP#=Computer Channel Used by Accelerometer or Potentiometer depending the test.
The portion P# indicate the number of the potentiometer connected

*= In test SBPRE-T3-TP, the computer channel was used by a Potentiometer P3 and P9

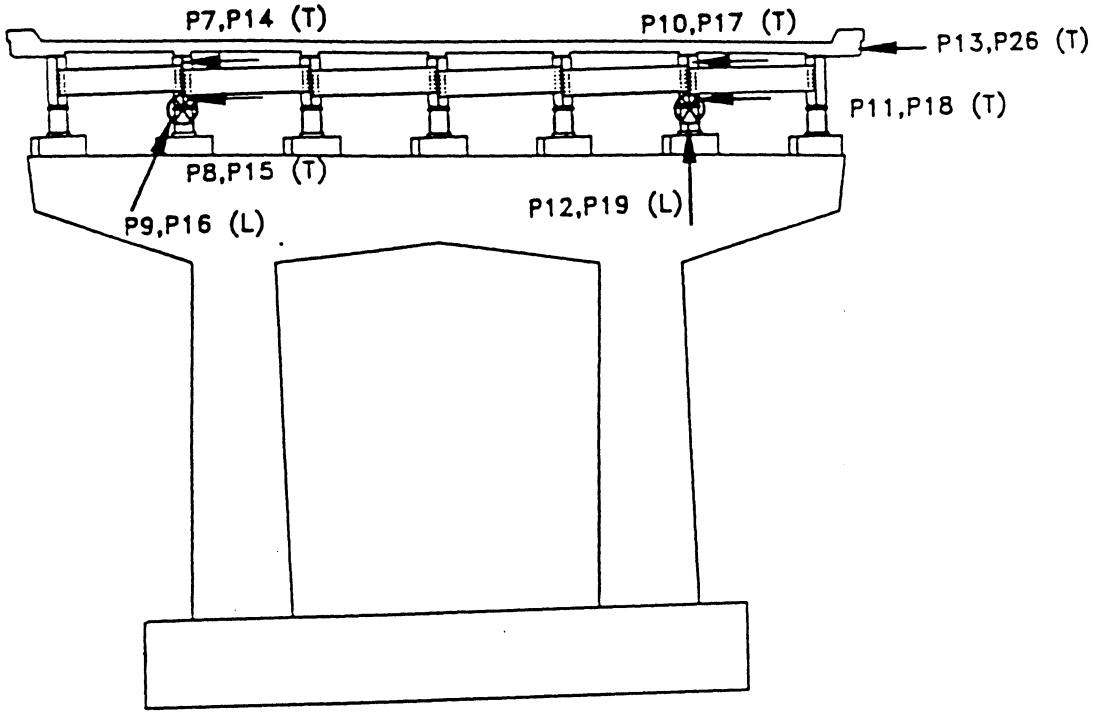

⊗ = Longitudinal Potentiometer
P7,8,9,10,11,12,13 = North Pier – Potentiometers
P14,15,16,17,18,19,26 = South Pier – Potentiometers
L = Longitudinal Direction of the Bridge
T = Transverse Direction of the Bridge
V = Vertical Direction of the Bridge

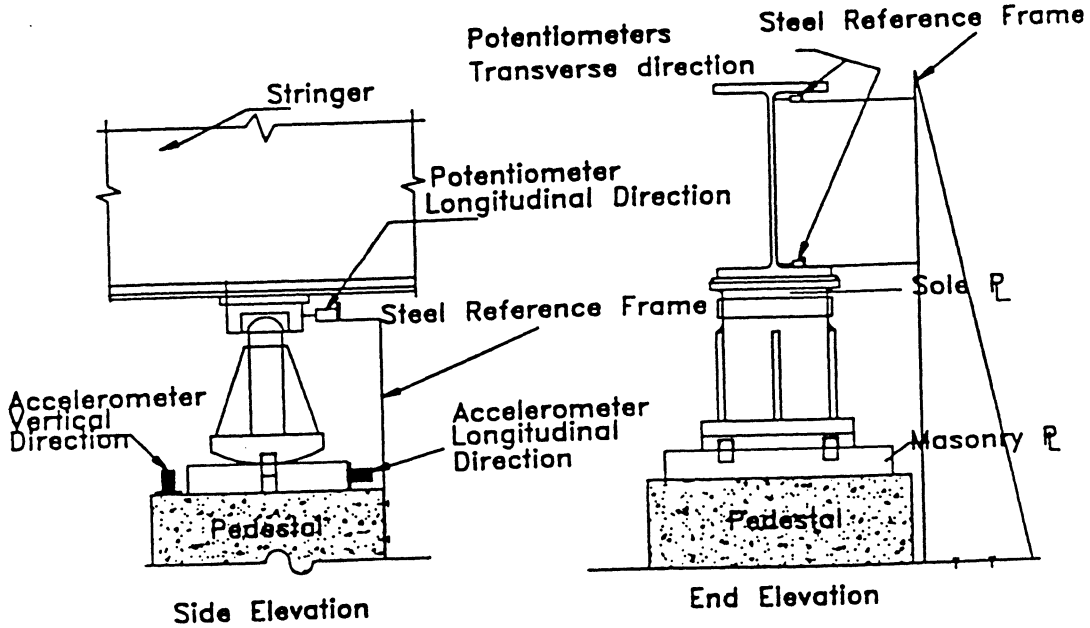

FIGURE 2-28 Pontentiometer Locations at the Piers

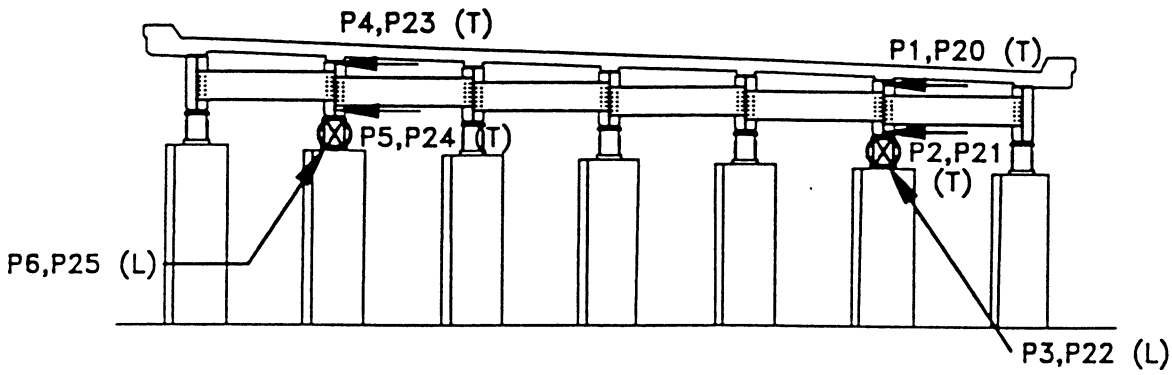

⊗ = Longitudinal Potentiometers
P1,2,3,4,5,6 = North Abut.
P20,21,22,23,24,25 = South Abut.
L = Longitudinal Direction of the Bridge
T = Transverse Direction of the Bridge
V = Vertical Direction of the Bridge

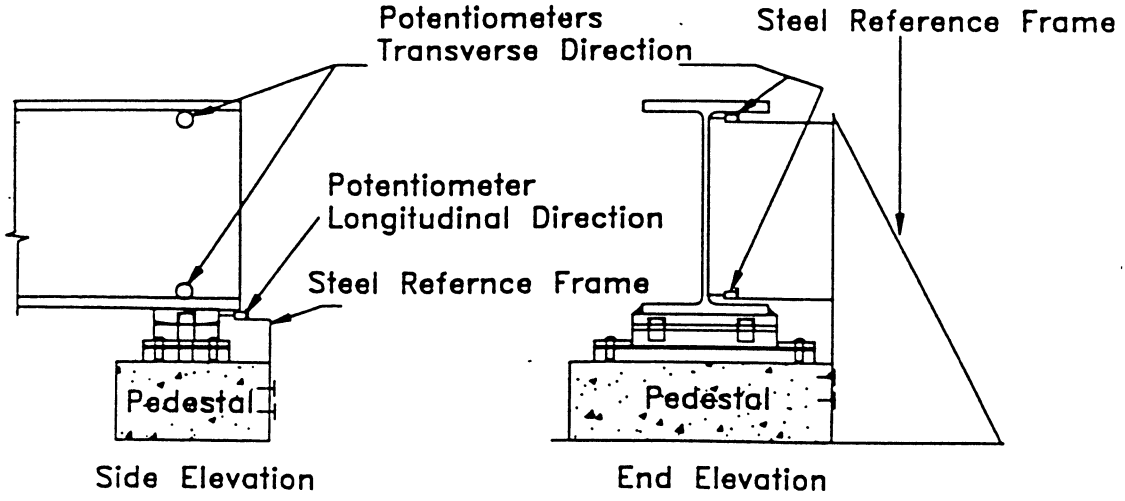

FIGURE 2-29 Pontentiometer Locations at the Abutments

TABLE 2-4 Potentiometer Locations - Pre-Retrofitted Bridges

Southbound Bridge			Northbound Bridge		
Accel.	**Location**	**Direction**	**Accel.**	**Location**	**Direction**
P1	North Abutment	Transverse	P1	North Abutment	Transverse
P2	North Abutment	Transverse	P2	North Abutment	Transverse
P4	North Abutment	Transverse	P4	North Abutment	Transverse
P5	North Abutment	Transverse	P5	North Abutment	Transverse
P7	North Pier	Transverse	P7	North Pier	Transverse
P8	North Pier	Transverse	P8	North Pier	Transverse
P10	North Pier	Transverse	P10	North Pier	Transverse
P11	North Pier	Transverse	P11	North Pier	Transverse
P14	South Pier	Transverse	P14	South Pier	Transverse
P15	South Pier	Transverse	P15	South Pier	Transverse
P17	South Pier	Transverse	P17	South Pier	Transverse
P18	South Pier	Transverse	P18	South Pier	Transverse
P20	South Abutment	Transverse	P20	South Abutment	Transverse
P21	South Abutment	Transverse	P21	South Abutment	Transverse
P23	South Abutment	Transverse	P23	South Abutment	Transverse
* * P24	South Abutment	Transverse	* * P24	South Abutment	Transverse
P13	Deck	Transverse	P13	Deck	Transverse
P26	Deck	Transverse	P26	Deck	Transverse
* P3	North Abutment	Longitudinal	P3	North Abutment	Longitudinal
P6	North Abutment	Longitudinal	P6	North Abutment	Longitudinal
* P9	North Pier	Longitudinal	P9	North Pier	Longitudinal
P12	North Pier	Longitudinal	P12	North Pier	Longitudinal
P16	South Pier	Longitudinal	P16	South Pier	Longitudinal
P19	South Pier	Longitudinal	P19	South Pier	Longitudinal
P22	South Abutment	Longitudinal	P22	South Abutment	Longitudinal
* * P25	South Abutment	Longitudinal	* * P25	South Abutment	Longitudinal

* = In tests SBPRE-T1-OP and SBPRE-T2-OP the computer channels were used by the Accelerometers AP3 and AP9

* * = Instrument installed but not connected to the computer

TABLE 2-5 Accelerometer Locations-Post-Retrofitted Bridges

Southbound Bridge

Accel.	Location	Direction
AP3	Deck	Transverse
A1	Deck	Transverse
A2	Deck	Transverse
A3	Deck	Transverse
AP9	Deck	Transverse
A4	Deck	Transverse
A5	Deck	Transverse
AP16	Deck	Transverse
A6	Deck	Transverse
A7	Deck	Transverse
AP22	Deck	Transverse
A8	North Abutment	Transverse
A13	North Pier	Transverse
A19	South Pier	Transverse
A22	South Abutment	Transverse
A9	North Abutment	Vertical
A11	North Pier	Vertical
A14	North Pier	Vertical
A17	South Pier	Vertical
A20	South Pier	Vertical
A23	South Abutment	Vertical
A25	Deck	Vertical
A26	Deck	Vertical
A27	Deck	Vertical
A28	Deck	Vertical
A29	Deck	Vertical
A30	Deck	Vertical
A10	North Abutment	Longitudinal
A12	North Pier	Longitudinal
A15	North Pier	Longitudinal
A18	South Pier	Longitudinal
A21	South Pier	Longitudinal
A24	South Abutment	Longitudinal

Northbound Bridge

Accel.	Location	Direction
AP3	Deck	Transverse
A1	Deck	Transverse
A2	Deck	Transverse
A3	Deck	Transverse
AP9	Deck	Transverse
A4	Deck	Transverse
A5	Deck	Transverse
AP16	Deck	Transverse
A6	Deck	Transverse
A7	Deck	Transverse
AP22	Deck	Transverse
A8	North Abutment	Transverse
A13	North Pier	Transverse
A19	South Pier	Transverse
A22	South Abutment	Transverse
A9	North Abutment	Vertical
A11	North Pier	Vertical
A14	North Pier	Vertical
A17	South Pier	Vertical
A20	South Pier	Vertical
A23	South Abutment	Vertical
A25	Deck	Vertical
A26	Deck	Vertical
A27	Deck	Vertical
A28	Deck	Vertical
A29	Deck	Vertical
A30	Deck	Vertical
A10	North Abutment	Longitudinal
A12	North Pier	Longitudinal
A15	North Pier	Longitudinal
A18	South Pier	Longitudinal
A21	South Pier	Longitudinal
A24	South Abutment	Longitudinal

TABLE 2-6 Potentiometer Locations-Post-Retrofitted Bridges

Southbound Bridge

Accel.	Location	Direction
P1	North Abutment	Transverse
P2	North Abutment	Transverse
P4	North Abutment	Transverse
P5	North Abutment	Transverse
P7	North Pier	Transverse
P8	North Pier	Transverse
**P10	North Pier	Transverse
P11	North Pier	Transverse
P14	South Pier	Transverse
P15	South Pier	Transverse
**P17	South Pier	Transverse
P18	South Pier	Transverse
P20	South Abutment	Transverse
P21	South Abutment	Transverse
P23	South Abutment	Transverse
P24	South Abutment	Transverse
P13	Deck	Transverse
P26	Deck	Transverse
P3	North Abutment	Longitudinal
P6	North Abutment	Longitudinal
P9	North Pier	Longitudinal
**P12	North Pier	Longitudinal
P16	South Pier	Longitudinal
**P19	South Pier	Longitudinal
P22	South Abutment	Longitudinal
P25	South Abutment	Longitudinal

Northbound Bridge

Accel.	Location	Direction
P1	North Abutment	Transverse
P2	North Abutment	Transverse
P4	North Abutment	Transverse
P5	North Abutment	Transverse
P7	North Pier	Transverse
P8	North Pier	Transverse
**P10	North Pier	Transverse
P11	North Pier	Transverse
P14	South Pier	Transverse
P15	South Pier	Transverse
**P17	South Pier	Transverse
P18	South Pier	Transverse
P20	South Abutment	Transverse
P21	South Abutment	Transverse
P23	South Abutment	Transverse
P24	South Abutment	Transverse
P13	Deck	Transverse
P26	Deck	Transverse
P3	North Abutment	Longitudinal
P6	North Abutment	Longitudinal
P9	North Pier	Longitudinal
**P12	North Pier	Longitudinal
P15	South Pier	Longitudinal
**P19	South Pier	Longitudinal
P22	South Abutment	Longitudinal
P25	South Abutment	Longitudinal

** = Instrument installed but not connected to the computer

potentiometers were used for this kind of test. One computer was adequate to acquire all of the data. The tests were performed selecting the kind of traffic that could produce significant accelerations. The computer was triggered approximately 2 seconds before a heavy vehicle arrived at the bridge. Channels were then scanned over the next 20 seconds.

The quick-release tests were performed with traffic control. Before the bars which crossed the deck were installed, one of the lanes was closed for the day. During each release test, the bridge was completely closed to the traffic and remained closed for approximately 30 seconds after the release. In all of the tests a 20 second window was used to acquire data. Immediately following each test, partial data reduction was carried out in the field to verify the results and check for possible malfunction of some instruments. In total three different tests were conducted on the Southbound and on the Northbound bridges. Table 2-7 summarizes the tests performed over the pre-retrofitted Northbound and Southbound bridges. The table describes the type of test, where a one pier test corresponds to a non-symmetric loading condition with respect to the center of the bridge and a two pier test to a symmetric loading condition. Also the table presents the maximum load applied in each case and the type of release system used during the test.

After retrofitting the two bridges, some 50 ambient vibration tests were performed, 25 on each bridge. These tests followed the same procedure and instrument locations described for the tests undertaken prior to retrofitting. All of the ambient vibration tests were conducted in advance of the snap-back tests. During the snap-back test accelerometers were located in the exterior girders, reading in the vertical direction, in order to corroborate the results obtained from the ambient vibration tests.

The procedures used in the snap-back tests of the bridges after retrofitting were similar to the procedures used in the earlier tests prior to retrofitting. Table 2-8 summarizes the number of tests done, type of test, and the applied load. Table 2-9 presents the residual and maximum displacements for each test. During the day of the test, and before any snap-back test was performed, a initial reading was done without any vehicle crossing the bridge or load in the

TABLE 2-7 Test Characteristics-Pre-Retrofitted Bridges

Southbound Bridge

Load Cell	Location	Test Name	Type of Test	Load (kN)	Release System
L1 + L2	North Pier	SBPRE-T1-OP	One Pier	0	
L3 + L4	South Pier	SBPRE-T1-OP	One Pier	639	Fuse Bar - South Pier
L1 + L2	North Pier	SBPRE-T2-OP	One Pier	0	
L3 + L4	South Pier	SBPRE-T2-OP	One Pier	598	Fuse Bar - South Pier
L1 + L2	North Pier	SBPRE-T3-TP	Two Pier	707	Oil Quick Release Sys.
L3 + L4	South Pier	SBPRE-T3-TP	Two Pier	699	Oil Quick Release Sys.

Notes

Location: North Pier = The force was applicated at the deck level over the pier mentioned

Test Name: SBPRE= Southbound Bridge Preretrofitted
T1= Test #1
OP= One Pier (Pulling Condition)

Northbound Bridge

Load Cell	Location	Test Name	Type of Test	Load (kN)	Release System
L1 + L2	North Pier	NBPRE-T1-TP	Two Pier	394	Oil Quick Release Sys.
L3 + L4	South Pier	NBPRE-T1-TP	Two Pier	396	Oil Quick Release Sys.
L1 + L2	North Pier	NBPRE-T2-TP	Two Pier	552	Oil Quick Release Sys.
L3 + L4	South Pier	NBPRE-T2-TP	Two Pier	529	Oil Quick Release Sys.
L1 + L2	North Pier	NBPRE-T3-TP	Two Pier	663	Oil Quick Release Sys.
L3 + L4	South Pier	NBPRE-T3-TP	Two Pier	668	Oil Quick Release Sys.

Notes

Location: North Pier = The force was applicated at the deck level over the pier mentioned

Test Name: NBPRE= Northbound Bridge Preretrofitted
T1= Test #1
TP= Two Piers (Pulling Condition)

TABLE 2-8 Test Characteristics - Post-Retrofitted Bridges

Southbound Bridge

Load Cell	Location	Test Name	Type of Test	Load (kN)	Release System
L1 + L2	North Pier	SBPOST-T1-TP	Two Piers	384	Mechanical Fuse
L3 + L4	South Pier	SBPOST-T1-TP	Two Piers	290	Mechanical Fuse
L1 + L2	North Pier	SBPOST-T2-TP	Two Piers	555	Mechanical Fuse
L3 + L4	South Pier	SBPOST-T2-TP	Two Piers	520	Mechanical Fuse
L1 + L2	North Pier	SBPOST-T3-OP		0	
L3 + L4	South Pier	SBPOST-T3-OP	One Pier	604	Mechanical Fuse
L1 + L2	North Pier	SBPOST-T4-OP		0	
L3 + L4	South Pier	SBPOST-T4-OP	One Pier	679	Fuse Bar - South Pier

Notes

Location: North Pier = The force was applicated at the deck level over the pier mentioned

Test Name: SBPOST= Southbound Bridge Post-Retrofitted Bridge
T3= Test #3
OP= One Pier (Pulling Condition)

Northbound Bridge

Load Cell	Location	Test Name	Type of Test	Load (kN)	Release System
L1 + L2	North Pier	NBPOST-T1-OP	One Pier	521	Mechanical Fuse
L3 + L4	South Pier	NBPOST-T1-OP		0	
L1 + L2	North Pier	NBPOST-T2-TP	Two Pier	615	Mechanical Fuse
L3 + L4	South Pier	NBPOST-T2-TP	Two Pier	607	Mechanical Fuse
L1 + L2	North Pier	NBPOST-T3-OP		0	
L3 + L4	South Pier	NBPOST-T3-OP	One Pier	573	Mechanical Fuse

Notes

Location: North Pier = The force was applicated at the deck level over the pier mentioned

Test Name: NBPOST= Northbound Bridge Post-Retrofitted Bridge
T1= Test #1
TP= Two Piers (Pulling Condition)

TABLE 2-9 Maximum and Residual Displacements

Post-Retrofitted Southbound Bridge

Residual Displacements

Location	SBPOST-T1-TP (mm)	SBPOST-T2-TP (mm)	SBPOST-T3-OP (mm)	SBPOST-T4-OP (mm)
North Abutment	2.08	1.74	3.80	3.64
North Pier	1.28	1.69	1.38	1.48
South Pier	6.32	6.50	8.68	8.66
South Abutment	7.39	7.42	11.35	11.20

Maximum Displacements

Location	SBPOST-T1-TP (mm)	SBPOST-T2-TP (mm)	SBPOST-T3-OP (mm)	SBPOST-T4-OP (mm)
North Abutment	14.22	28.47	7.18	5.20
North Pier	15.13	31.37	12.92	13.66
South Pier	15.62	34.82	26.00	25.52
South Abutment	15.74	37.03	34.86	33.00

Notes

Residual Disp. : Measure respect to the test "0" (first of the day, without load and traffic)
Maximum Disp.: Maximum initial disp. of test "i+1"- Final disp. of test "i"
Test Name: SBPOST= Southbound Bridge - Post-Retrofitted
T3= Test #3
OP= One Pier (Pulling Condition)

Post-Retrofitted Northbound Bridge

Residual Displacements

Location	NBPOST-T1-OP (mm)	NBPOST-T2-TP (mm)	NBPOST-T3-OP (mm)
North Abutment	0.13	0.13	0.15
North Pier	0.12	0.13	0.14
South Pier	0.05	0.02	0.05
South Abutment	0.23	0.22	0.23

Maximum Displacements

Location	NBPOST-T1-OP (mm)	NBPOST-T2-TP (mm)	NBPOST-T3-OP (mm)
North Abutment	6.47	8.94	0.15
North Pier	4.69	11.23	4.65
South Pier	3.20	17.17	12.62
South Abutment	2.18	21.41	18.28

Notes

Residual Disp. : Measure respect to the test "0" (first of the day, without load and traffic)
Maximum Disp.: Maximum initial disp. of test "i+1"- Final disp. of test "i"
Test Name: NBPOST= Northbound bridge - Post-Retrofitted
T3= Test #3
OP= One Pier (Pulling Condition)

tension bar system. The difference between the final deformation after each test, and this initial test called "test zero" is the so called residual displacement. The maximum displacement was computed as the difference between the measured displacement before the structure was released and the final displacement of the previous test. The Southbound and Northbound bridges were tested in October and November of 1994 with average ambient temperatures of 60°F and 53°F, respectively. The ambient temperatures during the evenings prior to the tests were around 42°F.

2.7 Expansion Joint Characteristics and Test

The contribution of the expansion joint showed in figure 2-30a to the overall stiffness in the transverse direction of the bridge is of interest. In most cases the contribution of the expansion joint working in shear is thought to be insignificant in comparison with the capacity provided by other structural elements, especially if these are very stiff. For the Southbound and Northbound bridges, armored expansion joints system were prescribed by the NYSDOT, with a nominal width of 102 mm and 64 mm at the south and north abutment in the Southbound bridge and nominal width of 89 mm for both abutments of the Northbound bridge. The prescribed width after installation at 68°F was 61 mm and 38 mm for the south and north abutment of the south bound and 57 mm in the Northbound.

In order to investigate its possible stiffness contribution, a simple test to estimate the expansion joint properties was conducted. The tests were performed on two different pairs of expansion joints as illustrated in figure 2-30b. Both pairs, shown on the photograph in Figure 2-30b consisted of 64 mm and 102 mm wide specimens. The smaller and larger specimens are representative of the north and south abutment expansion joints, respectively. Note that the profile of the two pairs are slightly different. Both were tested in compression and shear and the average results adopted. This is because it is not known precisely what joint type the contractor used in the field.

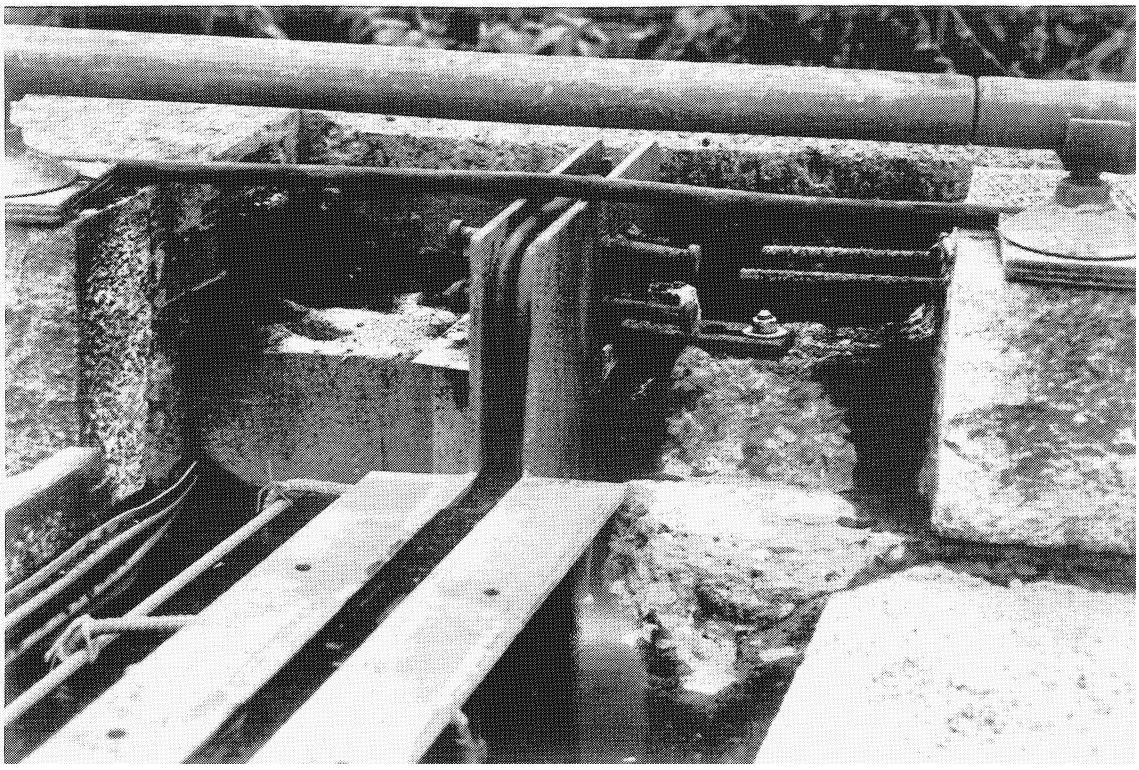

(a) General View

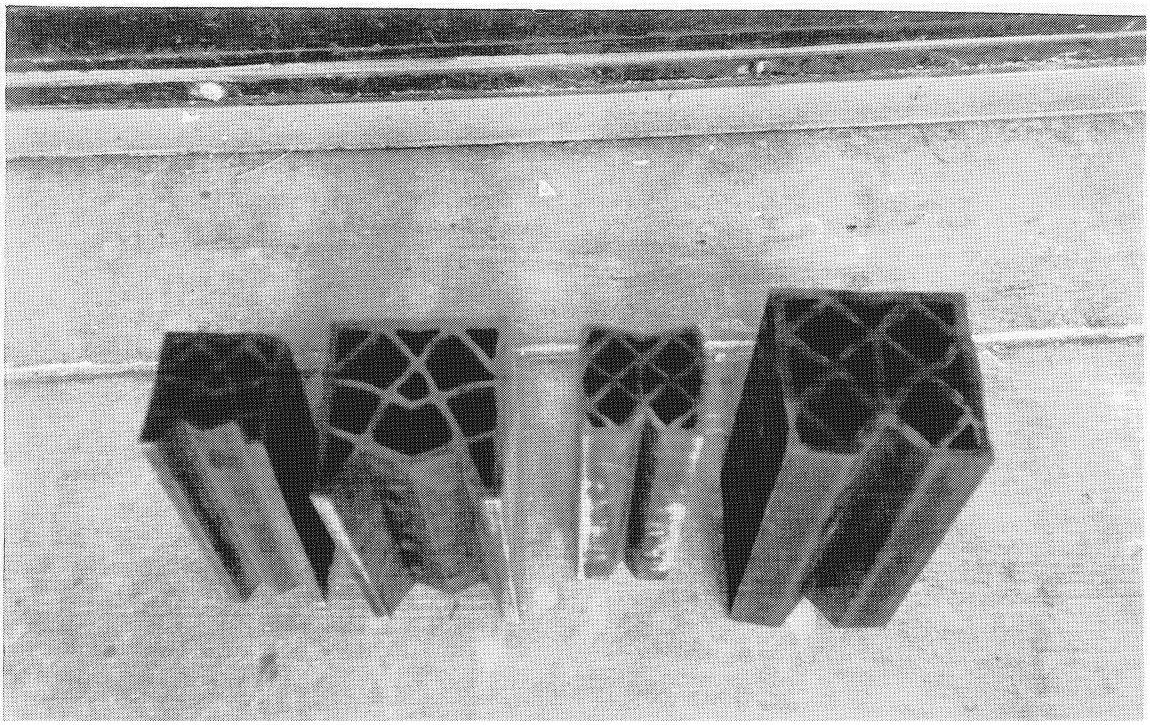

(b) Pair #1 and Pair #2

FIGURE 2-30 Bridge Expansion Joints

Figure 2-31a and 2-31b show the setup for the expansion joint test. In this setup, the seal is located between two mild steel plates, but not sealed to them as it is done in the field. The results obtained with this approach are expected to be conservative.

Two kind of tests were conducted on each specimen, compression and shear. For the compression test, the load was applied slowly and the vertical deformation was read. Figures 2-32a and 2-32b show the results obtained for these tests. In all of the tests, three well defined parts were observed. The first part corresponds to the initial deformation of the seal. For this portion the interior "honeycomb" remains "stable" and the load increases with the deformation. In the second part, the "honeycomb" collapses and the deformation increases with constant or even decreasing load. The final portion corresponds to the case where the "honeycomb" is completely compressed and the system starts to gain load again. During these tests, it was observed that there were variations of some 15% between similar tests with the same specimen and the same load. Therefore, it was decided to perform 3 tests to each specimen and report the results as the average of these tests.

The shear tests were performed applying steps of loads after the seal was compressed to a certain magnitude, measuring the shear deformation after each step was finished. Figures 2-32c and 2-32d show the results obtained for each seal and for each axial load. From figures 2-32c and 2-32d it is possible to infer that the initial stiffness of the seal depends on the axial load. This load in the field changes continuously, depending on different factors such as temperature, creep, etc. Thus it is difficult to define a unique initial stiffness for the seal. In order to estimate an initial stiffness, it was decided to use the average of the secant stiffness computed at a force equal to the 50% of the "yielding" point (K_1).

Figure 2-33 shows the coefficient of friction of the joints vs. displacement, obtained by dividing the results of the shear test by the axial load. The figure shows that independent of the kind of seal, the force necessary to slide the steel plate located at the top with respect to the seal is slightly less than the axial force sustained by the seal at the moment of the test. Thus for these

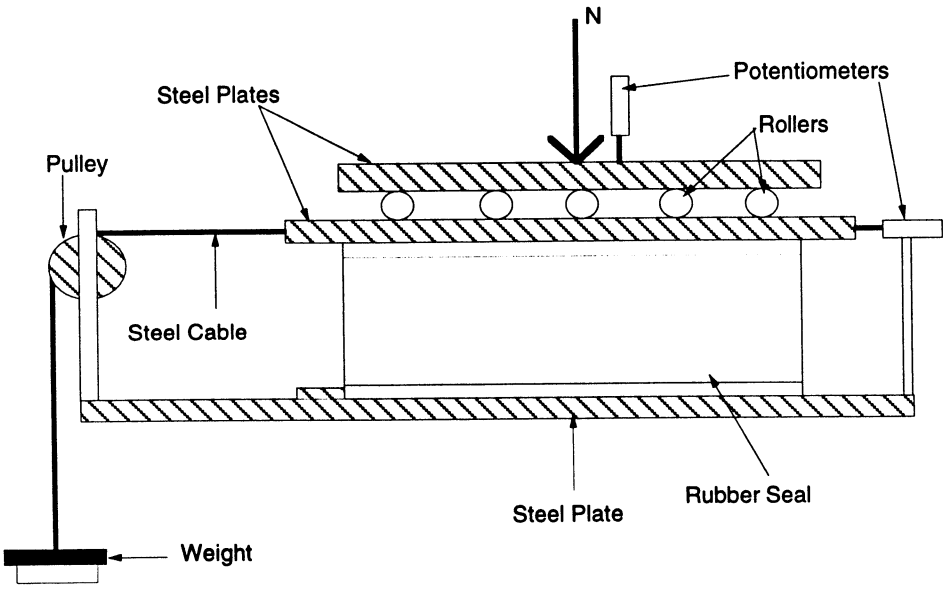

a) Longitudinal Section

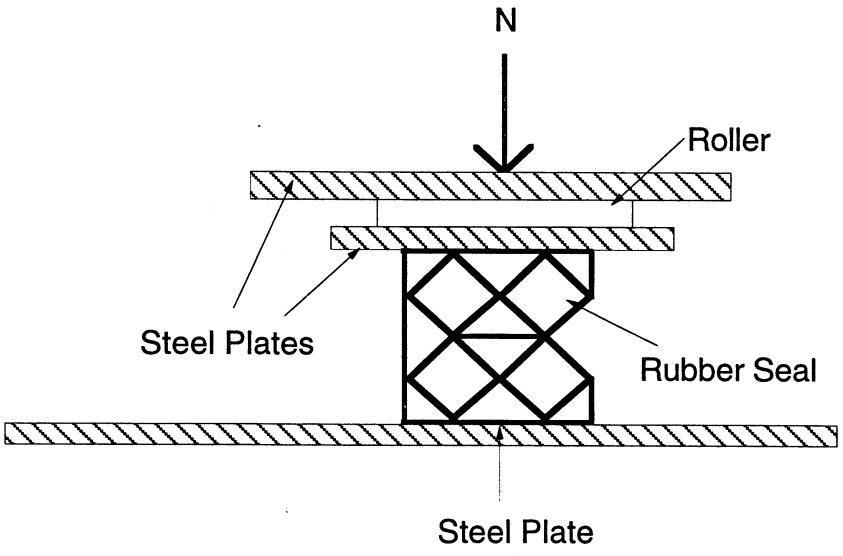

Cross Section A-A

b) Front View

FIGURE 2-31 Expansion Joints Test Setup

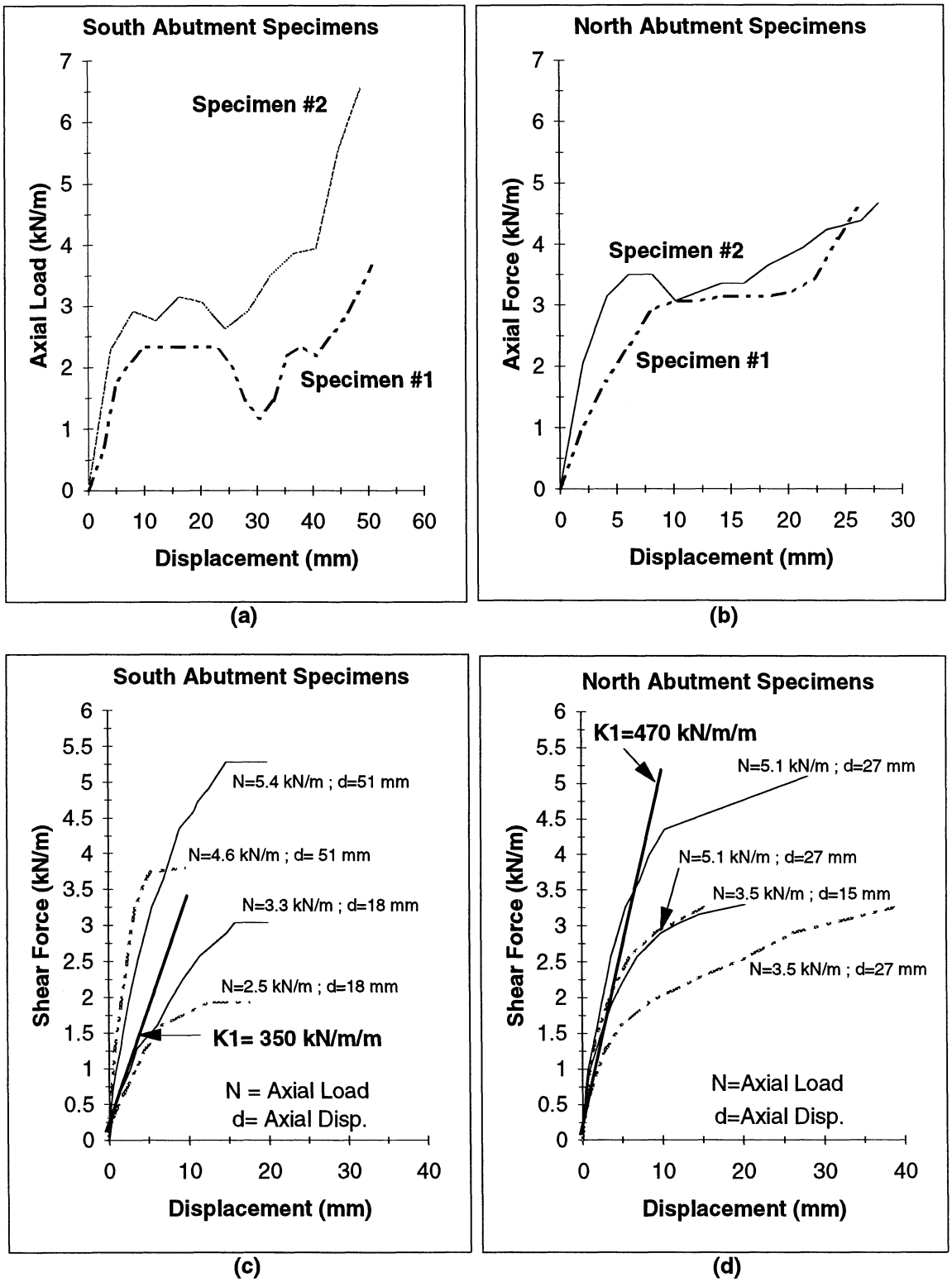

FIGURE 2-32 Southbound Bridge - Expansion Joint Test

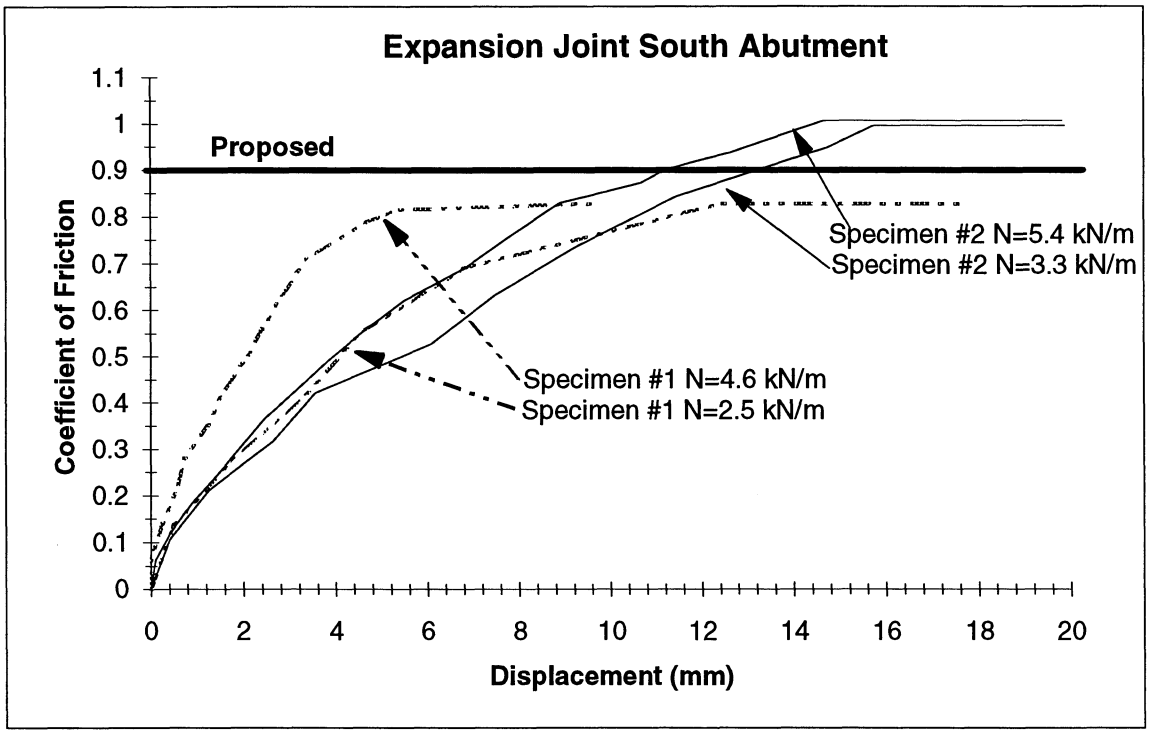

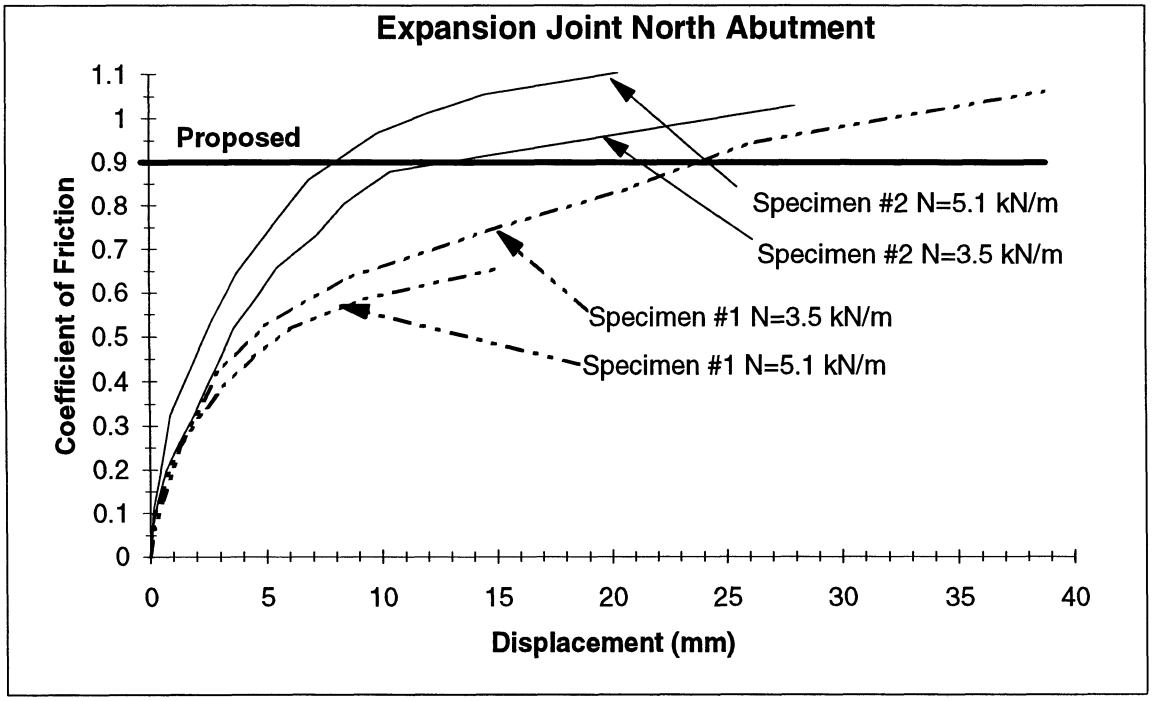

FIGURE 2-33 Southbound Bridge - Expansion Joint Coefficient of Friction

seals a frictional coefficient of 0.9 is proposed in order to estimate the frictional force developed in the expansion joint after the seal slides.

In order to be able to define a bilinear spring to model the expansion joint, the existing axial load in the field was obtained from figure 2-32a and 2-32b using as input the difference between the measured width of the expansion joint in the field and the nominal size of each seal. With these values of 38 mm in the south and 20 mm in the north abutment, respectively, a compression load of around 3.3 kN/m for the south abutment and 3.5 kN/m for the north abutment were obtained from the figures. Then the bilinear spring is defined as a spring with initial stiffness of 5173 kN/m (350 kN/m/m × 14.78 m) and a "yield" force of44 *kN* (3.3 kN/m × 0.9 × 14.78 m) for the south abutment and for the north abutment6947 kN/m (470 kN/m/m × 14.78 m) and 47 kN (3.5 kN/m × 0.9 × 14.78 m), respectively. The "yield" deformation was assumed for all of the cases as 8 mm.

It is important to mention that the results presented here give just an estimate of the contribution of the expansion joint to the overall behavior. A more extensive study should be conducted in order to consider other factors, such as aging, dirt and salt in the joints, roughness of the steel angles, etc.

For the Northbound bridge, where no specimen was tested, and since the size of the joint is in between that of the other two, the initial stiffness value was extended as the average of the values reported for the Southbound 5311 kN/m (410 kN/m/m × 12.95 m). A 0.9 frictional coefficient was used for the computation of the "yield" force of 40 kN (3.4 kN/m × 9 × 12.95 m).

SECTION 3
ANALYTICAL MODELS, DATA ANALYSIS AND SYSTEM IDENTIFICATION OF THE EXPERIMENTAL RESULTS WHEN THE BRIDGES WERE SEATED ON STEEL BEARINGS

3.1 INTRODUCTION

The dynamic response of a linear elastic structural system is the sum of a discrete set of independent, predictable motions (Stroud, 1985). This is the basis for the great majority of structural dynamic analyses. Such motions are often called either "normal modes of vibration", "natural modes of vibrations", "characteristic modes of vibration", "modes of vibration" or just "modes".

A mode is completely characterized by three properties: (1) its natural (or resonant) frequency, (2) its damping behavior (or the rate at which it dissipates energy), and (3) its mode shape.

A modal test is the experimental determination of the modal characteristics (i.e., resonant frequency, damping behavior, and mode shape) for some of the modes of vibration of a structural system. The most frequent use for a modal test is to establish the credibility of an analytical model. If there is some expected service load for a structure that cannot possibly or practically be simulated, it is necessary to qualify the structure by analysis. An accepted procedure is to develop a mathematical representation of the structure (probably a finite element model) and compute its modal properties. Then a prototype, or perhaps the actual structure, is tested and its modal characteristics are measured. If the analytically and experimentally derived modes are similar, the analyst has a basis for confidence that his computational model has been validated.

The first portion of this section (3.2 - 3.6) presents the background and the methodology of system identification techniques used to extract the structural dynamic properties described

above. The second portion (3.7) shows the application of the methodology to the experimental results obtained from the pre-retrofitted bridges.

3.2 Modal Test and System Identification Background

Modal testing has been used as an effective engineering tool for about forty-five years. Early efforts had modest goals, perhaps only to identify resonant frequencies. In the late 1960's several technical breakthroughs made possible a dramatic expansion in modal testing. In particular, Cooley and Tukey (1965) introduced the fast Fourier transform (FFT). The growing capability of relatively low-cost microcomputers permitted small computers to be dedicated to test and analysis functions. These and other achievements provided the basis for a revolution in modal-testing technology. Minicomputer systems complete with software for data acquisition and on-line analysis became commercially available. Other computer-based systems were developed for the application of classical modal-test methods. Data analysis techniques based on signal-processing concepts were introduced and refined.

There is abundant information in the area of modal testing (e.g., Ewins 1984; Allemang, 1983; Brown, 1980). These references cover different topics from the design of the test to the analysis and interpretation of the results. Several studies of full scale structures, using different methodologies, have been reported (e.g., Somaprasad 1991, Trifunac 1970a, 1970b and Douglas, 1982). In addition applied system identification has developed (Beck 1978, McVerry 1979).

Two of the most important aspects of any modal analysis are the system used to excite the structure and the methodology used to reduce the data. Of the different excitation alternatives (Salawu 1995), ambient and transient vibrations were used for tests of the subject bridges. For the data reduction, several frequency domain method and one time domain method were developed specifically for this project. A brief discussion of the excitation alternatives used and the system identification methodology follows.

3.3 Excitation Methods

3.3.1 Ambient Excitation

It is sometimes advantageous or even necessary to use ambient excitation. Modal characterization of a structure that is in service is sometimes possible by simply measuring the structure's response to its service environment. For very large or inaccessible structures, ambient excitation may be the only available means of excitation. Among the sources of ambient excitation are wind, wave action, acoustic disturbances, "on-board" equipment, and traffic.

Advantages of ambient excitation include the fact that no force excitation system is required. The measured responses are the result of actual service disturbances. Disadvantages include the fact that ambient excitation is difficult or impossible to measure. Response levels may also be inadequate, making a large volume of data necessary.

3.3.2 Forced Excitation

Forced excitation is based on either eccentric mass shaking or by quick release testing and examining the free vibration dynamic response. Free vibration testing is conducted by introducing an initial displacement or velocity to the structure and measuring its transient response. The initial displacement has been typically induced by pulling and quickly releasing the structure. Douglas (1976) reported testing bridges by this procedure, utilizing crawler-tractors equipped with electrical solenoid triggers which quickly released cables. The required set-up is simple in concept for bridges, however, may be impractical in case of non-isolated buildings due to increased height and weight. The introduction of an initial force-displacement state makes it possible to obtain the stiffness of the structure which can be used in conjunction with the dynamics results to calibrate the analytical model. With this approach it is also possible to introduce displacements larger than the elastic yield displacements, making the methodology suitable to be used with isolated bridges, where the non-linear behavior is of special interest. The disadvantage is that generally it is difficult to excite the higher modes of a structure merely by an initial displacement applied in one direction and location.

An alternative to the initial displacement quick-release methodology is the impact testing technique (Raghavendrachar, 1992). This also leads to a free-vibration response but with a high frequency content, which would therefore incorporate the participation of many more modes than may be activated by an initial displacement.

3.4 Analysis Methods

A variety of techniques has been developed for analyzing structural response measurements to estimate modal properties (Stroud, 1985). Like the excitation and measurement choices, the choice of an analysis method is difficult due to the diversity of options available to the analyst. System identification analysis may be subdivided into two categories: Frequency-domain approaches and time-domain approaches. The categories are described as follows.

3.4.1 Frequency Domain Analysis

There are several methods within this category that have different degrees of complexity. The simplest are the "peak picking" and the Frequency-Domain Curvefit (FDC) method proposed by Brown (1976). A more complex approach is the Simultaneous Frequency Domain (SFD) method proposed initially by Coppolino (1981). There are also variations within these methods (Klosterman 1971, Richardson 1974). Provided that there are no closely spaced frequencies or high damping effects to be accounted for, most of the above mentioned methods work satisfactorily.

3.4.2 Time Domain Analysis

There are several methods that use time-domain measurements to estimate modal parameters. The methods are: (1) the complex-exponential algorithm (Brown, 1976), (2) Ibrahim (1976, 1977) time-domain (ITD) analysis, (3) poly-reference analysis (Vold, 1982), and (4) the Eigensystem realization algorithm (ERA) analysis (Pappa, 1984). Each of these techniques uses free-response measurements sampled at a constant interval. The methods described above are robust. However, in many cases they require a high level of computational capacity, and in other cases the frequencies and damping are mathematically "complex". This makes practical applications in civil engineering difficult.

3.4.3 Discussion of System Identification Methods

3.4.3.1 Previous Methods for Quick-Release Experiments

Most researchers who work in the system identification area agree that, independent of the method used, different outcomes will result from different initial "seeding" of the solution search technique owing to the poor conditioning of this class of problem. It could be said that implementing various system identification techniques becomes somewhat of an art rather than a rigorous science. In some methods where it is necessary to assume initial values, or in others where it is necessary to distinguish between "real modes" and "noise modes" an experienced analyst is needed to make the correct decision. In general, most of these methods were developed for mechanical or aeronautical uses where the input excitation can be measured. That improves the predictions considerably. Only the Ibrahim time-domain approach which was initially proposed for free vibration and a variation of a curve fitting method in the frequency domain proposed by Richardson (1988) were designed for quick-release experiments.

In the field experiment of the subject bridges, two main factors influenced the decision to propose an alternate method. The first one was the set of closely spaced modes observed in the tests of the pre-retrofitted bridges; the second was the high equivalent viscous damping of the post-retrofitted bridges. These two phenomena reduce the effectiveness of the frequency domain method. It was thus considered necessary to introduce a time domain method compatible with the experiments conducted to complement and corroborate the results of the "peak peaking" frequency domain method.

3.4.3.2 Proposed Time Domain System Identification

The general solution for free vibration in a SDOF system may be written in the form:

$$u = [u_0 \cos(\omega_d t) + (v_0 + u_o \xi \omega)/\omega_d \sin \omega_d t)]e^{-\xi \omega t} \qquad \textbf{(3-1)}$$

and for a MDOF system

$$u_r = \sum_{r=1}^{n} \phi_r [A_r \cos(\omega_{d_r} t) + (B_r + A_r \xi_r \omega_r) / \omega_{d_r} \sin(\omega_{d_r} t)] e^{-\xi_r \omega_r t} \quad (3\text{-}2)$$

where

$$A_r = (\{\phi\}^T [M] \{u_0\}) / M_r \quad (3\text{-}3)$$

$$B_r = (\{\phi\})^T [M] \{v_0\} / M_r \quad (3\text{-}4)$$

$$M_r = \{\phi\}^T [M] \{\phi\} \quad (3\text{-}5)$$

where u_0 = initial displacement, v_0 = initial velocity, ξ = damping, ω = natural frequency, $[M]$ = mass matrix and $\{\phi\}$ = mode shape vector. If the natural modes are normalized so that $M_r = 1$, they are said to form an ortho-normal set of vectors. Then M_r becomes the unit matrix, that is,

$$\{\phi_r\}^T [M] \{\phi_r\} = 1 \quad (3\text{-}6)$$

Substituting (3-3), (3-4) and (3-5) in (3-2) and using a 2 DOF system as an example for the derivation with the following initial conditions:

$$u_0 = \begin{pmatrix} u_{01} \\ u_{02} \end{pmatrix} \; ; \; v_0 = \begin{pmatrix} 0 \\ 0 \end{pmatrix} \quad (3\text{-}7)$$

$$\begin{Bmatrix} A_1 \\ A_2 \end{Bmatrix} = \begin{pmatrix} \phi_{11} & \phi_{21} \\ \phi_{12} & \phi_{22} \end{pmatrix} \begin{pmatrix} m_1 & 0 \\ 0 & m_2 \end{pmatrix} \begin{pmatrix} u_{o1} \\ u_{o2} \end{pmatrix} = \begin{Bmatrix} \phi_{11} m_1 u_{o1} + \phi_{21} m_2 u_{o2} \\ \phi_{12} m_1 u_{o1} + \phi_{22} m_2 u_{o2} \end{Bmatrix} \quad (3\text{-}8)$$

where m_1 = mass at coordinate 1, m_2 = mass at coordinate 2, u_{01} = initial displacement at

$$\begin{Bmatrix} B_1 \\ B_2 \end{Bmatrix} = \begin{pmatrix} \phi_{11} & \phi_{21} \\ \phi_{12} & \phi_{22} \end{pmatrix} \begin{pmatrix} m_1 & 0 \\ 0 & m_2 \end{pmatrix} \begin{pmatrix} v_{o1} \\ v_{o2} \end{pmatrix} = \begin{Bmatrix} \phi_{11} m_1 v_{o1} + \phi_{21} m_2 v_{o2} \\ \phi_{12} m_1 v_{o1} + \phi_{22} m_2 v_{o2} \end{Bmatrix} = \begin{Bmatrix} 0 \\ 0 \end{Bmatrix} \quad (3\text{-}9)$$

coordinate 1, and u_{02} = initial displacement at coordinate 2, equation (3-2) reduces to:

$$u_r = \sum_{r=1}^{n} \phi_r A_r \left[\cos(\omega_{dr} t) + (\xi_r \omega_r)/\omega_{dr} \sin(\omega_{dt})\right] e^{-\xi_r \omega_r t} \tag{3-10}$$

or expanding:

$$\begin{aligned} u_1 = {} & \phi_{11}(\phi_{11} m_1 u_{o1} + \phi_{21} m_2 u_{o2}) \left[\left(\cos(\omega_{d1} t) + \frac{\omega_1}{\omega_{d1}} \xi_1 \sin(\omega_{d1} t)\right) e^{(-\xi_1 \omega_1 t)}\right] \\ & + \phi_{12}(\phi_{12} m_1 u_{o1} + \phi_{22} m_2 u_{o2}) \left[\left(\cos(\omega_{d2} t) + \frac{\omega_2}{\omega_{d2}} \xi_2 \sin(\omega_{d2} t)\right) e^{(-\xi_2 \omega_2 t)}\right] \end{aligned} \tag{3-11}$$

and

$$\begin{aligned} u_2 = {} & \phi_{21}(\phi_{11} m_1 u_{o1} + \phi_{21} m_2 u_{o2}) \left[\left(\cos(\omega_{d1} t) + \frac{\omega_1}{\omega_{d1}} \xi_1 \sin(\omega_{d1} t)\right) e^{(-\xi_1 \omega_1 t)}\right] \\ & + \phi_{22}(\phi_{12} m_1 u_{o2} + \phi_{22} m_2 u_{o2}) \left[\left(\cos(\omega_{d1} t) + \frac{\omega_2}{\omega_{d2}} \xi_2 \sin(\omega_{d2} t)\right) e^{(-\xi_2 \omega_2 t)}\right] \end{aligned} \tag{3-12}$$

Calling

$$u_{11} = [\phi_{11}(\phi_{11} m_1 u_{o1} + \phi_{21} m_2 u_{o2})] \tag{3-13}$$

$$u_{12} = [\phi_{21}(\phi_{11} m_1 u_{o1} + \phi_{21} m_2 u_{o2}] \tag{3-14}$$

$$u_{21} = [\phi_{21}(\phi_{11} m_1 u_{o1} + \phi_{21} m_2 u_{o2}] \tag{3-15}$$

$$u_{22} = [\phi_{22}(\phi_{12} m_1 u_{o1} + \phi_{22} m_2 u_{o2}] \tag{3-16}$$

Then equations (3-11) and (3-13) can be rewritten as,

$$u_1 = u_{11}\left[\left(\cos(\omega_{d1}\,t) + \frac{\omega_1}{\omega_{d1}}\,\xi_1 \sin(\omega_{d1}\,t)\right) e^{(-\xi_1\omega_1 t)}\right] + u_{12}\left[\left(\cos(\omega_{d2}\,t) + \frac{\omega_2}{\omega_{d2}}\,\xi_2 \sin(\omega_{d2}\,t)\right) e^{(-\xi_2\omega_2 t)}\right] \quad \textbf{(3-17)}$$

$$u_2 = u_{21}\left[\left(\cos(\omega_{d1}\,t) + \frac{\omega_1}{\omega_{d1}}\,\xi_1 \sin(\omega_{d1}\,t)\right) e^{(-\xi_1\omega_1 t)}\right] + u_{22}\left[\left(\cos(\omega_{d2}\,t) + \frac{\omega_2}{\omega_{d2}}\,\xi_2 \sin(\omega_{d2}\,t)\right) e^{(-\xi_2\omega_2 t)}\right] \quad \textbf{(3-18)}$$

From equations (3-17) and (3-18), it can be inferred that the total displacement at any point in the structure is the sum of the components of each mode; also that there are three unknowns in each component: amplitude, frequency and damping. Of these three unknown components two form part of a transcendental equation (frequency and damping) and one is outside (amplitude). The location of these parameters which are to be identified significantly influences the choice of methodology to solve the problem.

The methodology proposed and employed for this study is conceptually straightforward and can be described using equation (3-10). If in these equations it is assumed that some starting values were given for the frequencies and damping, then the values of the amplitudes that provide the best fitting for these starting values can be found using a multi-linear regression approach. After this first step, and using some appropriate optimization technique, new values for damping and frequency can be obtained. During this second step the values of the amplitudes found during the first step remain constant. The procedure described above is repeated until the function is minimized using a least squares approach.

The method as described above minimizes $2(NM)$ nonlinear parameters using a quasi-Newton technique (damping and frequencies) where NM = number of modes. This portion is the most time consuming part of the process. The remaining NS variables where NS = number of instruments considered, are determined solving a system of simultaneous linear equations.

In mathematical terms, the method can be described as the minimization of the sum of the squares of the residual errors between the time history of the instrument and the analytical function proposed, or as expressed in equation (3-19).

$$\varepsilon = \sum_{t=1}^{\sigma} (\varepsilon_\omega)^2 \tag{3-19}$$

In indicial notation

$$\varepsilon = \varepsilon_\omega . \varepsilon_\omega \tag{3-20}$$

where ε_ω is the difference between the experimental value and the value of the function for a given point in time. The proposed function (equations 3-17 and 3-18) for a 2DOF system is a nonlinear function of ω (frequency) and ξ (damping) and a linear function of u (amplitude). An iterative optimization process was implemented where the nonlinear optimization process was combined with a multi-linear regression to reduce the computation time.

According to Masri (1985), the statement of the nonlinear portion of the optimization process can be summarized as follows:

Consider the problem of minimizing a scalar function $f(x)$ of n variables

$$x = (x_1, x_2, ..., x_n)^T \tag{3-21}$$

where x is a vector in the n-dimensional Euclidean space R^n. Thus the aim is to find a local solution to the problem minimizing

$$f(x) \quad , \quad x \varepsilon R^n \tag{3-22}$$

The value of vector x which satisfies equation (3-21) is referred to as the minimizer of $f(x)$ and denoted by x^*. Let the gradient vector $g(x)$ be defined by:

$$g(x) = \overline{V}f(x) = \left(\frac{\partial f}{\partial x_1}, \frac{\partial f}{\partial x_2}, \ldots, \frac{\partial f}{\partial x_n}\right)^T \tag{3-23}$$

and let an $(n \times n)$ real symmetric matrix $[G(x)]$, called the Hessian matrix, be given by:

$$[G(x)] = \nabla(\nabla f^T) = \nabla^2 f(x) \begin{bmatrix} \frac{\partial^2 f}{\partial x_1 \partial x_1}, & \frac{\partial^2 f}{\partial x_1 \partial x_2}, \ldots, & \frac{\partial^2 f}{\partial x_1 \partial x_n} \\ \frac{\partial^2 f}{\partial x_2 \partial x_1}, & \frac{\partial^2 f}{\partial x_2 \partial x_2}, \ldots, & \frac{\partial^2 f}{\partial x_2 \partial x_n} \\ & \vdots & \\ \frac{\partial^2 f}{\partial x_n \partial x_1}, & \frac{\partial^2 f}{\partial x_n \partial x_2}, \ldots, & \frac{\partial^2 f}{\partial x_n \partial x_n} \end{bmatrix} \tag{3-24}$$

where the "del" operator is defined as:

$$\nabla = \left(\frac{\partial}{\partial x_1}, \frac{\partial}{\partial x_2}, \ldots, \frac{\partial}{\partial x_n}\right)^T \tag{3-25}$$

With the use of Taylor series expansion for function $f(x)$ and $g(x)$ about the initial point $x^{(0)}$ and about a point x in the neighborhood of the minimizer x^*. Consider now a point x in the neighborhood of the minimizer x^*

$$x = x^* + \delta \tag{3-26}$$

From this and making use of the fact that a local minimum, $f(x)$ must have zero slope and positive curvature

$$g(x^*) = 0 \tag{3-27}$$

and

$$\delta^T[G(x^*)]\delta > 0 \qquad \textbf{(3-28)}$$

It can be shown (Aoki, 1971) that for x^* to be a minimum of $f(x)$, it is sufficient that $g^* = 0$ and that $[G*]$ be positive definite.

As can be seen from the description above, to obtain the minimizer of $f(x)$ is necessary to compute the Hessian matrix which includes second partial derivatives. This task may be tiresome and even impossible to compute. An alternative to avoid this problem is the use of a Quasi-Newton method.

Unlike the classical Newton method where curvature information about $f(x)$ is directly provided at every step of the iteration by the Hessian matrix $[G(x)]$, the Quasi-Newton method use information regarding $f(x)$ and its gradient $g(x)$. This is obtained from several iteration steps, to develop approximate curvature information regarding $f(x)$ without explicitly forming the Hessian matrix.

The need to calculate second derivatives of f, to invert $[G]$, and to ensure that $[G]$ is positive definite can be avoided by using the Quasi-Newton method in which $[G^{(k)}]^{-1}$ is approximated by a symmetric positive definite matrix $[H^{(k)}]$ which is updated from iteration to iteration. Note that in this method, only first derivatives are required. The method also has significant advantages, compared to the classical Newton Method, with regard to the descent property and the number of numerical operations per iteration.

The linear portion of the optimization process can be solved using the concepts of multi-linear regression, which is an extension of linear regression where y is a linear function of two or more variables. For example, y might be a linear function of x_1 and x_2, as in:

$$y = a_0 + a_2 x_1 + a_2 x_2 \tag{3-29}$$

Such an equation is particularly useful when fitting experimental data where the variable being studied is often a function of two other variables. For these two dimensional cases, the regression "line" becomes a "plane".

As with the previous cases, the "best" values of the coefficients are determined by setting up the sum of the squares of the residuals:

$$S_r = \sum_{i=1}^{n} (y_i - a_0 - a_1 x_{1,i} - a_2 x_{2,i})^2 \tag{3-30}$$

and differentiating with respect to each of the coefficients:

$$\frac{\partial S_r}{\partial a_0} = -2 \sum (y_i - a_0 - a_1 x_{1,i} - a_2 x_{2,i}) \tag{3-31}$$

$$\frac{\partial S_r}{\partial a_1} = -2 \sum x_{1,i} (y_i - a_0 - a_1 x_{1,i} - a_2 x_{2,i}) \tag{3-32}$$

The coefficients yielding the minimum sum of the squares of the residuals are obtained

$$\frac{\partial S_r}{\partial a_2} = -2 \sum x_{2,i} (y_i - a_0 - a_1 x_{1,i} - a_2 x_{2,i}) \tag{3-33}$$

by setting the partial derivatives equal to zero and expressing equations (3-31) to (3-33) as a set of simultaneous linear equations:

$$n a_0 + \sum x_{1,i} a_1 + \sum x_{2,i} a_2 = \sum y_i \tag{3-34}$$

$$\sum x_{1,i} a_0 + \sum x_{1,i}^2 a_1 + \sum x_{1,i} x_{2,i} a_2 = \sum x_{1,i} y_i \tag{3-35}$$

or in general form, and using matrix notation,

$$\sum x_{2,i} a_0 + \sum x_{1,i} x_{2,i} a_1 + \sum x_{2,i}^2 a_2 = \sum x_{2,i} y_i \tag{3-36}$$

$$\begin{bmatrix} n & \sum x_{1,i} & \sum x_{2,i} & \cdots & \sum x_{m,i} \\ \sum x_{1,i} & \sum x_{1,i}^2 & \sum x_{2,i} x_{1,i} & \cdots & \sum x_1 x_{m,i} \\ \sum x_{2,i} & \sum x_{2,i} x_{1,i} & \sum x_{2,i}^2 & \cdots & \sum x_2 x_{m,i} \\ \cdot & \cdot & \cdot & & \cdot \\ \cdot & \cdot & \cdot & & \cdot \\ \cdot & \cdot & \cdot & & \cdot \\ \sum x_{m,i} & \sum x_{m,i} x_{1,i} & \sum x_{m,i} x_{2,i} & \cdots & \sum x_{m,i}^2 \end{bmatrix} \begin{bmatrix} a_0 \\ a_1 \\ a_2 \\ \cdot \\ \cdot \\ \cdot \\ a_m \end{bmatrix} = \begin{bmatrix} \sum y_i \\ \sum x_1 y_i \\ \sum x_{2,i} y_i \\ \cdot \\ \cdot \\ \cdot \\ \sum x_{m,i} y_i \end{bmatrix} \tag{3-37}$$

Summarizing, the general procedure can be described as follows:

1) Assume initial starting values ξ and ω in equation (3-10) normally extracted from some preliminary analysis or from the Fourier spectra of some of the instruments.
2) Using multi-linear regression, obtain the linear coefficients from equation (3-37) using u_i instead of a_i as notation.
3) Using a nonlinear procedure obtain the values of frequencies and damping (ω, ε).
4) Repeat the process until the convergence is reached or the error between two successive iterations is less than the fixed tolerance.

The process described above can be performed by computer using any of the mathematical routines available (e.g., IMSL). These routines are powerful and fast. However, as with many of the simultaneous curve fitting methods (Time domain or Frequency domain), although the minimum error is mathematically correct, it may not necessarily be the "best fit". As all of the instruments are reduced at the same time a weight factor should be defined for each of them in order to account for differences in the maximum acceleration, noise, importance, etc. This introduces a new variable into the problem. To address this issue, it was decided to apply the procedure described above to each instrument separately. After the frequencies, damping and modal displacement were found for all of the instruments individually, final values for the

frequencies and damping were found using a weighted computation. The solution of the equation (3-37) with the final damping and frequencies provides the modal displacements. The procedure described increased the time to solve the problem but decreased the amount of memory needed, making it possible to solve the problem in a commercially available spreadsheet. The spreadsheet software EXCEL (1993) was used in this study. Figure 3-1 presents a typical curve fitting result for one accelerometer (A4) during a test. Also shown in figure 3-1 is the predicted displacement obtained using the results of the proposed system identification. The specific test for this aforementioned example was SBPRE-T2-OP. Such terminology is used throughout where SB = southbound, PRE = pre-rehabilitation, T2 = test number 2, OP = pulled at one pier.

The procedure used in this project can be summarized as follows:

1) Derive the equation (3-10) and obtain the acceleration expression.
2) With initial estimation of ξ and ω, and using the matrix inversion option of any available spreadsheets, solve equation (3-37) for $\boldsymbol{a} = \boldsymbol{u}$ (initial displacement).
3) Using the solver option, minimize the error between the experimental values and the function values (equation 3-19).
4) Repeat the problem until converged.
5) With the results obtained for all of the instruments, compute the final frequency and damping, using the expressions:

$$C_i = \frac{\frac{Pa_i}{\varepsilon_i}}{\sum \frac{Pa_i}{\varepsilon_i}} \qquad \textbf{(3-38)}$$

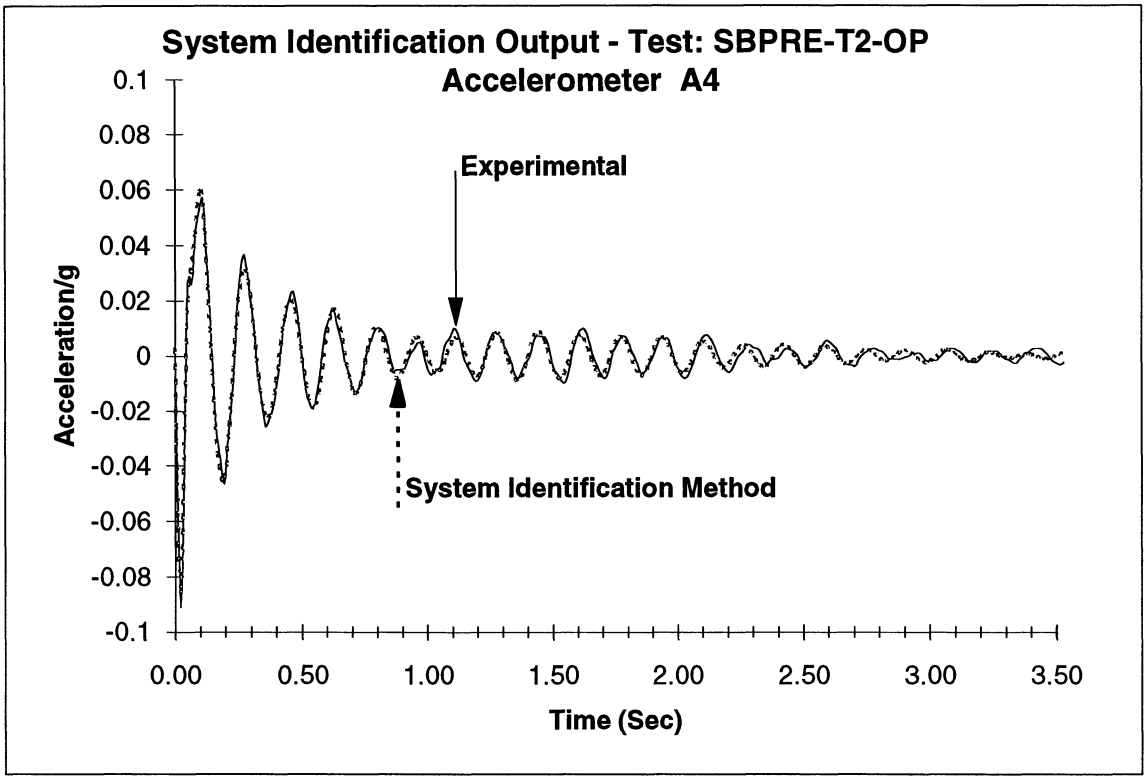

Acceleration Time History

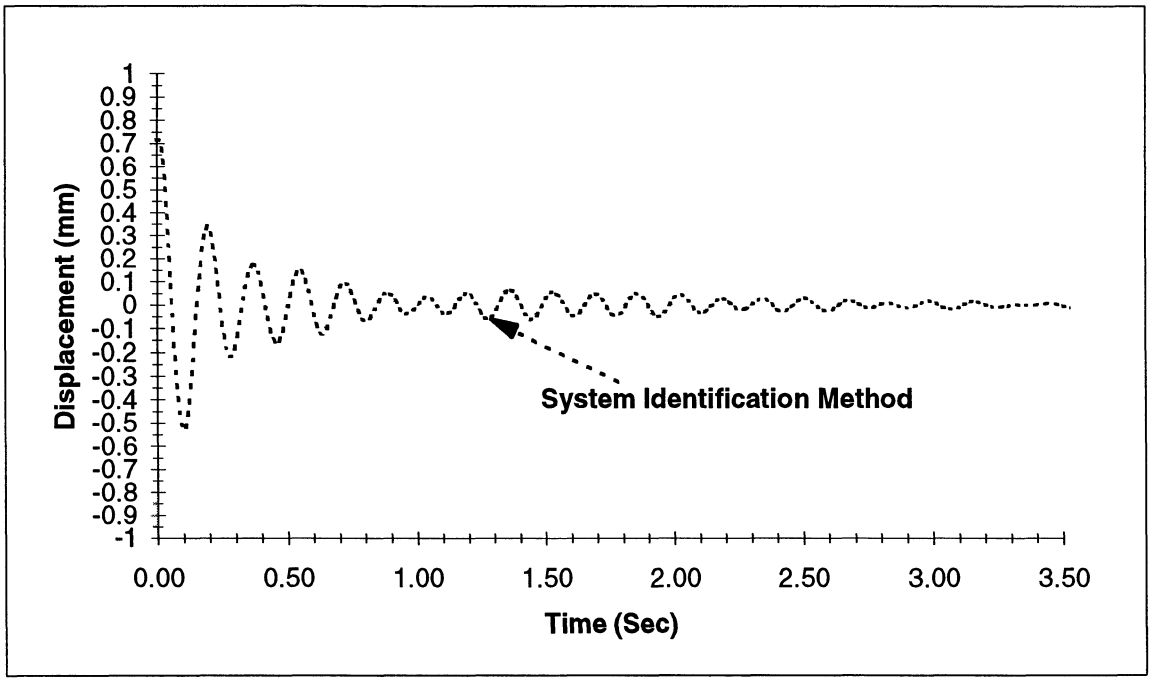

Displacement Time History

FIGURE 3-1 System Identification Typical Output

6) where ε_i = error in the optimization of the instrument "I", Pa_i = maximum peak acceleration of the instrument "I", ω_j = final frequency "j", ω_{ji} = value of the frequency "j" at the instrument "I", ξ_j = final damping "j", and ξ_{ji} = value of the damping "j" at the instrument "I".

7) Substitute the final frequency and damping of each instrument in the spreadsheet

$$\omega_j = \sum C_i \omega_{ji} \tag{3-39}$$

$$\xi_j = \sum C_i \xi_{ji} \tag{3-40}$$

and obtain the final modal displacements.

3.5 Advantages and Disadvantages of Proposed Method

1. Advantages of the proposed method can be summarized as follows:

   a) It is easy to understand and apply.
   b) The problem can be solved with basic tools.
   c) It can solve problems with closely spaced modes and relatively high damping.
   d) It provides the time history of acceleration, velocity and displacement.
   e) The summary of the modal displacements at time zero provides a good estimate of the initial displacements, which is difficult to obtain by the integration of the acceleration and is a good indicator of the static stiffness of the system.
   f) It can be modified easily to solve problems with initial velocity (impulsive loads) or initial velocity and displacements at the same time.

2. Disadvantages include the following:

   a) The method is time consuming.

b) It cannot solve problems with more than 6 different predominant frequencies due to the large number of variables to minimize. This makes the method not recommended for cases where extremely noisy signals are used and this noise is strong or predominant.

3.6 NUMERICAL EXAMPLES

Two examples are presented here to demonstrate the method. The first example is a three story building where the mass, damping and stiffness were assumed and an initial displacement was introduced as the source of vibration. With these assumptions the frequencies, mode shapes, and the exact total acceleration in each floor was computed using the modal superposition approach. Later, treating these acceleration time histories as if they were very clean experimental results, the proposed methodology was applied to compare the identified frequencies, mode shapes, and damping with the exact results. The second example is a quick-release test performed on a scale model of a three story reinforced concrete building. The test was performed applying a force of 8.9 kN at the third Floor. After the quick-release test, the structure was subjected to a white noise excitation on the shaking table. A complete description of the structural characteristics and the dynamic properties can be found in (Pekcan et al., 1995).

Figure 3-2 shows the structure for example 1 with the computed frequencies and mode shapes. It also presents the initial modal displacements. The table in figure 3-2 also compares the exact solution with the proposed methodology and the initial modal displacements, good agreement between the two is evident. Due to the absence of good data on bridges, figure 3-3 shows a three story building used for theory validation in example 2. Fourier spectra of the accelerometers located in each floor is presented in figure 3-4, while figure 3-5 compares the experimental results and the analytical predictions, and table 3-1 compares the mode shapes using different approaches. As can be inferred from the graphs and tables, good agreement was found using the proposed methodology and the results from the physical experiments. In both examples the solution was for a total of only six nonlinear variables (three frequencies and three damping factors) and nine linear variables (three initial displacements per accelerometer). The

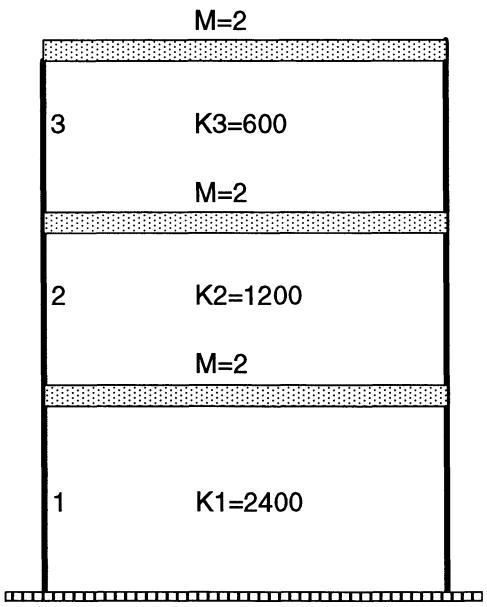

Mass Matrix

M	0	0
0	M	0
0	0	M

Stiffness Matrix

K3	-K3	0
-K3	K3+K2	-K2
0	-K2	K1+K2

Initial Displacements

Floor	Disp.(mm)
3	51
2	26
1	0

Frequencies		**Damping**		**Mode Shapes**		**Initial Modal Disp.**	
Analytical (Hz)	Identified (Hz)	Analytical (% Critical)	Identified (% Critical)	Analytical	Identified	Analytical (mm)	Identified (mm)
1.85	1.85	3	2.99	1 0.54 0.18	1 0.54 0.20	27.88 15.00 5.47	27.89 15.00 5.46
4.36	4.37	2	2	-0.67 1 0.58	-0.67 1 0.58	22.00 -33.00 -19.00	22.00 -33.00 -19.00
7.31	7.30	1	1	0.08 -0.52 1	0.09 -0.52 1	1.17 -7.08 13.71	1.17 -7.09 13.73

FIGURE 3-2 Time Domain System Identification - Example #1

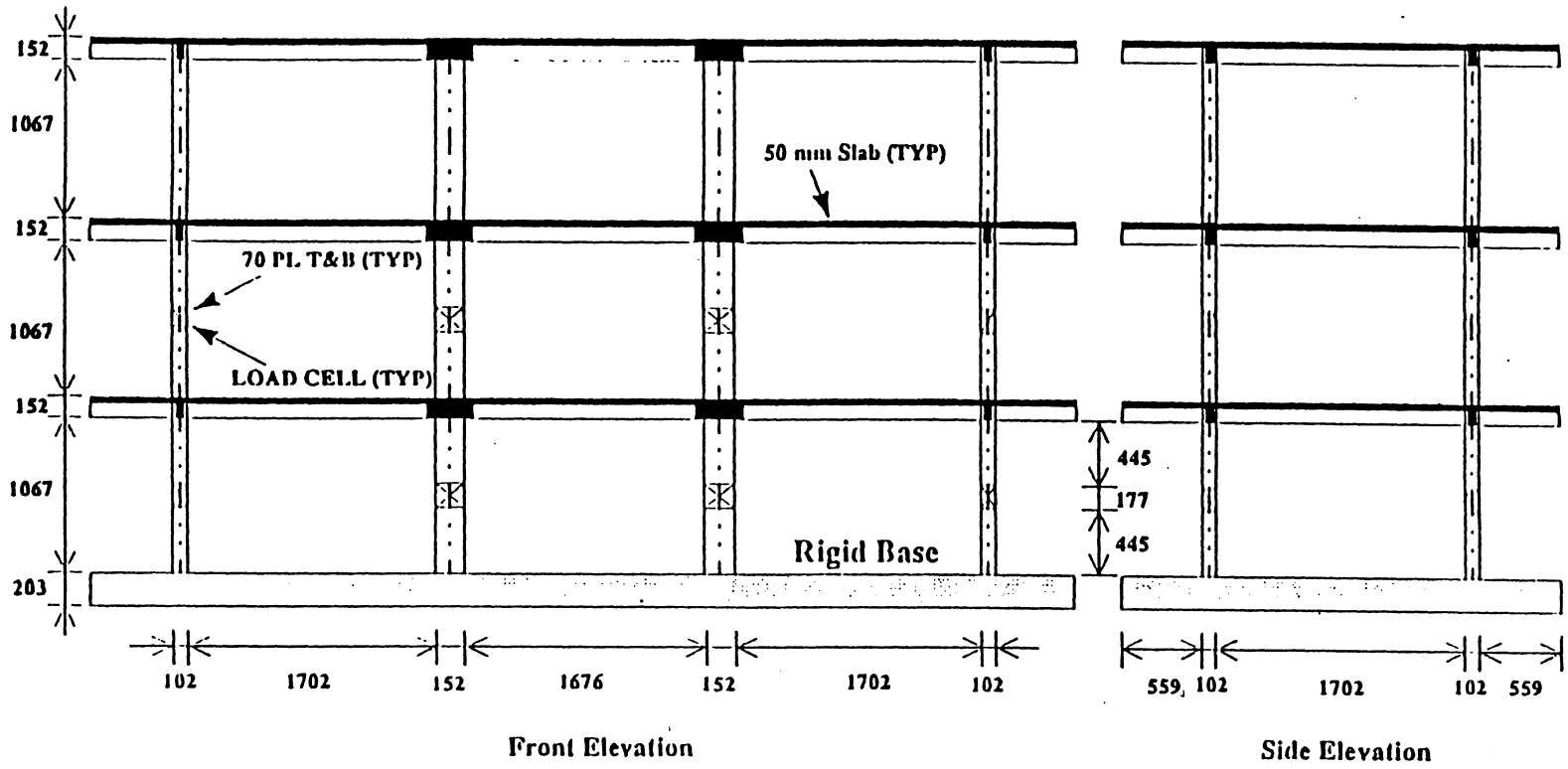

* All dimensions are in millimeters

FIGURE 3-3 Test Structure - Front and Side Elevation by Pekcan et al. (1995)

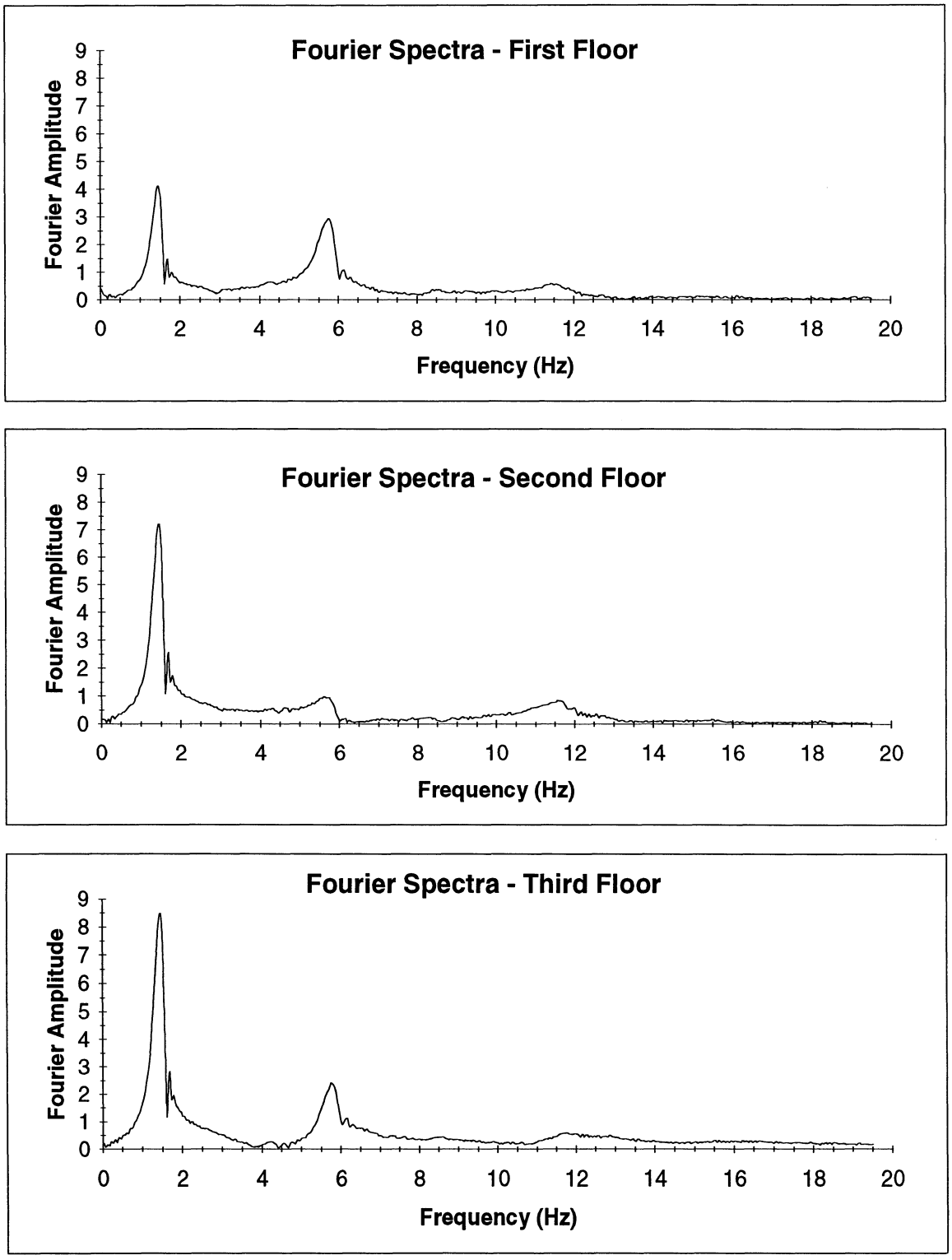

FIGURE 3-4 Experimental Fourier Spectra for Example #2

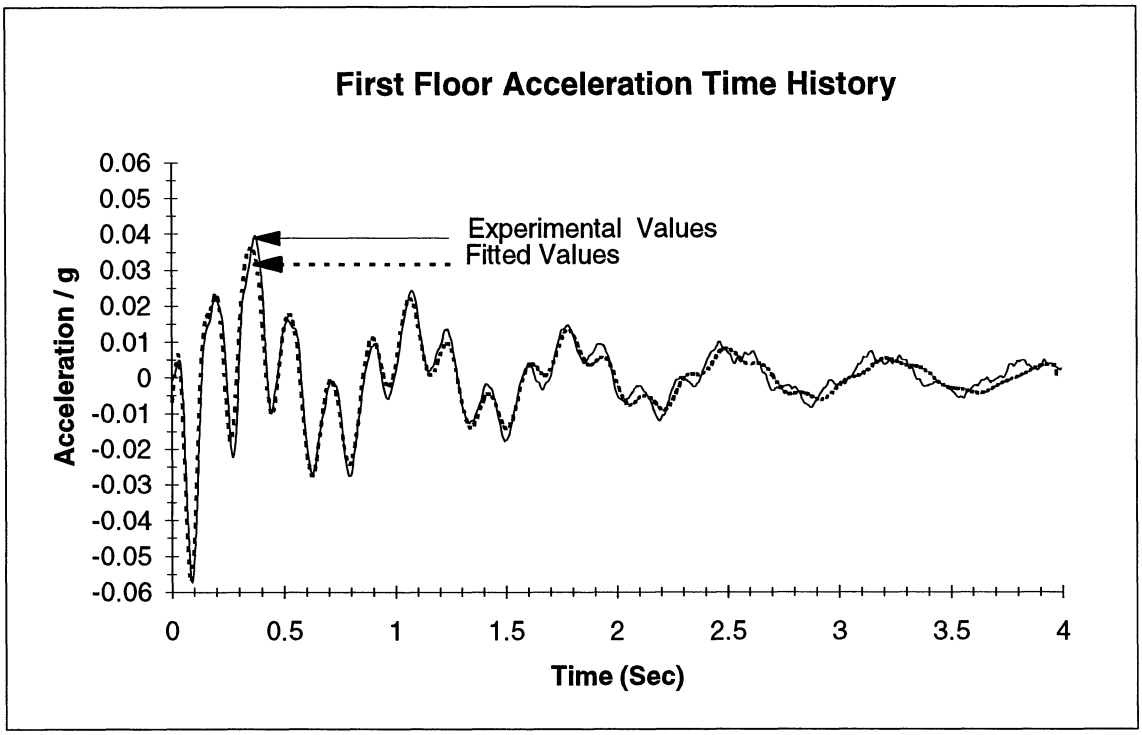

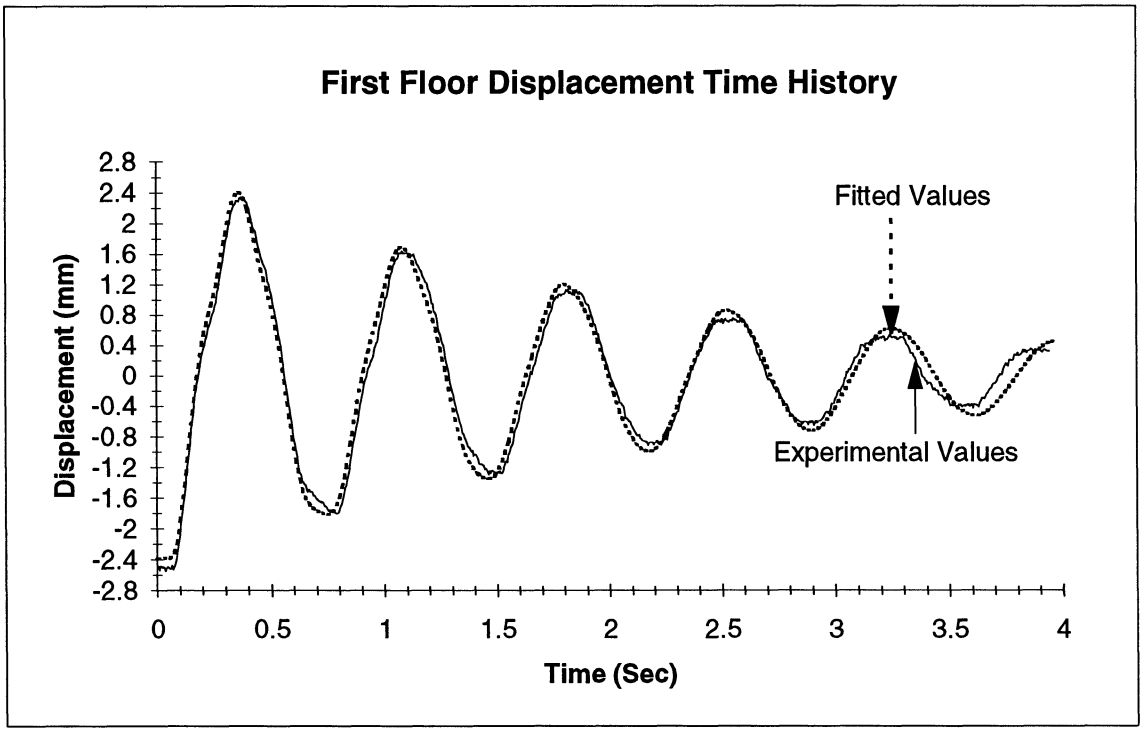

FIGURE 3-5 Experimental and Fitted Values for Example #2

TABLE 3-1 Comparison of the Results for the Example #2

Frequencies

Method		
Time Domain	Fourier Spectra	Transfer Function
Hz	Hz	Hz
1.37	1.44	1.32
5.62	5.76	5.51
11.3	11.52	11.35

Damping

Method		
Time Domain	Fourier Spectra	Transfer Function
% Critical	% Critical	% Critical
0.05	0.08	0.06
0.031	0.054	0.05
0.06	0.02	0.04

Mode Shapes Comparison

Mode Shape Method			**Mode Shape** Method			**Mode Shape** Method		
1.37	1.44	1.32	5.62	5.76	5.51	11.3	11.52	11.35
Time Domain	Fourier Spectra	Transfer Function	Time Domain	Fourier Spectra	Transfer Function	Time Domain	Fourier Spectra	Transfer Function
1	1	1	-0.73	-0.82	-0.74	-0.38	-0.59	-0.52
0.84	0.85	0.86	0.38	0.31	0.28	1	1	1
0.47	0.48	0.51	1	1	1	-0.68	0.69	-0.69

Initial Displacement

Floor	Quick Release	Time Domain
	(mm)	(mm)
1	2.5	2.4
2	4.9	4.6
3	6.6	5.6

predicted displacements in both examples were very close to the displacements observed in the experiment. This clearly shows one advantage of the method. Finally, it can be concluded that the use of this method in combination with the simple frequency domain "peak picking method" is a powerful tool to identify the dynamic characteristics of structures tested using the quick-release test methodology.

3.7 Selected Experimental Results

This section of the report presents selected experimental results obtained from the field experiments performed on the pre-retrofitted bridges. The frequencies and mode shapes were obtained using the methodology described above and from the "Peak Picking Method". This last method is performed computing the Fourier amplitude spectra and the phase spectra for each accelerometer. The frequencies are obtained by reading the ordinates of the graph under a well defined peak. The mode shape in a given direction for a given frequency is estimated by constructing a normalized vector dividing the Fourier amplitude of each accelerometer station by the largest value for the direction being considered. The phase spectra were used to identify the arithmetic sign of the modes.

To avoid errors, several precautions should be taken before the Fourier spectra is computed. For example, augment the time history with enough zeroes to reduce inaccuracies. This and other suggestions can be found elsewhere (Ramirez, 1985; Harris, 1978; Veletsos, 1985). In this project the main concern was to identify the characteristics of the bridge in the transverse direction, which was the direction in which the bridge was excited. The construction of the vertical modes was accomplished using the normalized modes obtained by using the quick-release test data, augmented by the information obtained from the ambient vibration test which oriented deck-level accelerometers in the vertical direction. In order to estimate the longitudinal modes, a normalized vector in the longitudinal direction was computed following the procedure described above. This vector helps in the mode shape identification, providing an estimate of the relative motion between the different locations where the accelerometers were installed. The

damping of each mode was extracted when possible from the Fourier spectra using the classical half power method and from the time domain methods proposed in this study.

Figure 3-6 compares the experimental time histories of transverse deck-level accelerations in each of the three spans with the result of the application of the time domain method presented earlier. As can be seen a good agreement was observed; the frequencies and damping were in conjunction with the initial modal displacement parameters which were extracted from the optimization process. The mode shapes were obtained constructing a normalized vector of the initial modal displacements. Tables 3-2 and 3-3 present the average frequencies and modes shapes obtained using the combined time domain and frequency domain ("peak picking") method. Figure 3-7 presents the frequencies vs damping extracted using this approach.

Figure 3-8 presents the time histories of vertical accelerometers A26 and A27 located on the exterior girder and compares the Fourier spectra of these accelerometers for the ambient vibration and the snap back test. From this figure, it is possible to infer that the vertical modes have one dominant frequency around 4.48 Hz. Also from the graph it can be seen that there is a second frequency around 4.11 Hz which corresponds to the first vertical mode. The figure shows that the results from ambient vibration are similar to the results obtained from the snap back tests demonstrating the use of ambient vibration tests to corroborate the identification of vertical modes.

Figure 3-9 shows time histories of selected accelerations and displacements for the test SBPRE-T2-OP (Southbound one pier test-fuse bar release system). The Fourier spectra of these records are presented in figure 3-10. From the comparison of the Fourier spectra of the accelerometers and the potentiometers reading in the transverse direction it can be seen that there are two well defined peaks between 5.4 and 6.02 Hz. From the Fourier spectra of the longitudinal potentiometer P16, it is possible to see the same two close peaks around the same frequencies. It is clear then that there is not a pure transverse or longitudinal mode. The first modes are coupled in the transverse and longitudinal directions and they are very close. The

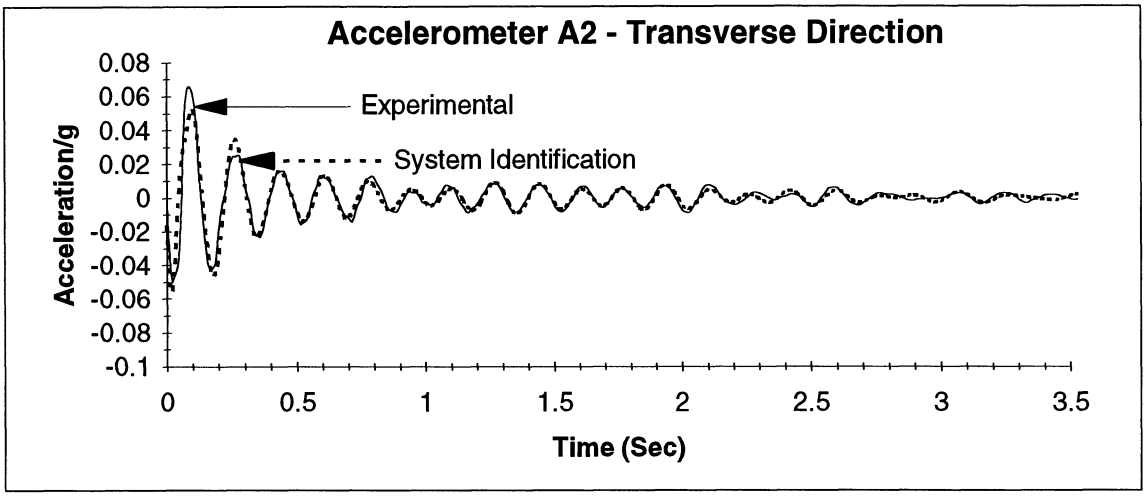

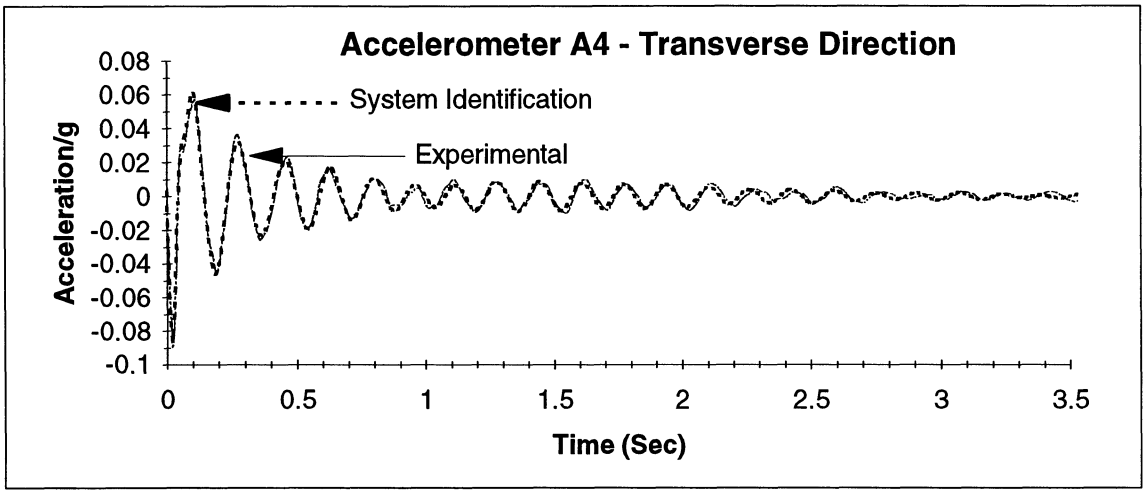

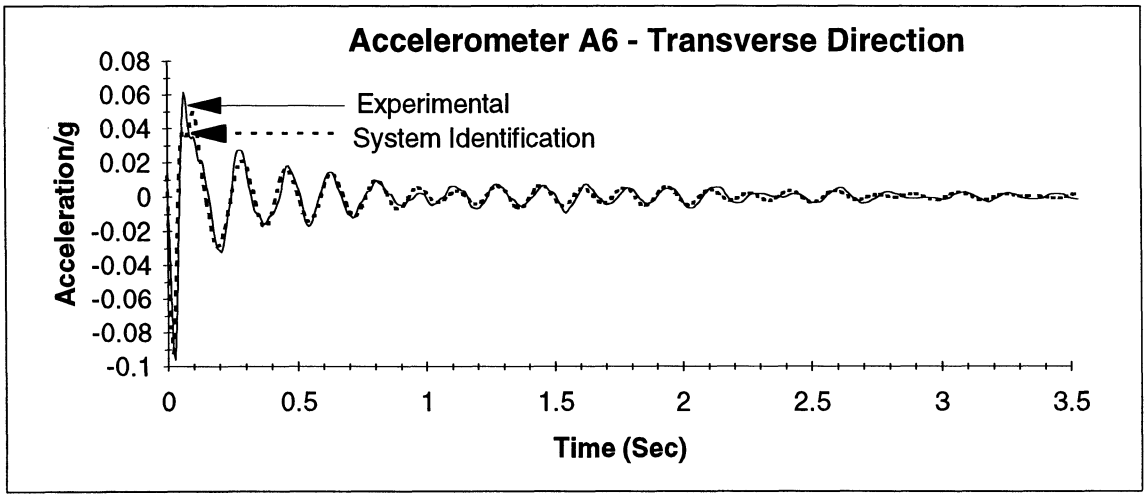

FIGURE 3-6 Experimental and Fitted values for the Test SBPRE-T2-OP

TABLE 3-2 Southbound Bridge-Experimental Frequencies and Mode Shapes

Accel.	Location	Test Type	Direction	Frequency 4.11	4.47
A1	Deck	Ambient vib.	Vertical	-0.25	0.06
A2	Deck	Ambient vib.	Vertical	-0.32	0.07
A3	Deck	Ambient vib.	Vertical	0.63	-0.14
A4	Deck	Ambient vib.	Vertical	0.88	-0.23
A5	Deck	Ambient vib.	Vertical	0.61	-0.15
A6	Deck	Ambient vib.	Vertical	-0.23	0.06
A7	Deck	Ambient vib.	Vertical	-0.19	0.06
A25	Deck	Ambient vib.	Vertical	-0.32	0.19
A26	Deck	Ambient vib.	Vertical	1	-0.73
A27	Deck	Ambient vib.	Vertical	-0.29	0.18
A28	Deck	Ambient vib.	Vertical	-0.2	-0.29
A29	Deck	Ambient vib.	Vertical	0.58	1
A30	Deck	Ambient vib.	Vertical	-0.15	-0.21

				Frequency 4.47	5.44	6.01	9.12
AP3	Deck	Snap Back	Transverse	0.51	0.58	0.65	1
A1	Deck	Snap Back	Transverse	0.75	0.69	0.73	0.88
A2	Deck	Snap Back	Transverse	1	0.88	0.91	0.79
AP9	Deck	Snap Back	Transverse	0.88	0.89	0.92	0.57
A3	Deck	Snap Back	Transverse	0.61	0.98	1	0.37
A4	Deck	Snap Back	Transverse	0.49	1	1	-0.05
A5	Deck	Snap Back	Transverse	0.53	0.98	0.95	-0.56
AP16	Deck	Snap Back	Transverse				
A6	Deck	Snap Back	Transverse	0.75	0.71	0.7	-0.92
A7	Deck	Snap Back	Transverse	0.59	0.57	0.56	-0.94
AP22	Deck	Snap Back	Transverse				
A8	N. Abutment	Snap Back	Transverse	0.3	0.35	0.37	0.61
A13	N. Pier	Snap Back	Transverse	0.59	0.55	0.56	0.45
A19	S. Pier	Snap Back	Transverse	0.49	0.5	0.45	-0.6
A22	S. Abutment	Snap Back	Transverse	0.16	0.17	0.15	-0.32

				Frequency 4.47	5.44	6.01	9.12
A10	N. Abutment	Snap Back	Longitudinal	-0.07	0.09	0.15	-0.13
A12	N. Pier	Snap Back	Longitudinal	-0.75	0.24	0.44	-20
A15	N. Pier	Snap Back	Longitudinal	1	0.22	0.4	-0.04
A18	S. Pier	Snap Back	Longitudinal	0.48	1	1	1
A21	S. Pier	Snap Back	Longitudinal	-0.65	0.82	0.66	0.49
A24	S. Abutment	Snap Back	Longitudinal	0.15	0.12	0.23	0.02

TABLE 3-3 Northbound Bridge - Experimental Frequencies and Mode Shapes

Accel.	Location	Test Type	Direction	Frequency 4.18	4.61	6.91	9.00	12.11
A1	Deck	Ambient vib.	Vertical	-0.19	0.06	0.17	-0.38	-0.24
A2	Deck	Ambient vib.	Vertical	-0.24	0.08	0.2	-0.4	-0.17
A3	Deck	Ambient vib.	Vertical	0.6	-0.24	-0.5	-0.08	-0.28
A4	Deck	Ambient vib.	Vertical	0.84	-0.36	-0.68	-0.06	-0.14
A5	Deck	Ambient vib.	Vertical	0.6	-0.27	-0.47	-0.23	0.25
A6	Deck	Ambient vib.	Vertical	-0.16	0.08	0.12	0.16	-0.62
A7	Deck	Ambient vib.	Vertical	-0.15	0.07	0.11	0.18	-0.65
A25	Deck	Ambient vib.	Vertical	-0.22	-0.18	-0.11	1	0.22
A26	Deck	Ambient vib.	Vertical	1	-0.9	0.77	0.2	0.13
A27	Deck	Ambient vib.	Vertical	-0.16	0.12	-0.07	-0.13	0.75
A28	Deck	Ambient vib.	Vertical	-0.15	-0.19	-0.2	-0.86	0.19
A29	Deck	Ambient vib.	Vertical	0.66	1	1	-0.16	0.13
A30	Deck	Ambient vib.	Vertical	-0.11	-0.15	-0.15	0.23	1

				Frequency 4.61	5.82	6.12
AP3	Deck	Snap Back	Transverse			
A1	Deck	Snap Back	Transverse	0.89	0.72	0.77
A2	Deck	Snap Back	Transverse	1	0.81	0.85
AP9	Deck	Snap Back	Transverse			
A3	Deck	Snap Back	Transverse	0.64	0.96	0.97
A4	Deck	Snap Back	Transverse	0.55	1	1
A5	Deck	Snap Back	Transverse	0.57	0.97	0.97
AP16	Deck	Snap Back	Transverse			
A6	Deck	Snap Back	Transverse	0.75	0.74	0.73
A7	Deck	Snap Back	Transverse	0.62	0.61	0.59
AP22	Deck	Snap Back	Transverse			
A8	N. Abutment	Snap Back	Transverse	0.28	0.3	0.28
A13	N. Pier	Snap Back	Transverse	0.43	0.55	0.56
A19	S. Pier	Snap Back	Transverse	0.44	0.46	0.46
A22	S. Abutment	Snap Back	Transverse	0.22	0.27	0.21

				Frequency 4.61	5.82	6.12
A10	N. Abutment	Snap Back	Longitudinal	-0.16	0.31	0.3
A12	N. Pier	Snap Back	Longitudinal	-0.38	0.82	0.75
A15	N. Pier	Snap Back	Longitudinal	1	0.71	0.6
A18	S. Pier	Snap Back	Longitudinal	0.29	1	1
A21	S. Pier	Snap Back	Longitudinal	-0.76	0.67	0.61
A24	S. Abutment	Snap Back	Longitudinal	0.13	0.2	0.2

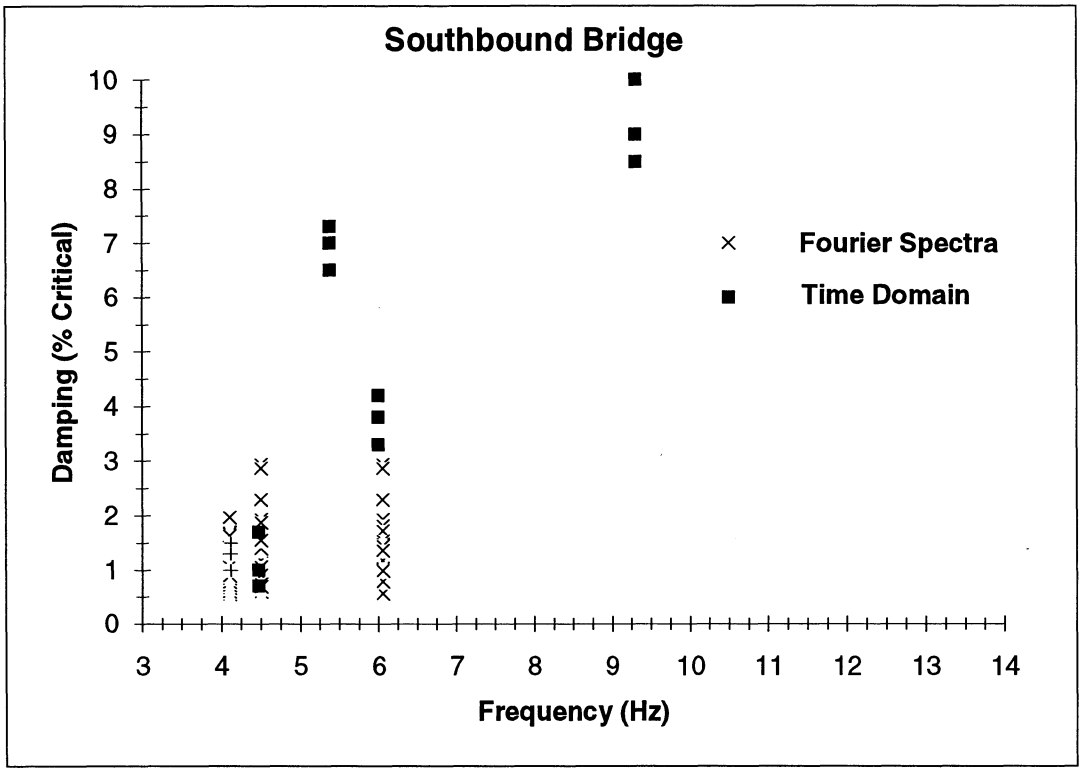

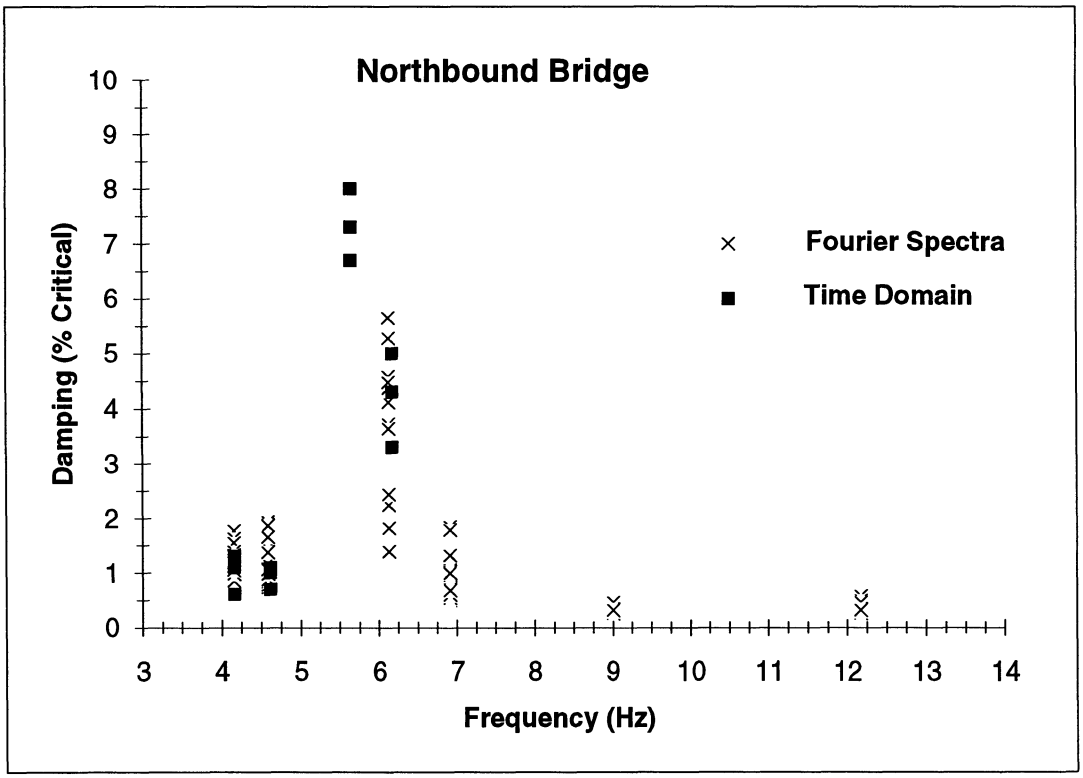

FIGURE 3-7 Average Damping vs Frequency for the Pre-retrofitted bridges

Southbound Bridge Selected Experimental Time Histories

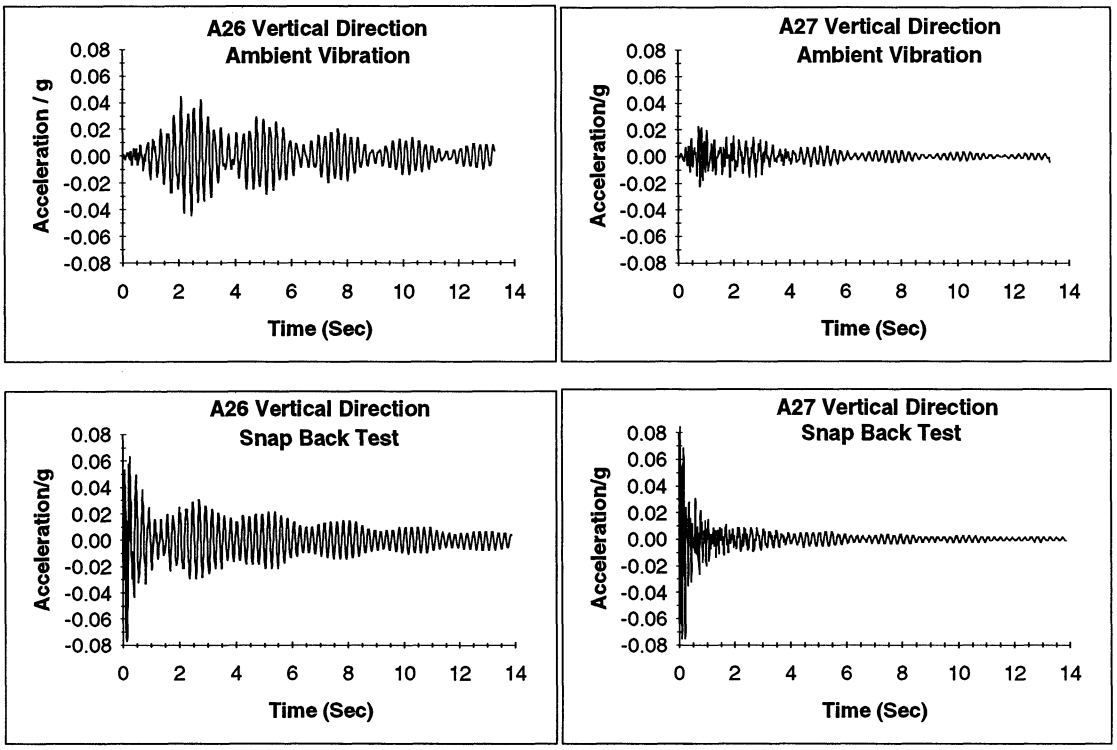

Southbound Bridge Experimental Fourier Spectra

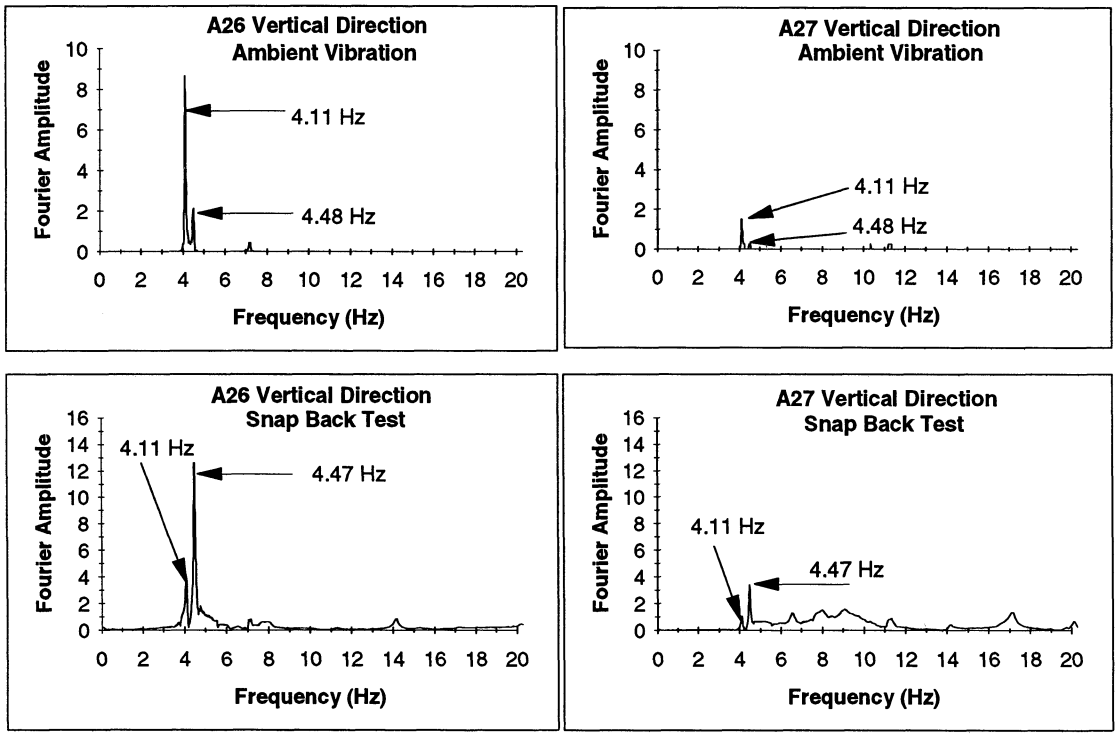

FIGURE 3-8 Ambient Vibration Test #7 vs Snap Back Test SBPRE-T2-OP

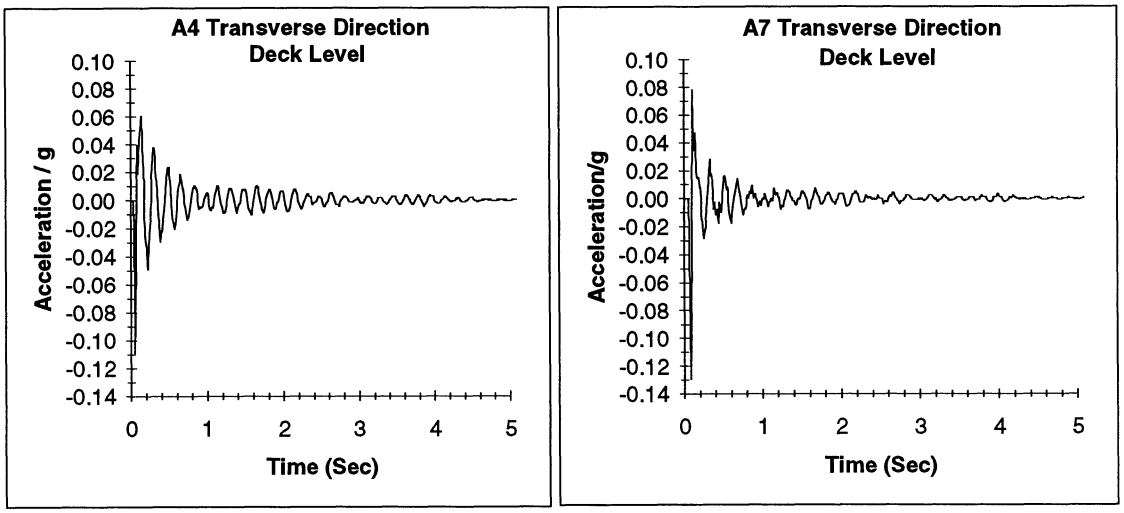

Acceleration

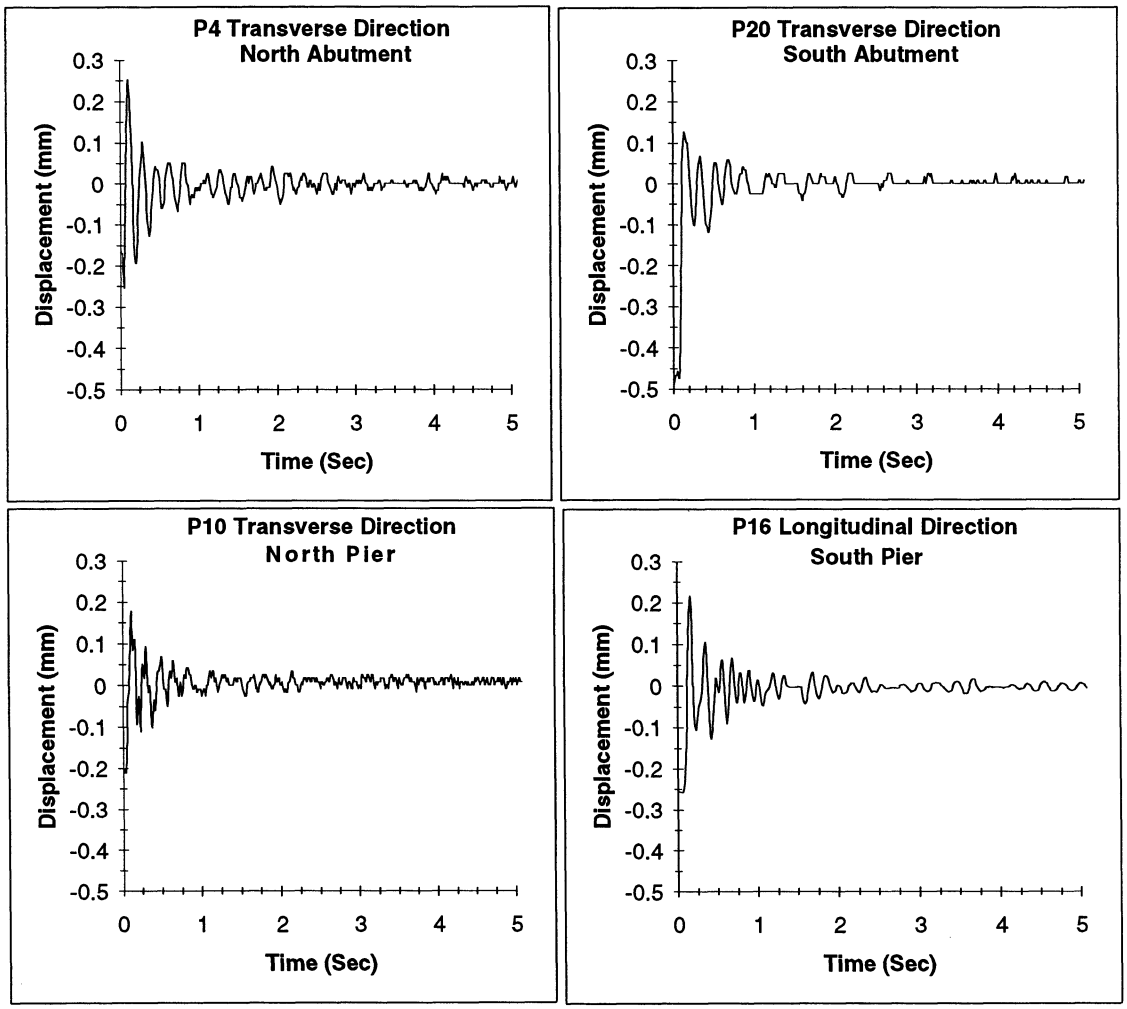

Displacement

Figure 3-9 Time Histories for the Test SBPRE-T2-OP

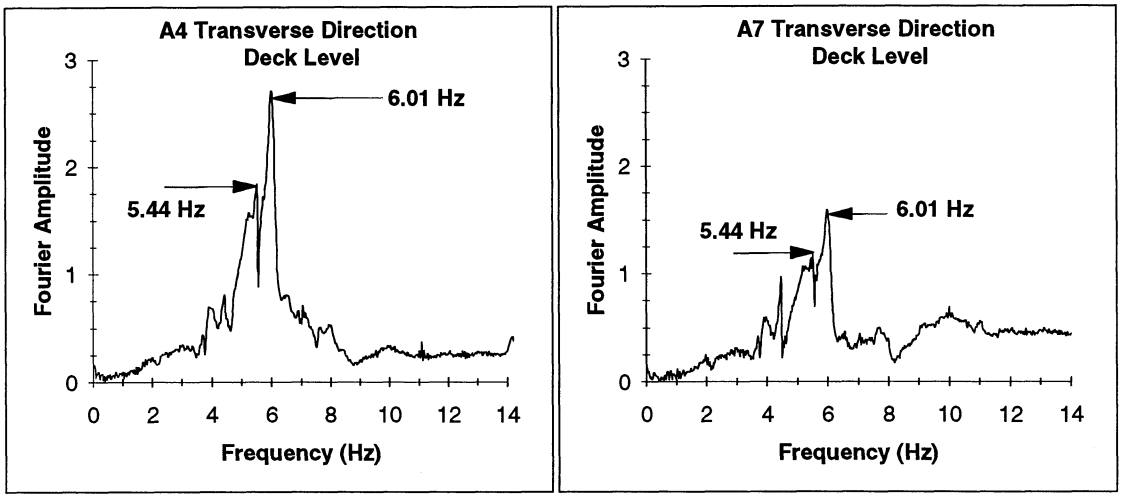

Acceleration

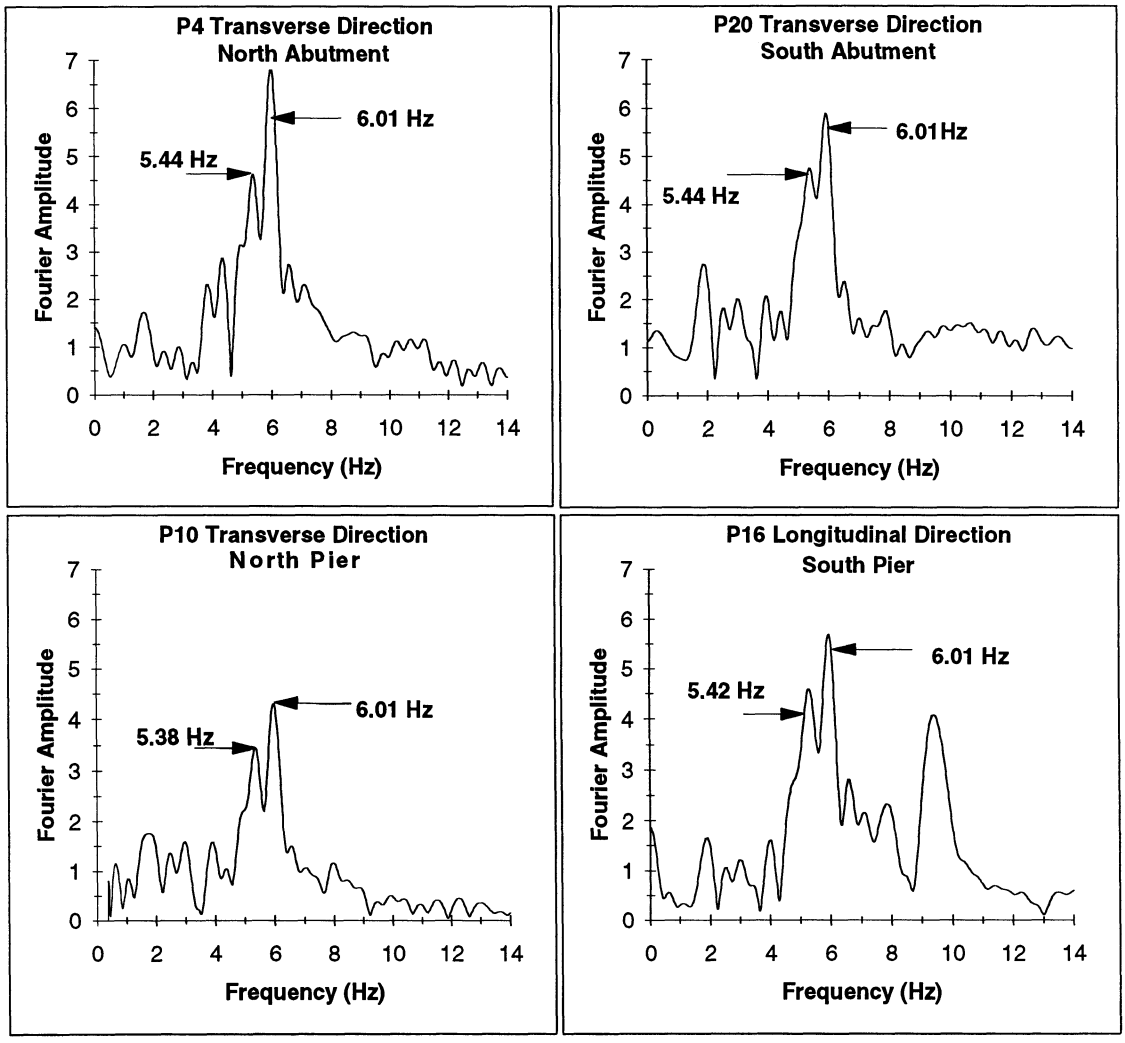

Displacement

Figure 3-10 Fourier Spectra for the Test SBPRE-T2-OP

Fourier spectra show that the snap-back test did not exhibit high frequencies and the peaks located after 10 Hz were very weak.

In order to obtain an estimate of the frequency values in the range between 6 and 10 Hz, two alternatives were evaluated. The first one was the computation of the power spectral density (PSD) after a bandpass filter (with first passband starting at 7 Hz and a first stopband at 20 Hz). The second was more simple and consisted of computing the PSD after two acceleration time histories located at the same distance from the center of stiffness were added or subtracted. The addition tended to cancel the rotational component and increase the translations. The opposite occurs with the subtraction.

Figure 3-11 shows the time history of the load in conjunction with the time history of transverse deck-level accelerometer A7 for the test SBPRE-T2-OP, which had a fuse bar as its release system. From the figure it can be inferred that the time to unload the structure is sufficiently less than a complete cycle of vibration. The graph also shows, however, that the load release is not instantaneous, taking around 40 ms reduce to a value close to zero.

For the Northbound bridge, the data reduction was performed using the same methodology as that described earlier for the Southbound bridge. Figure 3-12 shows the time history of the vertical deck-level accelerometers A26, A27 for the ambient vibration and snap back test. From comparison with the Fourier spectra, characteristics similar to those described previously for the Southbound bridge are evident in the Northbound bridge as well.

Figure 3-13 shows a typical transverse acceleration time history at the deck level of the bridge from one of the quick-release tests. There are typical time histories of free vibration response with the decay in amplitude being dependent on the inherent damping for that mode. It is evident that the vertical damping (A16) is significantly smaller than the longitudinal and transverse directions. Figure 3-14 shows the Fourier spectra of these accelerometers. From the spectra, it can be seen that observed behavior was similar to that described for the Southbound. In the Northbound bridge, the release system used (sudden release of the pressure in the jack)

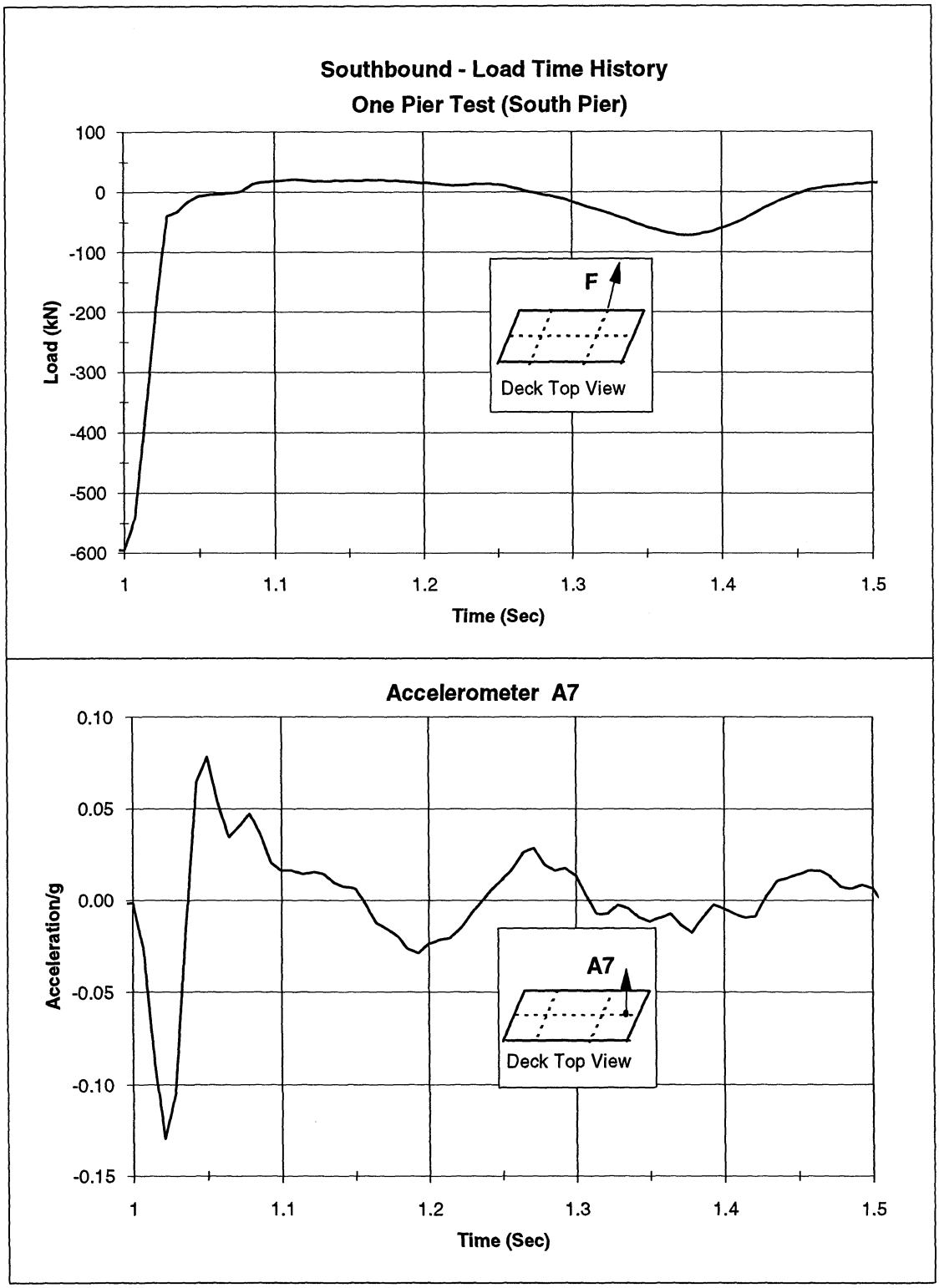

Figure 3-11 Load and Acceleration Time History for the Test SBPRE-T2-OP

Northbound Bridge Selected Experimental Time Histories

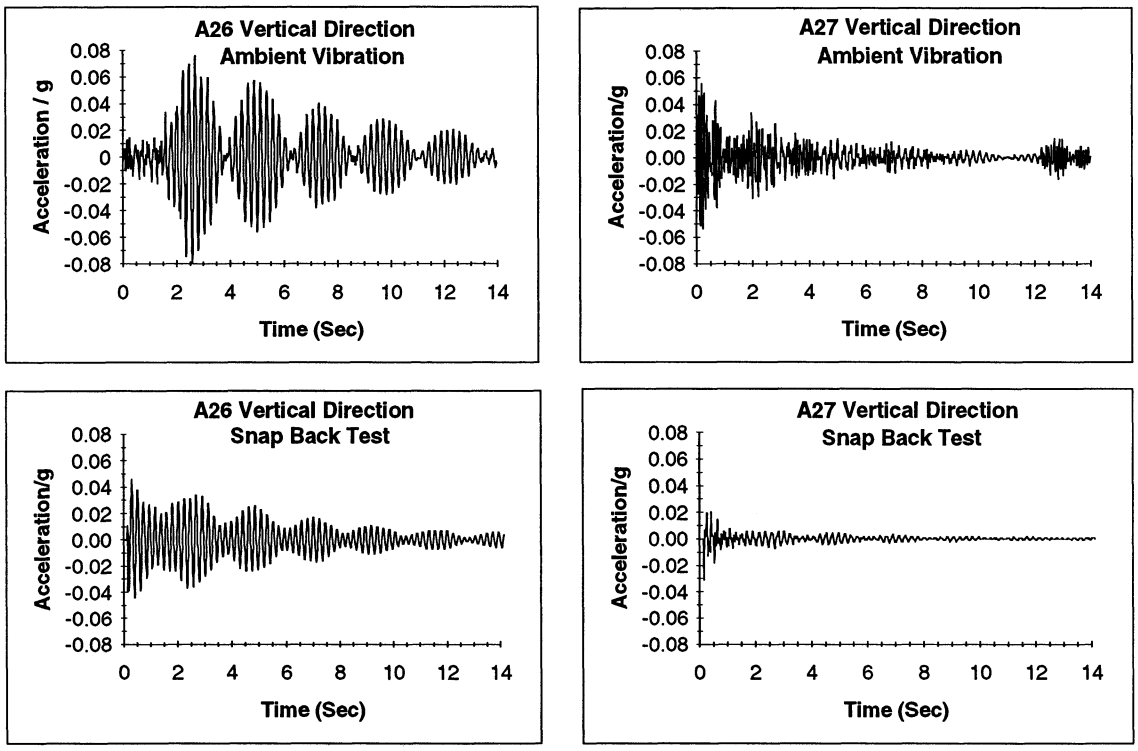

Northbound Bridge Experimental Fourier Spectra

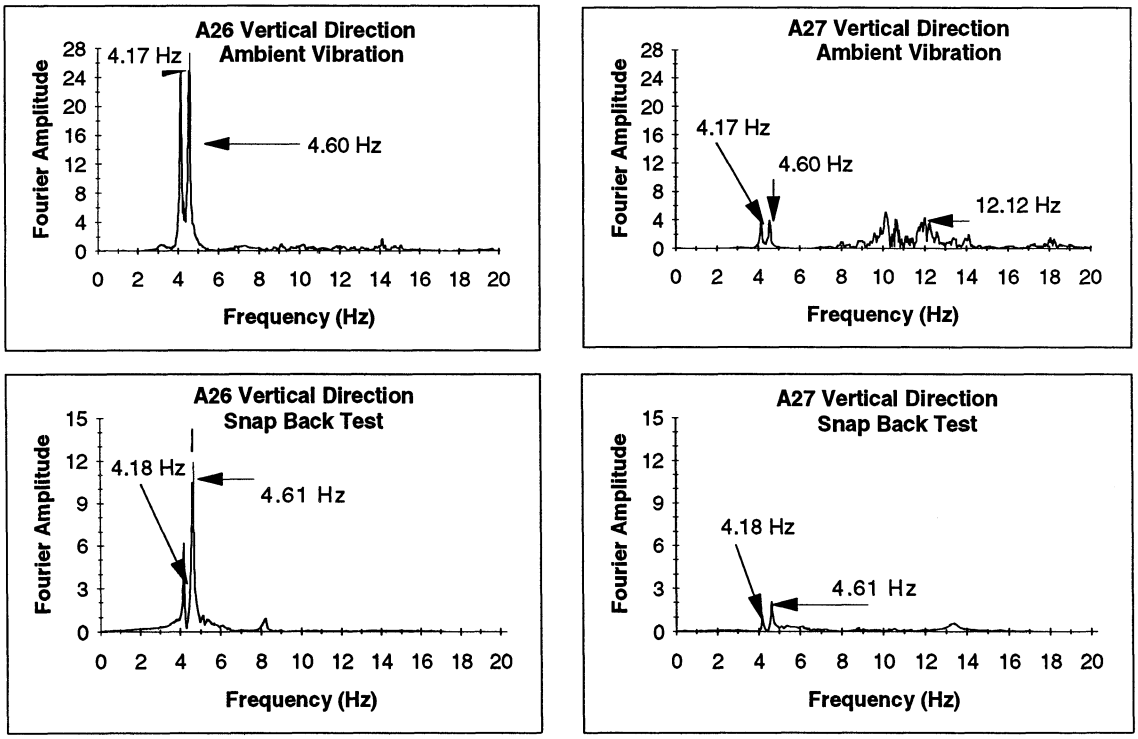

FIGURE 3-12 Ambient Vibration Test #5 vs Snap Back Test NPRE-T3-TP

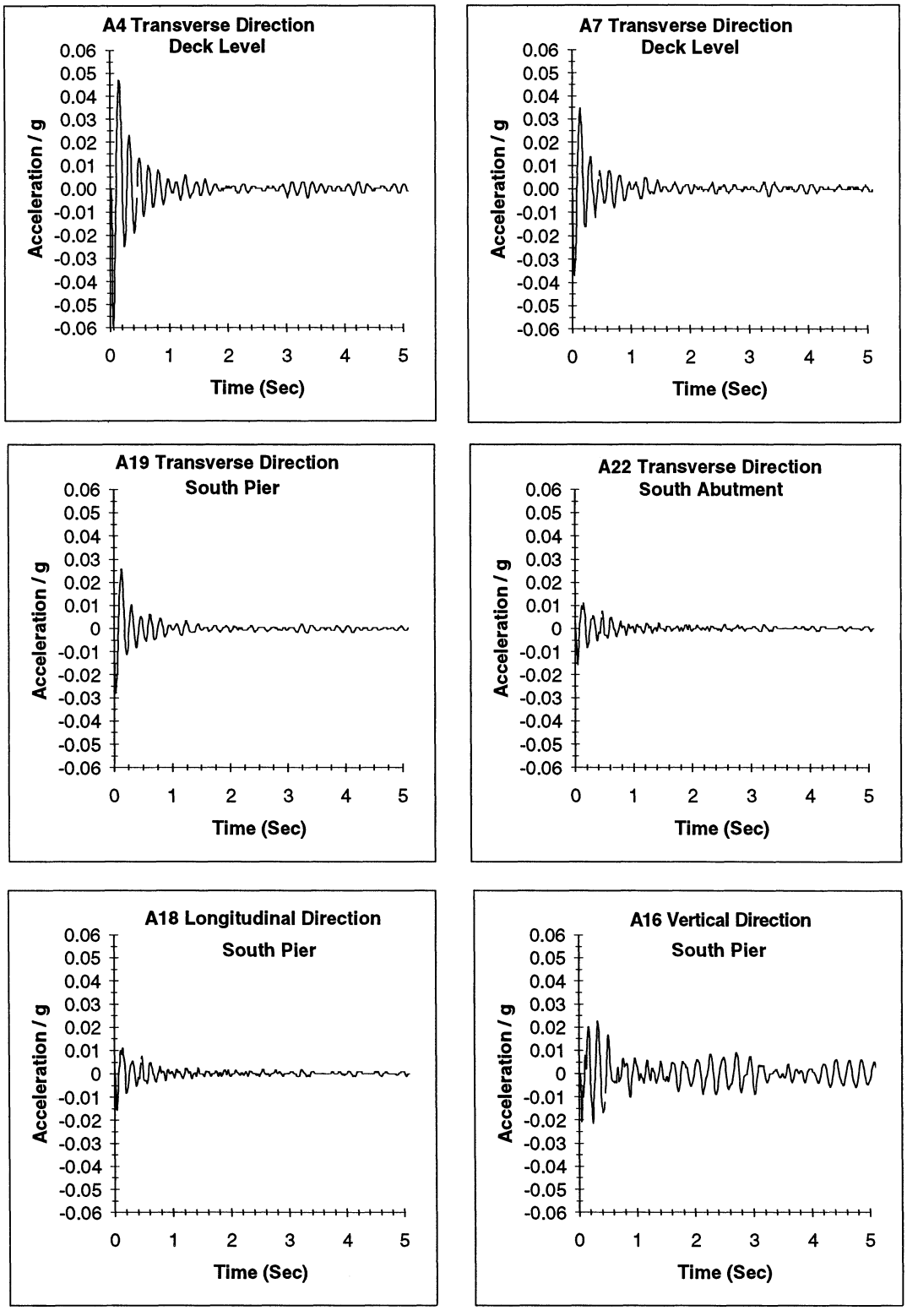

FIGURE 3-13 Acceleration Time History for the Test NPPRE-T3-TP

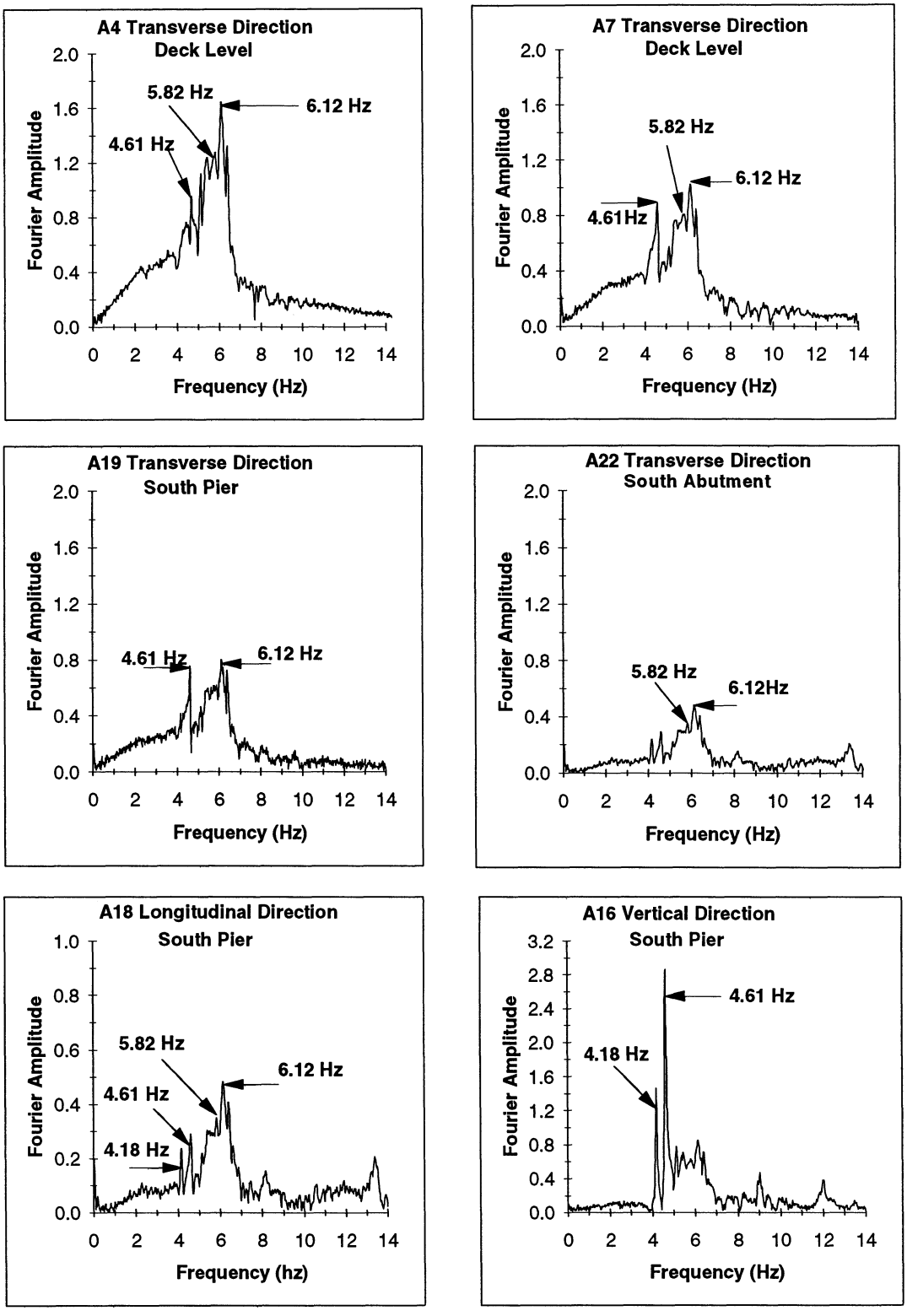

FIGURE 3-14 Acceleration Fourier Spectra for the Test NBPRE-T3-TP

as explained in Section 2 prevented the bridge from reaching higher accelerations. This unfortunately contributed to a poor definition of the predominant frequencies. As for the Southbound bridge, figure 3-15 shows the load time history in conjunction with the acceleration time history of the accelerometer A7 for the test NBPRE-T3-TP. As can be seen, the structure completes the first cycle before it is totally unloaded. The jack unfortunately works in this first portion of the test as a damper, reducing the response of the structure.

This section of this report presents, firstly, the development of tools used to identify the most important dynamic properties from the experimental results. Secondly, it shows some of the results obtained from the test. Section 4 uses these results to construct and calibrate analytical models of the bridges for further predictions.

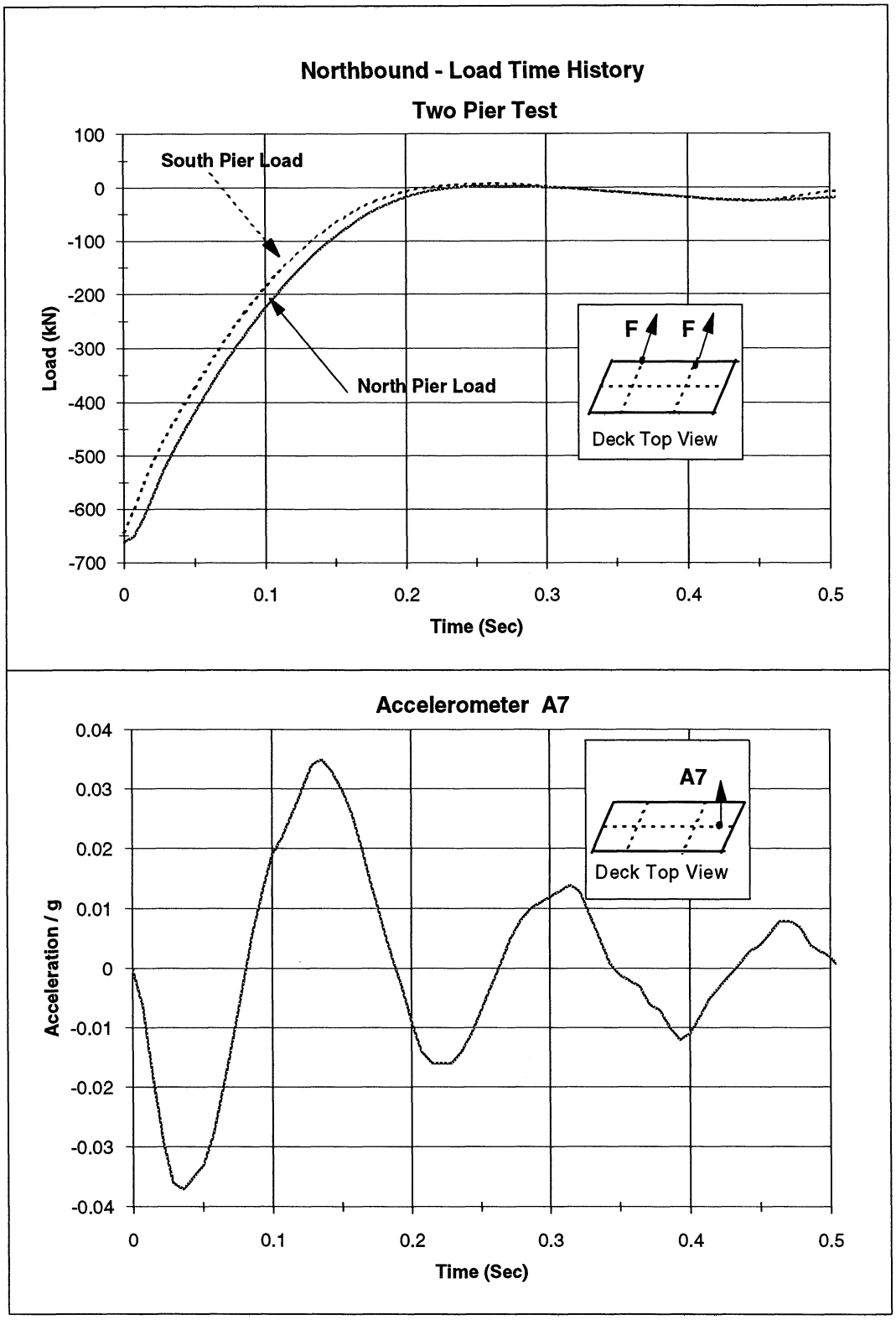

FIGURE 3-15 Load and Acceleration Time History for the Test NBPRE-T3-TP

SECTION 4
COMPARISON OF STRUCTURE MODELING PREDICTIONS WITH THE EXPERIMENTAL RESULTS WHEN THE BRIDGES WERE SEATED ON STEEL BEARINGS

4.1 INTRODUCTION

The main objectives in conducting a full scale experiment are not only to record the behavior of the structure under real site conditions (soil, construction defects, material differences, etc.), but also to use the results to validate, modify or propose analytical modeling techniques that can be used to predict the behavior of the structure under conditions similar to those observed during the experiment. After this objective is achieved, the generated models can be used to investigate the seismic vulnerability of the subject structure.

Due to the fact that both bridges prior to bearing rehabilitation evidently remained linear elastic, it was decided to construct a 3D elastic finite element model of sufficient detail to recapture the salient features observed in the experiments. This model was then adapted to develop a simpler 2D representation that could still capture the essential features of the transverse vibration response. This 2D model could then be augmented to handle nonlinear behavior observed in the post-retrofit experiments and expected under strong excitations.

4.2 ELASTIC 3D FINITE ELEMENT MODEL

The Northbound and Southbound bridge models understandably have similar characteristics, since the bridges were constructed at the same time with similar materials (concrete deck on steel girders). They were assumed to have the same material properties. The general description contained herein is valid for both bridges. Differences between the bridges will be explicitly noted.

The computer program SAP90 (1992), a general purpose elastic finite element program for static and dynamic structural analysis, was used to construct the model presented here. Figure 4-1 presents a general view of the three dimensional model. Figures 4-2 and 4-3 present

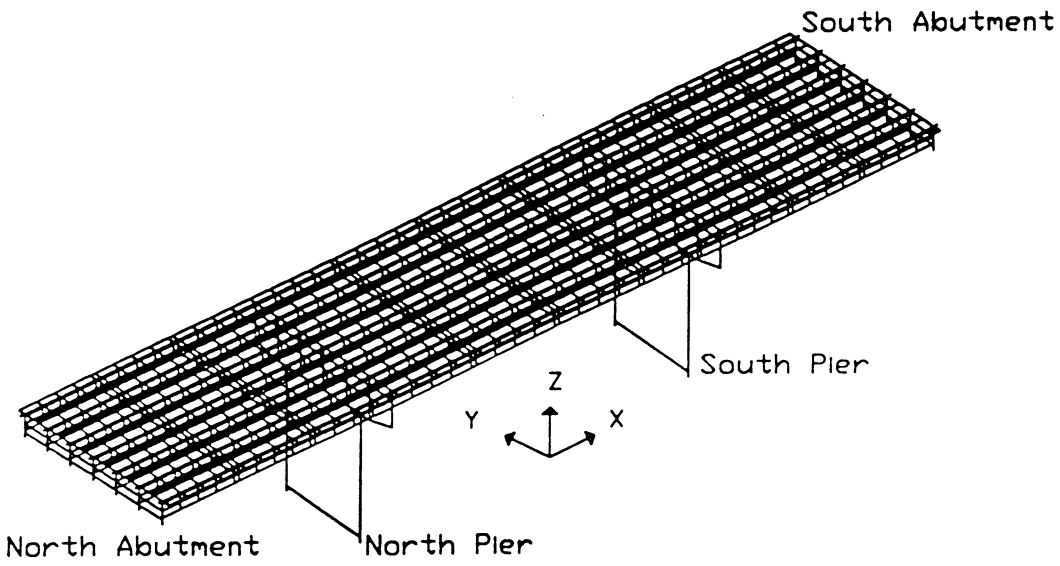

(a) Shell and Frame Elements

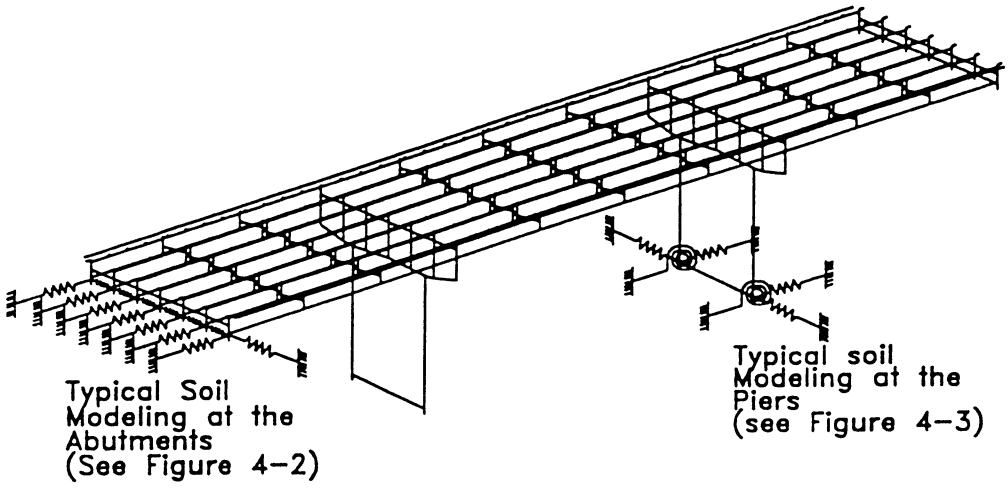

(b) Frame Elements

FIGURE 4-1 General View of the 3D FEM Including the Soil-Interaction Springs

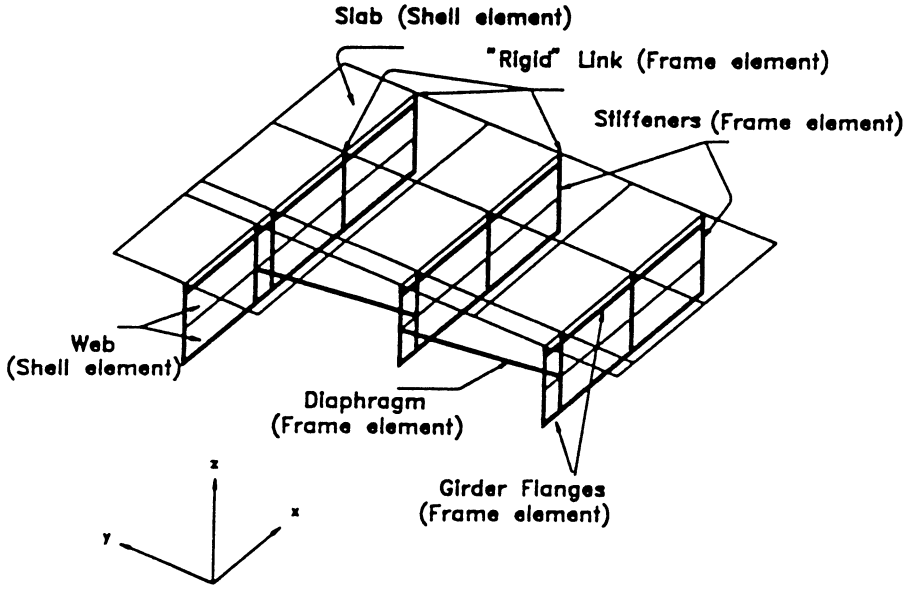

(a) Deck

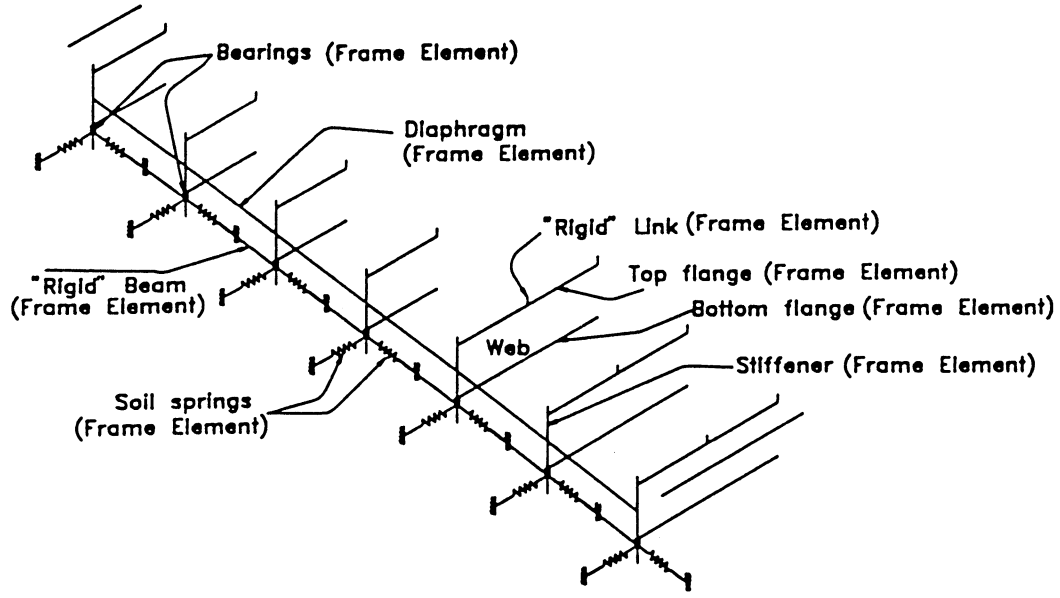

(b) Abutment

FIGURE 4-2 Deck and Abutment Details of the SAP90 3D Finite Element Model

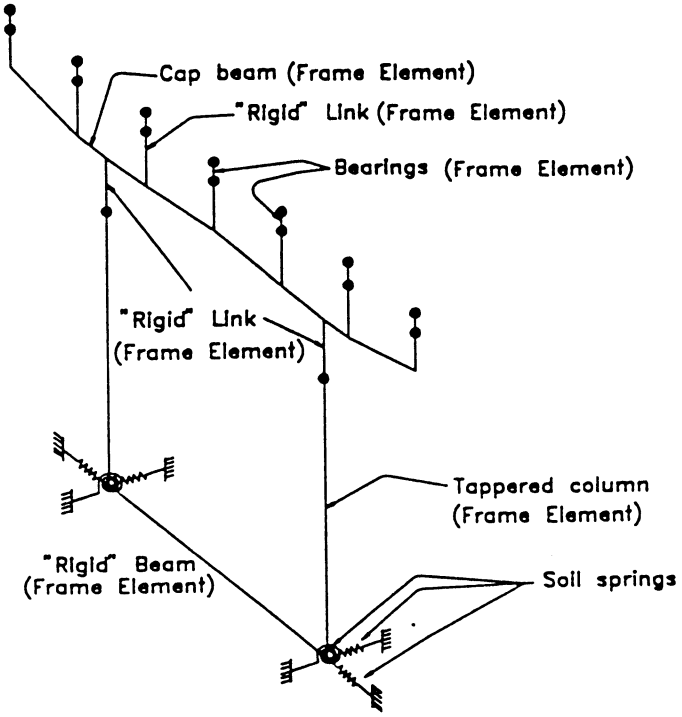

(a) Pier

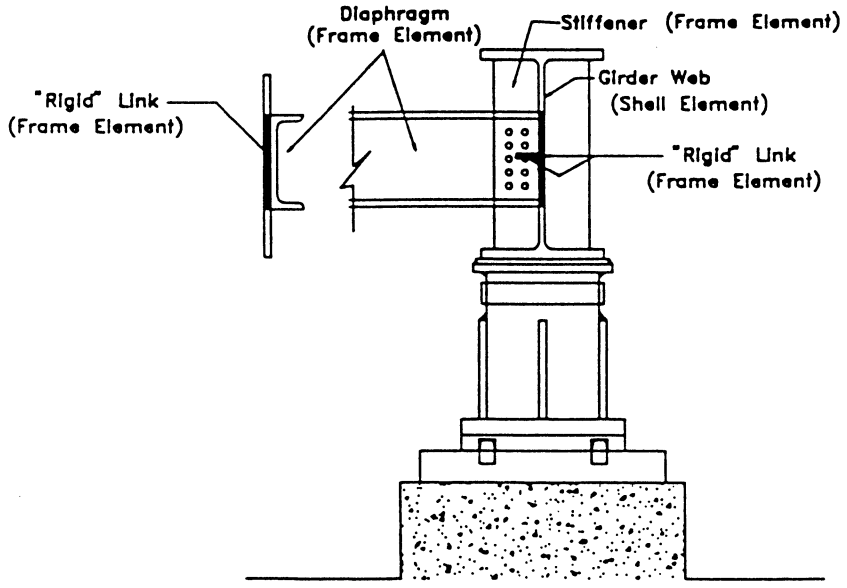

(b) Diaphragm

FIGURE 4-3 Pier and Diaphragm Details of the SAP90 3D Finite Element Model

the model details of the deck, piers, abutment and diaphragm, respectively, and figure 4-4 shows the joint discretization used in this model.

A shell element with membrane and plate bending behavior was selected to model the slab and the web of the girders. Frame elements were used to represent the flanges of the girders. The shell elements of the slab were located in a plane passing through the centroid of the slab and were connected to the tops of the girders using near-rigid links. The properties of these rigid links were defined based on a convergence study whereby the elastic modulus of the links was chosen such that the displacements at the deck and top of the girders were nearly the same. Stiffeners and diaphragms were also included in the model using frame elements. The columns and the cap beams in the piers were modeled using tapered frame elements. Beams with mass per unit length equivalent to that of the pile cap in the piers and that of the pile cap and wall in the abutment were used to model the foundation. The pedestals where the bearings were mounted were considered as an integral part of the near rigid beam illustrated in figure 4-3. This beam was defined between the center of the cap beam and the bottom of the bearings.

At the foundation level, the displacements of the pier joints were constrained in the direction of the soil springs in order to force the foundation of the pier to move as a rigid body. All of the other degrees of freedom at the foundation level were restrained. Similar solutions were adopted in the abutments where the only possibilities of movement were in the direction of the soil springs.

The bearings were modeled using a frame element connecting the bottom girder flange to the foundation level in the abutments and to the top of the pedestal in the piers. The rotation of the top and bottom of the bearings were constrained in the transverse direction of the bridge (strong direction of the bearings) and a pin connection was declared at the top of the bearings in the longitudinal direction of the bridge.

Soil interaction was by included using springs connected to the midplane of the foundation pile cap. The spring values were provided by researchers from the University of

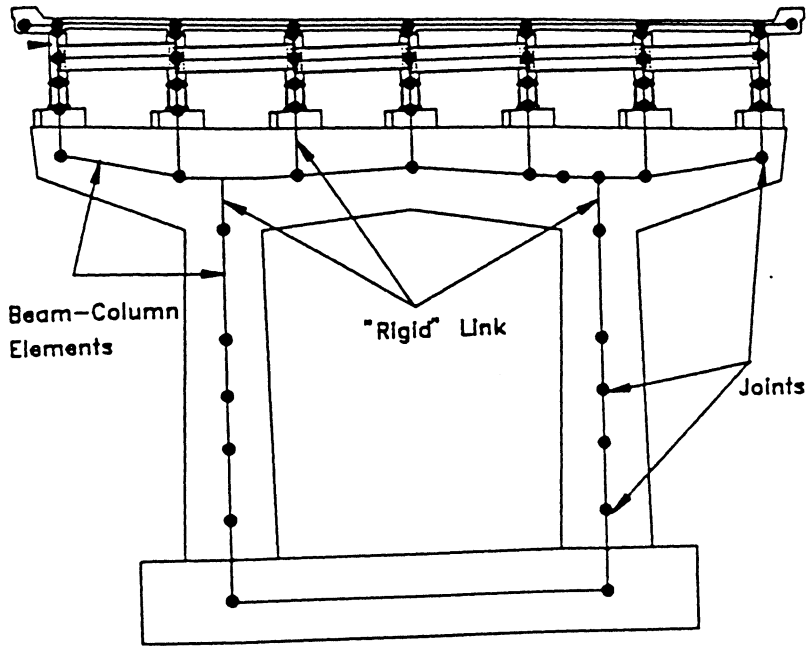

(a) Pier

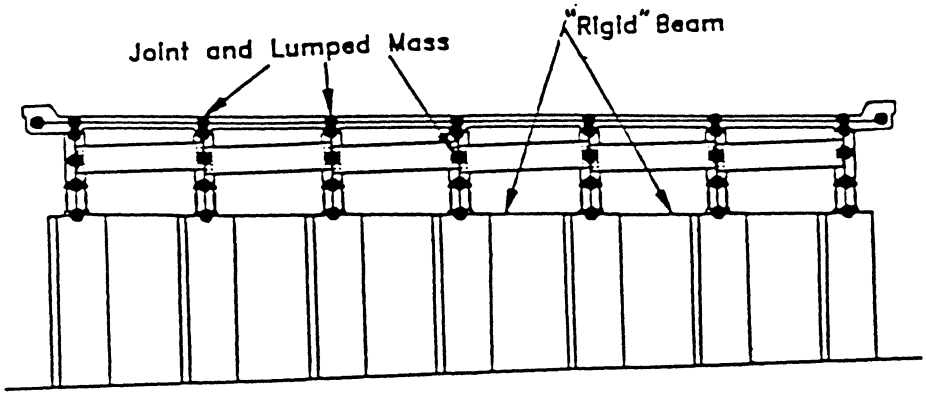

(b) Abutment

FIGURE 4-4 Joint Discretization

Nevada at Reno who undertook companion research for the express purpose of predicting the effects of the foundation and soil on dynamic behavior of the Southbound bridge (Douglas et al., 1994).

Figure 4-5 shows the load vs. deformation and stiffness curve for the piers, and figure 4-6 shows the stiffness vs. load for abutments, respectively. From the foundation and soil characteristics, the companion study used an equivalent linear iterative procedure (Maragakis 1992, 1995) to compute the stiffness versus displacement curves for different load conditions. The methodology proposed by Maragakis et al. is based in an iterative procedure, where the displacement of the foundation system (abutment or pile cap) for a certain load level is obtained after an interactive process. During this process, the strains at different depths in the soil mass are computed, and the properties of the solid element used to model the soil (elasticity and shear modulus) are updated according to the level of strain found. The process is repeated using the same level of load until the difference in between successive iterations is less than 5%.

Three loading cases were used in this study of soil spring stiffnesses. The first case was a lateral load applied to the longitudinal direction of the foundation (transverse to the bridge) and the other two cases were lateral loads and couple loadings applied to the transverse direction of the foundation. Six lateral load and five levels of force couples (emulating overturning moments) were used in the calculation. The companion study found that the soil above the pile cap had a significant influence on the deformation and the stiffness of the foundation. According to this research, the deformation of the foundation model in the longitudinal direction of the foundation (transverse to the bridge), without the soil above the pile cap was more than 40% higher than the model with the soil above the pile cap, correspondingly, the stiffness in the former model was lower than the latter model. As it was shown in figure 2-3, the level of soil in the Southbound bridge was much higher around the north pier than the south pier bent. Therefore, it was decided to use the increased soil stiffness values due to soil level in the north pier and use the regular values for the south pier.

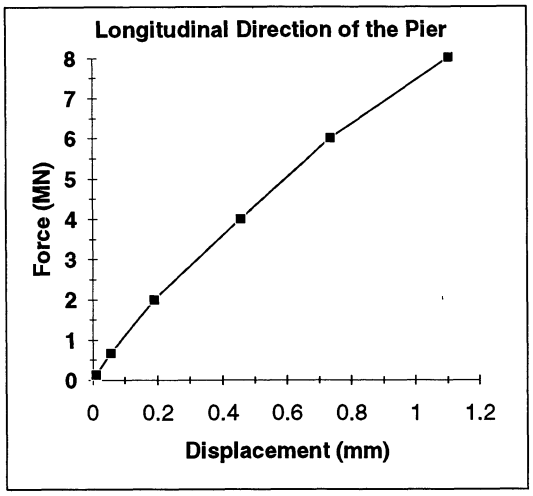

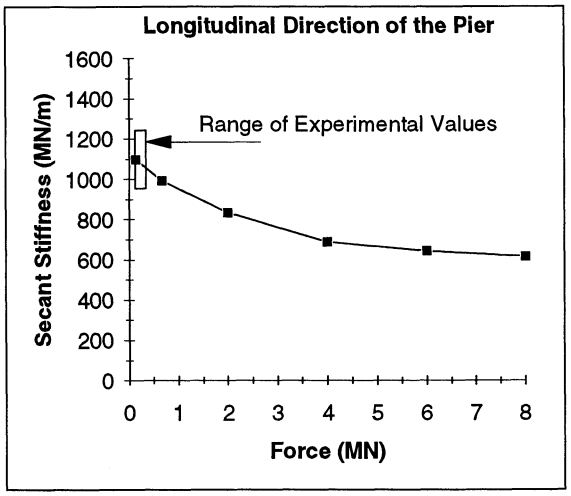

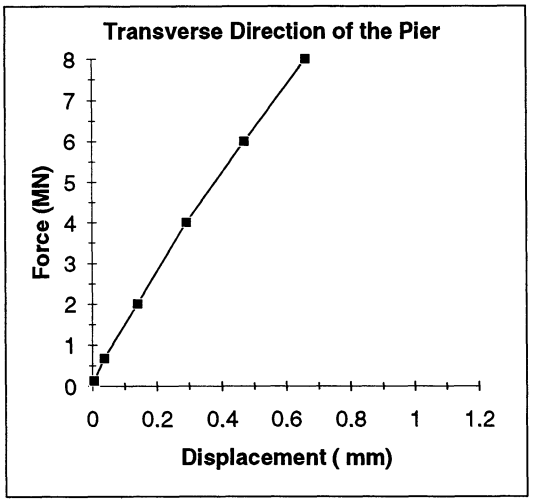

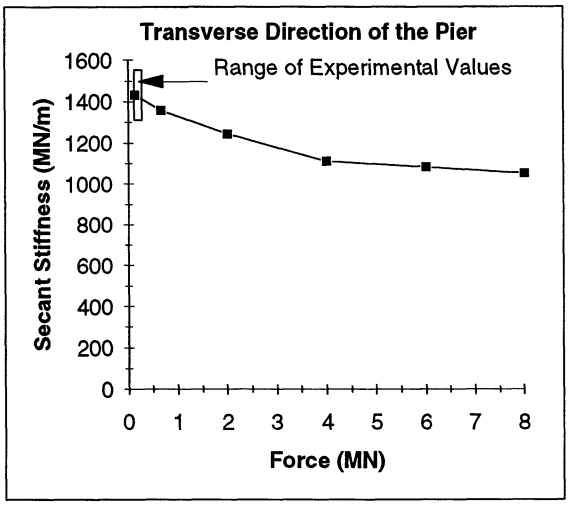

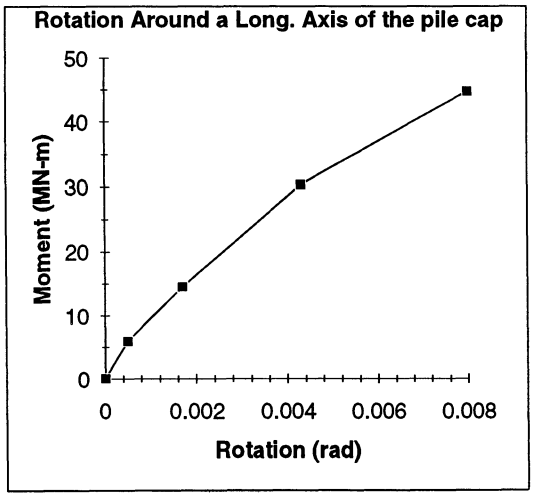

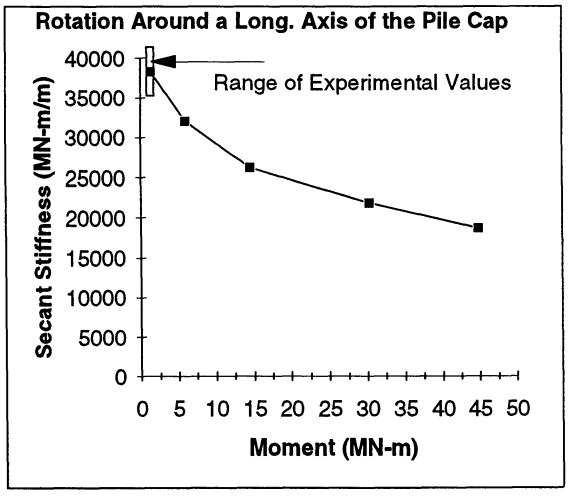

Southbound Bridge - South Pier

FIGURE 4-5 Soil-Structure Interaction Curves for the Pier Bent by Douglas (1994)

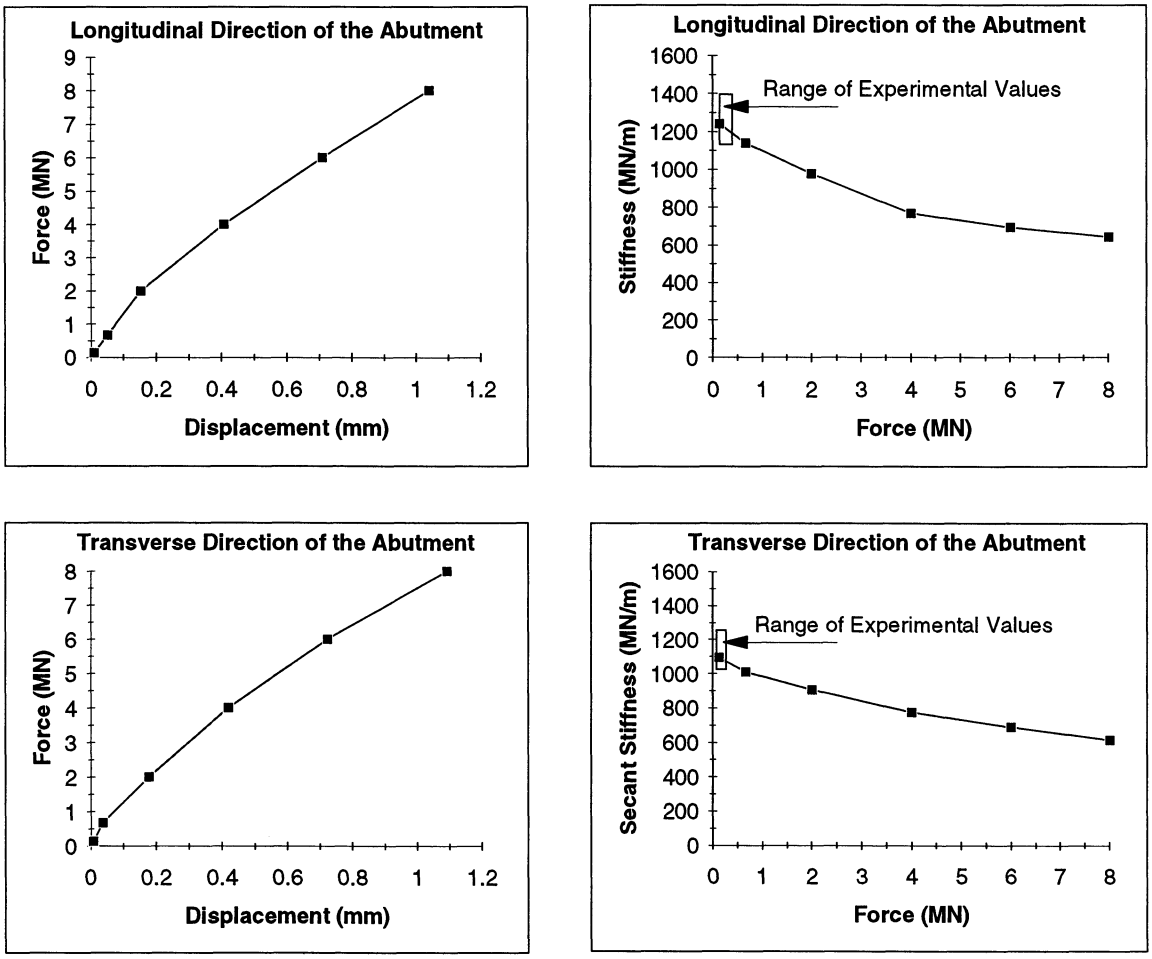

FIGURE 4-6 Soil-Structure Interaction Curves for the Abutment by Douglas (1994)

For the Northbound bridge no explicit information about the soil was available. Due to similarities between the foundation systems, the soil springs' stiffness values were estimated in the abutments by multiplying the Southbound bridge soil springs by a factor of (20/22 = 0.9). This scales the number of piles in the abutment between the Northbound (20) and Southbound (22) bridges. This factor is also close to the average ratio between the dimensions of the pile caps.

It should be emphasized that there are differences between the number of piles and the amount of soil over the pile caps of the Northbound and Southbound bridges as described previously in Section 2. Douglas reported that the amount of soil over the pile cap produced a significant increase in the stiffness of the foundation. In the Northbound piers, there is only 1.2 m of clear distance between the ground and the bottom of the cap beam. This situation made it difficult to define soil spring values, especially considering the soil around the bridge pier columns was loose. In the absence of a specific analysis, values scaled from the Southbound bridge were adopted for this study.

It is important to mention that the soil spring stiffness values provided by Douglas for the Southbound bridge and the modification of these values for the Northbound bridge were used only as an initial estimate. A sensitivity study was conducted in order to investigated the effect of each kind of spring on the dynamic behavior (frequencies and mode shapes). With this information several changes in the initial values were made in order to obtain a better agreement between the analytical predictions and the experimental results. In most of the cases the initial values for the Southbound bridge were near to the final values; only in the abutment was it necessary to make some minor adjustments.

In the Northbound bridge, due to the large amount of soil surrounding the pier bents and the low level of acceleration observed during the tests, the identification of soil springs and bearings stiffness was difficult. The results reported in table 4-1 are in the transverse direction of the bridge, showing a good correlation with the values found for the Southbound bridge.

TABLE 4-1 SAP90-3D Finite Element Model
Properties for Bridges Seated on Steel Bearings

Southbound Bridge SAP90 Model			Northbound Bridge SAP90 Model		
Description			**Description**		
General Properties	**Values**	**Units**	**General Properties**		MPa
Concrete Strength	41	MPa	Concrete Strength	41	MPa
Concrete Modulus	30442	MPa	Concrete Modulus	30442	
Concrete Poisson Ratio	0.20		Concrete Poisson Ratio	0.20	MPa
Concrete Shear Modulus	12684	MPa	Concrete Shear Modulus	12684	kN/m^3
Concrete Unit Weight	24	kN/m^3	Concrete Unit Weight	24	MPa
Steel Modulus	200000	MPa	Steel Modulus	200000	MPa
Steel Poisson Ratio	0.30		Steel Poisson Ratio	0.30	
Steel Unit Weight	77	kN/m^3	Steel Unit Weight	77	kN/m^3
Bearings Stiffness	(Per Brg)		**Bearings Stiffness**	(Per Brg)	
North Abut. Transverse	227	kN/m	North Abut. Transverse	227	kN/m
North Abut. Longitudinal	1000	kN/m	North Abut. Longitudinal	133	kN/m
North Pier Transverse	65	kN/m	North Pier Transverse	65	kN/m
North Pier Longitudinal	10	kN/m	North Pier Longitudinal	243	kN/m
South Pier Transverse	65	kN/m	South Pier Transverse	65	kN/m
South Pier Longitudinal	2	kN/m	South Pier Longitudinal	243	kN/m
South Abut. Transverse	267	kN/m	South Abut. Transverse	267	kN/m
South Abut. Longitudinal	1000	kN/m	South Abut. Longitudinal	133	kN/m
Total Soil Stiffness			**Total Soil Stiffness**		
North Abut. Transverse	1226	MN/m	North Abut. Transverse	1051	MN/m
North Abut. Longitudinal	978	MN/m	North Abut. Longitudinal	1182	MN/m
North Pier Transverse	1095	MN/m	North Pier Transverse	1459	MN/m
North Pier Longitudinal	1299	MN/m	North Pier Longitudinal	1459	MN/m
North Pier Rotational	3430	MNm/rad	North Pier Rotational	12202	MNm/rad
South Pier Transverse	919	MN/m	South Pier Transverse	1459	MN/m
South Pier Longitudinal	1051	MN/m	South Pier Longitudinal	1459	MN/m
South Pier Rotational	2686	MNm/rad	South Pier Rotational	12202	MNm/rad
South Abut. Transverse	1481	MN/m	South Abut. Transverse	1182	MN/m
South Abut. Longitudinal	949	MN/m	South Abut. Longitudinal	1182	MN/m
Masses			**Masses**		
Total Mass Abutments	445	tonne	Total Mass Abutments	347	tonne
Total Mass Piers	193	tonne	Total Mass Piers	129	tonne
Total Mass Pile Caps	265	tonne	Total Mass Pile Cap	170	tonne
Total Mass Deck	689	tonne	Total Mass Deck	555	tonne
% Gross Inertia			**% Gross Inertia**		
Abutment	100	%	Abutment	100	%
Piers	100	%	Piers	100	%

Note: 1 tonne = 1 Mg = 1000 Kg mass, the weight of 1 tone mass = 9.81 kN

However, in the longitudinal direction of the bridge (transverse to the excitation), the value reported are only estimated from error minimization analyses.

Due to the fact that the contractor had removed approximately the first 75 mm of the concrete deck and cast a new overlay before any tests were conducted, the gross moment of inertia was used for the concrete slab (no reduction in the moment of inertia by cracking). A visual inspection of the robust piers and a preliminary analysis showed that the same assumption could be used for the piers. In both cases (assuming that the concrete had gained 50% in strength during the last 28 years in accordance with recommendations of Buckle and Friedland (1995), the concrete strength of 41 MPa with a concrete modulus of 30441 MPa and unit weight of 24 kN/m^3 were used for the deck slabs and piers. These and other important properties of the 3D Finite element model are presented in table 4-1. The bearing stiffness and the soil stiffness values reported in table 4-1 and used in the 3D FEM were obtained after some adjustments were made to the initial values provided by the references (Douglas, 1994; Mander 1996). The adjustments were made assuming that in most of the cases, the provided values were accurate with a tolerance of $\pm 15\%$. This variation accounts for field conditions that are not reflected in the laboratory tests of the bearings or in the analytical predictions of soil behavior. With this tolerance, several trials were done, and the pattern of change extracted. With this information, a correction in the model stiffness values were made in order to obtain a better fitting between the experimental and analytical prediction. The mass of the superstructure (girders, deck, etc.) and foundation were determined from the drawings. Due to the high initial stiffness of the bearings in comparison with the expansion joint, it was decided not to include these in the model because of the insignificant contribution of the joint to the overall stiffness.

4.3 Simplified 2D Finite Element Model

The use of a 3D finite element model is highly recommended when the characteristics of the structure require special consideration, but it is admittedly overly complex for routine structures like those investigated in the present study. If the structure does not behave elastically, the use of a complex 3D model considerably increases the computer analysis time and makes impractical the use of this approach when a parametric or approximate study is to be

done. However, perhaps more importantly, the availability of such models is questionable and 2D nonlinear models need to be resorted to instead. Thus this subsection describes the construction of a 2D finite element model which is intended to be used not only for linear behavior of the pre-retrofit bridges, but also for subsequent study of the non-linear behavior of the post-retrofit bridges.

In order to produce a general model, the derivations were conducted using basic principles of mechanics and dynamics. The model was designed to be used with the program DRAIN-2DX (Prakash et al. 1992). At this style of system identification analysis, only the bearings and soil were considered to be able to reach the inelastic range. The basic concept used to construct the simplified model is illustrated in figure 4-7. The model is formed by layers that represent different portions of the structure. Each layer is formed by one or more structural elements that are connected with the contiguous layer only at specific points where the load is transferred ("A" and "B"). Any load applied for example at layer 1 will "travel" through all of the layers before reaching the support. Thus, the total deformations at the point where the load was applied is the sum of the deformation of each individual layer. Figures 4-7 to 4-14 help provide an understanding of the 2D model used in this study and the following description of the parameters' computation.

Figure 4-8 shows the general description of the different layers and figure 4-9 the numeration used in this model. In this figure it can be seen by what load path inertial forces applied to the deck (layer #1) transfer to the diaphragms and then to the bearings (both in layer #2). Finally the forces pass through the cap beam and pier bents before reaching the pile cap or directly to the foundation at the abutments. All of these elements plus the soils springs belong to the layer #3. The "rigid" links observed in layer #1 which represent the slab at each support force the joints 1, 5, and 9 at the north abutment for example to translate the same amount as the center of the slab defined by joint 13. This assumption is equivalent to saying that all of the points located in the slab over the supports have the same transverse or longitudinal displacement. The definition of these rigid links allows the installation of two groups of diaphragms and two groups of bearings. Each group of diaphragms or bearings re-

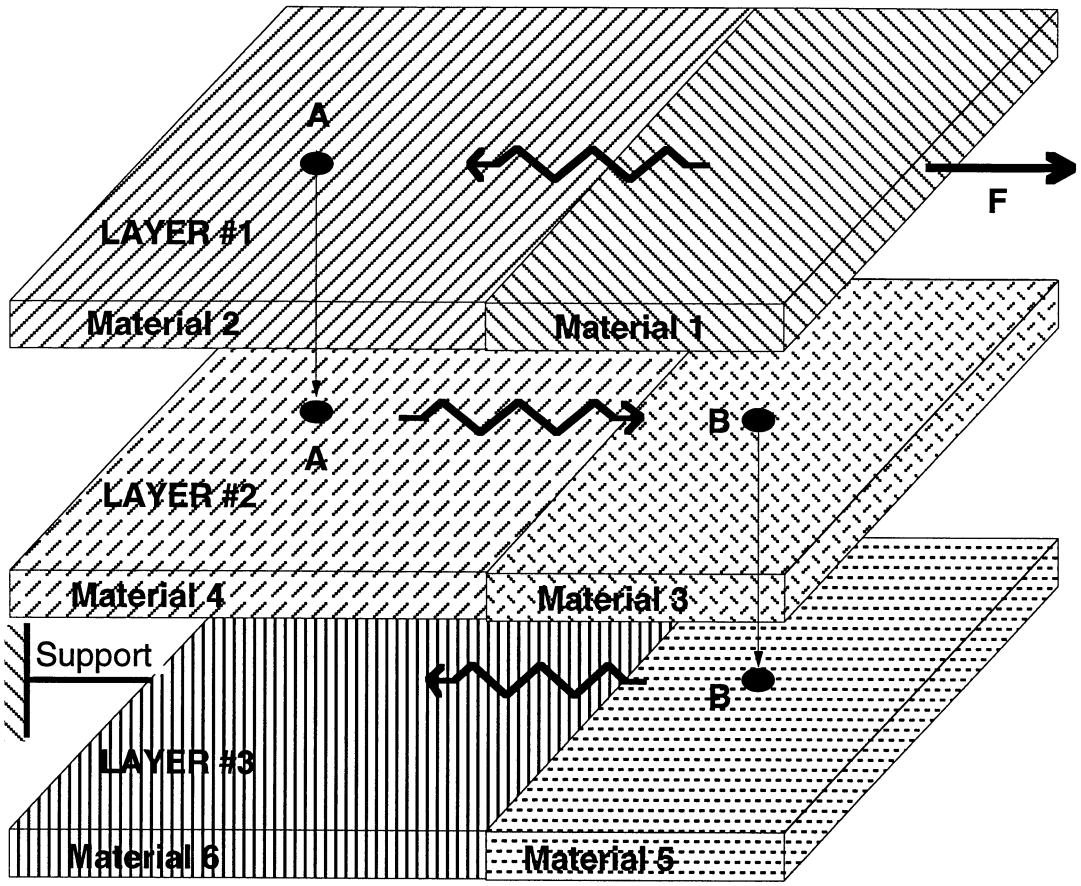

(a) Conceptual Load Path

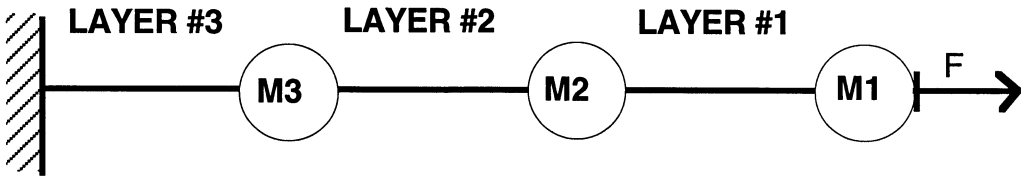

(b) Schematic Representation of the 2D Model

FIGURE 4-7 Basic concept of the Simplified Model

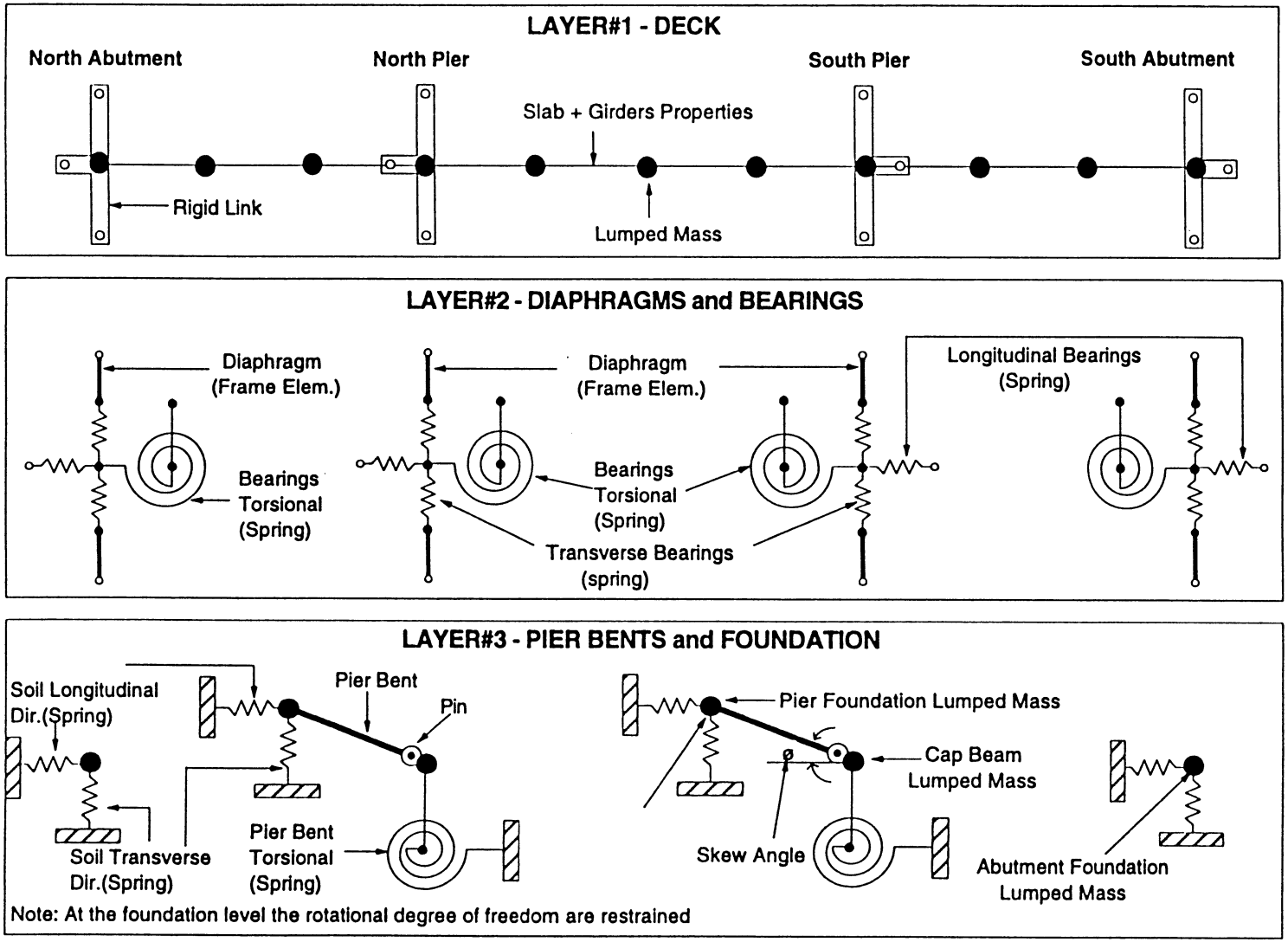

FIGURE 4-8 Simplified DRAIN2DX model - Components Description

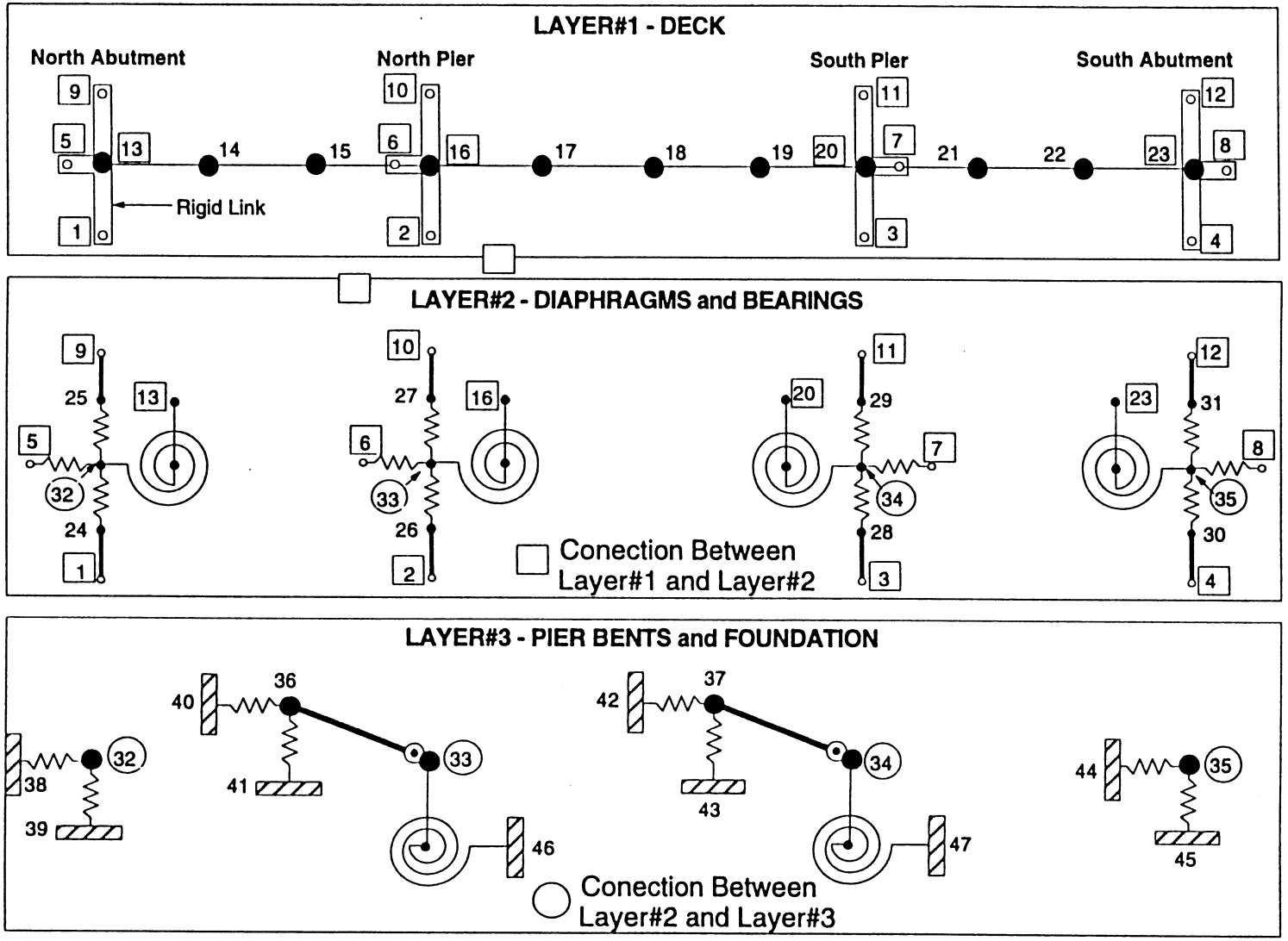

FIGURE 4-9 Simplified DRAIN2DX Model - Members Connectivity

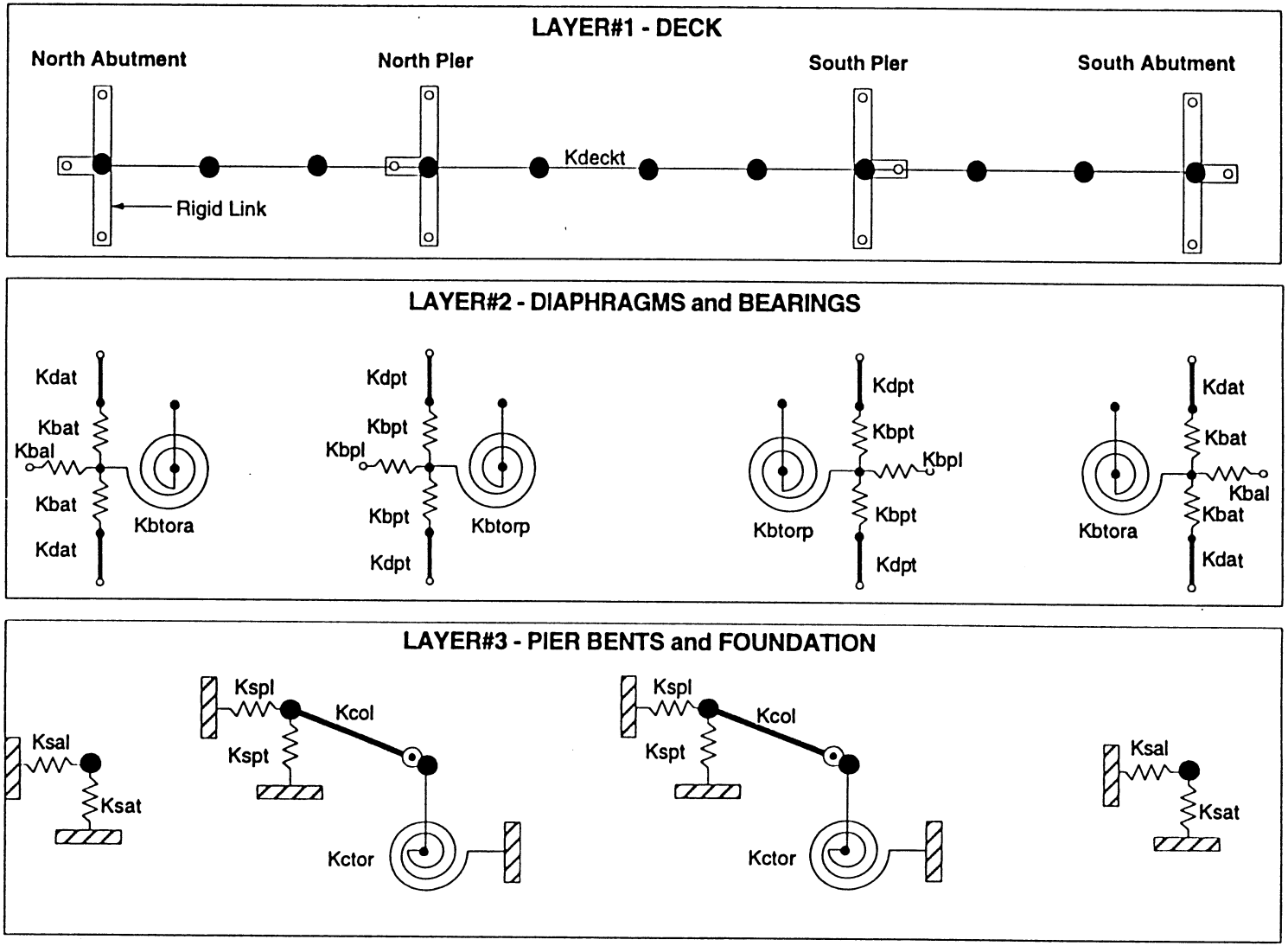

FIGURE 4-10 Simplified DRAIN2DX Model - Stiffness Nomenclature

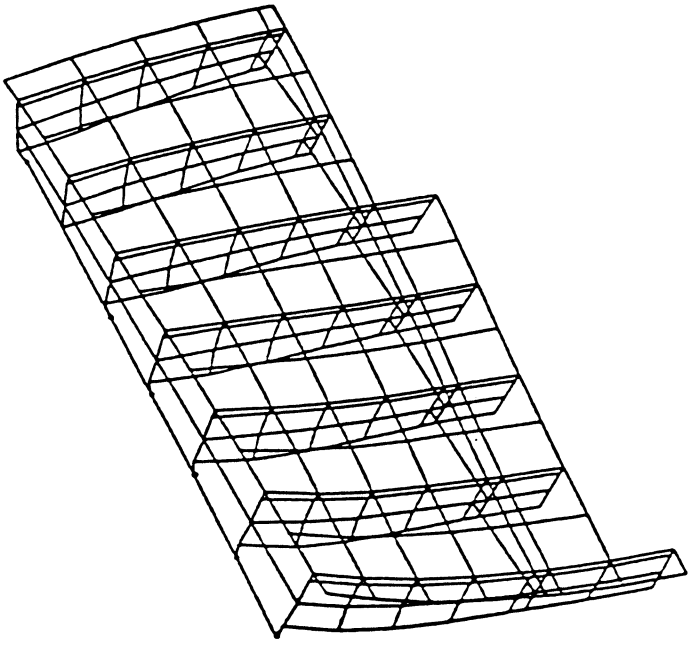

(a)

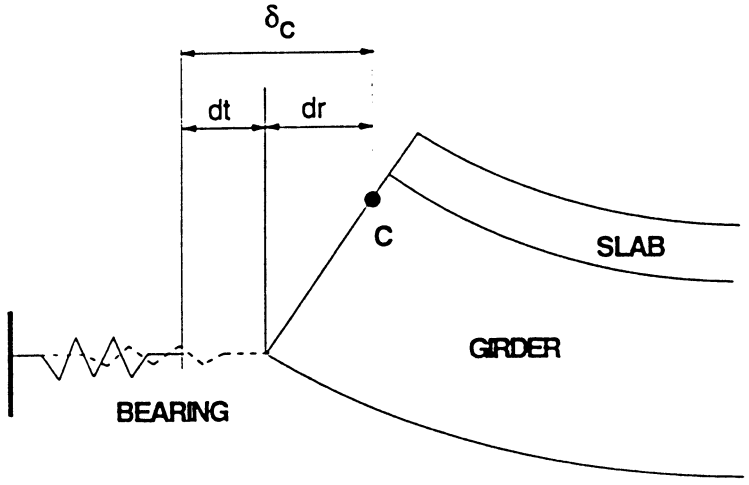

(b)

FIGURE 4-11 Torsional Behavior of the Deck at the Abutments

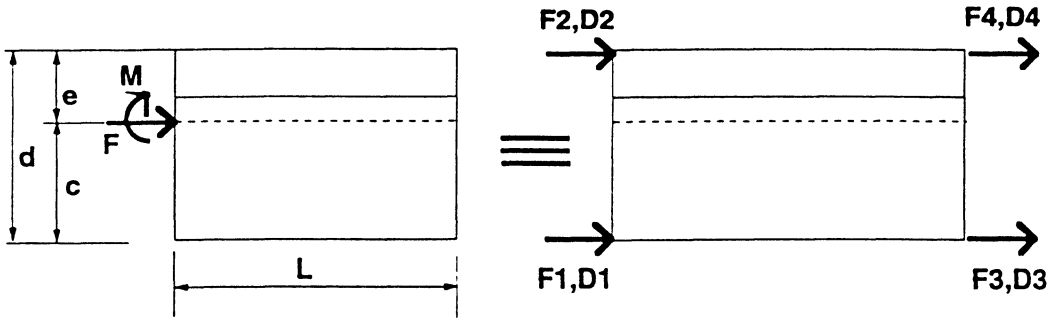

(a)

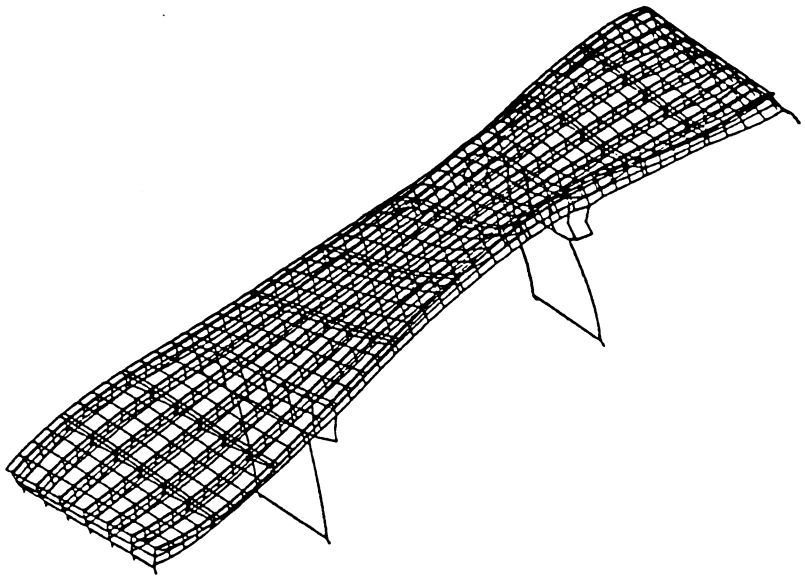

(b)

FIGURE 4-12 Equivalent Beam System

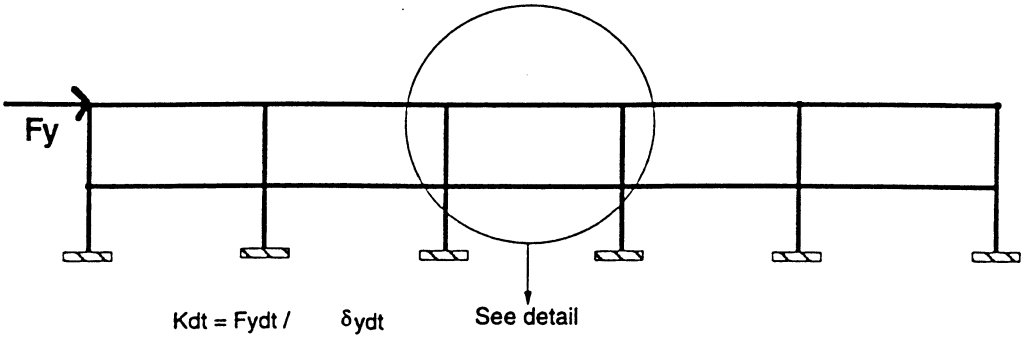

Where:

Fydt = Force applied in the transverse direction

δydt = Displacement of the frame system in the transverse direction

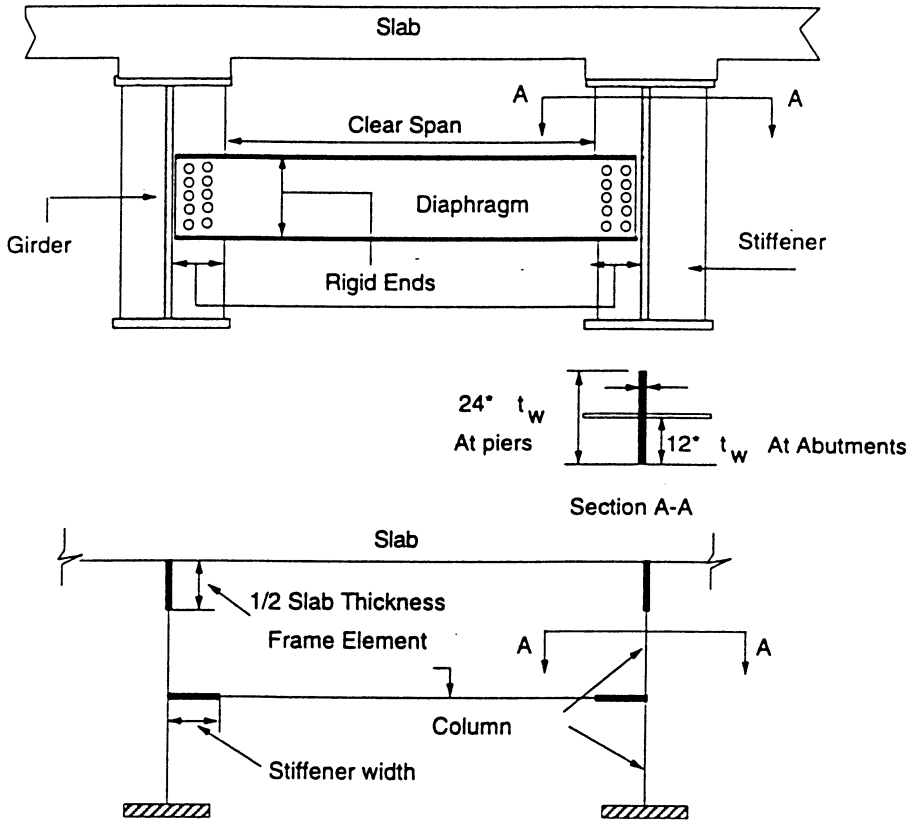

FIGURE 4-13 Diaphragm Frame System - Stiffness Computation

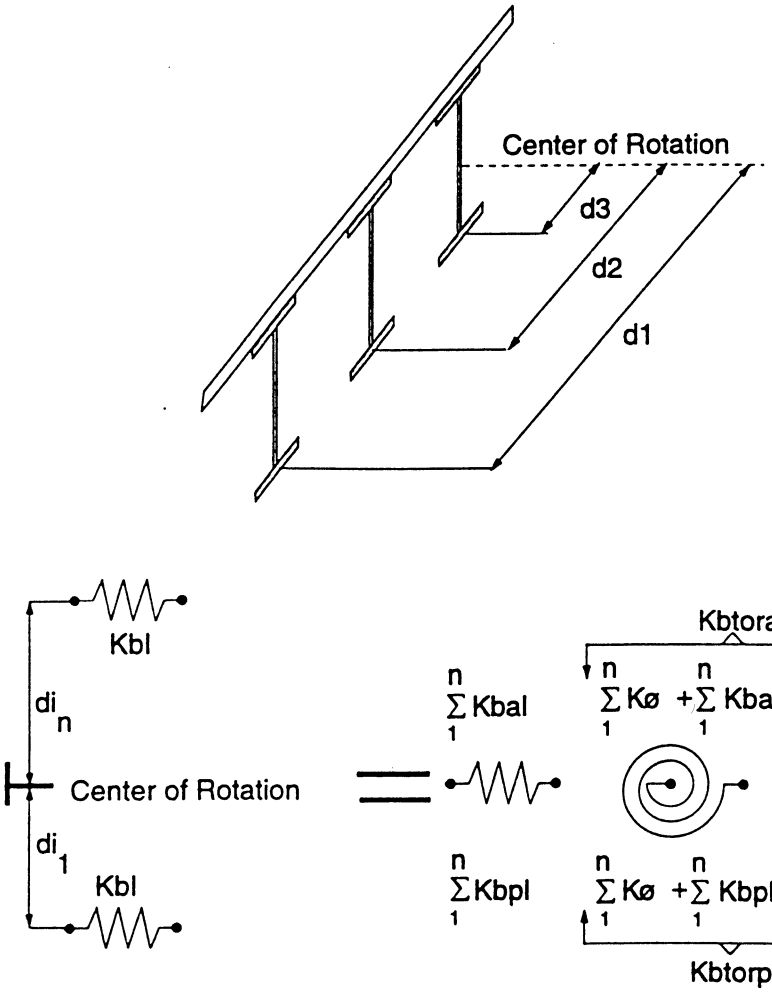

Where:

di = Distance between the bearing "i" and the center of rotation
Kbl = Stiffness of each bridge bearing in the long. direction
Kø = Torsional stiffness of the bearing around a vertical Axis - (assumed cero)
Kbal = Stiffness of the bearing at the abutment in the long. direction
Kbpl = Stiffness of the bearing at the pier bent in the long. direction
Kbtora = Torsional stiffness of the bearings system at the abutments
Kbtort = Torsional stiffness of the bearings system at the pier bent

FIGURE 4-14 Equivalent Longitudinal and Torsional Springs at the Bearings

present half of the total bearing or diaphragm stiffness, 3.5 times the individual value reported in table 4-1 for the Southbound and 3 for the Northbound. It is important to note that the definition of these two groups was done with the idea that under a transverse load one of the bearing groups at the same support (abutment or pier) is in tension, and the other is in compression. Then it is possible to model the behavior of the bearings that have different properties only by defining different properties in tension and compression.

The torsional springs defined and abutments and piers in layer #2 account for the torsional effect of the bearings. Although these uncouple the bearing in the longitudinal direction in two different springs, one rotational and one transitional, the simplification allows a significant reduction in the number of degrees of freedom making it unnecessary to define all of the bearings in the longitudinal direction for an analysis in the transverse direction. It also reduces the number of nonlinear elements in the model, keeping the modeling tractable. The torsional springs located in layer #3 and connected to the top of the piers account for the torsional stiffness between the cap beam and the pile cap. The program DRAIN-2DX has the capability of defining connection elements (type 4) that do not require specification of the length of the element; only the stiffness of the element that connects the two joints is necessary. Using this approach, all of the rotational springs were defined.

The layers are connected between them at common joints as indicated in figure 4-9. The masses of the model were lumped at the important joints and are shown in figure 4-8 as solid dots. A small dot represents a joint location. At the top of the piers a pin was defined in order to facilitate the definition of a cantilever element (pier bent) whose axial stiffness corresponds to the longitudinal stiffness of the pier bent (considering in the bridge direction) and where bending stiffness corresponds to the transverse stiffness of the pier bent. The pin uncouple the bending of the cantilever (pier bent) with the torsion transmitted by the bearings and resisted by the torsional pier bent spring (K_{ctor}).

Figure 4-10 shows the nomenclature used to define the various springs. In general the first letter after the K represents the element considered; thus s = soil, c = column,

b = bearing, d = diaphragm. The second represents the location; thus a = abutment, p = pier; and the third the direction considered; thus t = transverse, l = longitudinal. In some cases, this nomenclature does not apply directly as in the torsional springs where for example K_{btorp} = stiffness, bearing, torsional, pier. The stiffness matrix for a 2D beam column element can be transformed from coordinate d to e according to the following equation:

$$[K]_e = [H]^T[K]_d[H] \tag{4-1}$$

where $[H]$ = transformation matrix between coordinates d to e.

4.4 Model Characterization

4.4.1 Abutments

In order to construct a reliable model, is necessary to understand the behavior of the structure that is to be modeled. The behavior of the bridges at their abutments is very complex, including not only translation in the transverse and longitudinal directions of the deck but also rotation of the deck about a vertical axis.

Figure 4-11 a shows the magnified deformed shape of the 3D SAP90 model at the abutment under the static load preceding the snap-back test. From the figure, it is clear that there is a rotation of the deck respect to a vertical axis at the abutment, and it can also be seen that the deck suffers a vertical deformation, which is most significant in the exterior girders. This observed behavior at the ends can be explained by studying the deformation of the deck when a transverse load is applied. If the deck system (slab + girders) is considered as a long beam, any transverse load will produce extension of the "fibers" located in the opposite side of the applied load (tension side) and a contraction of the "fibers" in the other side (compression side). Due to this behavior, the exterior girders will suffer more longitudinal deformation than the others. If the bearings at the abutments are free to move in the longitudinal direction, then

the girders do not suffer major vertical deformations. However, if the girders are restrained from moving in the longitudinal direction due to a high initial stiffness at the bearings, the top of the girder moves relative to the bottom which is restrained, producing a vertical deformation in the system.

In order to include this behavior in any simplified model, it is necessary to consider the following, especially at the abutments. The center of the transformed section of the deck which represents the location of the simplified deck system suffers a longitudinal displacement, which is the sum of the deformation of the bearing in the longitudinal direction (dt) and the translation (dr) due to the vertical deformation of the system by the reason described above and illustrated in figure 4-11b. In order to compute an equivalent bearing stiffness value that can account for both contributions, a simple approach is proposed herein as follows.

Using the transformed stiffness matrix proposed by Mander et al. (1993), reproduced here and illustrated in figure 4-12a:

$$[K]_d = \frac{E}{L}\begin{bmatrix} A & -A & 0 & 0 \\ -A & A & 0 & 0 \\ 0 & 0 & 4I & 2I \\ 0 & 0 & 2I & 4I \end{bmatrix} \qquad \textbf{(4-2)}$$

where E = modulus of elasticity, and A, I and L are respectively the area, moment of inertia and span length. Then:

$$[K]_e = \frac{E}{d^2\,L}\begin{bmatrix} 4I+Ae^2 & -4I+Ace & -2I-Ace & 2I-Ae^2 \\ -4I+Ace & 4I+Ac^2 & 2I-Ac^2 & -2I-Ace \\ -2I-Ace & 2I-Ac^2 & 4I+Ac^2 & -4I+Ace \\ 2I-Ae^2 & -2I-Ace & -4I+Ace & 4I+Ae^2 \end{bmatrix} \qquad \textbf{(4-3)}$$

where c = location of the neutral axis from the base, e = eccentricity and d = sum of c and e. It is possible to find a stiffness value of a spring connected in series with the longitudinal

bearing spring (K_{bal}) to reconstruct the behavior explained above. In order to define this spring, it is necessary to find the displacement of the coordinate 2 when all of the others are restrained. Later it is possible to find the displacement at the center of the transformed section of the deck for the same axial load and moment. From figure 4-12b, it is possible to assume for practical purposes, that the girders at the middle of the bridge do not suffer any longitudinal displacement. Also, if it is assumed that at coordinate 1 there is a bearing of infinite stiffness, then the solution of the equation (4-2) for the unknown reduces to:

$$[D_u] = [K_{22}]^{-1} [F_{k_2}] \tag{4-4}$$

where

$$[K_{22}] = \left[\frac{4EI}{d^2L} + \frac{EAc^2}{d^2L}\right] \tag{4-5}$$

and the displacement at the centroid of the transformed section for linear deformation can be expressed as:

$$\delta_c = \frac{\delta_2 c}{d} \tag{4-6}$$

where δ_c = displacement at the centroid of the transformed section and δ_2 = displacement at the coordinate 2 with an equivalent spring stiffness:

$$K_{dr} = F_{k_2} / \delta_c \tag{4-7}$$

where F_{k_2} = force applied at coordinate 2. The total equivalent bearing stiffness considering the deformation of the bearings and the rotation of the girders as the result of two springs in series. Then:

$$K_{bal} = \frac{K_{blon} \times K_{dr}}{(K_{blon} + K_{dr})} \qquad (4\text{-}8)$$

where K_{blon} = bearing stiffness at the abutments in the longitudinal direction.

The remaining stiffness of the springs located in the layer #2 can be computed using basic structural mechanics. Figure 4-13 shows a portion of the frame composed by girders, diaphragms and slab. The stiffness of the frame can be computed by applying a concentrated load at the deck level and determining the displacement at the center of the frame. The ratio between the force and the displacement is the total frame stiffness. Then each spring representing the diaphragm in the model (*Kabt, Kbpt*) is the half of the total stiffness value. The bearing spring can be computed as the product of the bearings values by the number of bearings considered in the group.

Figure 4-14 shows the procedure for the computation of the torsional stiffness K_{btorp}, K_{btora} of the bearings at the piers and abutments. The longitudinal effect of the bearings decoupled in two components, one transitional and one rotational. For this study the torsional stiffness of the bearing around a vertical axis (K_v) was not considered.

Based on the principles of mechanics, table 4-2 summarizes the procedure for the abutment stiffnesses computation. In table 4-2 where K_{dat} = diaphragm stiffness in figure 4-13, K_{bat_i} = stiffness of each bearing at abutment in the transverse direction, C_{bt} = number of bearings considered in the computation (transverse direction, C_{bt} = 3.5 for the Southbound, C_{bt} = 3 for the Northbound, C_{bl} = number of bearings considered in the computation (longitudinal direction), C_{bl} = 7 for the Southbound, C_{bl} = 6 for the Northbound, K_{bal_i} = stiffness of each bearing at abutment in the longitudinal direction, K_{btora} = torsional stiffness of the bearings system at the abutment, K_{sat} = stiffness of the soil at abutment in the transverse direction, and K_{sal} = stiffness of the soil at abutment in the longitudinal direction.

TABLE 4-2 Abutment Stiffness Computation

	Reference
$K_{dat} = K_{dt}/2$	Figure 4-13
$K_{bat} = K_{bat_i} C_{bt}$	Mander et al., 1996, Dicleli, 1995
$K_{bal} = K_{bal_i} C_{bl}$	Mander et al., 1996, Dicleli, 1995
$K_{btora} = \Sigma(k_\theta + k_{bal} d_i^2)$	Figure 4-14
K_{sat}	Douglas 1994, Maragakis 1992
K_{sal}	Douglas 1994, Maragakis 1992

4.4.2 Pier Stiffness

The equivalent stiffness of the pier bent model was computed using an approach similar to the approach used with the diaphragm. As the columns were modeled using a beam-column element, two properties needed to be defined -the inertia and the area. The inertia, as was explained, defines the stiffness of the pier bent in the transverse direction of the bridge and the area defines stiffness in the longitudinal direction. Figure 4-15 helps to describe the approach used and table 4-3 summarizes the values employed.

In table 4-3, K_{dp} = stiffness of the diaphragms system at pier, K_{dp} = stiffness of each bearing at the piers in the transverse direction K_{bp_i} = stiffness of a bearing at the piers in the longitudinal direction, K_{btorp} = torsional stiffness of the bearings system at the pier, K_{ctorp} = torsional stiffness of the columns system at pier, K_{pl} = stiffness of each column in the longitudinal direction, $K_{\theta_{bp}}$ = torsional stiffness of the column around a vertical axis passing through the center of the column, J = torsional constant, G = shear modulus, L = clear height of the column, b = shorter side of a rectangular section, c = longer side of a rectangular section, K_{pt} = stiffness of the pier in the transverse direction, I_{ec} = equivalent inertia of the

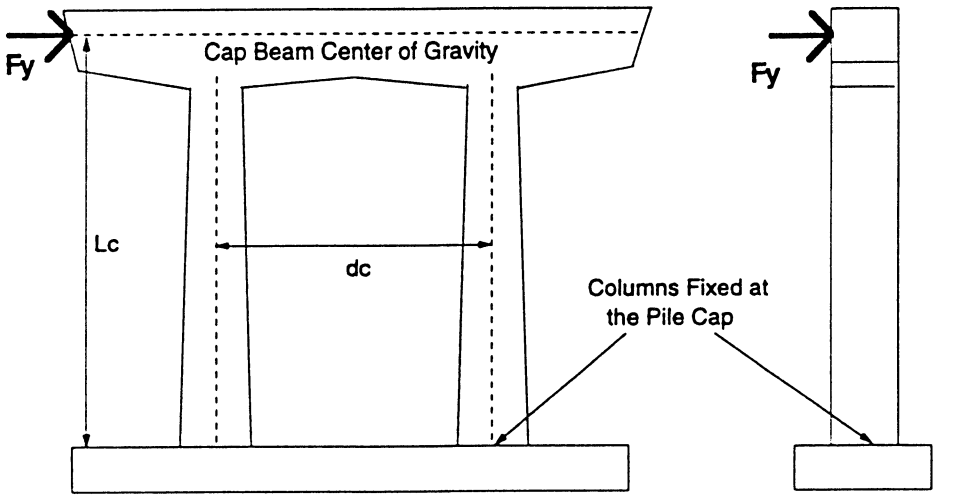

$K_{pt} = F_{ypt} / \delta_{ypt}$

$K_{pl} = F_{ypl} / \delta_{ypl}$

Where:

F_{ypt}= Force appied in the transverse direction

δ_{ypt} = Displacement of the pier in the transverse direction

F_{ypl} = Force appied in the longitudinal direction

δ_{ypl} = Displacement of the pier in the longitudinal direction

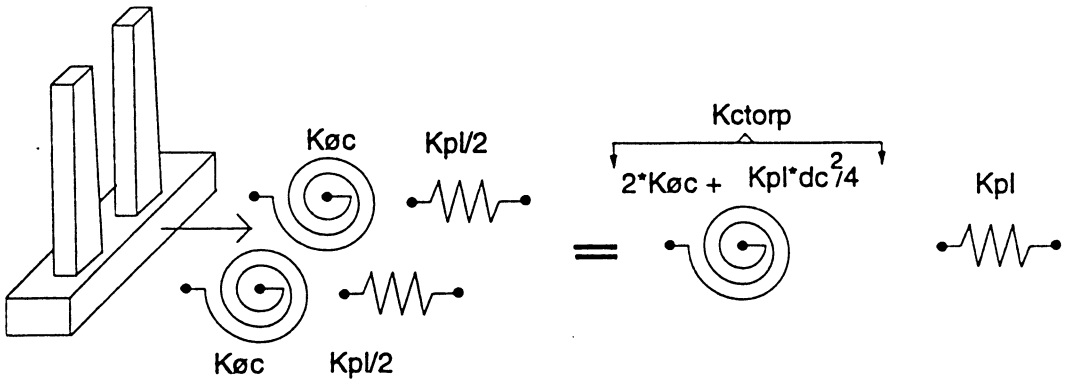

Where:

$K_{øc}$ = Torsional stiffness of each column

dc = Distance between the center of the columns

FIGURE 4-15 Pier Bent - Stiffness Computation

DRAIN-2DX pier bent, figures 4-8 and 4-15 and L_a = assumed length of the DRAIN-2DX column, E = assumed modulus of elasticity, A_{ec} = equivalent area of the DRAIN-2DX pier bent, Figure 4-8 and 4-15, K_{spt} = stiffness of the soil at piers in the transverse direction, K_{spl} = stiffness of the soil at piers in the longitudinal direction.

4.4.3 Deck Stiffness

The stiffness of the slab-girders system K_{deckt} in figure 4-10 was computed using the transformed section principles.

TABLE 4-3 Pier Stiffness Computation

Stiffness	Reference
$K_{dpt} = K_{dt}/2$	Figure 4-13
$K_{bpt} = k_{bpt_i} C_{bt}$	Mander et al. 1996, Premus 1993, Dicleli 1995
$K_{bpl} = K_{bpl_i} C_{bl}$	Mander et al. 1996, Premus 1993, Dicleli 1995
$K_{btorp} = \Sigma(K_\theta + K_{bpi} d_i^2)$	Figure 4-14
K_{spt}	Douglas 1994, Maragakis 1992
K_{spl}	Douglas 1994, Maragakis 1992
K_{pt}	Figure 4-15
K_{bl}	Figure 4-15
$K_{ctorp} = \Sigma\left[K_{\theta_c} + \frac{K_{pl}}{2}\left(\frac{d_c}{2}\right)^2\right]$	Figure 4-15
$K_{\theta_{bp}} = \frac{JG}{L_c}$	Ghali 1989
$K_{col}(A_{ec}, I_{ec})$	
$A_{ec} = \frac{K_{pl} L_a}{E}$; $I_{ec} = \frac{K_{pt}(L_a)^2}{3E}$	

4.4.4 Lumped Masses

The lumped masses showed in figure 4-8 were computed according to the tributary area approach where M_{d_i} = lumped mass of the deck at location i, M_{cp} = lumped mass of the cap beam at the top of the pier, I_{oc} = rotational mass of the cap beam at the top of the pier, M_a = lumped mass of the abutment at abutments, and M_{pf} = lumped mass of the pier foundation and portion of the columns.

Table 4-4 summarizes the property values used for the DRAIN-2DX model. The initial bearings stiffness values and the soil spring stiffness were initially taken form the SAP90 model. With these initial estimates, an adjustment similar to that done with the SAP90 3D model was performed in order to improve the fitting between the experimental results and the predicted results using DRAIN-2DX. It was found that it was only necessary to increase the stiffness of bearings at the south pier in the longitudinal direction in order to obtain results similar to those obtained using a 3D model. All of the other values were the same values as used in the SAP90 3D model. The table shows the properties for each group of elements. For example, the stiffness bearing at the north abutment of the Southbound bridge DRAIN-2DX model is 3.5 times larger than the values of the SAP90 3D model (Table 4-1) in the transverse direction and seven times in the longitudinal direction for the same location.

The SAP90 3D model described earlier was constructed in order to satisfy two basic requirements after the calibration with the experimental results: to predict the response of the structure for other conditions than the snap-back test, and to use this model as a basis for comparison with other models that allow no linear behavior. The DRAIN-2DX model was constructed in order to perform a nonlinear analysis of the bridges, before and after the retrofit with elastomeric bearings. A third model called SAP90 2D was constructed in order to compare the predicted results obtained using a typical engineering office approach and a more sophisticated model. Figure 4-16 shows the proposed SAP90-2D model; it is a derivation of the DRAIN-2DX model with the major difference that it does not account for longitudinal movement. The spring values in all cases were computed using the same approach as for the

TABLE 4-4 DRAIN2DX Model
Properties for Bridges Seated on Steel Bearings

Southbound Bridge DRAIN2DX Model			Northbound Bridge DRAIN2DX Model		
Description			**Description**		
General Properties	**Values**	**Units**	**General Properties**		
Concrete Modulus	30442	MPa	Concrete Modulus	30442	MPa
Concrete Poisson Ratio	0.20		Concrete Poisson Ratio	0.20	
Deck Properties			**Deck System**		
Tranformed Sec. Area	5.05	m^2	Tranformed Sec. Area	4.45	m^2
Tranformed Sec. Inertia	104.75	m^4	Tranformed Sec. Inertia	72.22	m^4
Diaphragm Stiffness			**Diaphragm Stiffness**		
Abutment	817	kN/m	Abutment	697	kN/m
Pier	854	kN/m	Pier	751	kN/m
Total Pier Stiffness			**Total Pier Stiffness**		
Transverse Direction	489	kN/m	Transverse Direction	611	kN/m
Longitudinal Direction	40	kN/m	Longitudinal Direction	68	kN/m
Torsional	1736	kN*m/rad	Torsional	2002	kN*m/rad
Bearings Stiffness	(Per Group of Brgs)		**Bearings Stiffness**	(Per Group of Brgs)	
North Abut. Transverse	793	MN/m	North Abut. Transverse	680	MN/m
North Abut. Longitudinal	6997	MN/m	North Abut. Longitudinal	800	MN/m
North Pier Transverse	227	MN/m	North Pier Transverse	195	MN/m
North Pier Longitudinal	68	MN/m	North Pier Longitudinal	1459	MN/m
South Pier Transverse	227	MN/m	South Pier Transverse	195	MN/m
South Pier Longitudinal	23	MN/m	South Pier Longitudinal	1459	MN/m
South Abut. Transverse	933	MN/m	South Abut. Transverse	800	MN/m
South Abut. Longitudinal	6997	MN/m	South Abut. Longitudinal	800	MN/m
Total Soil Stiffness			**Total Soil Stiffness**		
North Abut. Transverse	1226	MN/m	North Abut. Transverse	963	MN/m
North Abut. Longitudinal	978	MN/m	North Abut. Longitudinal	1182	MN/m
North Pier Transverse	1095	MN/m	North Pier Transverse	1459	MN/m
North Pier Longitudinal	1299	MN/m	North Pier Longitudinal	1459	MN/m
South Pier Transverse	919	MN/m	South Pier Transverse	1459	MN/m
South Pier Longitudinal	1051	MN/m	South Pier Longitudinal	1459	MN/m
South Abut. Transverse	1481	MN/m	South Abut. Transverse	1182	MN/m
South Abut. Longitudinal	949	MN/m	South Abut. Longitudinal	1182	MN/m
Masses			**Masses**		
Total Mass Abutments	445	tonne	Total Mass Abutments	347	tonne
Total Mass Piers	193	tonne	Total Mass Piers	129	tonne
Total Mass Pile Caps	265	tonne	Total Mass Pile Cap	170	tonne
Total Mass Deck	689	tonne	Total Mass Deck	555	tonne

Note 1 t = 1000 kg mass, weight of 1 t mass = 9.81 kN

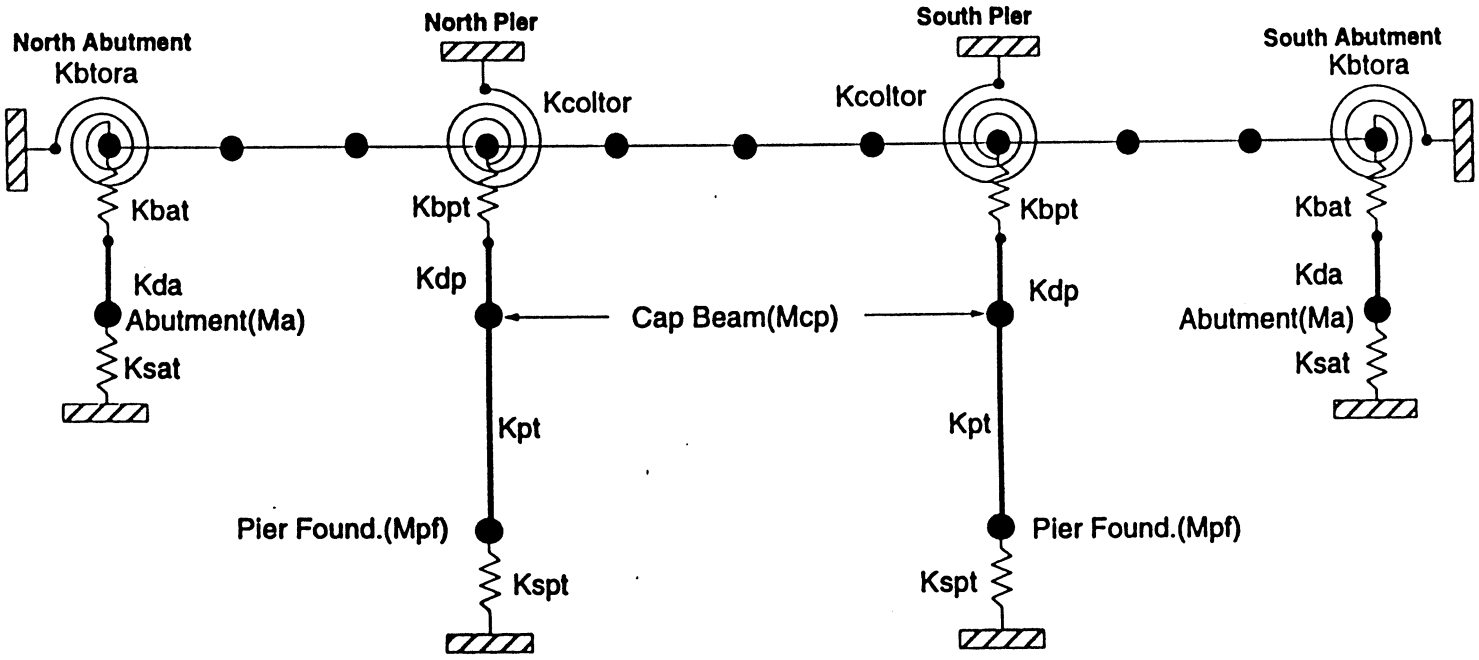

$$Kcoltor = \frac{Kbtorp * Kctor}{Kbtor + Kctor}$$

Where:

Kbtorp = Torsional Stiffness of the bearings system

Kctor = Torsional Stiffness of the pier bent System

FIGURE 4-16 Transverse Simplified Model (SAP-2D)

DRAIN-2DX model except that there was only one group of bearings and diaphragms at the supports.

4.5 Analytical Predictions

In order to compare the behavior predictions, two basic comparisons were made. The first comparison was the predicted frequencies and mode shapes vs. the experimentally observed frequencies and mode shapes. The second compared the analytically predicted time histories of the accelerometers with the experimental results, using as the input load in the analytical model the load-time-history obtained from the load cells bars at the moment of release. Prior to the instant of release, a simulated loading portion was added to the time history. The accuracy of the 2D finite element model to predict the elastic behavior was investigated by comparing the experimental frequencies and mode shapes with the prediction obtained from the 3D model for the same condition.

Figures 4-17 and 4-18 compare the first two Southbound vertical mode shapes and frequencies. In these figures, unless otherwise noted, SAP90 refers to the SAP90-3D model. The continuous heavy line represents the analytical prediction and the bold symbols the average experimental results. Each graph represents a different girder. Figures 4-19, 4-20 and 4-21 show the average experimental results for the transverse-longitudinal modes and the SAP90 and DRAIN-2DX predictions. Considering the immense complexity of the problem, it is considered that the analytical prediction shows excellent agreement with the experimental results, especially at the deck level, where the accelerations are greatest.

The two closely-spaced transverse-longitudinal modes can be explained by studying the behavior of the pier bents. Figure 4-22a shows the magnified deformation of the pier in the SAP90 model under a force similar to the force transmitted by the structure during the test. It can be seen from the static test that although the main force is transverse with a small component in the longitudinal direction the bent deforms basically in the longitudinal direction. This behavior is related to the skew angle of the pier bents, and the high stiffness of the piers

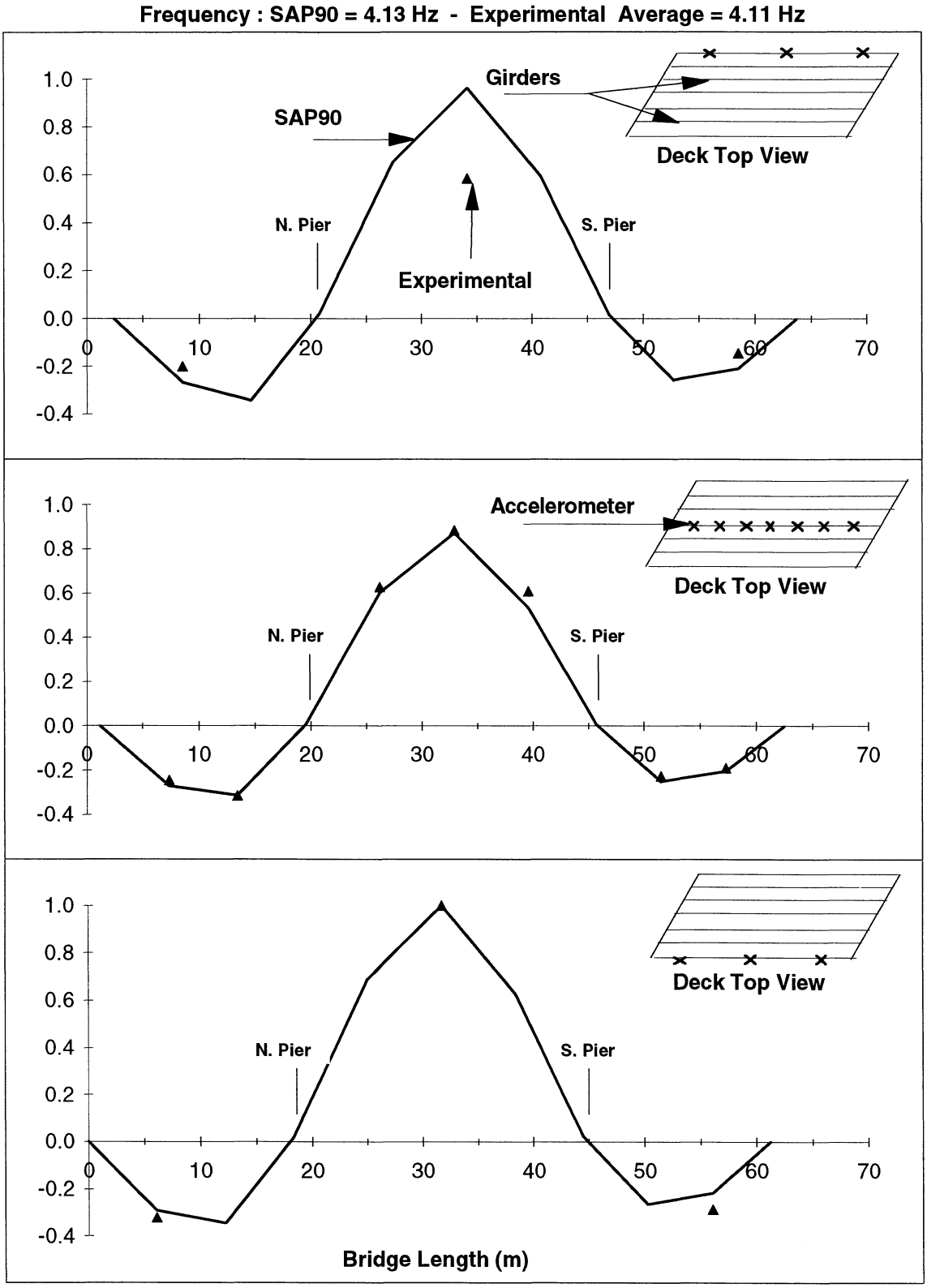

FIGURE 4-17 Southbound Bridge - First Vertical Mode

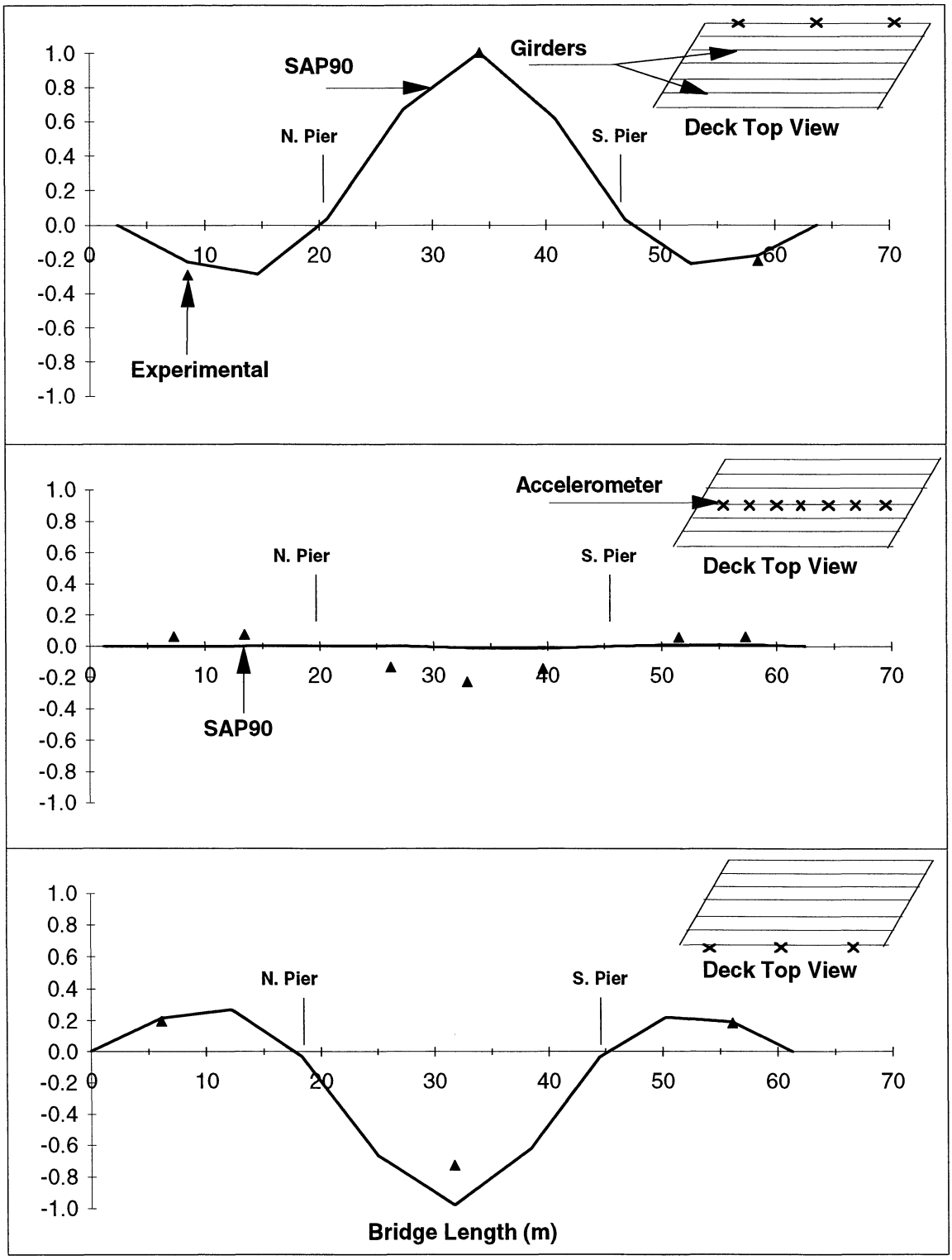

FIGURE 4-18 Southbound Bridge - Second Vertical Mode

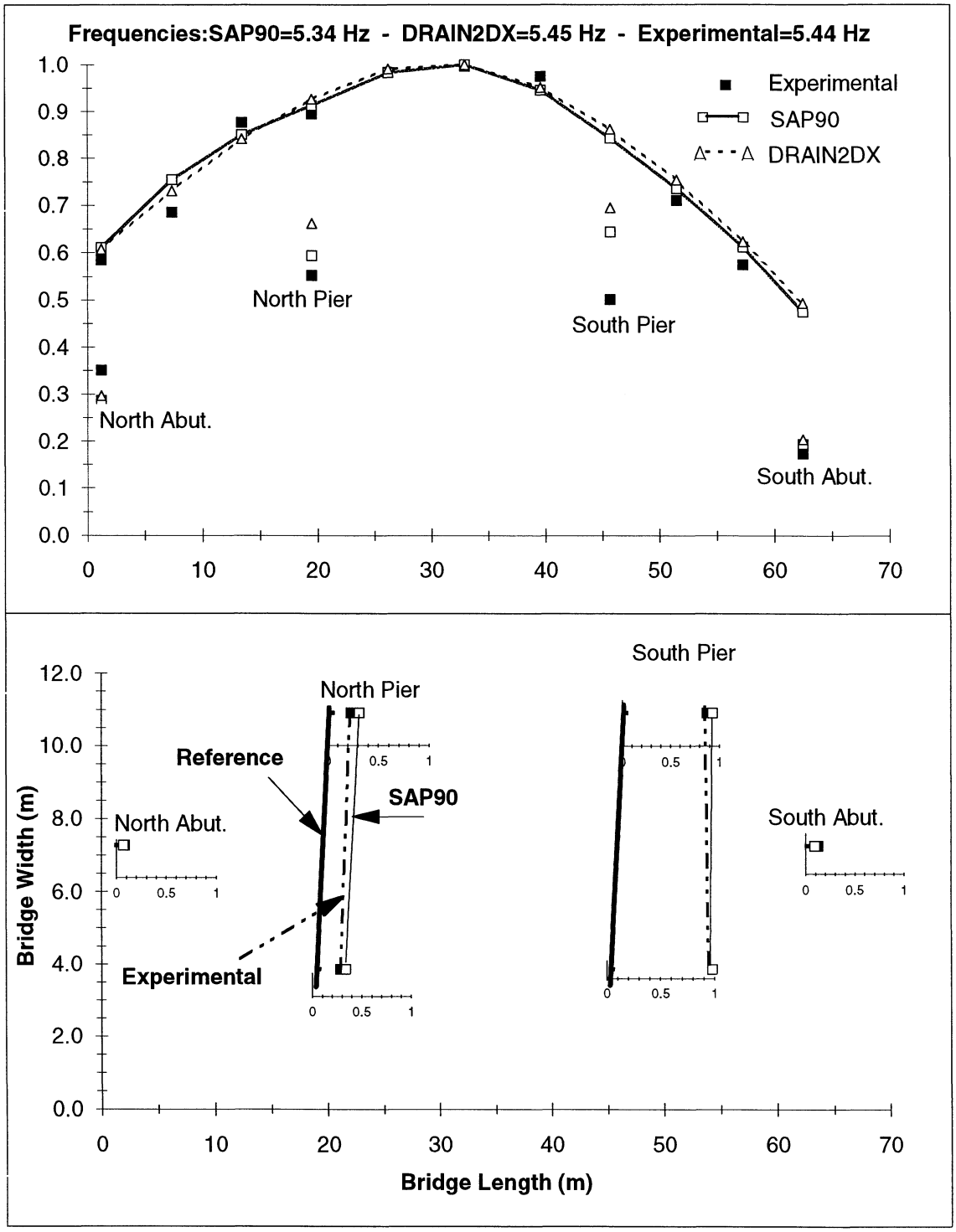

FIGURE 4-19 Southbound Bridge - First Transverse - Longitudinal Mode

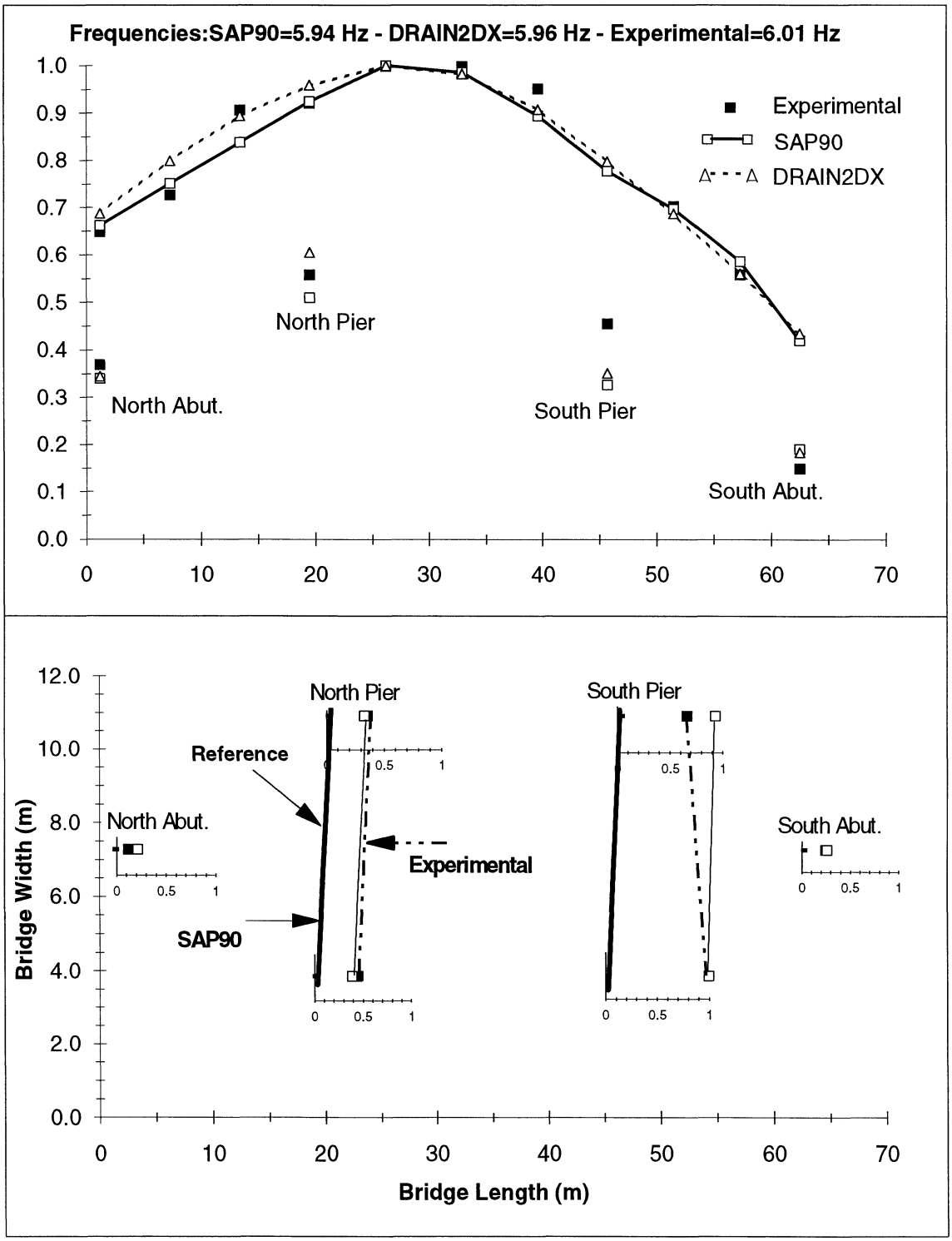

FIGURE 4-20 Southbound Bridge - Second Transverse - Longitudinal Mode

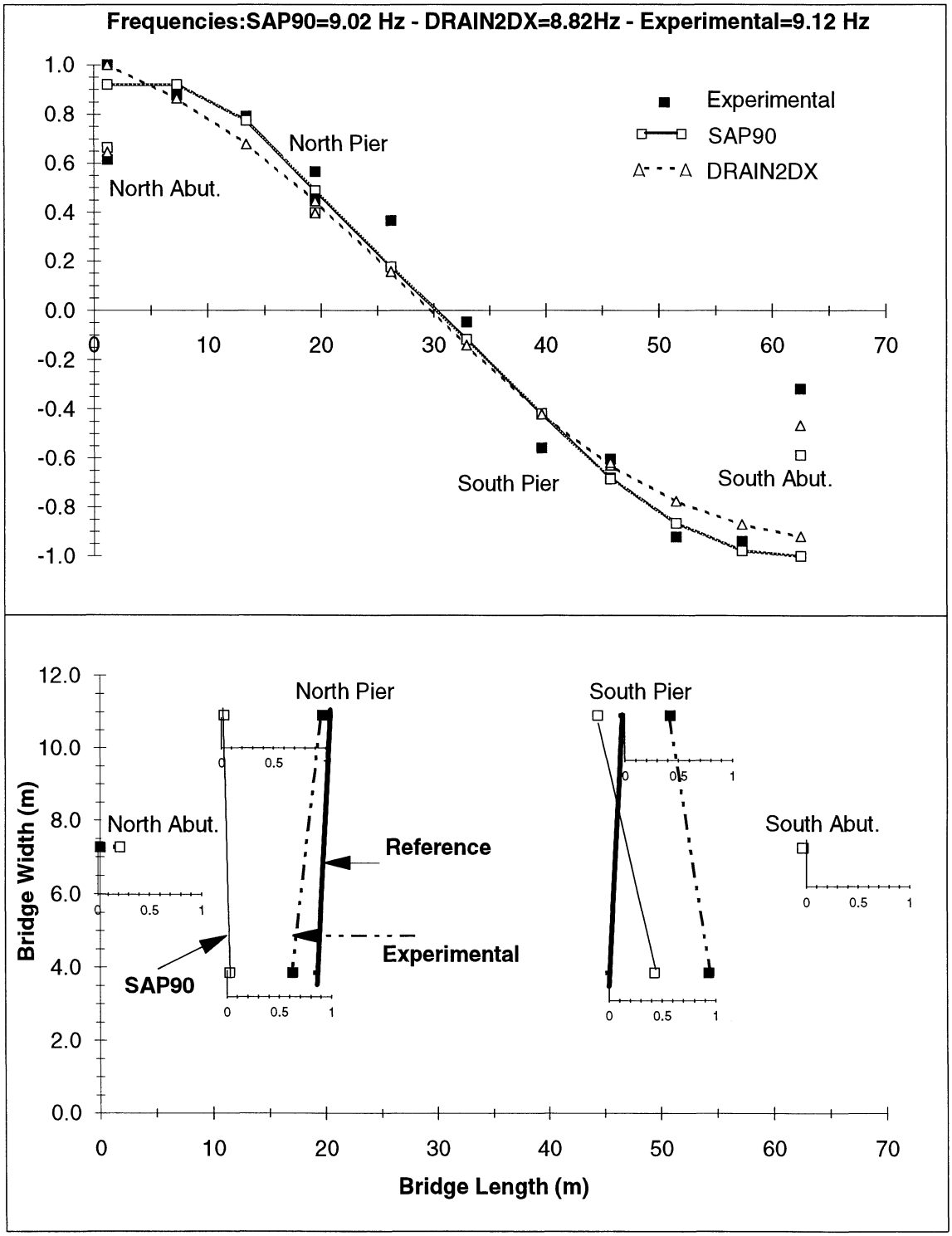

FIGURE 4-21 Southbound Bridge - Third Transverse Mode

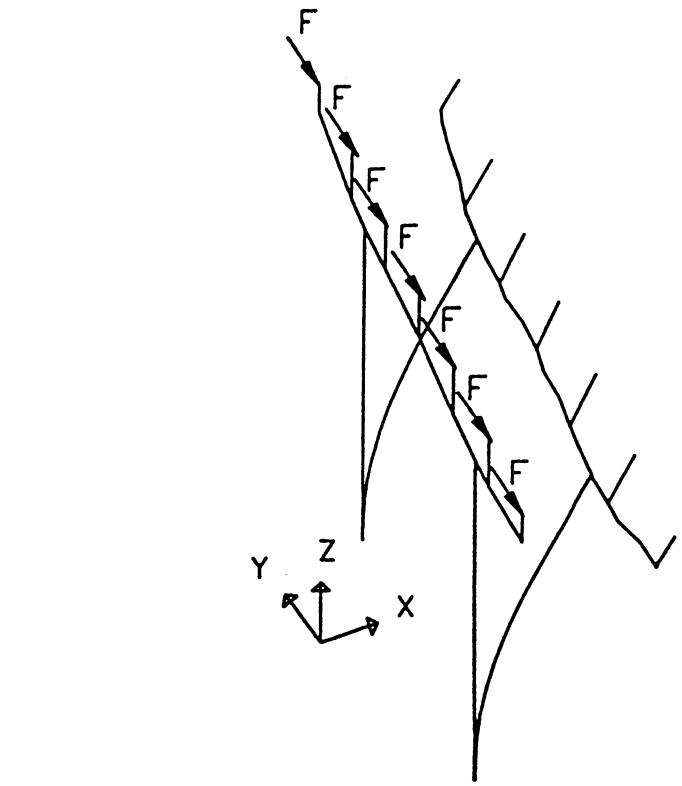

(a)

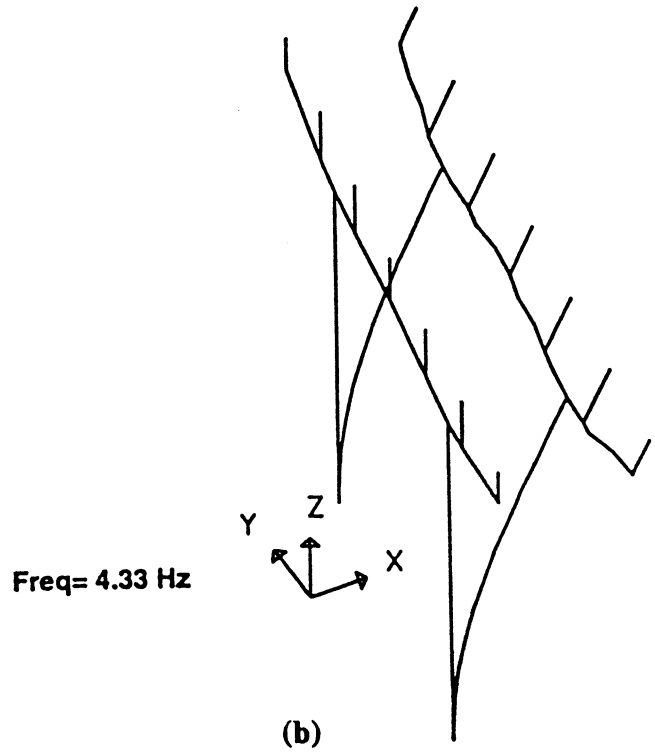

Freq= 4.33 Hz

(b)

FIGURE 4-22 Comparison Between Static Deformed Shape and First Mode of Vibration

in the transverse direction (of the bridge), and their low stiffness in the longitudinal direction. The first mode of vibration of the pier acting independently of the bridge as a cantilever is at a frequency of 4.5 Hz and is illustrated in figure 4-22b.

From the brief discussion above it is clear that any transverse deformation will be accompanied by a longitudinal deformation of the piers and, depending on the degree of connection between the structure and the pier bents, the piers could be excited at their own frequencies. For both bridges, as illustrated in Section 2, the south pier was connected to the structure with a high type fixed bearing which acts as a truss member (compression or tension) and the north pier with a high type expansion bearing which for our purposes is equivalent to a frame element pinned at the top.

Figures 4-23 and 4-24 compare the predicted acceleration time history using the proposed 3D finite element model and the experimental results for different locations. From the Fourier spectra, and considering the frequency of modes excited, the first 40 modes that are equivalent to frequencies up to 22 Hz and a 98% of the total participating mass, were used for the prediction although good agreement was observed with only 15 modes (frequencies up to 14 Hz). The model has a good correlation with the experimental data in the transverse and vertical direction including the pier and abutment. There are certain differences at the piers that can be attributed to two major factors. The first is the difficulty to reduce the data due to the low value of acceleration and noisy condition observed in the time history of the accelerometers located over the piers. The second is associated with the uncertainty in the modeling of the soil-interaction effect, especially in the north pier where the soil level was around 1.5 m under the cap beam.

Comparisons between the experimental and predicted mode shapes for the Northbound bridge are presented in figures 4-25 to 4-30. It can be seen that for this bridge the predicted and experimental values are also very close. Figures 4-31 and 4-32 show the experimental and analytical acceleration time history in the vertical and transverse directions. In this bridge the second vertical mode shape during the snap back test was predominant over the others. For this

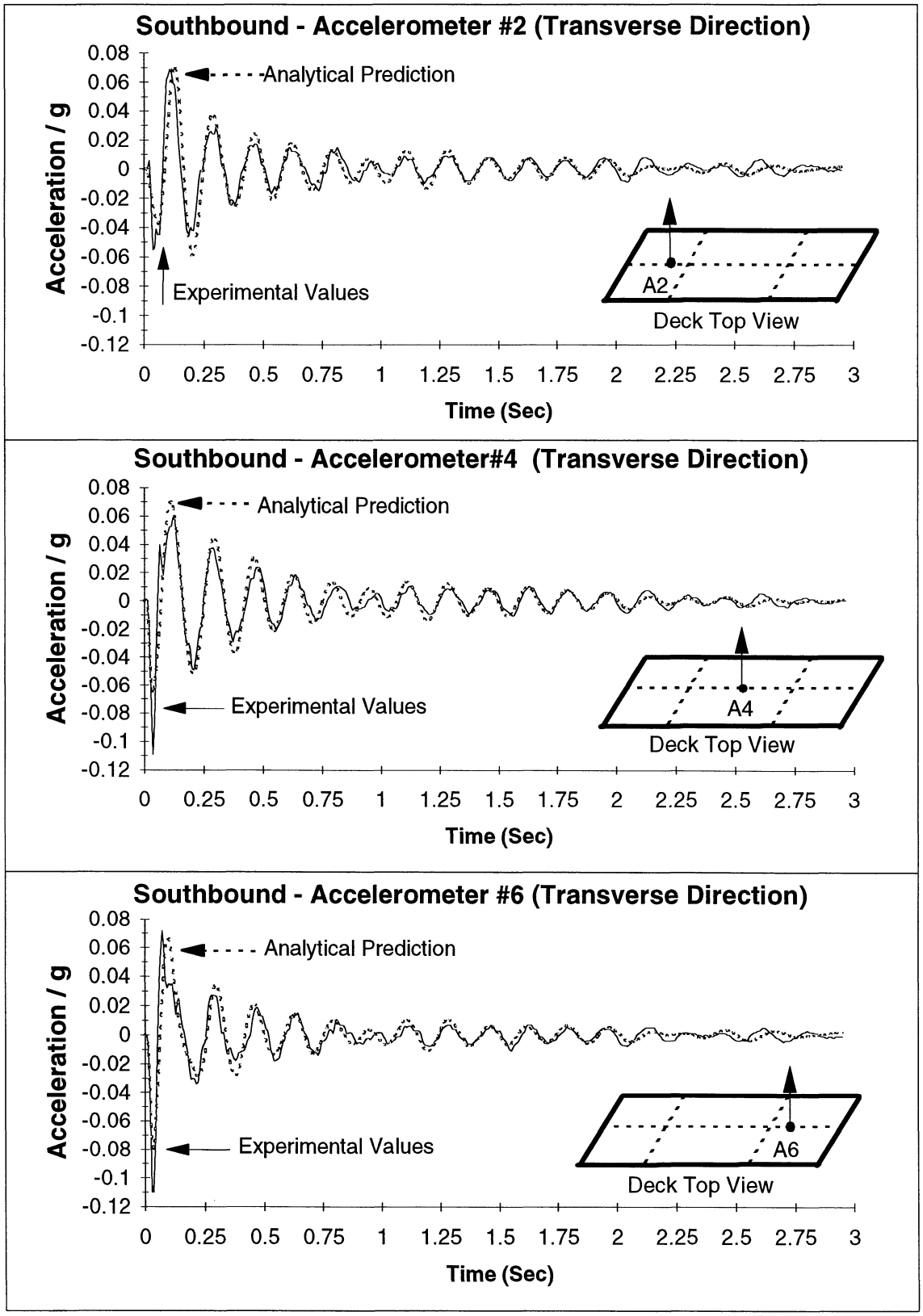

FIGURE 4-23 Southbound Bridge - Analytical vs Experimental SBPRE-T2-OP

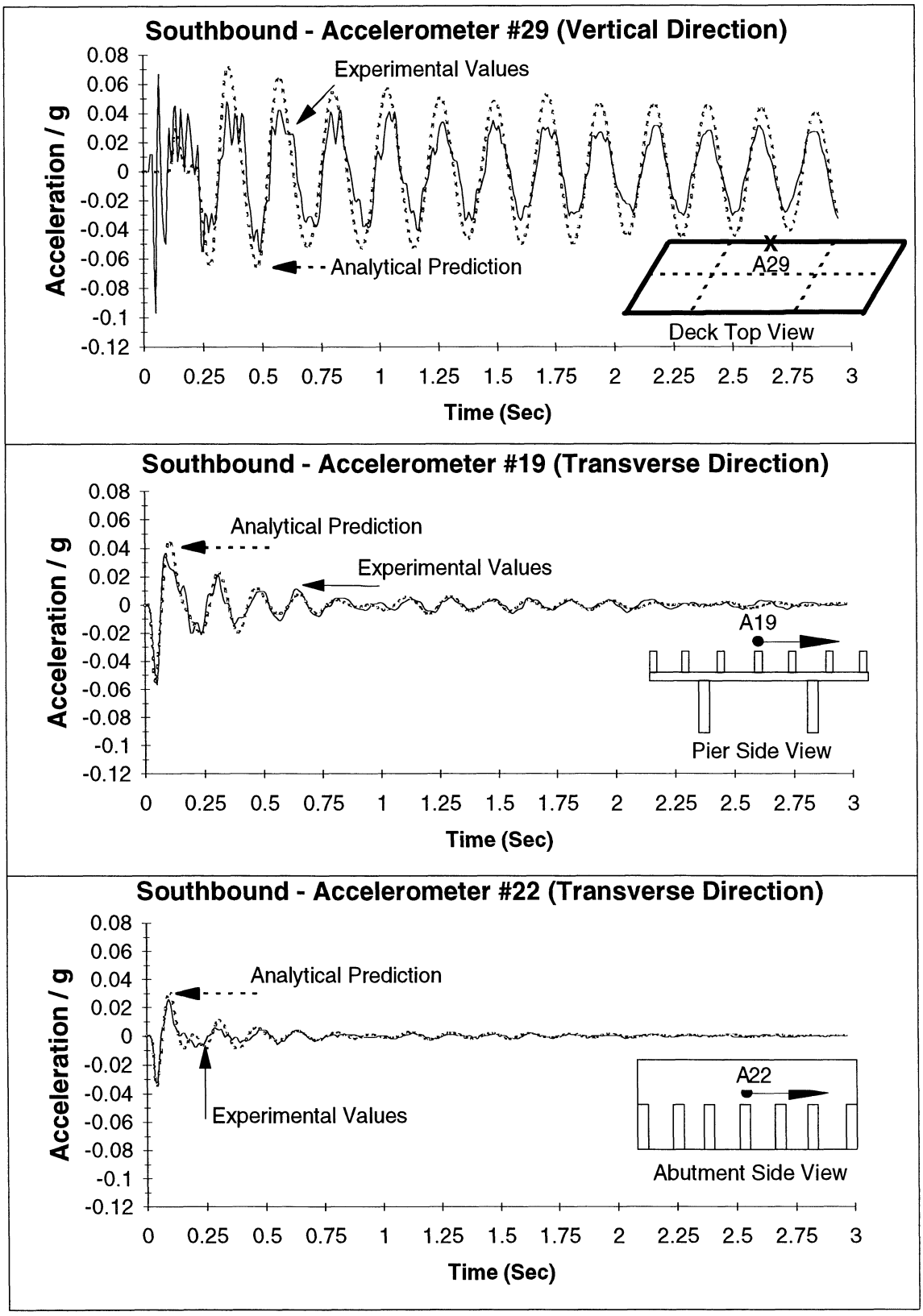

FIGURE 4-24 Southbound Bridge - Analytical vs Experimental SBPRE-T2-OP

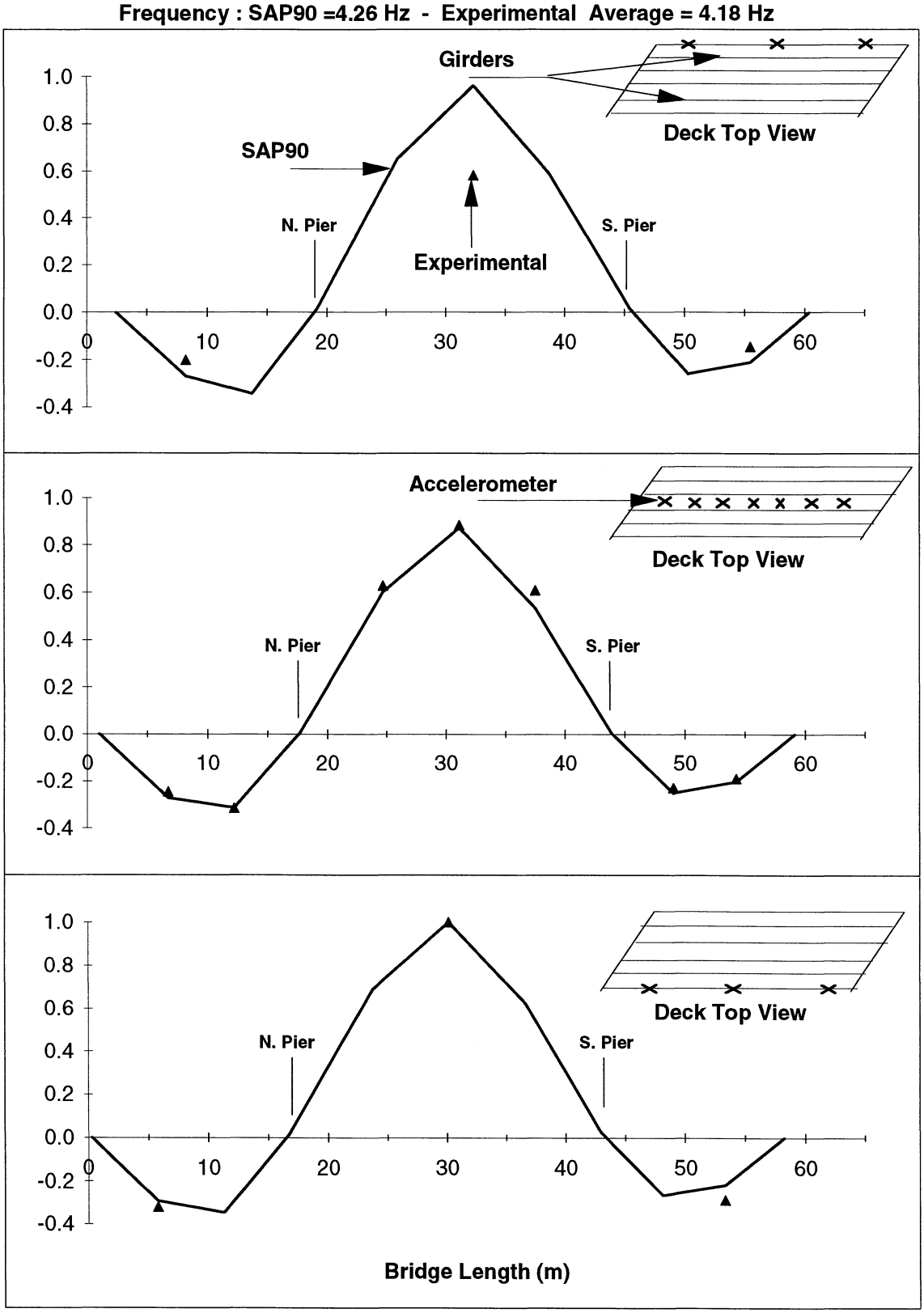

FIGURE 4-25 Northbound Bridge - First Vertical Mode

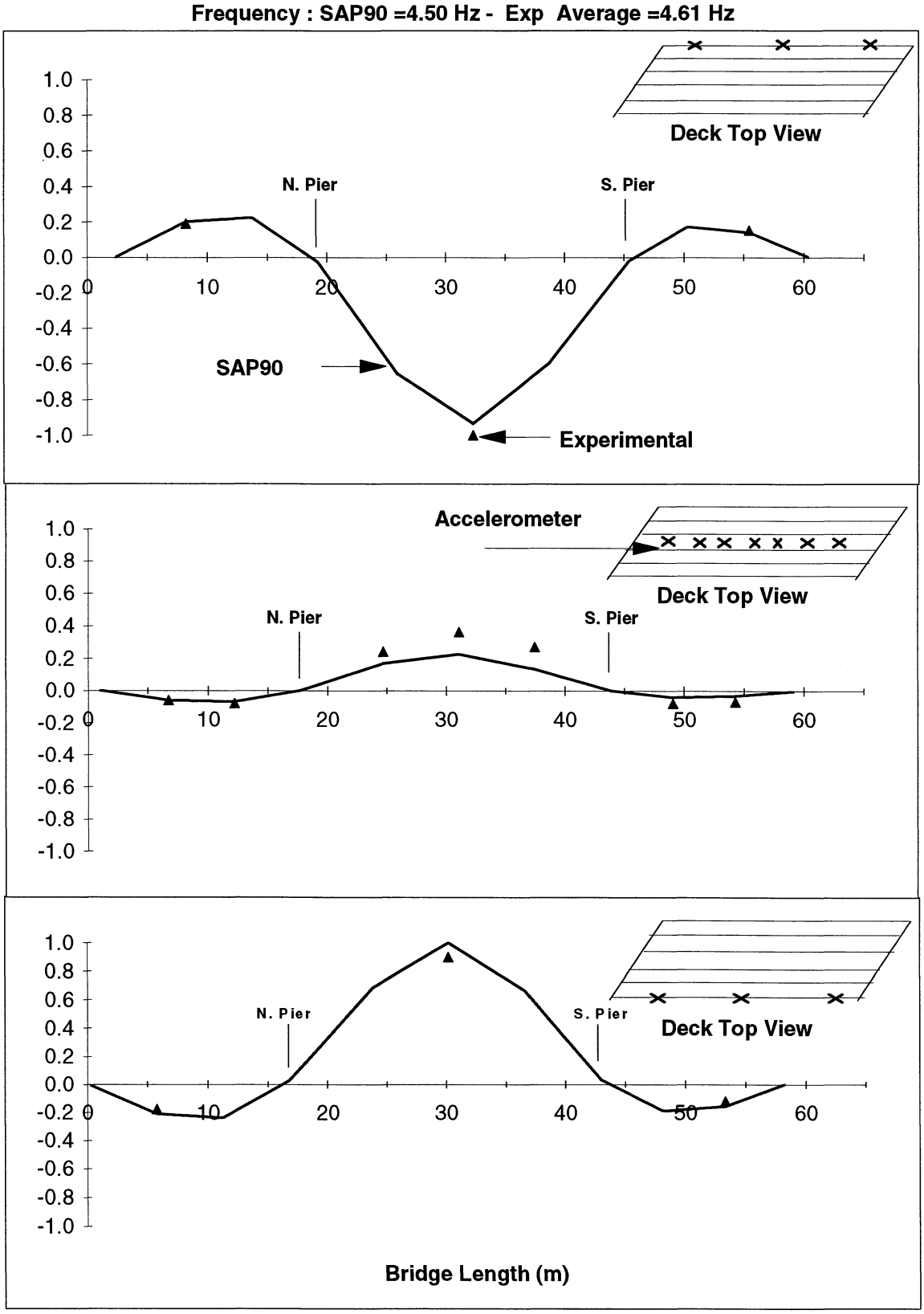

FIGURE 4-26 Northbound Bridge -Second Vertical Mode

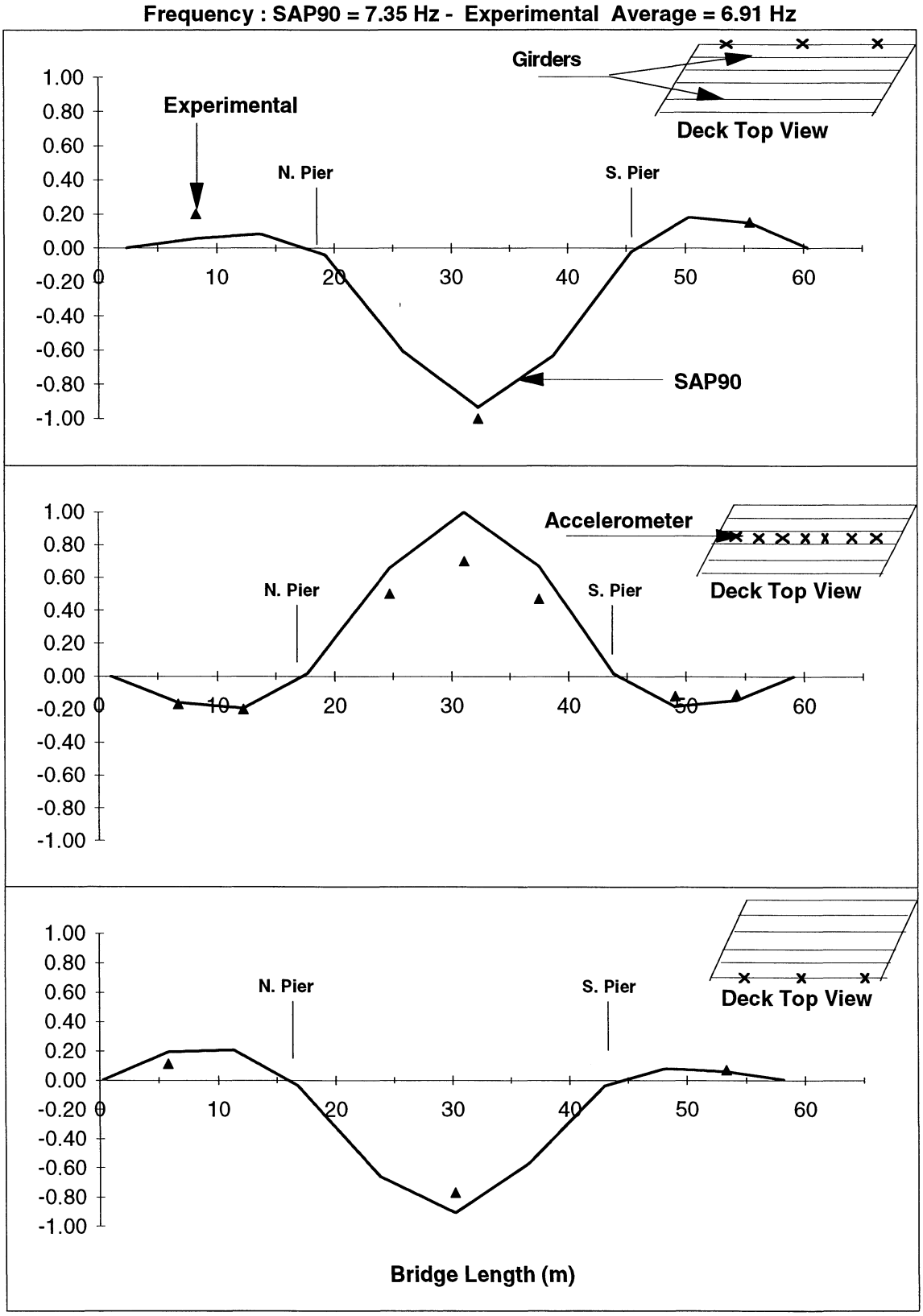

FIGURE 4-27 Northbound Bridge - Third Vertical Mode

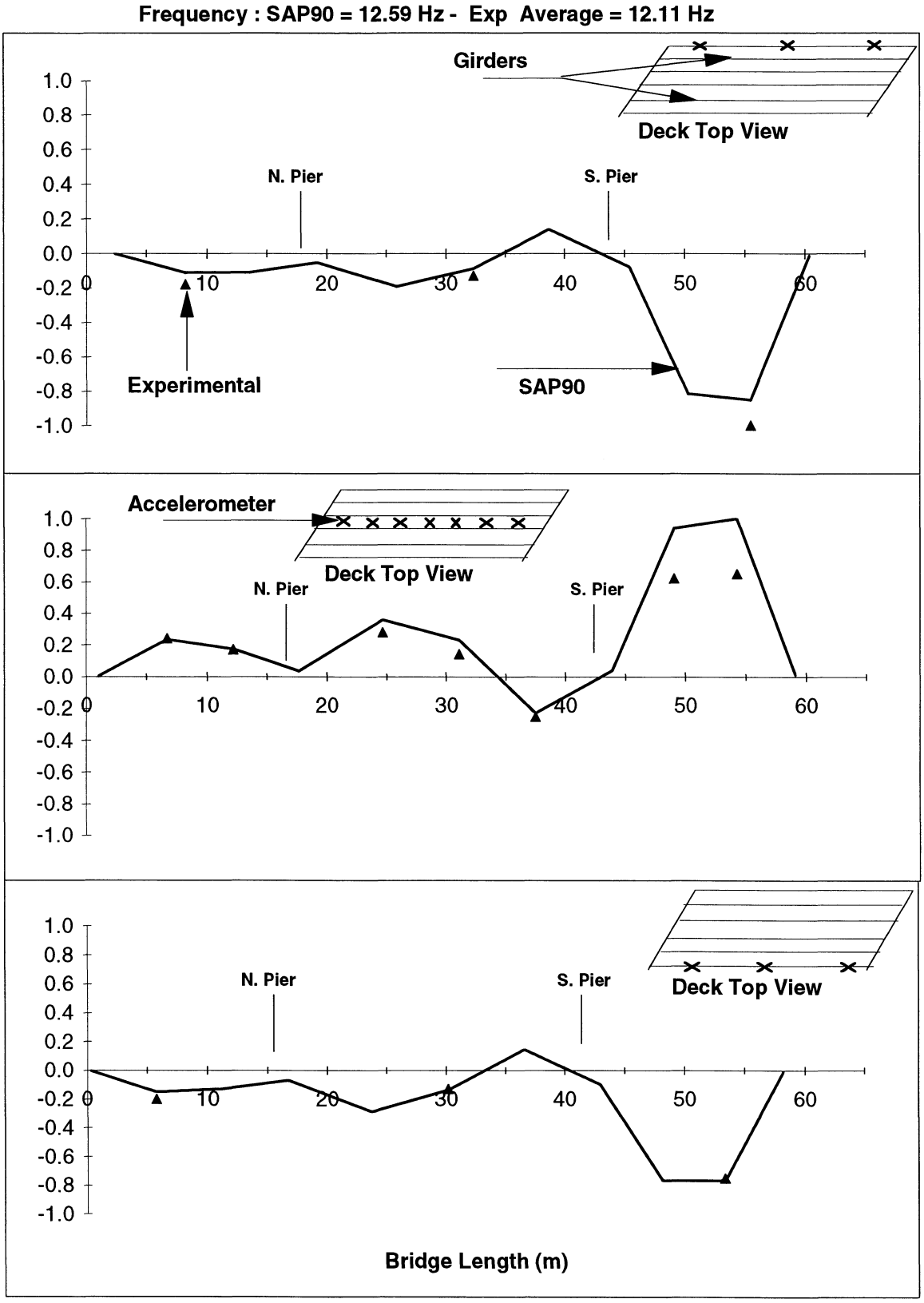

FIGURE 4-28 Northbound Bridge - Fourth Vertical Mode

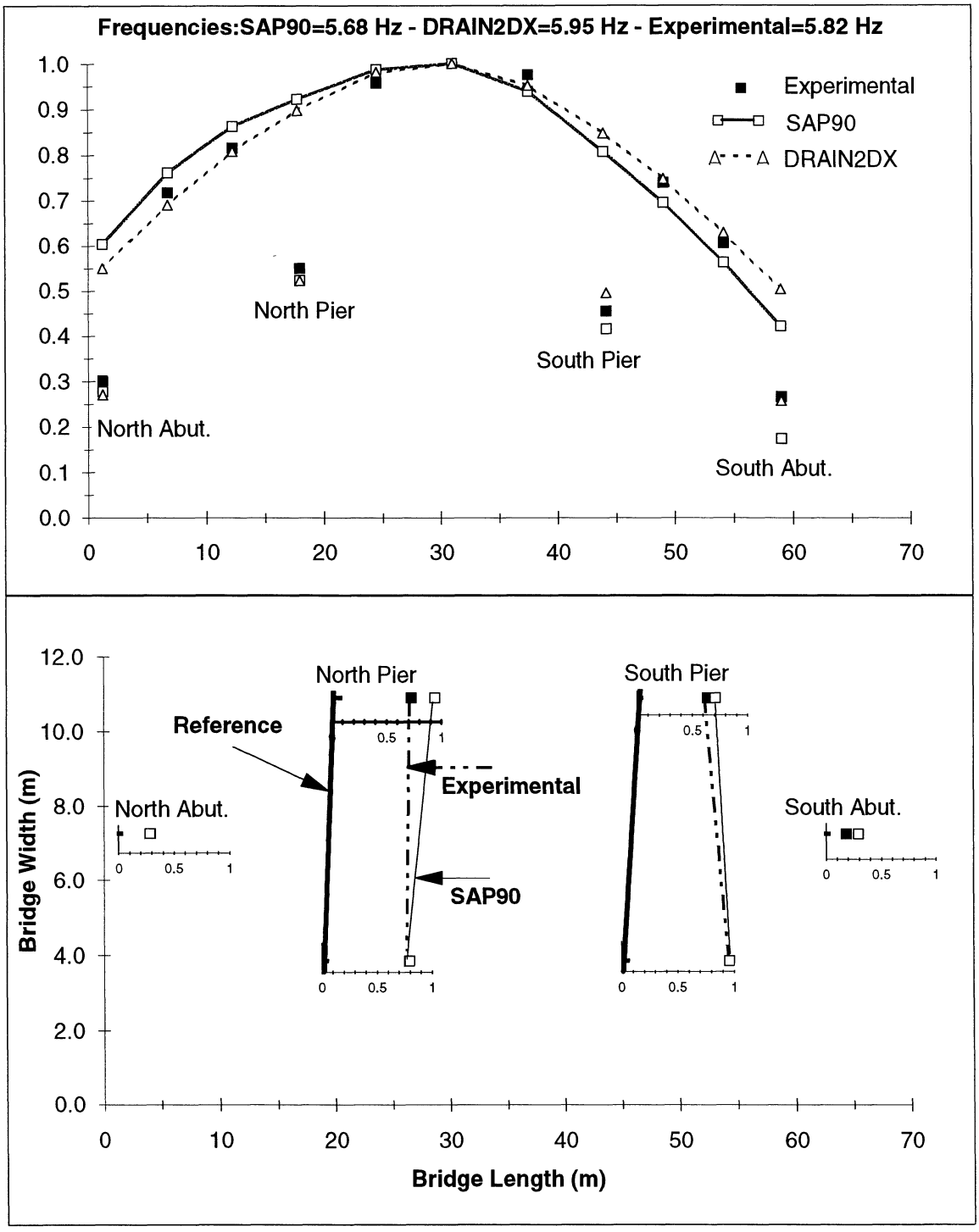

FIGURE 4-29 Northbound Bridge - First Transverse - Longitudinal Mode

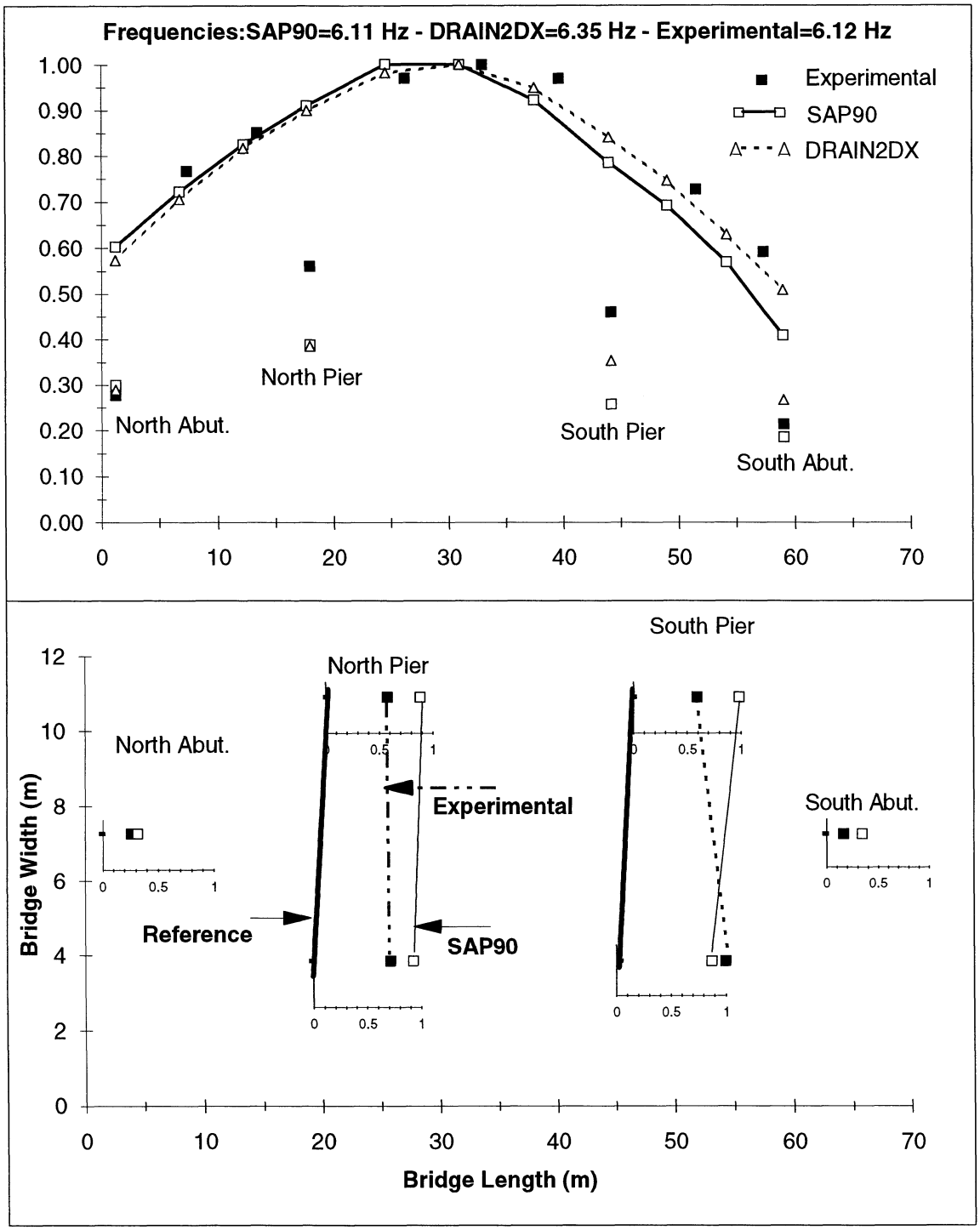

FIGURE 4-30 Northbound Bridge - Second Transverse - Longitudinal Mode

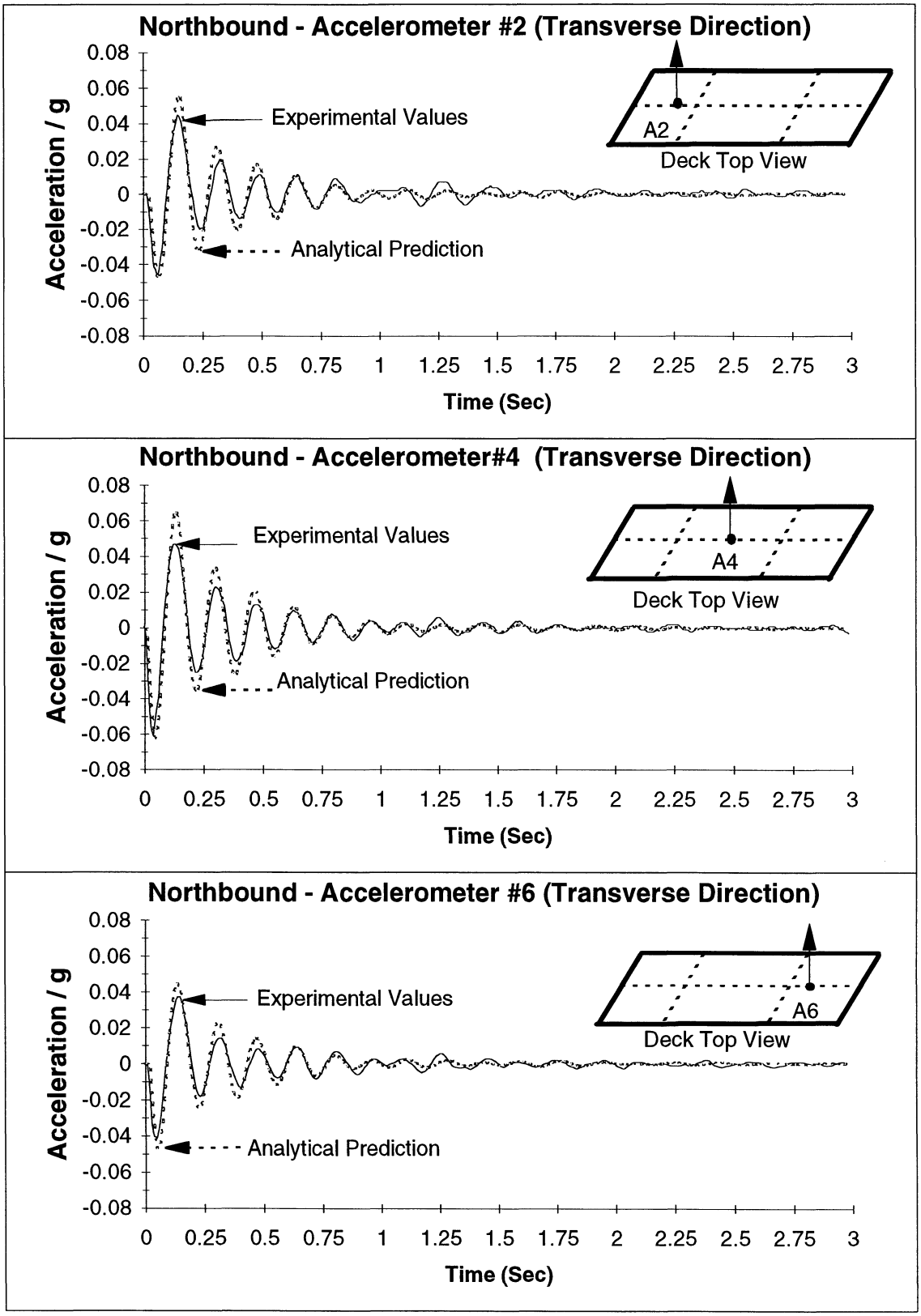

FIGURE 4-31 Northbound Bridge - Analytical vs Experimental - NBPRE-T3-TP

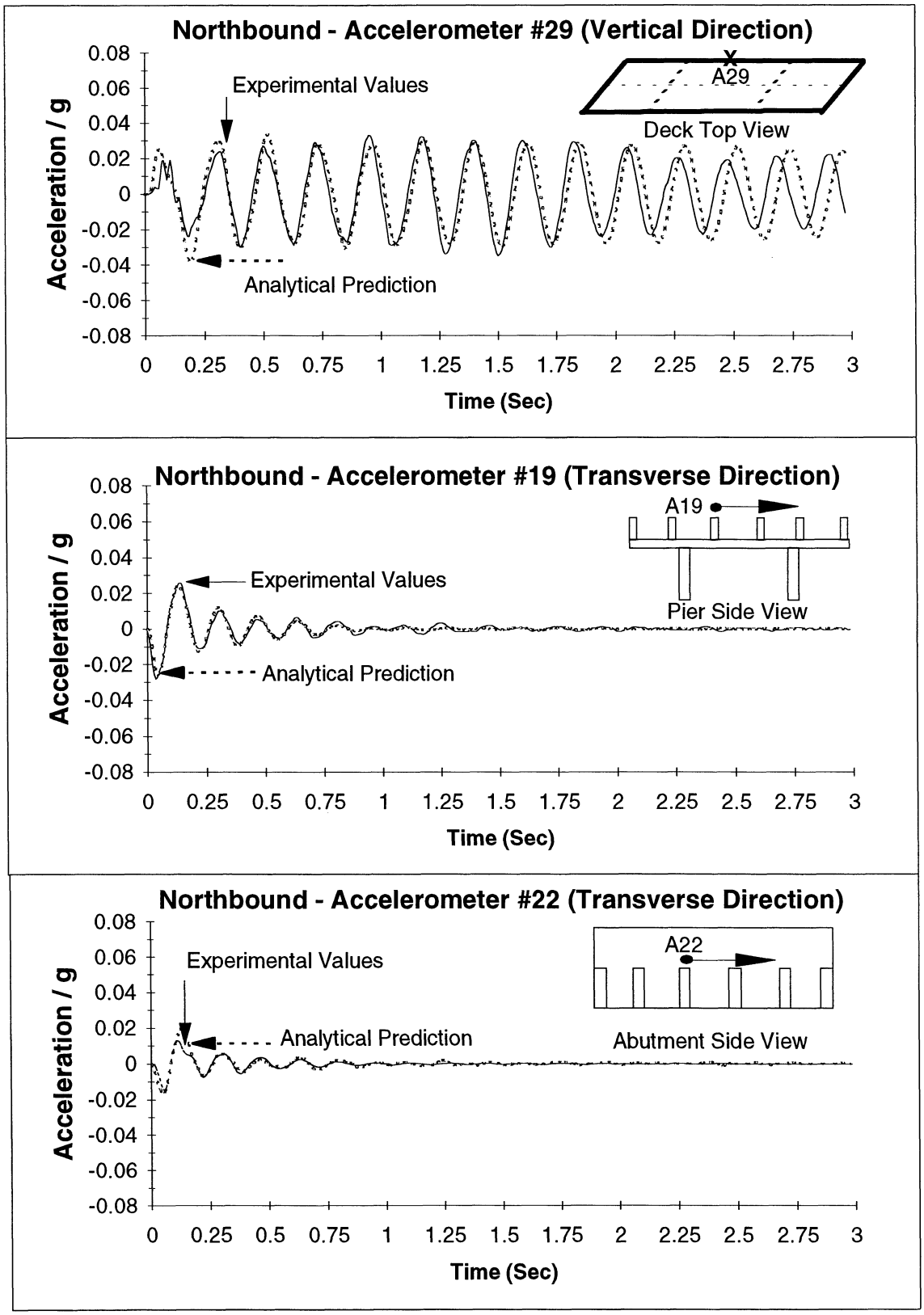

FIGURE 4-32 Northbound Bridge - Analytical vs Experimental - NBPRE-T3-TP

reason and due to a slight difference in the frequency predicted and the experimental results (4.50 Hz vs 4.61 Hz) and a very small damping, the time history shows an initial good agreement but this agreement is lost for the reasons given before.

4.6 Modeling Comparison

When deciding on the level of complexity of a structural model, most engineers need to find a solution that can balance factors as time, cost, accuracy, etc. Simplified models normally are a cost-effective way to solve the class of common regular structures. However, an oversimplification of the problem can produce substantial error that puts at risk veracity and credibility of the results. The construction of a simplified model is an art that combines knowledge, experience and a clear understanding of the fundamental parameters that govern the problem. For this project, three different models were constructed with different levels of complexity. All of them are compared here.

Before starting the comparison, is important to mention that as described before each model has a different level of complexity, model size, approximate time to run and other factors such as memory requirement which can be estimated from the following table 4-5.

TABLE 4-5 Model Comparison

			Type of Analysis	
Model	**Number of Joints**	**Degree of freedom per joint**	**Linear**	**Non-linear**
SAP90 3D	1830	$6(x, y, z, R_x, R_y, R_z)$	yes	no
DRAIN-2DX	47	$3(x, y, R_z)$	yes	yes
SAP90 2D	21	$2(y, R_z)$	yes	no

where x = translation in the X direction, y = translation in the Y direction, and z = translation in the Z direction, R_x = rotation around the X axis, R_y = rotation around the Y axis, and R_z = rotation around the Z axis.

Figure 4-33 compares the experimental mode shapes and the predictions using different models for the Southbound bridge. It is clear from the figure that there is a reasonable agreement among all of them and the experimental values. It is also clear that the differences observed between the 3D model and the 2D model are not substantial, even though in the latter the reduction of the number of DOF is more than 100 times. Figure 4-34 presents a summary of the first five transverse mode shapes and frequencies predicted by the models. It also presents the participating mass for each mode. The comparison between the 3D SAP90 model and DRAIN-2DX model show two mode shapes that look similar (shape 1) at frequencies around 5.5 and 6 Hz. For these models there is a coupled condition between the longitudinal and transverse direction that does not appear in the model SAP90-2D since the bridge in this model is restrained in the longitudinal direction ("x"). The first five mode shapes and frequencies predicted by each model are very close, with some differences in the participating mass, especially between the SAP90-3D and the model SAP90-2D.

To corroborate the possible differences in predictions between the models for a specific earthquake, the EL CENTRO 1940 N-S motion was used as input for the three models and the displacement time history was computed and compared. The first 15 seconds of the response are presented in figures 4-35 and 4-36. Figure 4-35 shows that the differences in the predictions using the 3D model and the DRAIN-2DX model were not significant in any of the directions (transverse or longitudinal) or at the pier level. In all of the cases, the DRAIN-2DX model was able to reconstruct the major peaks and in cases where there were differences, they were on the order of 9%. Figure 4-36 compares the results between the two SAP90 models. From the figure is clear that a reasonable agreement was observed between both models; the differences between the prediction for certain peaks were on the order of 12%.

The comparison between models shows that for regular structures, if the correct parameters that govern the problem are chosen, and if these parameters are computed using logical first principles of structural mechanics and dynamics, it is possible to construct models that can predict the behavior of the structure with an average error of only around 10% com-

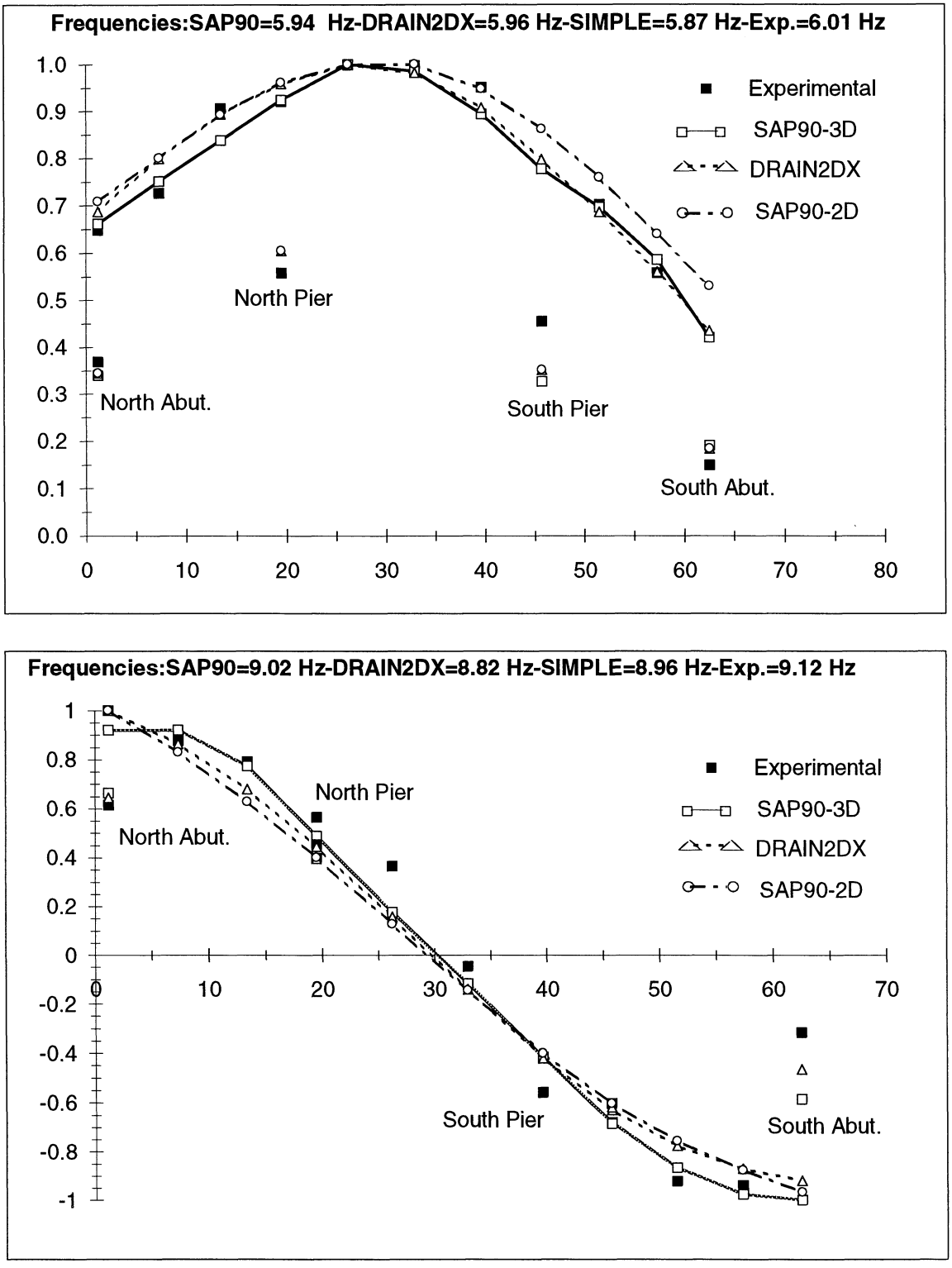

FIGURE 4-33 Southbound Bridge - Comparison Between Different Models

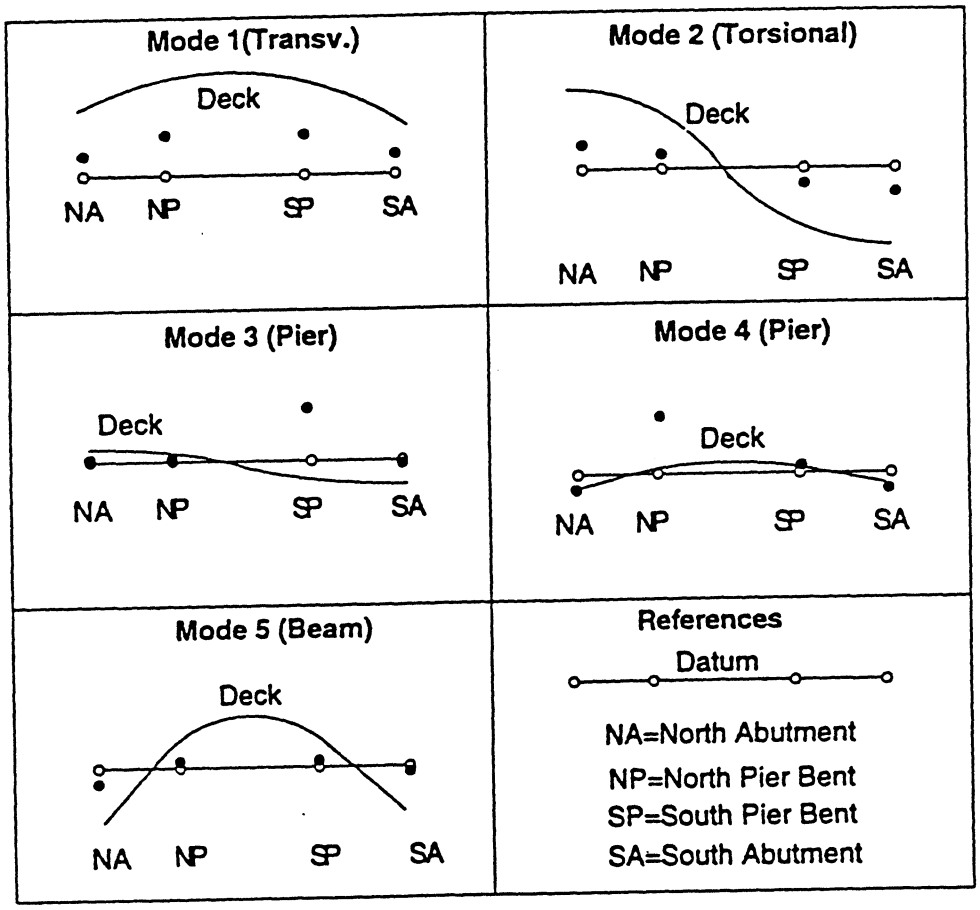

Mode	SAP90 -3D		DRAIN2DX		SAP90-2D	
	Freq.(Hz)	P.M.(%)*	Freq.(Hz)	P.M.(%)*	Freq.(Hz)	P.M.(%)*
1	5.34 5.94	35.0 30.0	5.45 5.96	39.0 33.0	5.86	75.0
2	9.02	0.15	8.82	0.10	8.95	0.26
3	11.86	2.50	12.00	3.27	11.99	3.28
4	12.43	1.91	12.58	0.06	12.60	1.89
5	13.72	7.88	13.83	11.0	14.04	18.53
Sum=		78%		86.5%		99%

*P.M. = Participating Mass

FIGURE 4-34 Results Comparison for Different Mathematical Models

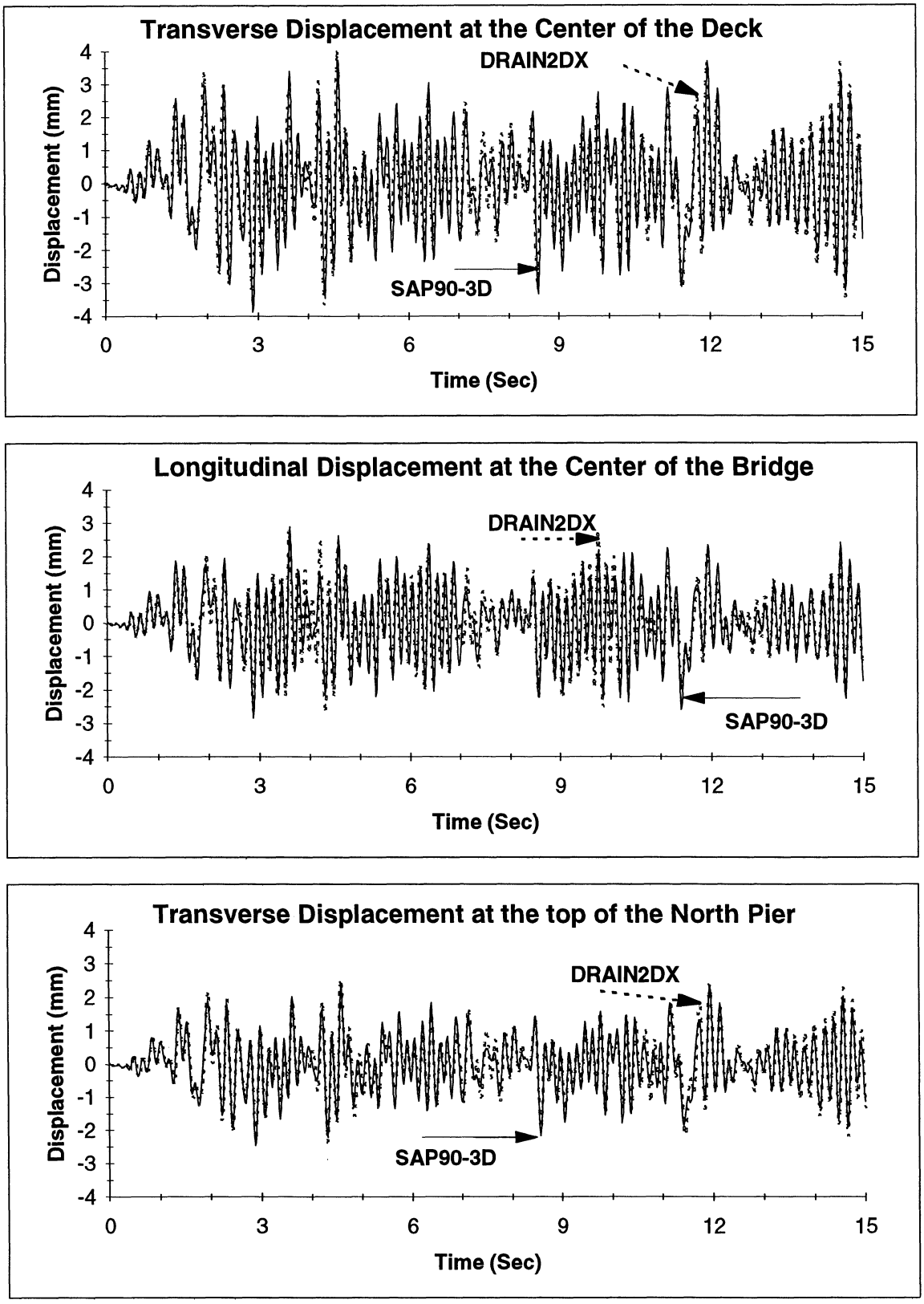

FIGURE 4-35 SAP90-3D vs DRAIN2DX-Southbound Models for EL CENTRO

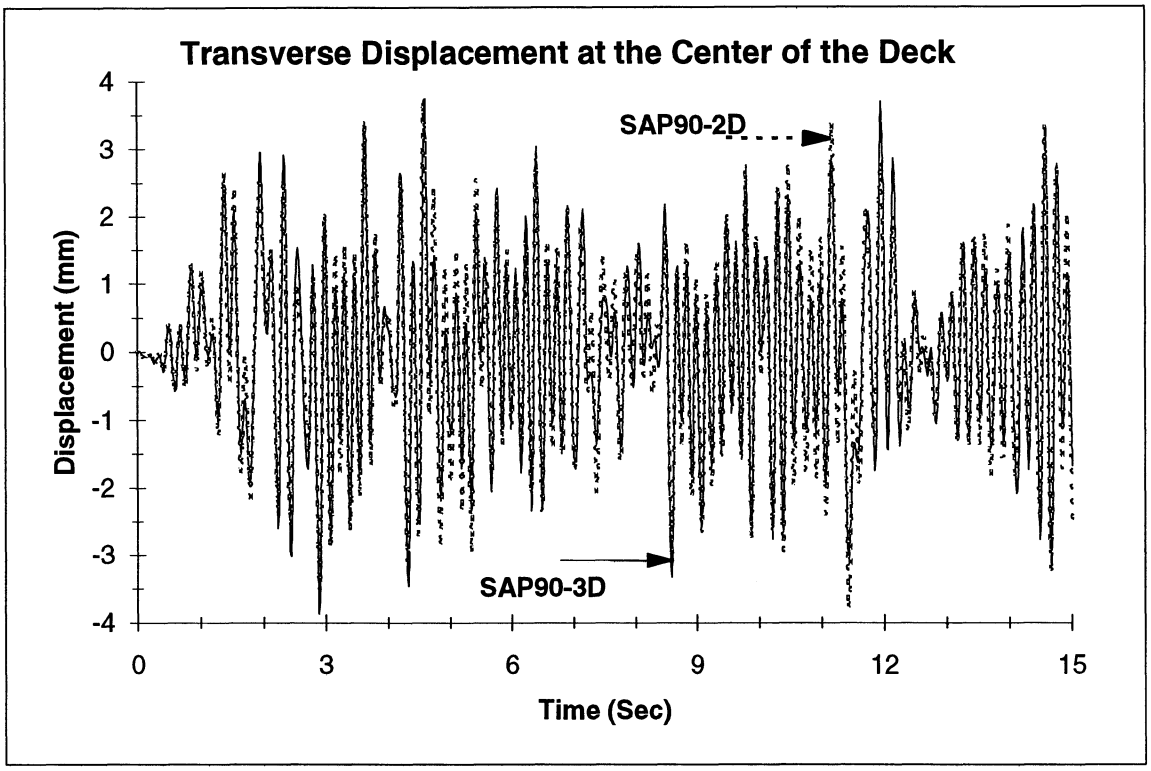

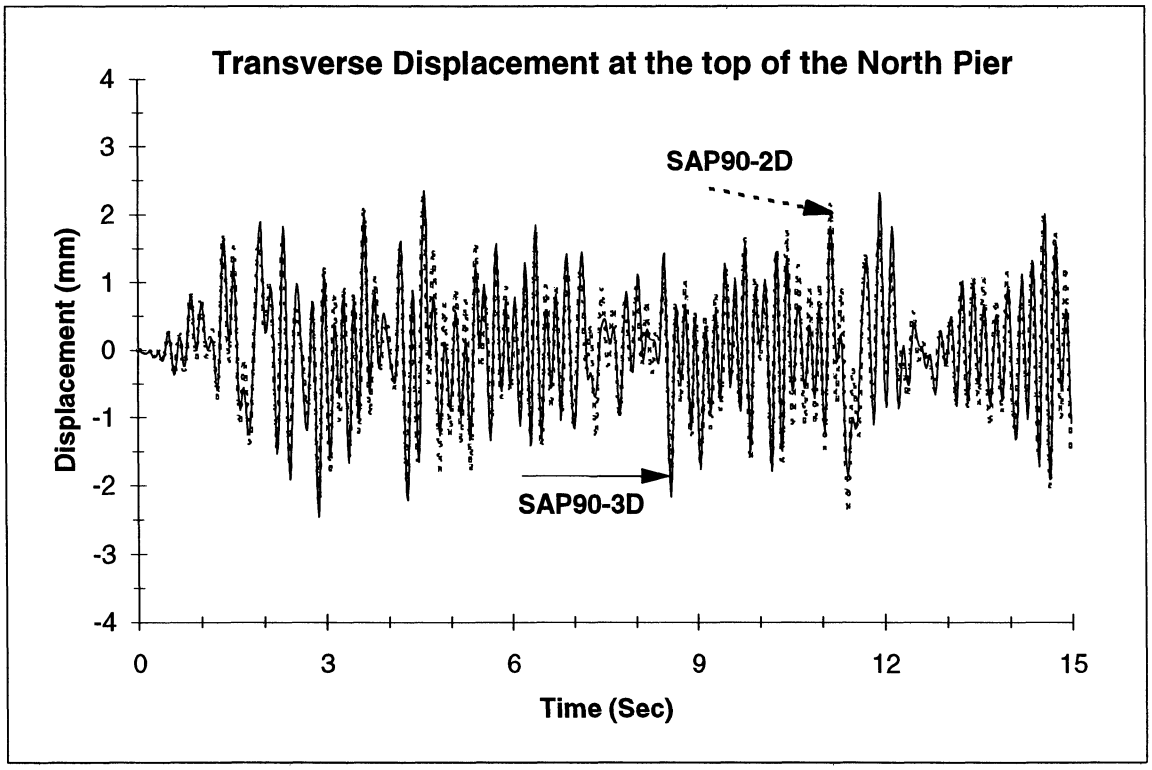

FIGURE 4-36 SAP90-3D vs SAP90-2D-Southbound Models for EL CENTRO

pared with a much more sophisticated model. The comparison presented here was done withthe intention to show that for regular slab-on-girder bridges, the simplified model can produce a good estimate. For preliminary studies, however, it is important to mention again that the reliability of this simplified model rests in a sound knowledge of the structural behavior.

SECTION 5
EXPERIMENTAL BEHAVIOR OF THE BRIDGES SEATED ON RUBBER BEARINGS

5.1 INTRODUCTION

The two principal concepts of base isolation are to lengthen the fundamental period of the vibration of structure and to increase the structural damping by mechanical means. Both of these, generally, reduce seismic response. The isolation approach can be appealing for seismic retrofit as it minimizes changes to the structure to be retrofitted.

The section goes on to consider the problems that arise during the structural identification of the dynamic properties for a system which does not exhibit linear behavior. The approach used to extract mode shapes and frequencies is explained. Finally, the results obtained from the field experimentation on the two investigated bridges are presented.

5.2 SYSTEM IDENTIFICATION OF THE POST-RETROFITTED BRIDGES

Section 3 discussed the different approaches that can be used to extract the dynamic properties of a structure after it is tested. The so-called system identification methodology provides important parameter values that help calibrate control parameters in the mathematical/ structural models. The methodologies presented in that section and the alternative proposed for this project were based on linear behavior of the structure. If the structure does exhibit a substantial nonlinear behavior, then the proposed methodology is no longer valid due to changes in the properties (frequencies, mode shapes, etc) with time. In the Southbound bridge where a substantial nonlinear behavior was expected, it was necessary to develop another approach to obtain the bearings' characteristic stiffness and "yield strength". For the Northbound bridge, where the non-linearities of the bearings were minor, it was possible to assume that the structure would behave linearly and apply the methodology described in Section 3 with certain modifications that will be described later. The first part of this subsection will introduce the reader to the problems that arise in the system identification approach when the structure has a

nonlinear behavior. Later the subsection will discuss the methodology proposed and utilized in this study to identify the dynamic characteristics and bearing stiffness of both bridges.

5.2.1 Background

Before presenting the methodology used to identify the dynamic properties of the post-retrofitted bridges, a brief discussion of certain basic dynamic principles and related research in the system identification of nonlinear structures is needed. The intention of this introduction is to present the problems which arise when a structure behaves in a non-linear fashion.

It is commonplace for structural engineers to describe structural dynamic behavior in terms of frequencies and mode shapes. In fact, design codes for both bridges and buildings incorporate these concepts in the computation of the design forces. The frequencies and mode shapes are the result of eigen solutions of the equations of motion of multi-degree-of-freedom systems. Under certain conditions these equations can be decoupled and the solution expressed in terms of a new coordinate system called principal coordinates. One of the basic assumptions used to solve these differential equations is that the properties of the structure remain constant during the time considered (stationary condition), which is equivalent to assuming that the structure remains linear-elastic. Other assumptions require that the structure has a low level of viscous damping. Under these two conditions real-numbered frequencies and mode shapes result from the solution of the differential equations of motion.

As expressed earlier, the base isolation concept is based on the notions of period shift and increase in energy dissipation via mechanical (hysteretic) damping. Such mechanical damping is often expressed in terms of equivalent viscous damping. If equivalent viscous damping exceeds 10 to 20% of critical, it is possible that the solution of the differential equations can produce complex frequencies and mode shapes. If the structural properties change with time due to nonlinear behavior, then the solution of the differential equations (frequencies and mode shapes) is valid only for a time interval in which the properties are considered constant. It is clear that if the structure has proportional damping no greater than 10% of critical and remains elastic, then the conventional concepts of frequencies and mode shapes can

be used. In other cases the solution of the differential equations using the conventional approach is an approximation of the exact solution and should be used with caution.

Tsai (1988) in his study of typical base isolated structures reported that the classical mode superposition technique can be used without significant error to evaluate the behavior of structures under the excitation of earthquakes which have dominant frequencies between 1 Hz and 10 Hz for general soil conditions. For heavily damped base isolated systems Tsai (1993) showed that the use of classical mode superposition can produce substantial errors. Kelly and Buckle (1986), using a shaking table test, showed that for structures isolated with rubber bearings, the classical modal approach can predict the experimental behavior. From this discussion and according to results reported by other researchers, the Northbound bridge, which has elastomeric rubber bearings, can be considered a linear structure. Therefore the system identification approach used in the pre-retrofitted bridges can be used to find its dynamic properties.

For the Southbound bridge, where non-linear behavior is expected for large transverse displacements, some other considerations should be pointed out before the system identification used will be discussed. Several previous research efforts have been conducted in the identification of the dynamic properties of nonlinear structures. Ghanem (1991) described and compared the use of the extended Kalman filter with other alternatives in his work. This identification technique, is considered to require substantial expertise, with a numerical convergence that is reached sometime. Ibrahim (1983) used his linear time domain solution to produce a quasi-linear identification system to predict the effective dynamic characteristics of a nonlinear system. Distefano (1974) has presented a least squares approach for the identification of a nonlinear SDOF system. Cifuentes (1984) proposed a methodology based on the restoring force time history of a SDOF system. The method can handle only a time record with a single frequency component; therefore bandpass filtering needs to be performed to isolate the frequency component of interest from other frequency components in an experimental record. Peng (1992) presents a method for hysteretic structures, based on the restoring force of each mode-like component. This approach, like that of Cifuentes, uses band-pass filtering so that the

coupling between these mode-like responses is minimized. Lam (1990) has reported another system identification technique used in the Mangatewai-iti bridge test. These researchers obtained the frequencies of the bridge from the Fourier spectra and the mode shape using a band-pass filter to isolate the frequency considered. Lam extracted the mode shapes from the comparison of the peaks of the band pass filtered acceleration time histories. It is evident that most of the proposed methods rely on band-pass filtering to isolate the frequency under consideration.

Several points should be made regarding the bandpass filter approach for the system identification of base isolated structures. According to Skinner (1993), the lower frequencies are controlled by the characteristics of the isolators and the higher frequencies by the structure's characteristics. Lower frequencies, which are the most important for design purposes, may be closely spaced due to the fact that the stiffness of the isolators is very small in comparison with the stiffness of the structure. As the structure tries to move as a rigid body, the transverse, longitudinal, and torsional modes around an axis perpendicular to the foundation are very close and may be highly damped. This situation makes the mode separation very difficult when using a band-pass filter. Also due to the damping the interaction between different closely-spaced frequencies cannot be evaluated easily. The results of the filtering process are therefore biased. Finally, to complicate the problem further, during the snap-back test of isolated structures with lead rubber bearings the bearings have an initial displacement greater than the "yield displacement". The inelastic portion ceases rapidly and after no more than one or two cycles the structure behaves linearly. This situation considerably limits the amount of data that can be acquired during the inelastic portion of the time history making it very difficult to extract parameters of interest from this region.

In summary, a structure that behaves inelastically does not have a constant value for its natural frequencies. Rather, frequencies vary according to the degree of inelastic response in the structure. However, it is possible to define a range of one or more dominant frequencies. The goodness of the assessed dominant frequencies also depends on the number of excursions

of the structure into the inelastic range. The kind of test used (one pier or two pier test), the hysteretic characteristics of the bearings, and the maximum displacement amplitude affect the non-linear portion of the time history but may have little or no effect on the elastic portion of the time history. By separating out the inelastic portion of the dynamic response, it is possible to find the dynamic characteristics of the elastic portion. Later with the help of a structural modeling technique, it is possible to reconstruct the nonlinear behavior.

5.2.2 Southbound System Identification

Based on the above discussion, it was decided to divide the time history of the quick-release tests into two portions. Figure 5-1 shows typical acceleration and displacement time histories for an accelerometer and potentiometer located at the south abutment. From the displacement time history, it can be seen that there are two well-defined portions. Portion 1 corresponds to larger deformations, and the second to the remaining data. Inelastic behavior can be assumed initially and is thus limited to Portion 1 since it occurs primarily in the first half-cycle. Portion 2 gives the elastic behavior that is assumed for the remainder of the time history.

To identify the dynamic properties from the elastic portion and from the frequency domain point of view, it is necessary to separate the elastic portion from the inelastic portion first. Four different windows were tested: Hanning, Hamming, Kaiser, and Super Gaussian. These windows help to minimize the leakage and in varying degrees separate any closely-spaced modes. They also affect the results in two different ways. The first, depending on the characteristics of the windows (major lobe height, side lobe, etc.) reduces the side lobes and the leakage but increases the energy concentrated in widening the major lobe. This produces a higher damping value when damping is extracted from the Fourier spectra using the half power method. The second change arises when the window is applied to the time history. The multiplication of time series by the chosen window is equivalent to convolve the two spectras. In order to correct the Fourier spectra of the time history, the window spectra needs to be deconvolved. These and other problems are described in the literature (Ramirez 1985; Harris

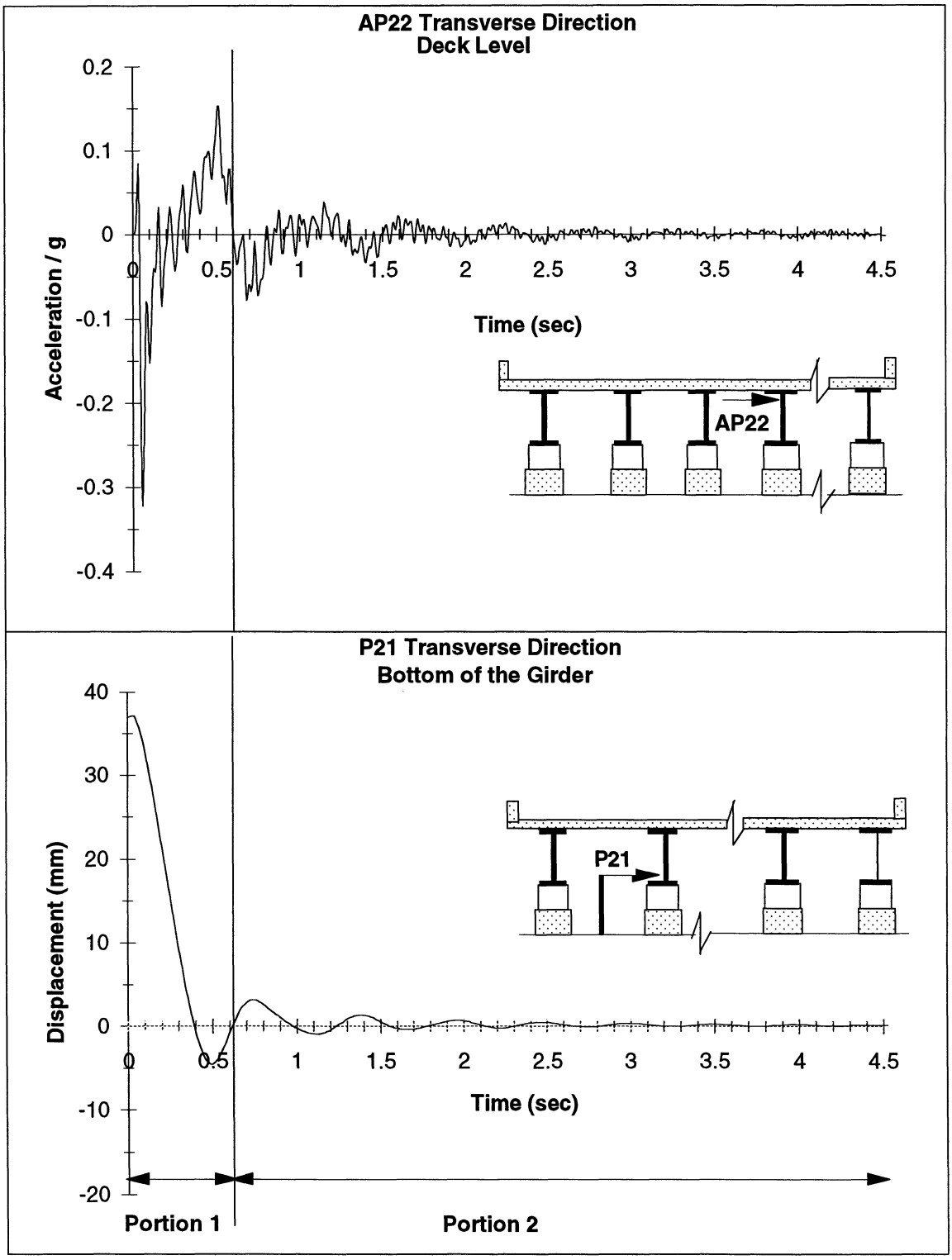

FIGURE 5-1 Typical Acceleration and Displacement Time History at the Abutment

1978; Richardson 1975; Veletsos 1985). It was found that for this study the Hanning, Hamming and Kaiser windows did not introduce significant errors and the Kaiser windows performed better than the others in separating the closely-spaced modes.

To extract the linear portion of the acceleration time history, the following procedure was used:

1) From the displacement time histories of all the potentiometers located at the bearings, the tentative starting time of elastic behavior was chosen as the longest time between the release of the structure and the end of the first cycle of all of the potentiometers in question.
2) Using a Kaiser window between the starting point defined in Step 1 and the end of the vibration, the elastic portion was extracted and augmented with zeroes until the total number of points in the time history was 8192.
3) The Fourier spectra was computed and the frequencies extracted.
4) Steps 2 and 3 were repeated assuming different starting times. The process was stopped when the frequencies of two consecutive steps did not differ by more than 5%.

From the procedure described above, it was found that a good estimate of the starting linear portion can be assumed at the end of the first cycle that starts from zero displacement. Due to the shape of the Kaiser window, which resembles an elongated bell, any additional inelastic behavior that may extend over the second cycle is reduced to small values, giving a negligible contribution over the total elastic portion.

With the elastic portion of the time history, the frequencies and mode shapes were extracted from the Fourier spectra following the procedure described for the pre-retrofitted bridges. The approximate damping values were obtained from the Fourier spectra using the half power method. In order to double check the values obtained by this methodology, the Time Domain method described in Section 3 was modified to include the possibility of initial velocity.

The initial time for the time domain curve fitting was taken as the end of the first cycle as defined above. The initial frequencies and damping values necessary for this process, were taken from the analysis of the Fourier spectra of the entire time history (elastic + inelastic portion). Table 5-1 presents the average of the experimental frequencies and mode shapes, extracted from the ambient vibration tests and from the elastic portion of the snap-back test, using the approach described above.

With the frequencies and mode shapes extracted from the elastic portion of the time history and with the data from the static test, an optimization process was used in order to extract the initial stiffness of the bearings in the transverse direction of the bridge. The optimization process used the simplified model SAP90-2D presented in Section 4 and reproduced as figure 5-2. In this model the only unknown characteristics are the bearings, all the others values, (mass, stiffness, etc.) were extracted from the pre-retrofitted results. The stiffness values of the bearings were obtained from a minimization process. In this process the error was computed as the difference between the predicted mode shapes, frequencies, static displacements at a low load level, and the experimental values. In order to check the results extracted from the use of the simple model, the final values of the identified initial stiffness were substituted into the 3D SAP90 finite element model described in Section 4, and the frequencies and mode shapes obtained from the analysis compared with the experimental values.

During the experiment, the accelerometers were installed in the transverse direction at the deck, piers and abutments as shown in figures 2-25 to 2-27. These instruments provided information that allowed the reconstruction of the translational component of the mode shapes but did not provide direct information of the rotational components. Then the problem should be expressed in terms of the known experimental values. To accomplish this objective and to reduce the computational time it was decided to use static condensation or Guyan (1965) reduction. This approach is widely used to reduce the size of the problem, and is well described in several references (Craig 1981, Paz 1991). The problem can be expressed as:

TABLE 5-1 Southbound Bridge - Experimental Frequencies and Mode Shapes

				Frequency			
Accel.	**Location**	**Test Type**	**Direction**	**3.97**	**4.31**	**6.87**	**9.16**
AP3	Deck	Ambient vib.	Vertical	-0.03	-0.03	-0.06	-0.13
A1	Deck	Ambient vib.	Vertical	-0.22	-0.07	-0.27	-0.89
A2	Deck	Ambient vib.	Vertical	-0.24	-0.05	-0.23	-0.64
AP9	Deck	Ambient vib.	Vertical	0.02	0.01	0.11	-0.14
A3	Deck	Ambient vib.	Vertical	0.55	0.21	0.68	-0.03
A4	Deck	Ambient vib.	Vertical	0.73	0.23	1.00	-0.16
A5	Deck	Ambient vib.	Vertical	0.53	0.18	0.77	-0.22
A16	Deck	Ambient vib.	Vertical	0.06	0.03	0.13	-0.05
A6	Deck	Ambient vib.	Vertical	-0.17	-0.06	-0.20	0.08
A7	Deck	Ambient vib.	Vertical	-0.16	-0.08	-0.25	0.09
AP22	Deck	Ambient vib.	Vertical	-0.01	-0.05	-0.06	0.02
A25	Deck	Ambient vib.	Vertical	-0.31	0.17	0.26	0.90
A26	Deck	Ambient vib.	Vertical	1.00	-0.63	-0.53	0.09
A27	Deck	Ambient vib.	Vertical	-0.25	0.16	0.10	-0.14
A28	Deck	Ambient vib.	Vertical	-0.19	-0.29	0.05	1.00
A29	Deck	Ambient vib.	Vertical	0.52	1.00	-0.93	0.11
A30	Deck	Ambient vib.	Vertical	-0.07	-0.11	0.09	-0.08
				Frequency			
				1.96	**3.13**	**14.03**	**27.79**
AP3	Deck	Snap Back	Transverse	1.00	-0.99	0.96	-0.93
A1	Deck	Snap Back	Transverse	0.99	-0.80	0.54	-0.25
A2	Deck	Snap Back	Transverse	0.97	-0.61	0.10	0.39
AP9	Deck	Snap Back	Transverse	0.97	-0.43	-0.29	0.89
A3	Deck	Snap Back	Transverse	0.95	-0.20	-0.39	0.54
A4	Deck	Snap Back	Transverse	0.92	0.04	-0.48	-0.06
A5	Deck	Snap Back	Transverse	0.90	0.26	-0.36	-0.69
AP16	Deck	Snap Back	Transverse	0.87	0.45	-0.12	-0.92
A6	Deck	Snap Back	Transverse	0.84	0.64	0.20	-0.40
A7	Deck	Snap Back	Transverse	0.82	0.82	0.60	0.36
AP22	Deck	Snap Back	Transverse	0.78	1.00	1.00	1.00
A8	N. Abutment	Snap Back	Transverse	0.02	-0.02	0.00	0.00
A13	N. Pier	Snap Back	Transverse	0.02	-0.01	0.00	0.00
A19	S. Pier	Snap Back	Transverse	0.02	0.01	0.00	0.00
A22	S. Abutment	Snap Back	Transverse	0.00	0.00	0.00	0.00

$$[M]\{\ddot{U}\} + [K]\{U\} = \{P\} \tag{5-1}$$

or

$$\begin{bmatrix} [M_{aa}] & 0 \\ 0 & 0 \end{bmatrix} \begin{Bmatrix} \{\ddot{U}_a\} \\ \{\ddot{U}_d\} \end{Bmatrix} + \begin{bmatrix} [K_{aa}] & [K_{ad}] \\ [K_{da}] & [K_{dd}] \end{bmatrix} \begin{Bmatrix} \{U_a\} \\ \{U_d\} \end{Bmatrix} = \begin{Bmatrix} \{P_a\} \\ 0 \end{Bmatrix} \tag{5-2}$$

$$[M_{aa}]\{\ddot{U}_a\} + [K_{aa}]\{U_a\} + [K_{ad}]\{U_d\} = [P_a] \tag{5-3a}$$

where $[M]$ = mass matrix, $[K]$ = stiffness matrix, $\{\ddot{u}\}$; $\{u\}$ = original set of coordinates, (acceleration or displacement), $[M_{aa}]$ = lumped mass matrix for active coordinates, $\{\ddot{U}_a\}$ = vector

$$[K_{da}]\{U_a\} + [K_{dd}]\{U_d\} = 0 \tag{5-3b}$$

of active coordinates (acceleration), $\{\ddot{U}_d\}$ = vector of dependent coordinates (acceleration), $\{U_a\}$ = vector of active coordinates (displacement), $\{U_d\}$ = vector of dependent coordinates (displacement), $[K_{aa}]$; $[K_{da}]$ = stiffness coefficients of the active coordinates, and $[K_{dd}]$ = stiffness coefficients of the dependent coordinates.

Equation (5-3b) provides a constraint equation which may be expressed as:

$$\{U_d\} = -[K_{dd}]^{-1}[K_{da}]\{U_a\} \tag{5-4}$$

By defining

$$-[K_{dd}]^{-1}[K_{da}] = [t] \tag{5-5}$$

equation (5-4) can be expressed as:

$$\{U_d\} = [t]\{U_a\} \tag{5-6}$$

or using the identity

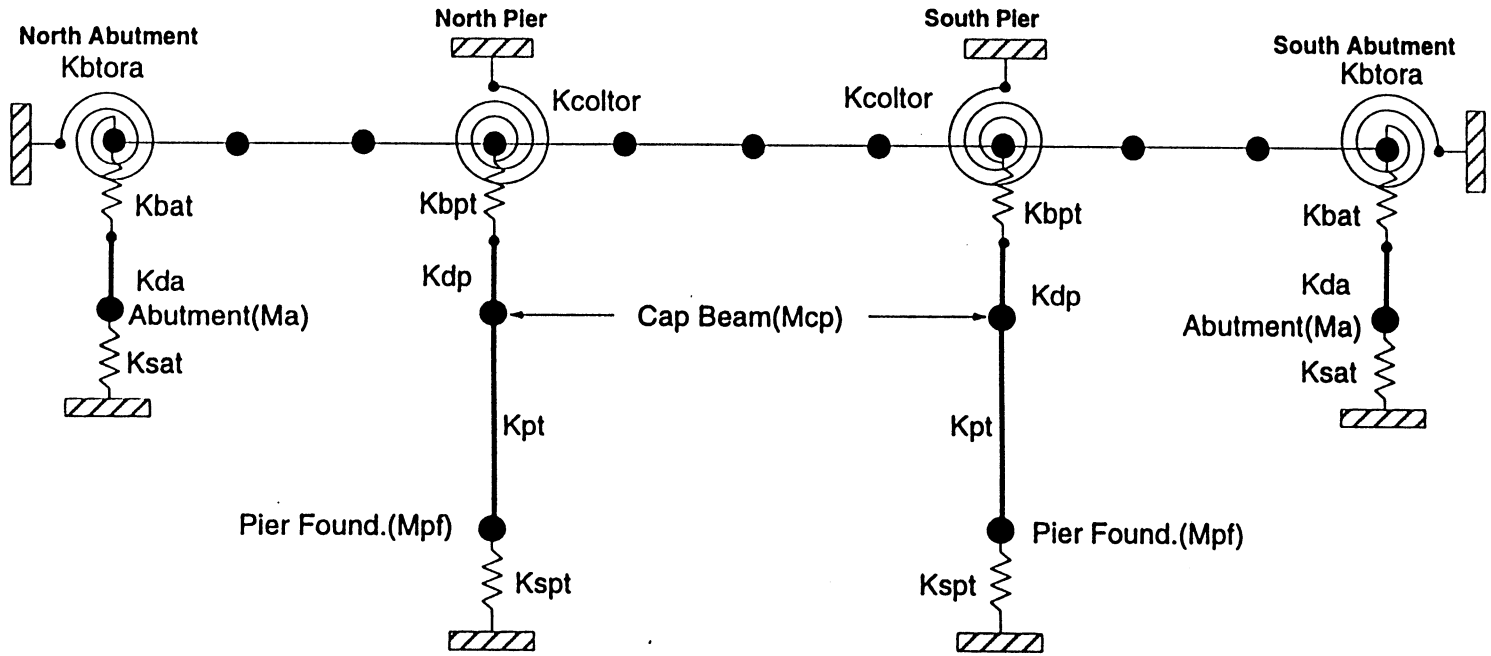

$$Kcoltor = \frac{Kbtorp * Kctor}{Kbtor + Kctor}$$

Where:

Kbtorp = Torsional Stiffness of the bearings system

Kctor = Torsional Stiffness of the pier bent System

FIGURE 5-2 Transverse Simplified Model (SAP-2D)

$$\{U_a\} = [I]\{U_a\} \tag{5-7}$$

it is possible to express:

$$\{U\} = \begin{Bmatrix} \{U_a\} \\ \{U_d\} \end{Bmatrix} = \begin{bmatrix} [I] \\ [t] \end{bmatrix} \{U_a\} \tag{5-8}$$

where transformation matrix $[T]$ may be defined as

$$[T] = \begin{bmatrix} [I] \\ [K_{dd}]^{-1}[K_{da}] \end{bmatrix} \tag{5-10}$$

$$\{U\} = [T]\{U_a\} \tag{5-9}$$

Making use of the transformation matrix $[T]$ it is possible to write the equation of motion (5-1) for the active coordinates $\{U_a\}$. If the mass of the structure is lumped at the joints, then the mass matrix is:

$$[\hat{M}_{aa}] = [T]^T[M][T] = \{[I][t]\}\begin{bmatrix} [M_{aa}] & 0 \\ 0 & 0 \end{bmatrix}\begin{Bmatrix} [I] \\ [t] \end{Bmatrix} = [M_{aa}] \tag{5-11}$$

and the stiffness matrix:

$$[\hat{K}_{aa}] = [T]^T[M][T] = \{[I][t]\}\begin{bmatrix} [K_{aa}] & [K_{ad}] \\ [K_{da}] & [K_{dd}] \end{bmatrix}\begin{Bmatrix} [I] \\ [t] \end{Bmatrix} \tag{5-12}$$

$$[\hat{K}_{aa}] = [K_{aa}] - [K_{da}]^T[K_{dd}]^{-1}[K_{da}] \tag{5-13}$$

Finally, equation (5-1) can be expressed as:

$$\left[\hat{M}_{aa}\right]\left\{\ddot{U}_{aa}\right\} + \left[\hat{K}_{aa}\right]\left\{U_{aa}\right\} = \left\{P_a\right\} \tag{5-14}$$

where $\left[\hat{M}_{aa}\right]$ = reduced mass matrix, and $\left[\hat{K}_{aa}\right]$ = reduced stiffness matrix. Thus the mode shapes and frequencies may be found from the solution of an eigenvalue problem using the condensed approach:

$$\left\{\left[\hat{K}_{aa}\right] - \omega^2\left[\hat{M}_{aa}\right]\right\}\{\phi\} = 0 \tag{5-15}$$

The static displacement $\{U_s\}$ using the condensed approach can be expressed as:

$$\left[\hat{K}_{aa}\right]\left\{U_s\right\} = \{P\} \tag{5-16}$$

$$\left\{U_s\right\} = \left[\hat{K}_{aa}\right]^{-1}\{P\} \tag{5-17}$$

If, as expressed by Skinner (1993), the lower modes are controlled by the characteristics of the isolators, then only the first modes should be used in the minimization process. The experimental results of the laboratory tests on the bearings were used as starting values. To constrain the problem, lower and upper bounds equal to 50% and 150% of the experimental values were adopted. From the load-displacement curve obtained during the loading process of the bridge, and for small loads, it can be assumed that the bearings behaved in a linear fashion. Then the static test could be included in the optimization process, forcing the stiffness not only to minimize the error between the experimental and analytical mode shapes, but also the static displacements of the bridge for a low level of load.

The procedure to obtain the initial stiffness of the bearings can be summarized as follows:

1) Construct a simple model of the bridge and lump the mass in the joints where experimental values can be obtained (figure 5-2).
2) Using the Guyan reduction, condense the degrees of freedom, leaving only the degrees of freedom where the instrument are located.

3) Extract the elastic portion of the acceleration time history, and compute the frequencies and mode shapes as described.

4) From the loading portion of the load vs displacement curve and for a low load value, extract the displacement of the structure at the points where the displacement transducers are located.

5) Using a conventional nonlinear, least-squares method (Quasi-Newton for this study), minimize the error of the expression:

$$F(k) = \sum F_M(k) + F_D(k) + F_\omega(k) = \sum_{i=1}^{N} W_i \xi_i^2 \qquad \textbf{(5-18)}$$

Where the terms in this are obtained as follows:

$$F_M(k) = \sum_{i=1}^{M} W_{M_i} \left[\{\phi\}_{E_i} - \{\phi\}_{A_i} \right]^2 \qquad \textbf{(5-19)}$$

From the frequencies and mode shapes (Step 3):

$$F_\omega(k) = \sum_{i=1}^{\omega} W_{\omega_i} \left[\omega_{E_i} - \omega_{A_i} \right]^2 \qquad \textbf{(5-20)}$$

From the load-displacement curve and for different load values (step 4):

$$F_D(k) = \sum_{i=1}^{D} W_{D_i} \left[\{U\}_{E_i} - \{U\}_{A_i} \right]^2 \qquad \textbf{(5-21)}$$

in which $\{\phi\}_{E_i}$ = experimental mode shape, $\{\phi\}_{A_i}$ = predicted mode shape using simplified model, $\{U\}_{E_i}$ = experimental displacement at each location for force P_i, $\{U\}_{A_i}$ = predicted displacement at each location for force P_i, W_{E_i} = experimental frequency, ω_{A_i} = predicted frequency using simplified model, W_{M_i} = modal weighing factor, W_{D_i} = displacement weighing factor, and W_{ω_i} = frequency weighing factor.

To obtain the properties of the static non-linear portion of the load-displacement hysteresis, a simple approach was used as follows. Assuming that the bearings located over the piers have identical linear properties, then the nonlinear behavior can be attributed solely to the lead-rubber bearings located at the abutments. It is also assumed that due that the aspect ratio between length and width is around four, the bridge moves as a rigid body. This assumption is in agreement with the findings of Turkington (1987). Then it is possible to consider only the translational effect and not include the rotational springs in figure 5-2 for the post yielding phase.

It was also found during the analysis with the SAP 90 3D model described in Section 4 that for the load applied during the pre-retrofitted tests which is approximately the same magnitude as the forces used in the post-retrofitted tests, the total static displacement at the deck was around 1 mm. For these bridges where the expected displacements were on the order of 40 mm and 25 mm for the South and Northbound, respectively, it is possible to assume that the total deformation is due mainly to the deformation of the bearings at the abutments and piers. With the help of the static loading portion of the test, and using the initial stiffness obtained following the procedure described above and the equations of equilibrium, it is possible to obtain the load vs deformation curve of the bearing using the following procedure:

Changing the bearings nomenclatures in figure 5-2 in order to differentiate the locations of the bearings:

$$K_{baN} = K_{bat} \text{ (North abutment)} \; ; \; K_{baS} = K_{bat} \text{ (South abutment)} \qquad \textbf{(5-22)}$$

From equilibrium

$$\Sigma F_y = K_{baN}\delta_{NA} + K_{bpt}\,\delta_{NP} + K_{bpt}\,\delta_{SA} + K_{baS}\,\delta_{SA} - P_{NP} - P_{SP} = 0 \qquad \textbf{(5-23)}$$

Making

$$
\begin{aligned}
F_{SA} &= K_{baS}\,\delta_{SA} \\
F_{SP} &= K_{PS}\,\delta_{SP} \\
F_{NP} &= K_{PS}\,\delta_{NP} \\
F_{NA} &= K_{baN}\,\delta_{NA}
\end{aligned}
\qquad \textbf{(5-24)}
$$

Taking moments around the North abutment

$$\Sigma M_{NA} = -P_{NP}L_{NP} - P_{SP}L_{SP} + F_{SA}L_T + F_{SP}L_{SP} + F_{NP}L_{NP} = 0 \qquad \textbf{(5-25)}$$

$$F_{SA} = \frac{P_{NP}L_{NP} + P_{SP}L_{SP} - F_{SP}L_{SP} - F_{NP}L_{NP}}{L_T} \qquad \textbf{(5-26)}$$

$$K_{baS} = \frac{P_{NP}L_{NP} + P_{S}L_{SP} - F_{SP}L_{SP} - F_{NP}L_{NP}}{L_T\delta_{SA}} \qquad \textbf{(5-27)}$$

and from equation (5-23)

$$F_{NA} = (P_{NP} + P_{SP}) - (F_{NP} + F_{SP} + F_{SA}) \qquad \textbf{(5-28)}$$

where K_{baN} = instantaneous stiffness of the bearing at the north abutment, K_{baS} = instantaneous

$$K_{baN} = \frac{(P_{NP} + P_{SP}) - (F_{NP} + F_{SP} + F_{SA})}{\delta_{NA}} \qquad \textbf{(5-29)}$$

stiffness of the bearing on the south abutment, K_{bpt} = elastic stiffness of the rubber bearings at the north and south pier (from previous elastic system identification), δ_{NP} = North pier bearing displacement, δ_{SP} = south pier bearing displacement, δ_{NA} = north abutment bearing displacement, δ_{SA} = south abutment bearing displacement, P_{NP} = force applied during the static test of the north pier, P_{SP} = force applied during the static test of the south pier, L_{SP} = distance from the south pier to the north abutment, L_{NP} = distance from the north pier to the north abutment, and L_T = total length of the bridge.

In order to include the contribution of the expansion joint to the overall stiffness of the system, the expansion joint was modeled as a spring acting in parallel with the bearings at the abutments. If the displacement of the bearings was less than the "yield" point of the expansion joint, then the forces at the expansion joints were computed as the product of the defined initial stiffness times the displacement. If the displacement of the bearings were greater than the joint "yield" displacement, then a constant frictional force as defined in subsection 2.6 was subtracted from the equilibrium equations (5-23).

Figure 5-3a compares the experimental load vs displacement obtained from the companion laboratory tests for a 50 mm maximum displacement in the bearings and the results obtained using the methodology presented above for the test SBPOST-T2-TP. As can be seen from the figure, the inferred field performance of the lead-rubber bearings is quite consistent with the behavior exhibited in the component test. It also can be appreciated from the graph that the south abutment bearings, have a slightly higher initial stiffness than the north abutments bearings. Using this graph, it is possible to define an initial stiffness for each bearing, a theoretical "yield point" and a "post-yielding" stiffness as illustrated in figure 5-3b. The comparison of laboratory test of the laminated rubber bearings located over the piers and the inferred field test results assuming linear behavior is illustrated in figure 5-3c.

Is important at this point to compare the obtained initial stiffness of the bearings and the contribution of the expansion joints to the overall stiffness. For small displacements, for which there is no yielding in the bearings or sliding in the expansion joints, the total stiffness at the abutment is the sum of the bearings' stiffness and the expansion joint's. Expressing the stiffness of the components as a percent of the total initial stiffness, then the expansion joints have a contribution of around 10% (5173 *kN/m* / (5173 *kN/m* + 6672 *kN/m* ×7)) and 13% (6947 *kN/m* / (6947 *kN/m* + 6255 *kN/m* × 7)) for the south and north abutment, respectively. For larger deformations the joints slide and a frictional force is generated. The total force at the abutment is equilibrated by this frictional force and the resisting forces at the bearings. For displacements on the order of 50 mm (50 % of the total rubber thickness) the joints carry 11% and 12% of the

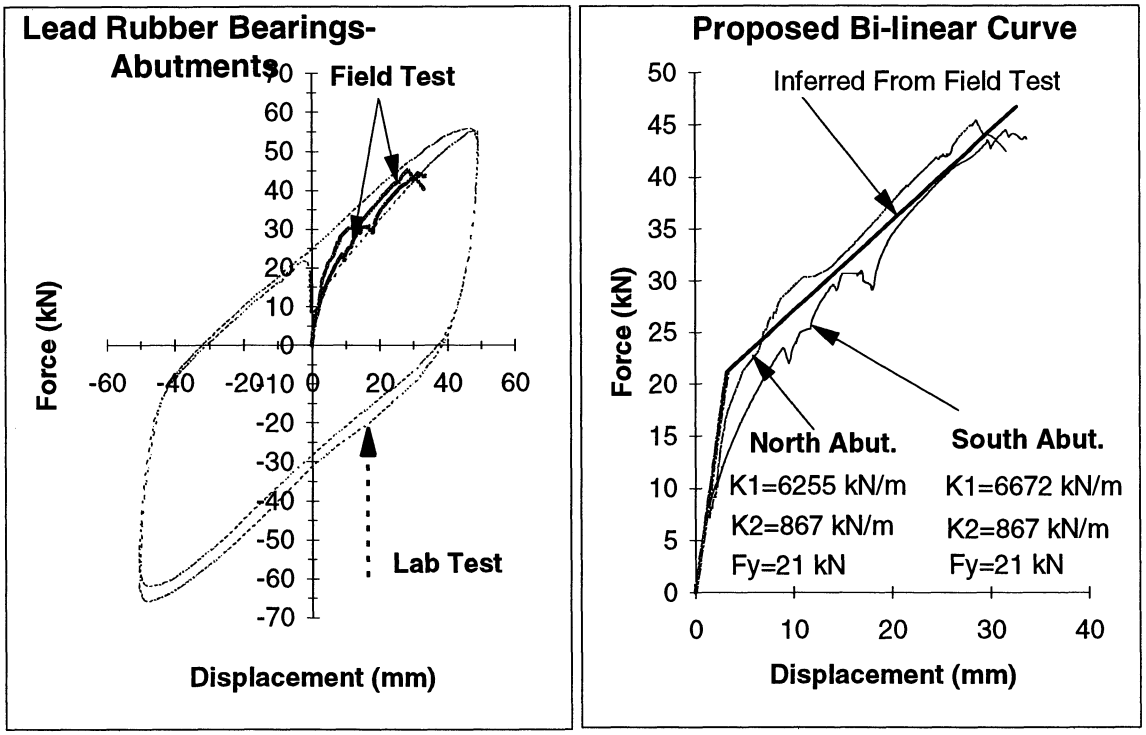

(a) (b)

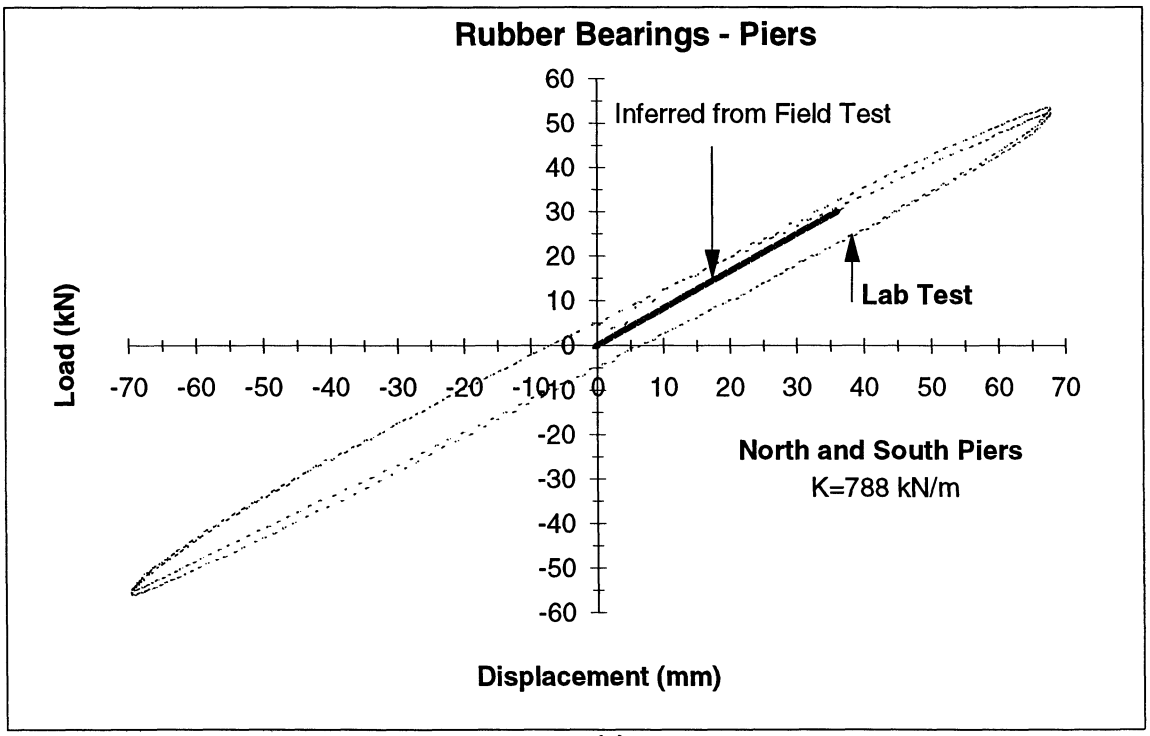

(c)

FIGURE 5-3 Lab Test vs Field Test Behavior - Two Piers Static Test

total force, and for 100 mm (100% of the total rubber thickness) 7% and 8% of the total force at the south and north abutment, respectively.

It is important to mention that identification of the post-yielding stiffness were extracted from a procedure that use the static test. At the moment other researchers (Douglas and co-workers at the University of Nevada, Reno) are conducting studies to identify the properties from the dynamic descendent portion of the bearings constitutive curves.

5.2.3 Northbound System Identification

As discussed, of the Northbound bridge can be assumed to behave linearly without significant error (Tsai, 1988; Kelly, 1986). The tools applied in the pre-retrofitted bridges which are valid for elastic structures can therefore also be used for the post-retrofit tests on the Northbound bridge. A minor modification was made, however, in the time domain approach in order to improve the prediction of the initial displacement of the structure. As explained in Section 3, the time domain approach employed is based on the curve fitting of the fundamental equation of free vibration, considering superposition of several modes. If the experimental measurement (e.g., displacement) is other than acceleration, the basic parameters to be minimized (frequencies, damping and amplitudes) are still the same. The only difference between acceleration and displacement is that the equation of the acceleration is the second derivative of the displacement. Thus, in the minimization process for a station where acceleration and displacement were both measured, the records can be simultaneously minimized if an appropriate factor is used to include the difference in the scale. The only restriction for this approach is that only absolute displacements should be used in conjunction with the acceleration which is also absolute. As described above in subsection 5.2.2, the displacement measured between the deck and the ground at the piers location (potentiometers P13 and P26) can be considered as absolute. These displacement time histories in conjunction with the acceleration time histories at the deck level at the pier location (accelerometers AP9 and AP16) were curve fitted at the same time. This approach forced the parameters to be identified to minimize the error between the experimental and fitted displacement and acceleration time histories. For weighting purposes the instruments were counted two times.

Figure 5-4a shows the comparison between the experimental acceleration and the predicted acceleration using the results obtained from the identification method. Figures 5-4b,c show the experimental and predicted displacement using the system identification methodology. It is evident from the good agreement obtained between the predicted time history and the experimental records that the method works very well. Table 5-2 summarizes the experimental frequencies and mode shapes. The results presented there are the average from the different tests.

Finally, the contribution of the expansion joint to the overall stiffness of the system, was considered using the same approach as that described for the Southbound bridge. For the Northbound bridge, where the stiffness of the bearings are lower than the bearings located at the abutments of the Southbound bridge, the contribution of the expansion joints to the overall initial stiffness of the bridge increases considerably. For the north abutment this contribution is around 21% (5311 *kN/m* / (5311 *kN/m* + 3320 *kN/m* × 6)) and 44% for the south abutment (5311 *kN/m* / (5311 *kN/m* × 1.1 *kN/m* × 6)). After the expansion joint slide (around 8 mm) the frictional force developed there is on the order of 40 kN which in terms of resisting elements at the abutments, is equivalent to considering that there are more than six bearings at the abutments, depending on the maximum deformation.

Figure 5-5 compares the lab experiments performed on the bearings and the predicted load deformation curve from the field test assuming linear behavior in the bearings. The results show that the stiffness of the bearing obtained from the field test, have a good agreement with the results obtained from the laboratory test, for the same deformation level as illustrated.

5.3 Experimental Results of the Post-Retrofitted Bridge Tests

This subsection presents the experimental results for the Northbound and Southbound bridges. The reported methodology to extract the data was described above and in Section 3. The frequencies and mode shapes are the average of consecutive tests performed the same day.

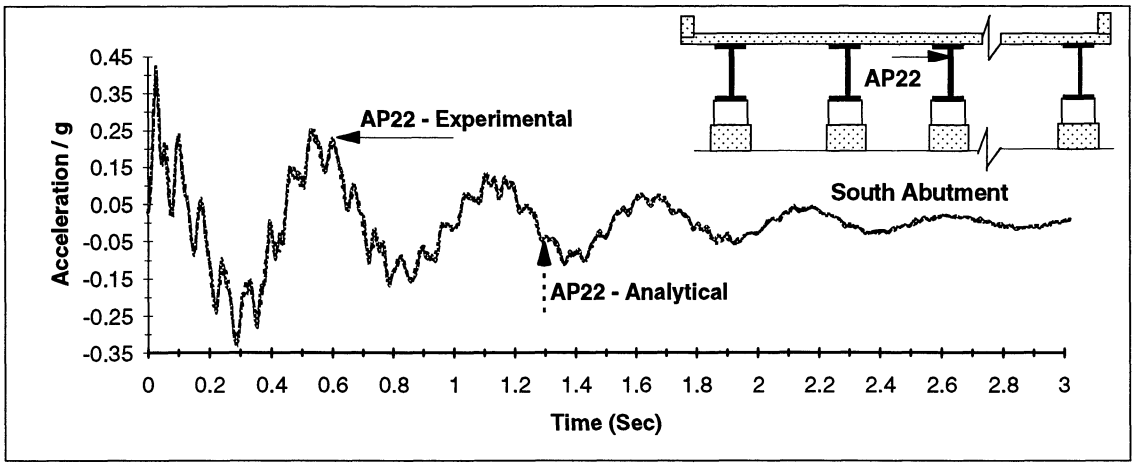

(a)

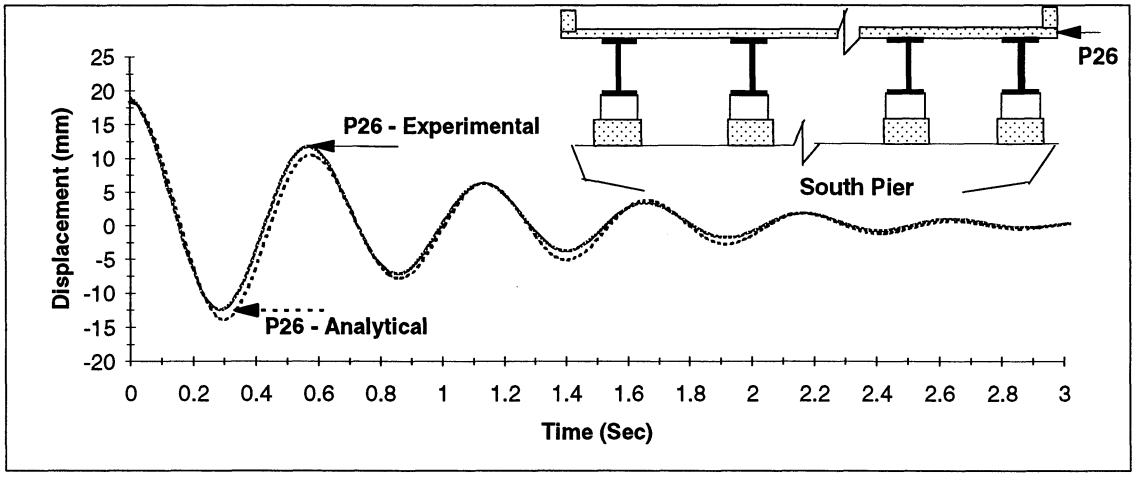

(b)

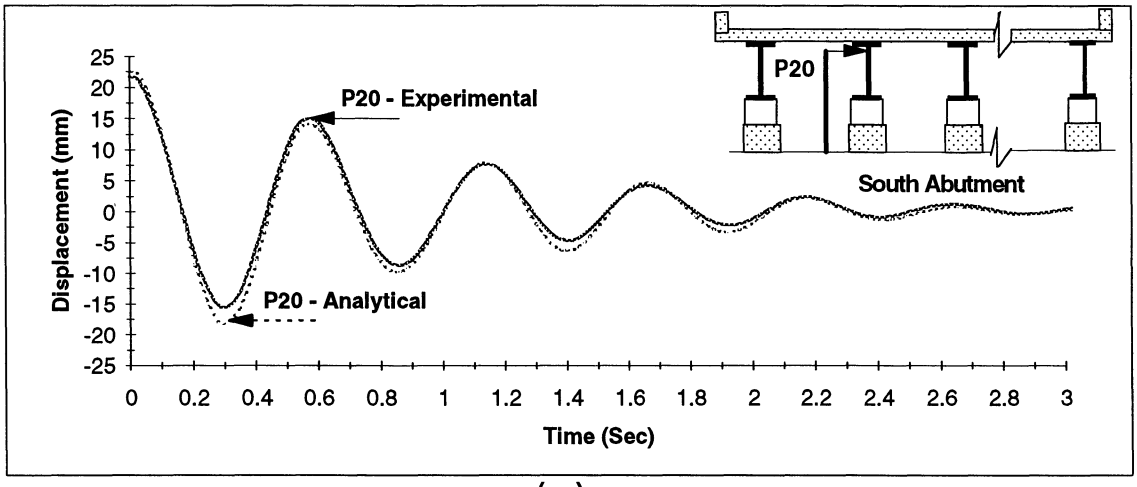

(c)

FIGURE 5-4 System Identification vs Experimental Values-NBPOST-T2-TP

TABLE 5-2 Northbound Bridge - Experimental Frequencies and Mode Shapes

				Frequency				
Accel.	**Location**	**Test Type**	**Direction**	**4.18**	**4.60**	**8.36**	**11.80**	**12.67**
AP3	Deck	Ambient vib.	Vertical	-0.02	-0.01	0.01	-0.12	0.03
A1	Deck	Ambient vib.	Vertical	-0.19	-0.03	0.10	-0.99	0.14
A2	Deck	Ambient vib.	Vertical	-0.22	-0.03	0.12	-0.91	0.11
AP9	Deck	Ambient vib.	Vertical	0.01	0.01	-0.04	-0.12	0.03
A3	Deck	Ambient vib.	Vertical	0.56	0.09	-0.68	0.10	0.17
A4	Deck	Ambient vib.	Vertical	0.79	0.14	-0.98	-0.14	0.14
A5	Deck	Ambient vib.	Vertical	0.53	0.11	-0.74	-0.24	-0.02
AP16	Deck	Ambient vib.	Vertical	0.03	0.01	-0.05	0.00	0.15
A6	Deck	Ambient vib.	Vertical	-0.16	-0.04	0.20	0.16	0.91
A7	Deck	Ambient vib.	Vertical	-0.13	-0.04	0.19	0.18	1.00
AP22	Deck	Ambient vib.	Vertical	-0.02	0.00	0.04	0.03	0.21
A25	Deck	Ambient vib.	Vertical	-0.27	0.15	-0.28	0.90	-0.11
A26	Deck	Ambient vib.	Vertical	1.00	-0.67	0.72	0.06	-0.06
A27	Deck	Ambient vib.	Vertical	-0.22	0.12	0.06	-0.35	-0.80
A28	Deck	Ambient vib.	Vertical	-0.20	-0.23	-0.10	1.00	-0.07
A29	Deck	Ambient vib.	Vertical	0.64	1.00	1.00	0.14	-0.06
A30	Deck	Ambient vib.	Vertical	-0.06	-0.10	-0.08	-0.11	-0.50

				Frequency				
				1.86	**2.26**	**2.88**	**14.00**	**28.50**
AP3	Deck	Snap Back	Transverse	0.16	-0.09	1.00	0.98	1.00
A1	Deck	Snap Back	Transverse	0.23	-0.04	0.82	0.54	0.29
A2	Deck	Snap Back	Transverse	0.31	-0.01	0.70	0.16	-0.37
AP9	Deck	Snap Back	Transverse	0.38	0.25	0.57	-0.21	-0.85
A3	Deck	Snap Back	Transverse	0.50	0.49	0.42	-0.56	-0.55
A4	Deck	Snap Back	Transverse	0.58	0.58	0.30	-0.62	0.25
A5	Deck	Snap Back	Transverse	0.68	0.67	-0.01	-0.51	0.81
AP16	Deck	Snap Back	Transverse	0.77	0.76	-0.30	-0.16	0.76
A6	Deck	Snap Back	Transverse	0.84	0.81	-0.40	0.21	0.35
A7	Deck	Snap Back	Transverse	0.92	0.88	-0.49	0.57	-0.26
AP22	Deck	Snap Back	Transverse	1.00	1.00	-0.61	1.00	-0.87
A8	N. Abutment	Snap Back	Transverse	0.01	-0.01	0.02	-0.01	-0.01
A13	N. Pier	Snap Back	Transverse	0.04	-0.04	0.03	-0.07	-0.20
A19	S. Pier	Snap Back	Transverse	0.04	-0.04	0.01	-0.04	-0.01
A22	S. Abutment	Snap Back	Transverse	0.01	-0.02	0.01	0.00	0.00

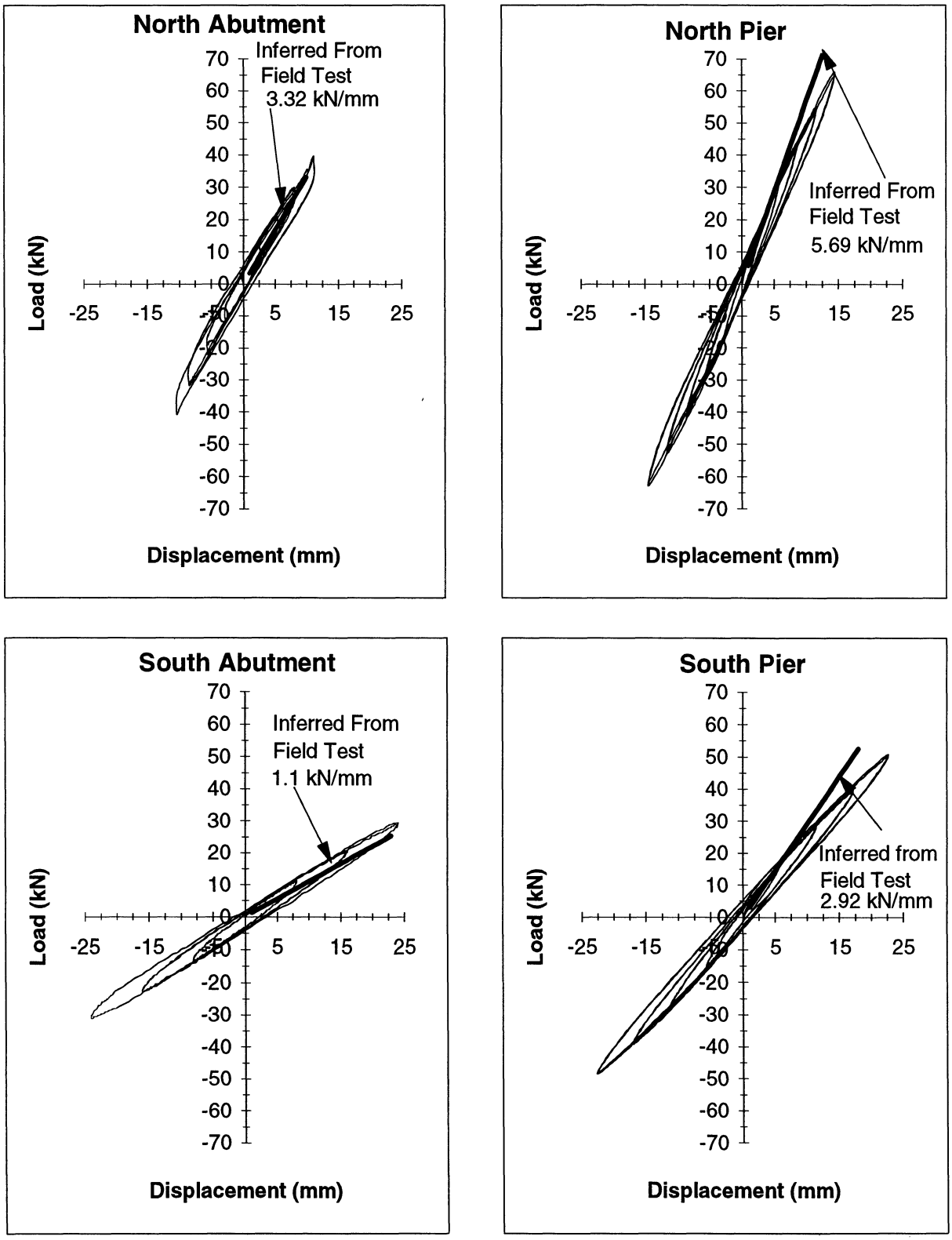

FIGURE 5-5 Lab Tests vs Inferred Stiffness from Test NBPOST-T2-TP

5.3.1 Southbound Bridge Results

The upper portion of figure 5-6 shows the acceleration time history in the vertical direction measured during one of the ambient vibration tests and from the snap back test. The lower portion of the same figure presents the Fourier spectra for the corresponding time history. It is possible to see from the peaks of the Fourier spectra that both tests predict modes at frequencies of 3.97 Hz, 4.31 Hz, and 6.87 Hz. These results show that although the magnitude of the maximum acceleration was small in the ambient vibration test (around $0.015g$) in comparison with the snap-back test ($0.09g$); the ambient vibration test can produce good estimates of the frequencies and shapes of vertical modes.

Figure 5-7 presents typical acceleration time histories for selected locations. Accelerometers AP3, AP22, AP9, and AP16 were located at the top of the flange at the north abutment, south abutment, north pier and south pier, respectively. The accelerometer A4 was located at the middle of the center span (approximately center of the bridge), and A19 at the top of the south pier. From comparison of the different time histories it is clear that the maximum accelerations ($0.27g$ and $0.34g$) were observed at the abutments where the lead rubber bearings were located. At the piers (rubber bearings without lead core bearing) the peak accelerations were around 0.16g. A similar value was observed at the center of the bridge. The time histories do not show smooth patterns, but rather the superposition of several dominant frequencies. The comparison between the time histories of accelerometers AP16 and A19 which were located at the same vertical plane passing through the pier bent but at different level (deck and pier), show a considerable difference in the peak acceleration. This difference clearly indicates that the deck behaved almost independently of the pier, the deck being effectively "isolated" from the pier.

As explained above, for the purpose of analysis of the experimental results, the acceleration time history was divided in two portions: the inelastic portion which is approximately the first half cycle, and the elastic portion which is the remaining portion of the time history. Figure 5-8 presents the Fourier spectra of the elastic portion of the acceleration time histories shown in figure 5-7. From the figure it can be seen that the dominant mode has

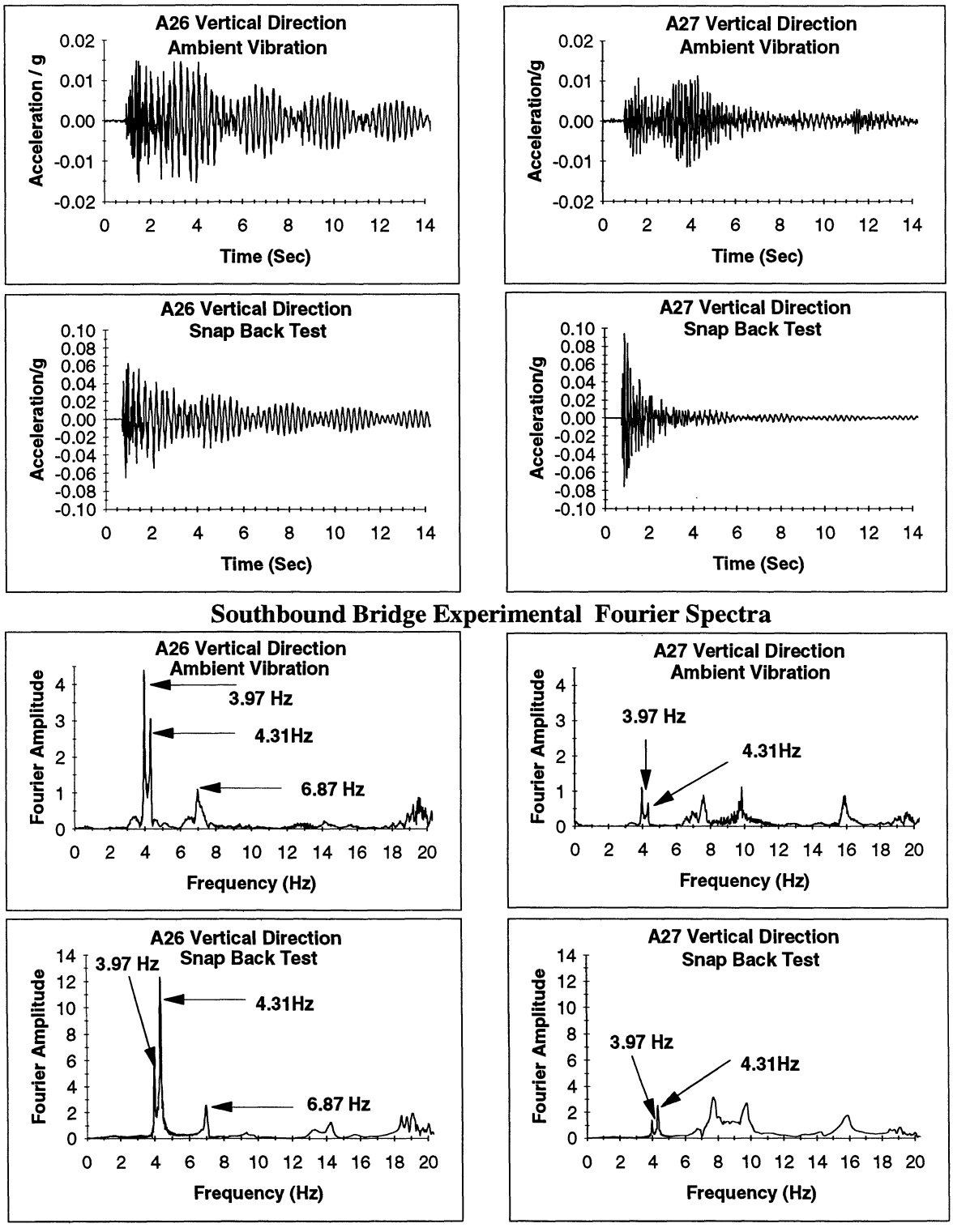

FIGURE 5-6 Comparison Between Ambient Vibration and Snap Back Test

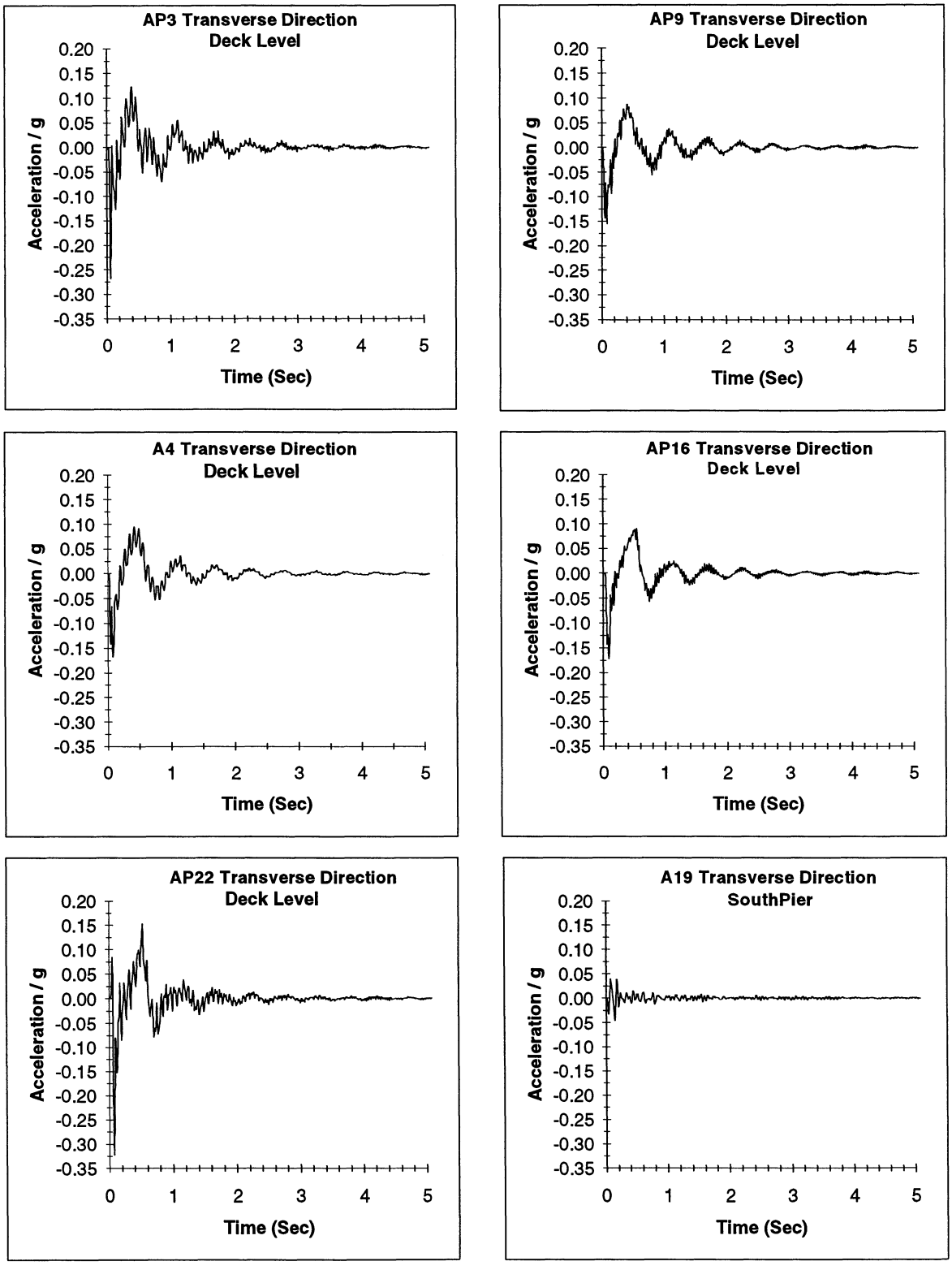

FIGURE 5-7 Acceleration Time Histories for the Test SBPOST-T2-TP

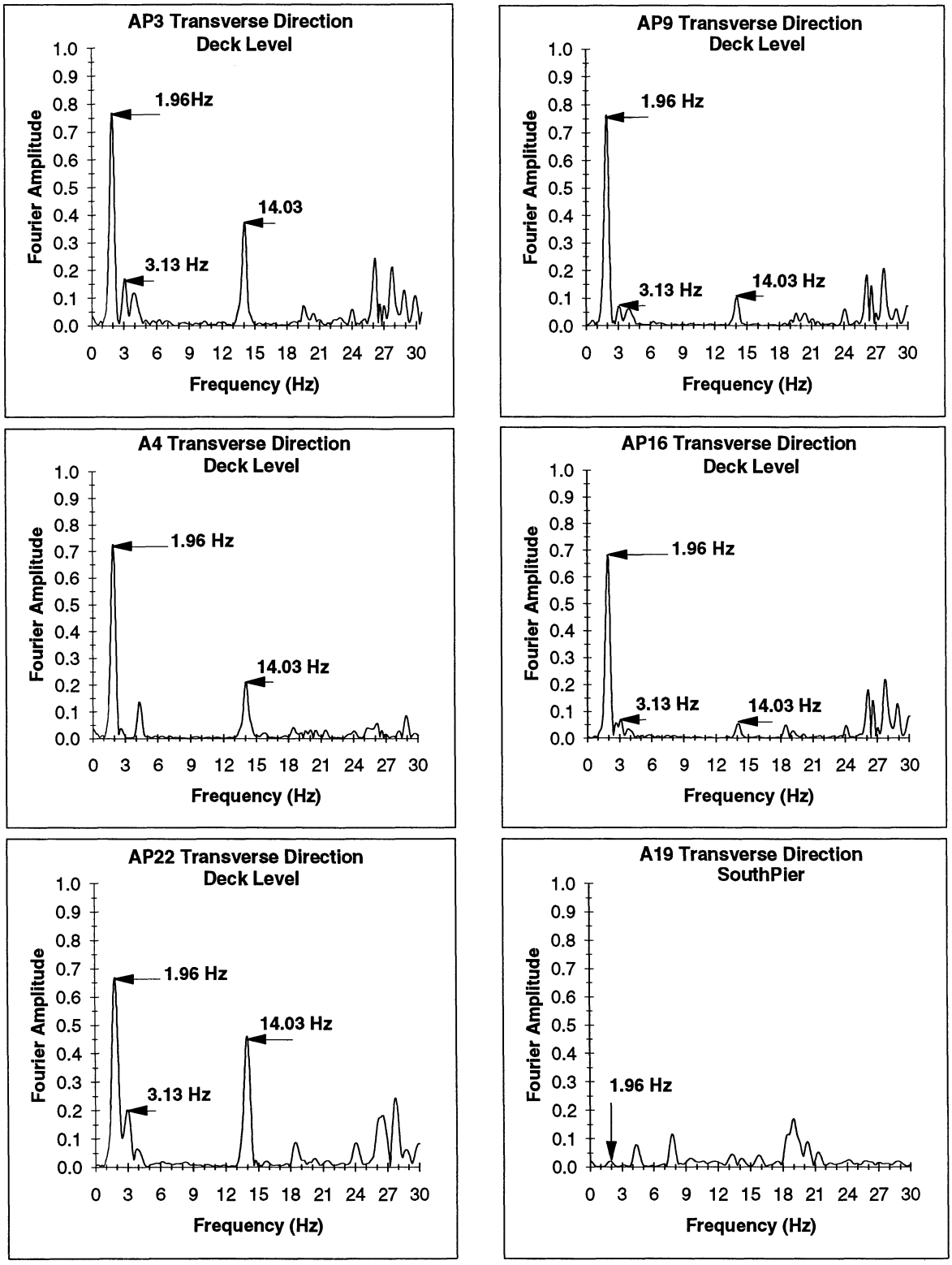

FIGURE 5-8 Fourier Spectra for the Elastic Portion-Test SBPOST-T2-TP

a frequency of 1.96 Hz, with a secondary mode at 3.13 Hz. There is also another important mode at 14.03 Hz and several other minor modes with frequencies over 25 Hz. The small value of the Fourier amplitude of the accelerometer A19, again shows the effectively "isolated" condition of the pier bent.

Certain researchers compute the Fourier spectra of the whole time history. This approach shown in figure 5-9 provides only a rough approximation of the overall dynamic response. It is of interest to note that the modes obtained using this approach have the same characteristics extracted with only the linear portion. The major difference is that as expected, the dominant frequency is lower (1.55 Hz) than the frequency observed in the Fourier spectra of the elastic portion (1.96 Hz).

Displacement time histories for the linear potentiometer displacement transducers at selected locations are presented in figure 5-10. This figure illustrates that in each case the vibration dies quickly and that the inelastic behavior is observed only in the initial part of the record. Figure 5-11 compares the time histories for potentiometer pairs located at the south pier and abutment. From figure 5-11a it can be seen that the displacement of the top and bottom of the girder relative to the pedestal are similar and that the girders do not suffer significant distortion. The comparison of the potentiometer P14 and potentiometer P26 which measured the displacement of the center of the deck relatively to the ground were also very close. It is thus clear from this figure that practically all of the total lateral displacement of the bridge results from bearing deformation. Figures 5-11b and 5-11c have an important implication for the modeling where simplification is desired: it is possible to replace all of the bearings located in the same support line with an equivalent simple bearing possessing the sum of the individual properties.

5.3.2 Northbound Bridge Results

The same approach used for the presentation of the Southbound experimental results is also used for the Northbound bridge. Where possible, the same accelerometer or potentiometer

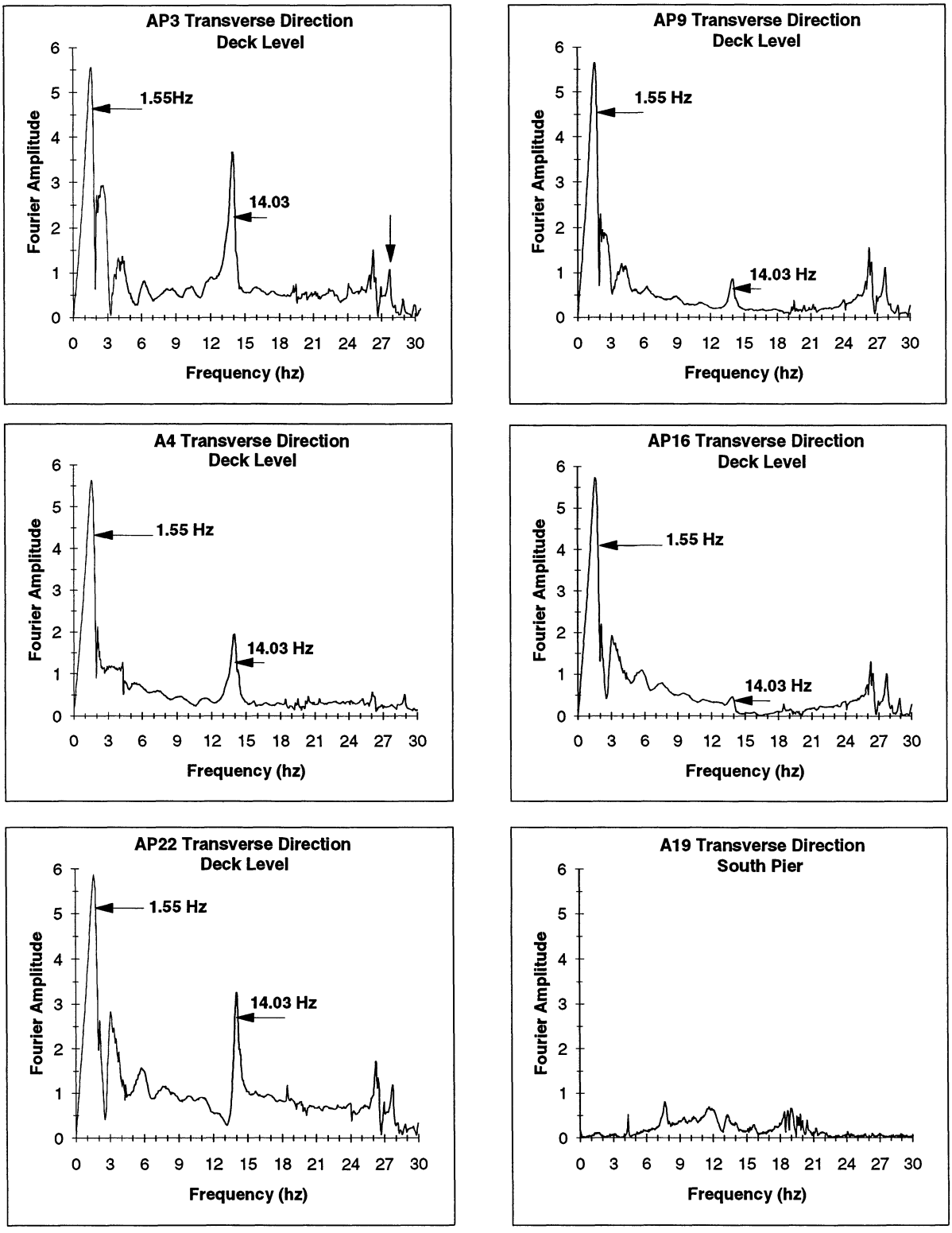

FIGURE 5-9 Fourier Spectra of the whole Acceleration Time History-SBPOST-T

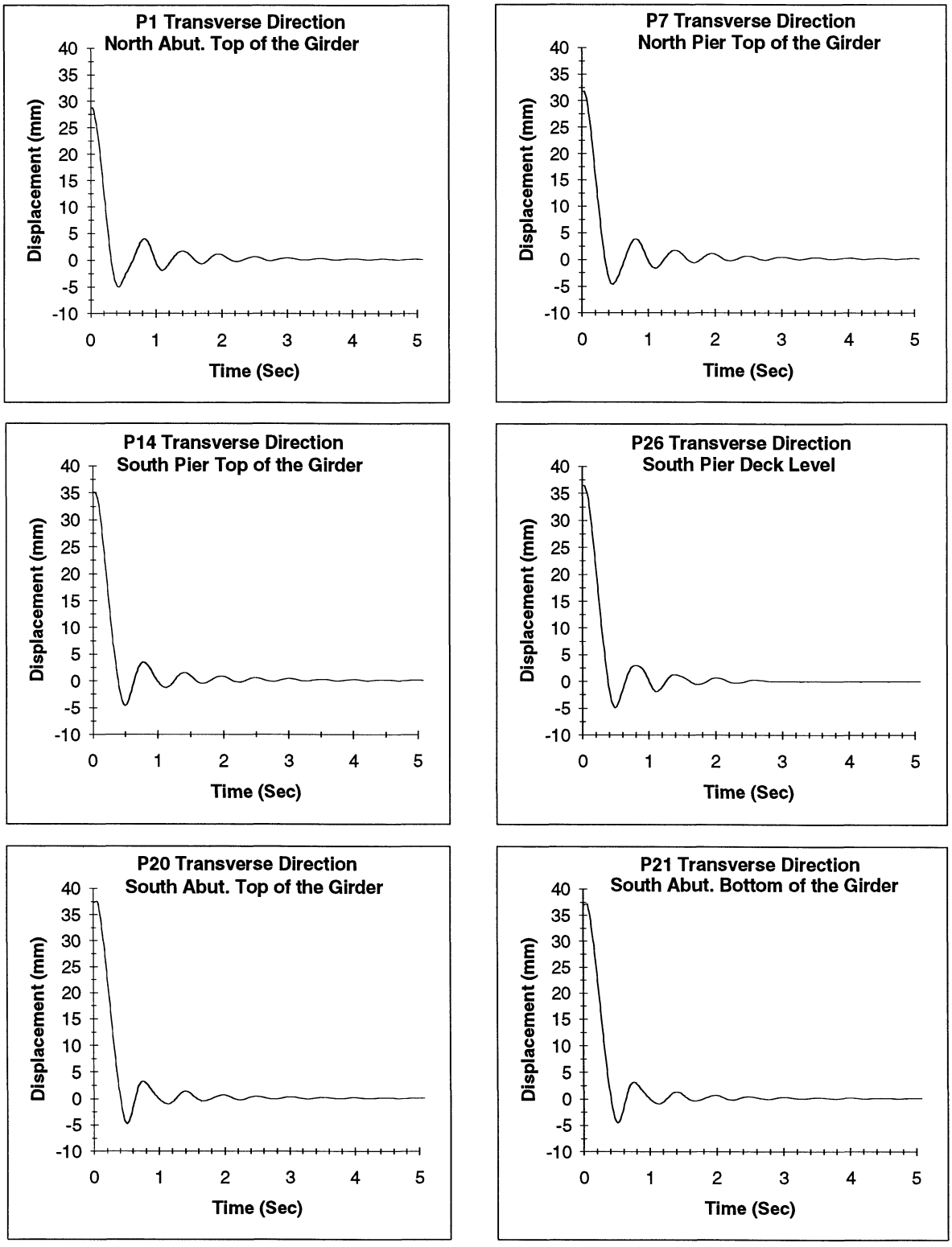

FIGURE 5-10 Displacement Time History for the Test SBPOST-T2-OP

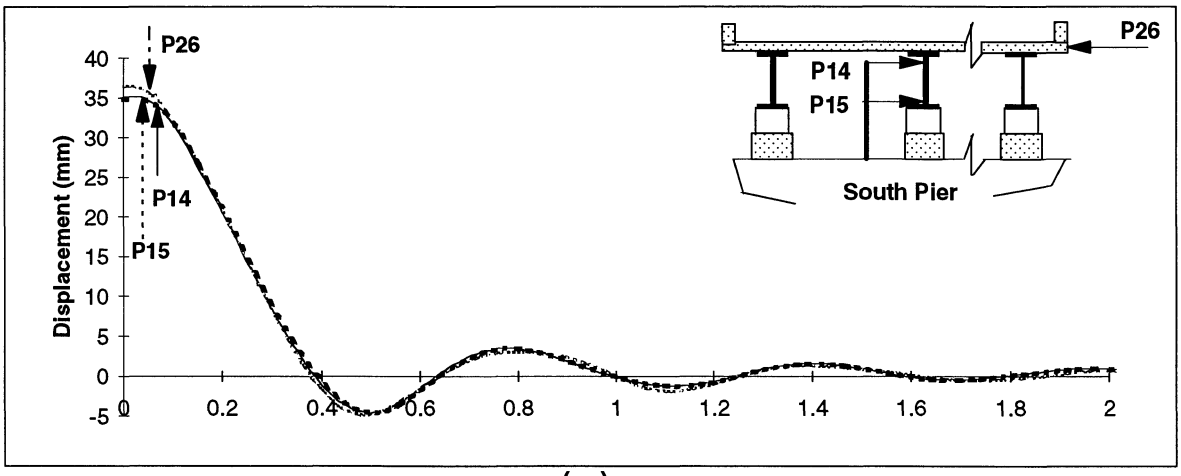

(a)

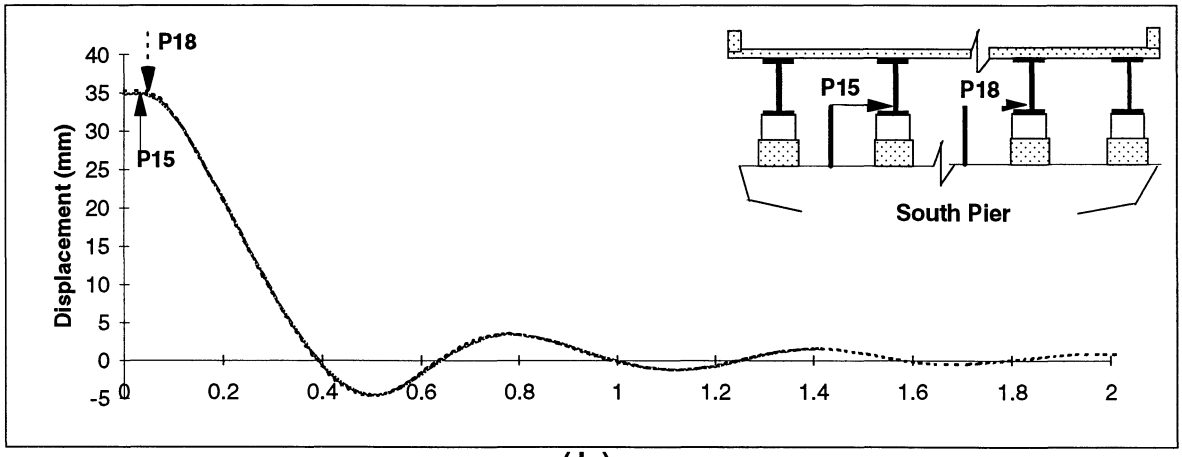

(b)

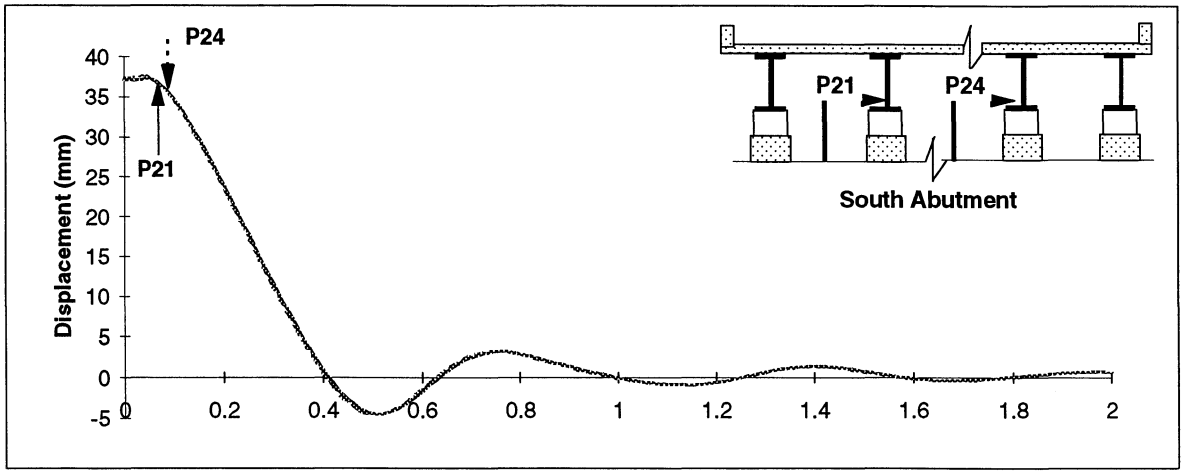

(c)

FIGURE 5-11 Displacement Time History for the Test SBPOST-T2-TP

locations presented for the Southbound bridge are used. This enables a comparison to be made of the response between the two bridges.

Figure 5-12 presents in the upper portion the acceleration time histories in the vertical direction from the ambient vibration test and snap-back test, and in the lower portion the Fourier spectra of these records. There were no major differences in the frequencies observed for the two different type of tests. Figure 5-13 shows typical acceleration time histories for the test NBPOST-T2-TP. The higher peak acceleration was observed in the south abutment (AP22) with a value close to 0.43g. At the south pier behavior similar to that described in the Southbound bridge can be seen. For the same vertical plane passing through the pier, the accelerometer located at the deck (AP16) showed a peak acceleration of 0.28g, while for the accelerometer located at the top of the pier the peak was around 0.05g. At other locations, the center of the bridge A4, the deck over the north pier AP9 and the deck over north abutment AP3, the peak accelerations were between 0.25 to 0.30g. The Fourier spectra of these records are presented in figure 5-14. From the figure, it can be seen that there is a dominant peak in the south abutment at a frequency around 1.86 Hz. The magnitude of this peak decreases through to the north abutment, clearly showing that the mode shape corresponding to this frequency resembles a cantilever beam. This behavior is in agreement with the bearings' stiffness distribution which are bigger in the north abutment and pier than in the south. Other frequency peaks can be observed at 2.88 Hz and 14 Hz.

Figure 5-15 presents the displacement time histories for selected potentiometer locations. From these time histories it is clear that the vibration does not die so quickly as was observed in the Southbound bridge. The potentiometers located in the south pier and abutments exhibit several well defined cycles before the movement died completely. Finally, figure 5-16 compares the displacements for different bearings at the same location, pier or abutment. As found for the Southbound bridge, most of the total displacements are attributed to the deformation of the bearings. There is only a very small difference in the record of the potentiometer P14 and P15 that can be attributed to the girder deformation. The diaphragm system worked to force all of

Northbound Bridge Experimental Time Histories- Amb#19 and NBPOST-T2-TP

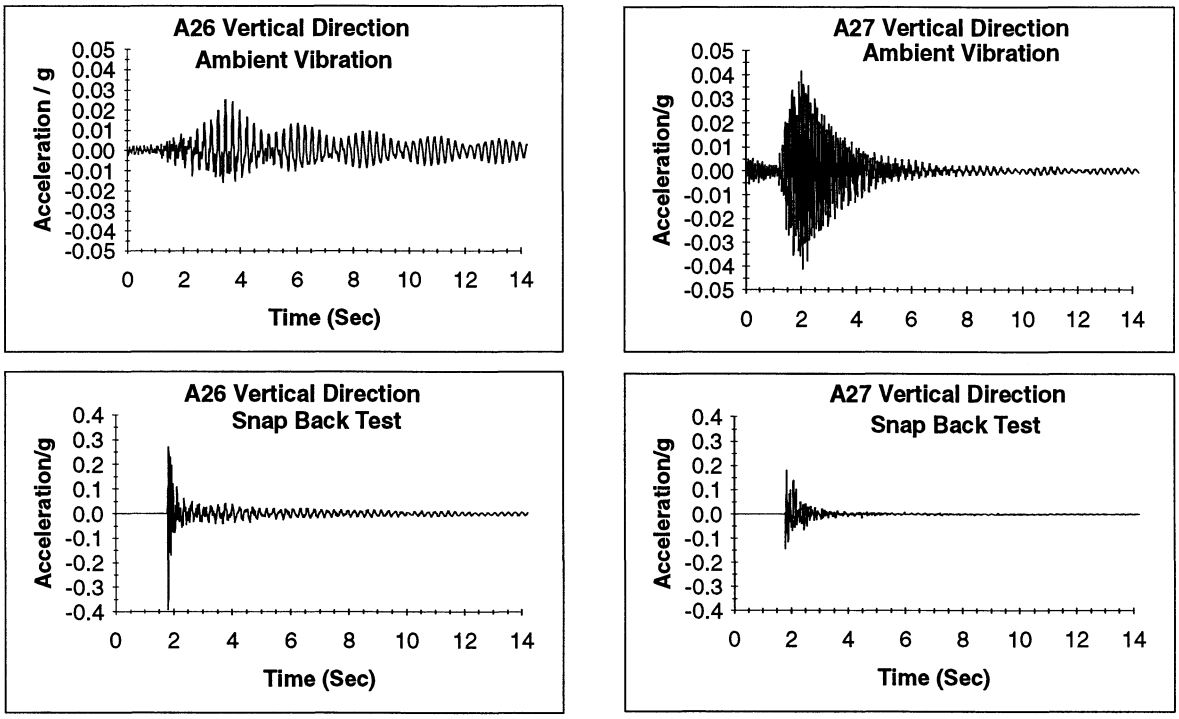

Northbound Bridge Experimental Fourier Spectra

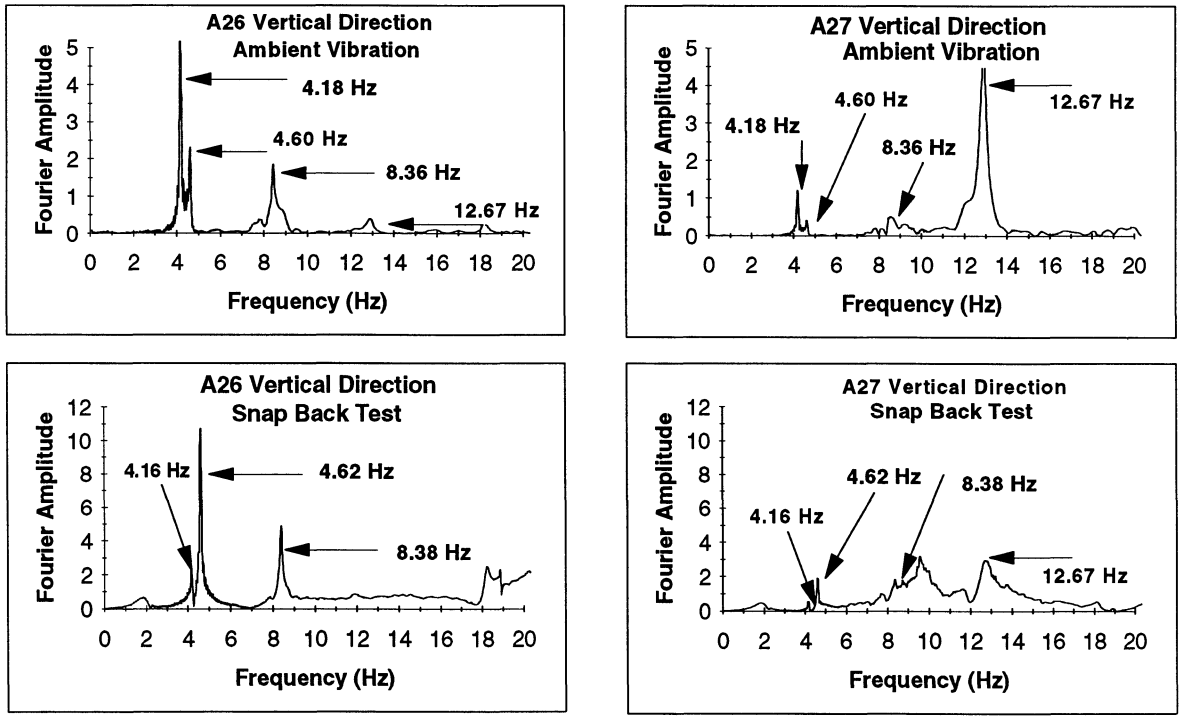

FIGURE 5-12 Comparison Between Ambient Vibration and Snap Back Test

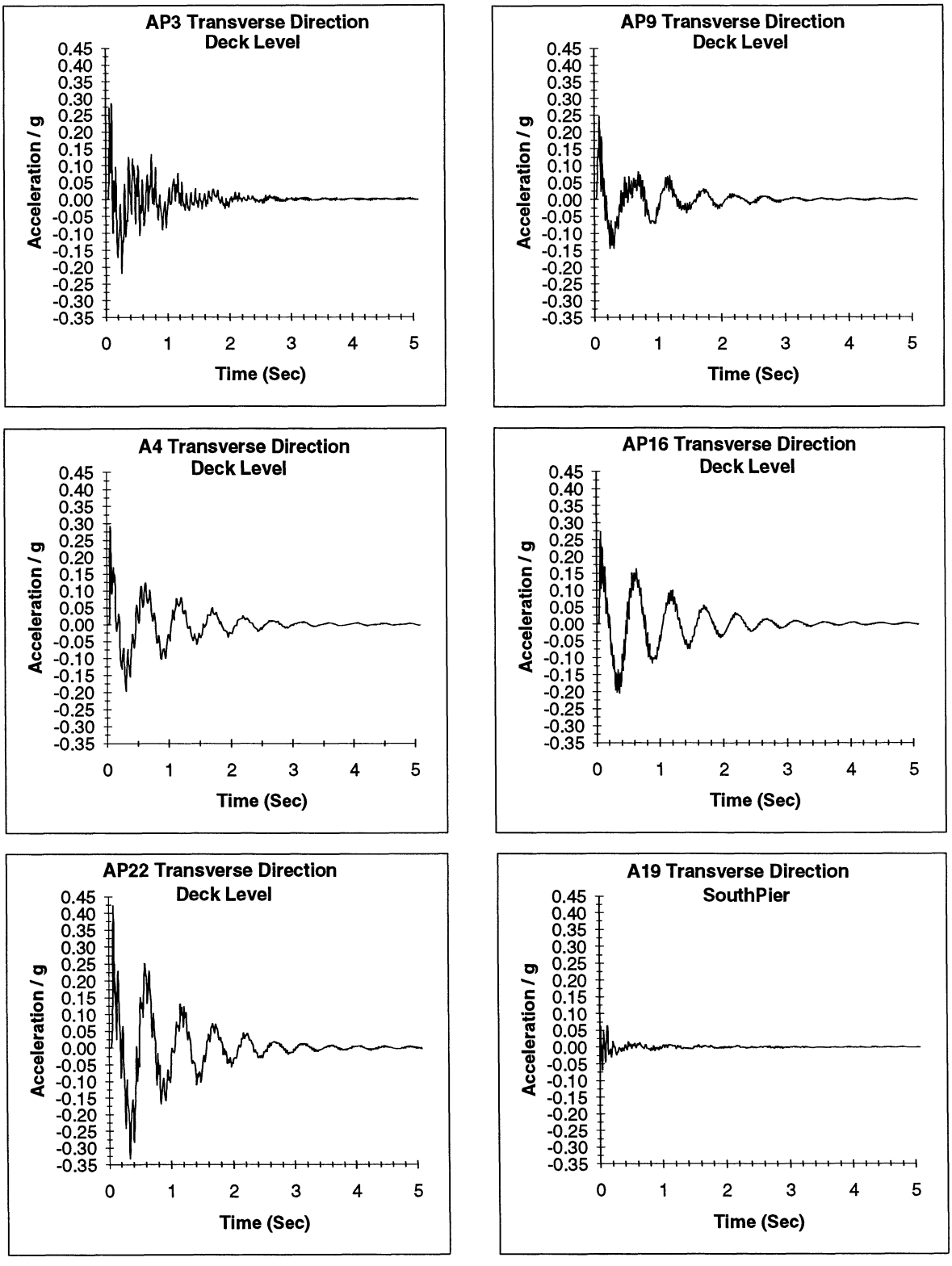

FIGURE 5-13 Acceleration Time History for the Test NBPOST-T2-TP

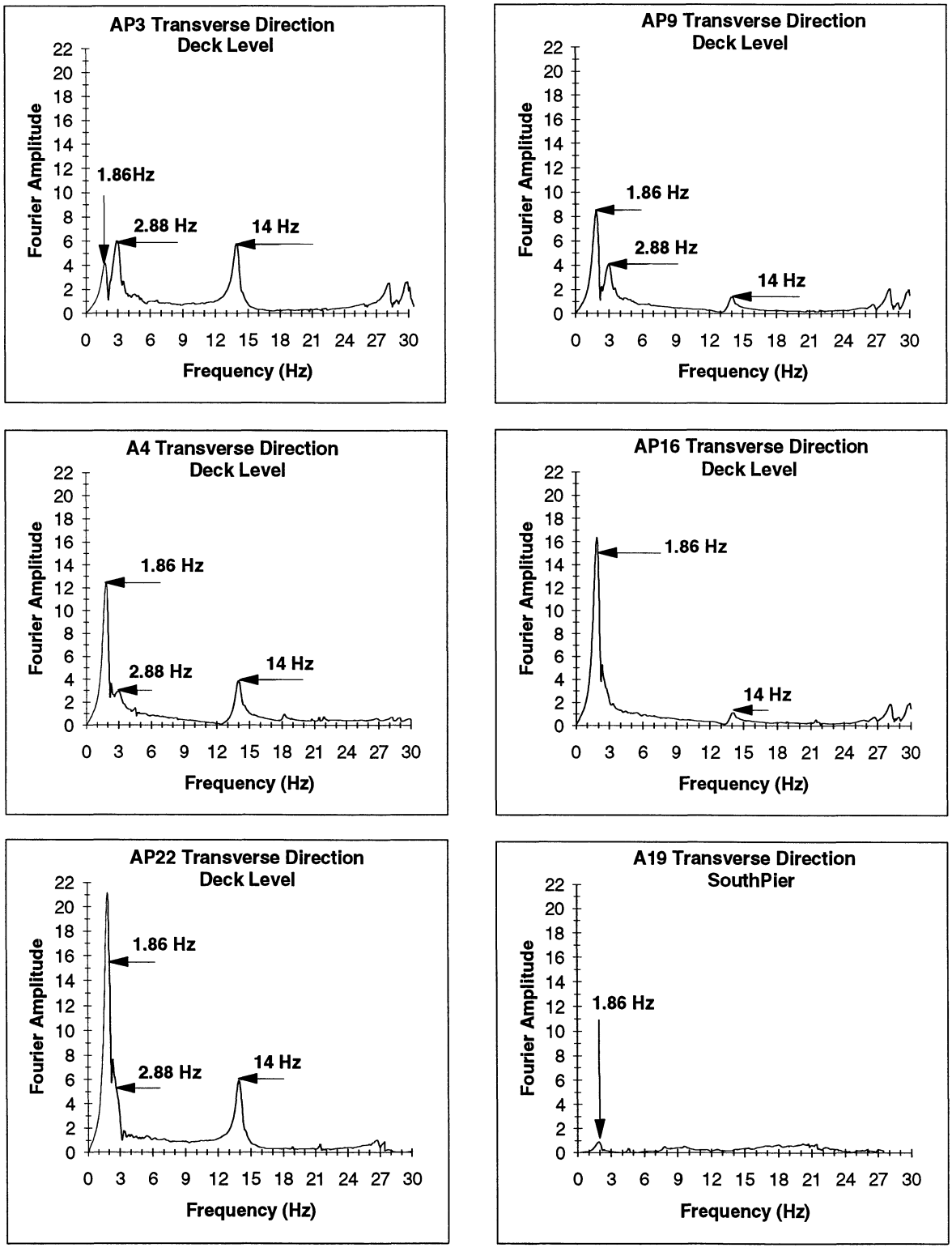

FIGURE 5-14 Fourier Spectra for the Test NBPOST-T2-TP

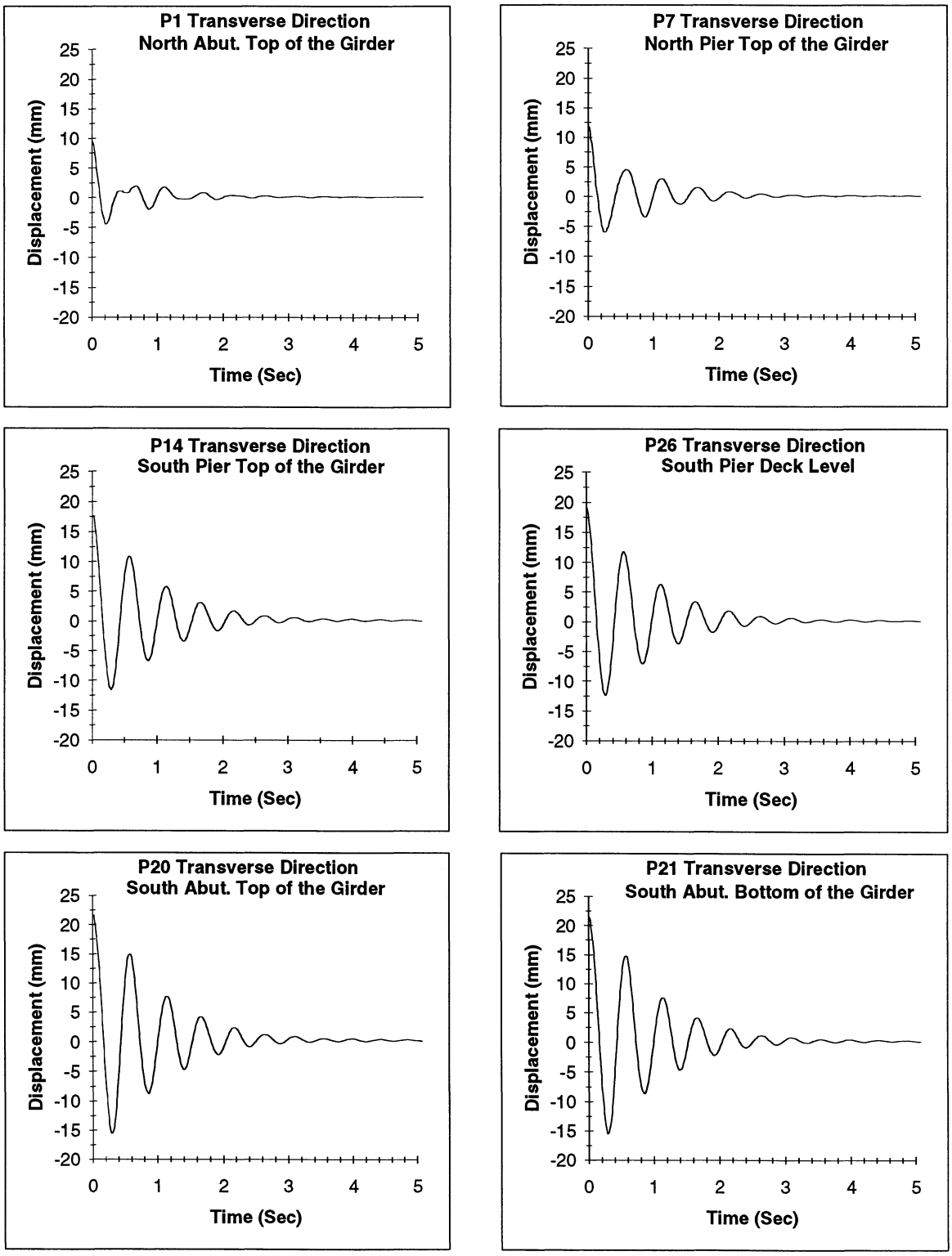

Figure 5-15 Displacement Time Histories for the Test NBPOST-T2-TP

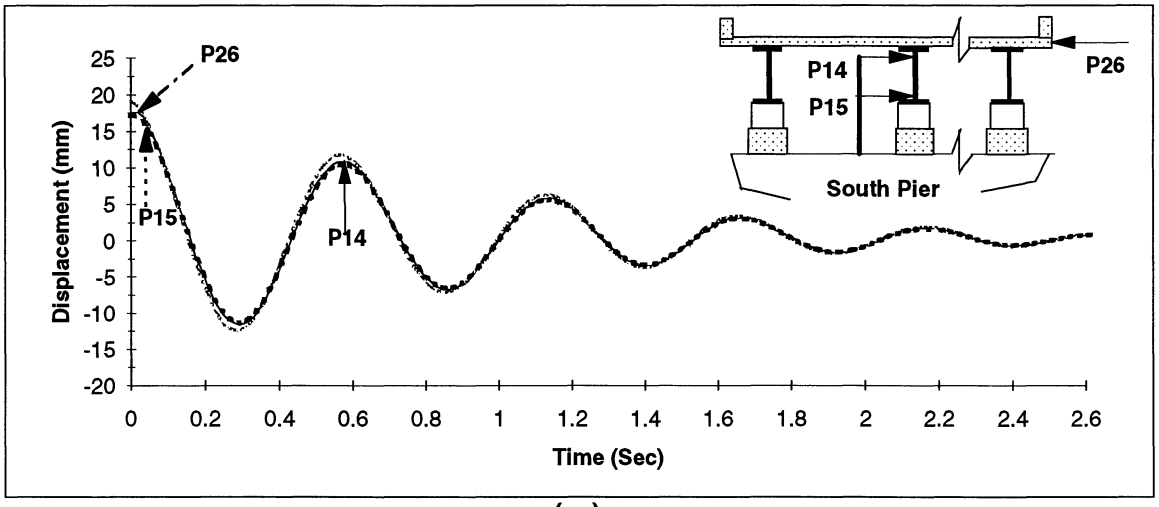

(a)

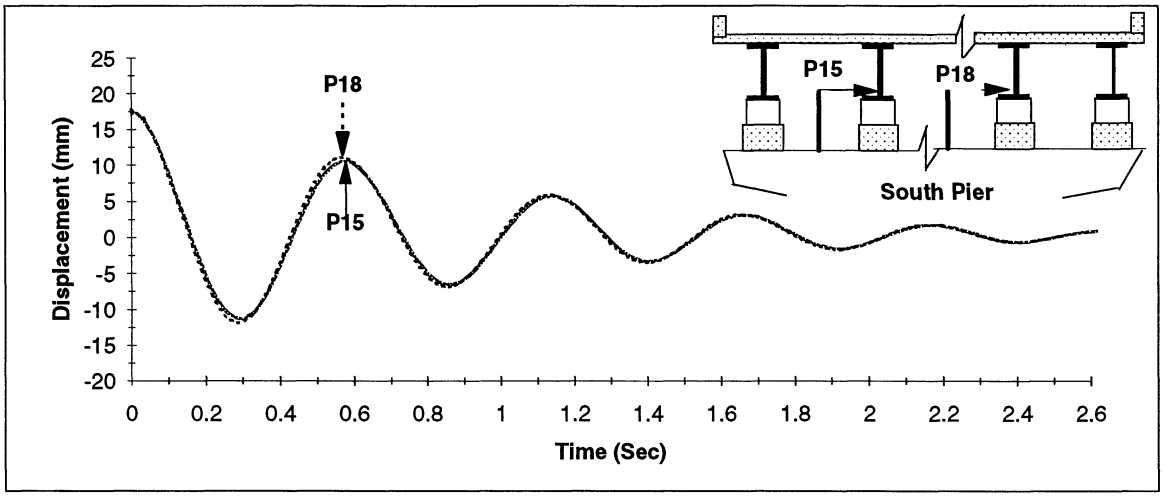

(b)

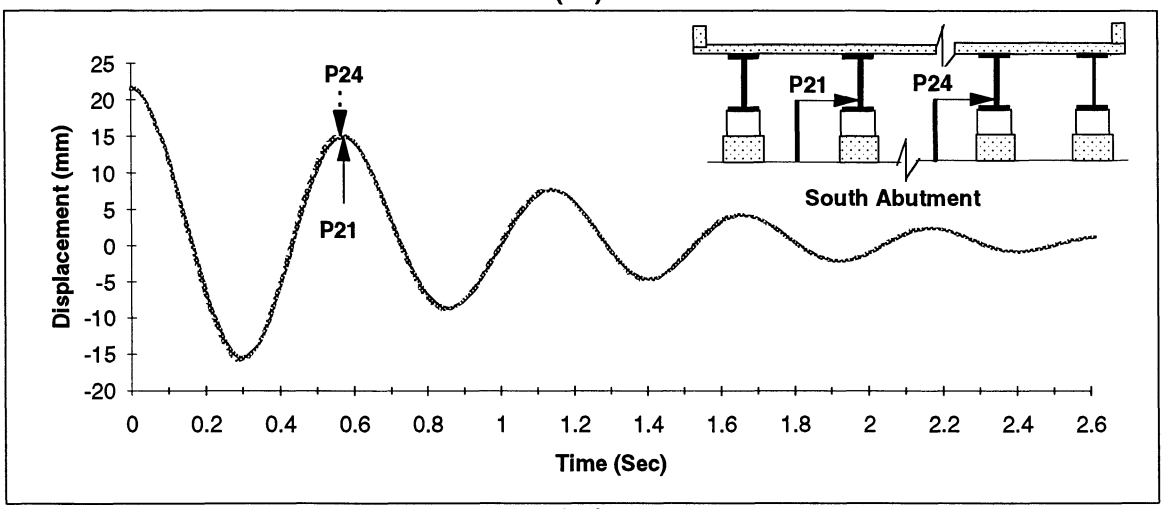

(c)

FIGURE 5-16 Displacement Time Histories for the Test NBPOST-T2-TP

the bearings in the same line of support to displace the same amount. This can also be seen when comparing potentiometers P15 vs P18 and P21 vs P24.

5.4 Damping in Post-Retrofitted Bridges

5.4.1 Damping Computation

For the purpose of modeling, not only are the stiffness and mass distribution important, but also the way in which energy is dissipated by the structure should be carefully modeled. According to Uang (1990), during an earthquake different energy dissipation mechanisms are involved as follows:

$$E_I = E_K + E_S + E_H + E_D \qquad \textbf{(5-30)}$$

where E_I = absolute seismic input energy, E_K = absolute kinetic energy, E_S = recoverable elastic strain energy, E_H = irrecoverable hysteretic energy dissipated by the inelastic action of the structural elements, and E_D = energy dissipated by damping.

Depending of the kind of analysis to be performed (linear or non-linear) and the characteristics of the program to be used, each of the energy components involved can be studied individually. In this study where two different programs were used SAP90 (linear) and DRAIN-2DX (nonlinear), different approaches were used to extract the damping values from the experimental results. The use of these methodologies provide the appropriate values that permit an accurate time-history modeling of the dynamic response.

The methodology used for this work is clearly presented in (Clough, 1975; Humar, 1990) and can be summarized as:

(i) Half Power Method

$$\xi = \frac{f_2 - f_1}{f_2 + f_1} \tag{5-31}$$

where $(f_2 - f_1)$ = difference between the frequencies at $\frac{1}{\sqrt{2}}$ the resonant frequencies, and $(f_2 + f_1)$ = sum of the frequencies measured at $\frac{1}{\sqrt{2}}$ the resonant frequency.

(ii) Logarithmic Decrement Method

$$\delta = \ln \frac{U_n}{M_n + 1} = 2\pi m\xi \frac{\omega}{\omega_d} \tag{5-32a}$$

for small damping

$$\xi = \frac{1}{2\pi m} \ln \frac{U_n}{U_{n+m}} \tag{5-32b}$$

where U_n = displacement measured at time and U_{n+m} = displacement measured "m" cycles after "n".

Equivalent Viscous Damping from Hysteretic Curves

An equivalent viscous damping can be computed based on equating hysteretic and strain energies (Humar, 1990).

$$\xi_{eq} = \frac{w_G}{4\pi w_s} = \frac{w_D}{2\pi K_{eq} x_D^2} \tag{5-33}$$

Equation(5-33) is similar to the AASHTO (1991) equation for the equivalent damping computation:

$$\xi_{eq} = \frac{1}{2\pi} \frac{Total\ Area}{\sum k_{max} d_i^2} \qquad (5\text{-}34)$$

where w_D = area of the hysteretic cycle, K_{eq} = equivalent elastic stiffness, x_D = displacement, total area = sum of the hysteretic area under the isolators, K_{max} = maximum effective stiffness, d_i = displacement at the center of rigidity of the isolation system.

It is important to make clear that the use of these equations (5-33 and 5-34) produce only an estimation of the equivalent viscous damping values. Each of these methods has its own advantages and restrictions as discussed by Clough (1975) and Humar (1991). For this study, and due to the complexity of the problem, a comparison of the results obtained from these methods is presented in figure 5-17 (Southbound bridge) and 5-18 (Northbound bridge). Because the equivalent hysteretic damping depends on the maximum deformation observed during the test, the test SBPOST-T2-TP was used to determine the damping factors for the Southbound bridge. The damping values obtained from the half power method were computed using the Fourier spectra of the elastic portion of the time history (e.g. figure 5-8). The results reported are the average of the values of all of the accelerometers reading in the same direction. The only exception was for the frequency of 3.13 Hz (torsional mode) where due to the poor definition of this mode in the Fourier spectra of the accelerometers located close to the center of the bridge (center of rotation) only the accelerometers AP3, A1, A7 and AP22 were used for the computation. The Time domain damping was obtained using the least square curve fitting method described in Section 3.

For the logarithmic decrement method, the displacement time histories of potentiometers P1, P3, P13, P26, P20 and P23 were used. The use of displacement time histories instead of acceleration time history has the advantage of filtering out the high frequencies, leaving only the fundamental mode. The equivalent hysteretic damping was computed using the load-deformation curve of figure 5-3. For this computation, it was assumed that the bearings described a complete cycle (including reversal) with the same maximum deformation as that observed in the field. Figure 5-17 shows that for half power method predicts damping values that are higher

Test: SBPOST-T2-TP

Half Power Method (Elastic Portion)			Time Domain Method (Elastic Portion)		
Mode	**Freq. (Hz)**	**Damping %**	**Mode**	**Freq. (Hz)**	**Damping %**
Vertical #1	3.97	1.7			
Vertical #2	4.31	1.2			
Vertical #3	6.87	1.8			
Vertical #4	9.16	2.4			
Transv #1	1.96	10.1	Transv #1	1.91	8.1
Transv #2	3.13	12	Transv #2	3.19	10
Transv #3	14.03	1.6	Transv #3	14	1.1

Logarithmic Decrement Method

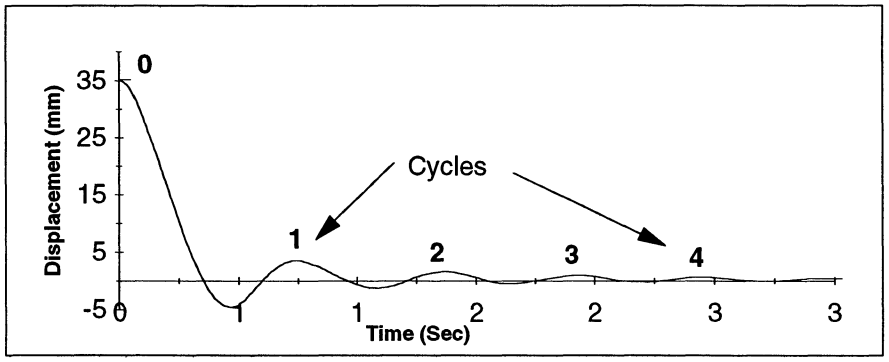

North Abutment			South Abutment		
Cycle	**Freq. (Hz)**	**Damping %**	**Cycle**	**Freq. (Hz)**	**Damping %**
1	1.28	36	1	1.37	39
2	1.75	13	2	1.69	14
3	1.79	8	3	1.72	10
4	1.85	7	4	1.82	7

Equivalent Viscous Damping From Hysteretic Curve

Location	Disp. (mm)	Fu (kN)	K (kN/mm)	Wd (kN-mm)	Damping (%)
N. Abut.	29	43	1.49	1874	24
	32	27	0.84	840	16
	35	29	0.84	972	15
S. Abut.	37	50	1.36	2459	21

AASHTO= 20

FIGURE 5-17 Post-Retrofitted Southbound Bridge - Damping Computation

Half Power Method			Time Domain Method		
Mode	Freq. (Hz)	Damping %	Mode	Freq. (Hz)	Damping %
Vertical #1	4.18	2.1			
Vertical #2	4.6	1.3			
Vertical #3	8.36	2.4			
Vertical #4	11.8	1.7			
Vertical #5	12.67	1.1			
Transv #1	1.86	12	Transv #1	1.81	12
Transv #2	2.88	13	Transv #2	2.75	15
Transv #3	14	1.8	Transv #3	13.95	1.6

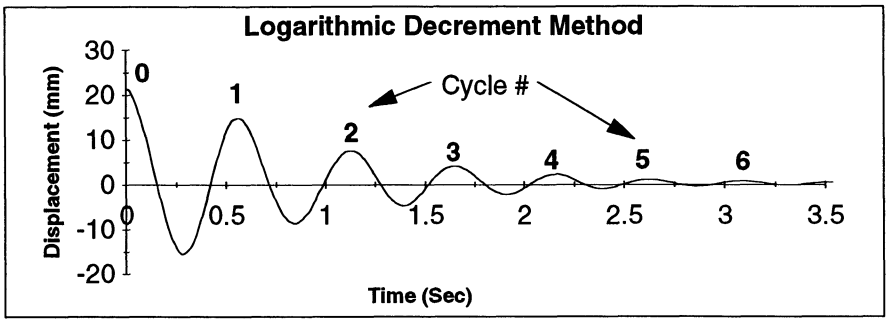

Logarithmic Decrement Method - AverageTest Values

Test: NBPOST-T2-TP			Test: NBPOST-T3-OP		
Cycle	Freq. (Hz)	Damping %	Cycle	Freq. (Hz)	Damping %
1	1.74	9.7	1	1.89	10.1
2	1.83	9.9	2	1.96	11.3
3	1.93	10.0	3	1.96	8.5
4	2.10	10.5	4	2.05	8.7
5	2.11	7.2	5	2.12	6.6
6	2.14	6.0	6	2.16	6.7

Using Points "0" and "5" only for Computation Purpose (5 Cycles)

Damping (%) = 9.2 Damping (%) = 8.7

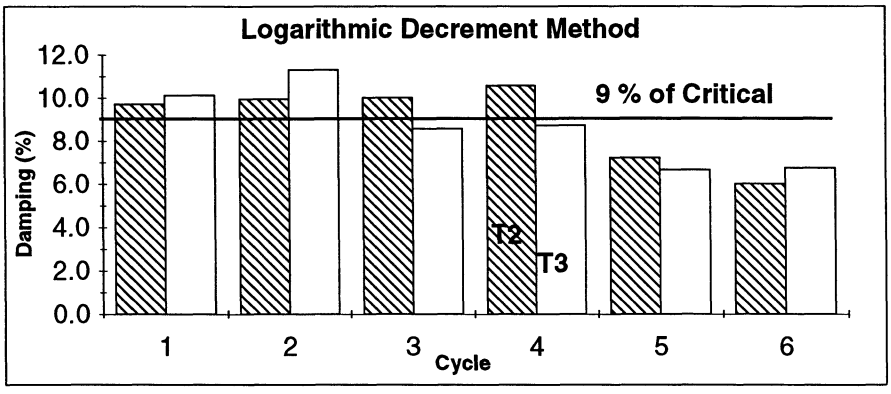

FIGURE 5-18 Post-Retrofitted Northbound Bridge - Damping Computation

than the values predicted using the time domain method. Those differences can be attributed to the effect of windowing the acceleration time history (the use of windows concentrates the energy under the main lobe Harris 1978). The use of the logarithmic method over the displacement time history showed in figure 5-17 that during the first cycle there is considerable energy dissipated (inelastic portion of the time history). Following this stage the damping values decrease to levels which are close to the time domain values for the first frequency. The frequencies computed for each cycle also show that there is a substantial change between the first cycle and the others. This is compatible with the observation, that after the first cycle the structure behaves in a linear fashion.

The computation of the equivalent viscous damping, using equation (5-33), shows that for the maximum displacements observed during the test, the corresponding average damping value is around 20% of critical.

In the Northbound bridge (figure 5-18) the damping computed by the half power method used the entire time histories of the accelerometers reading in the same direction (vertical or transverse). For the logarithmic decrement method, the damping values were computed as the average of the results obtained using the displacements time histories of the potentiometers P13, P26, P20 and P23. Potentiometers P1 and P3 were not used since, the fixed bearing installed at the north abutment did not allow a well defined free vibration time history. The results show that the damping values obtained using the half power method and the time domain approach are close. The logarithmic decrement method predict lower values than the other two method for similar frequency (around 1.9 Hz). It also was found that the damping decreases with bearing deformation, or in other words exhibits a strain dependent condition. The frequencies computed between cycles increase around 20% between the first and sixth cycle. This change clearly shows that although linear elastic behavior is somewhat assumed for the analysis, the stiffness of the bearings is strain dependent.

SECTION 6
TRANSIENT DYNAMIC ANALYSIS OF THE BRIDGES AFTER REHABILITATION WITH ELASTOMERIC BEARINGS

6.1 Introduction

A reliable model that can be used to predict the behavior of the structure should be able to reconstruct with a reasonable degree of agreement the observed behavior under the field test conditions. The first step in the construction of such a model is based on information provided by different sources such as construction drawings, component and material tests. If a computational model is well conceived, then the differences between the "theoretical" response and the observed behavior should be minimal. System identification techniques are sometimes necessary to correct faulty initial assumptions. In Section 4 it was shown that the proposed models for the pre-retrofitted bridges could be used to reconstruct with good agreement the behavior observed in the field. Section 5 presented the approach used to identify the dynamic characteristics of both post-retrofitted bridges and reported the experimental frequencies, mode shapes, displacements under static loads, and bearing properties. With this information and making use of the proposed pre-retrofitted models, the only changes were in order to adjust the model to the new bearing support condition. If the pre-retrofitted models with these property changes can reconstruct the observed field behavior of the post-retrofitted bridges, it can then be concluded that the proposed models are a reliable representation of the bridges and they can be confidently used for further predictive studies. The first portion of this section describes the modification made to the models used for the pre-retrofitted bridges – principally to include the behavior characteristics of the new bearings.

The section then goes on to compare the results obtained using the proposed models with the experimental results. The degree of agreement between the results is indicative of the reliability of the models for subsequent non-linear predictions.

6.2 Post-Retrofitted Analytical Models

Previously, Section 4 described two large 3D FEM models of the Northbound and Southbound bridges and a simpler 2D FEM for each bridge. In order to compare analytical predictions between the pre-retrofitted bridges and the post-retrofitted bridges the same tools were used. It was decided to use the 3D FEM and a 2D FEM model for the cases where the structure was assumed to behave linearly. In the Southbound post-retrofit case where non-linear behavior was expected two options were evaluated: a 3D FEM equivalent linear approach and a 2D model that can accommodate non-linear behavior. The latter model was proposed for situations where the combined soil and bearing non-linearities were potentially important in the prediction of the overall behavior of the structure.

The only major change in the 2D and 3D models between the pre and post-retrofitted bridges were the bearings properties. Table 6-1 summarizes the bearing properties used for the comparison between the field test and the analytical predictions. The shear stiffness of the bearings extracted from the identification process described in Section 5 and the axial and rotational stiffness from the laboratory experimental results were used to define a frame element that connected the foundation to the bottom of the girder in the 3D model. For the 3D model of the Southbound bridge, two different values of the shear stiffness were used. The first one corresponded to the analysis of the structure using the initial elastic shear stiffness obtained from the system identification and reported in table 2-6. This prediction corresponded to the case where there is not inelastic deformation, and the structure remained on the elastic branch of a representative bilinear force-displacement curve for the bearings. The second value corresponded to an analysis using an equivalent secant shear stiffness. This equivalent shear stiffness was defined using figure 5-5 as a line between the origin and the maximum experimental, transverse or longitudinal displacement in each instrumented bearing location. In the 2D model of the Southbound bridge, the initial shear stiffness, the "yield point", and the ratio between the initial and post yielding stiffnesses defined the bearing characteristics.

Similar information was provided to model the nonlinear behavior of the soil. Figure 6-1 illustrates the soil properties used in this study. For the 3D and 2D models of the Northbound

TABLE 6-1 Experimental Vs Analytical Time History-Bearings Properties

Southbound Bridge - Test: SBPOST-T2-TP

Axial Stiffness

Location	Stiffness (kN/m)	Modulus (MPa)
North Abutment	140101	221
North Pier	175125	248
South Pier	175125	248
South Abutment	140100	221

Rotational Stiffness

Location	Stiffness (kN-m/rad)
North Abutment	311
North Pier	497
South Pier	497
South Abutment	311

Shear Stiffness

Location	Shear Strain (%)	Fu (kN)	Qd (kN)	K1 (kN/m)	K2 (kN/m)
North Abut.	0.30	21	18	6255	867
North Pier	0.33	-	-	788	-
South Pier	0.37	-	-	788	-
South Abut.	0.39	21	18	6672	867

Northbound Bridge - Test: NBPOST-T2-TP

Axial Stiffness

Location	Stiffness (kN/m)	Modulus (MPa)
North Abutment	1593654	621
North Pier	1681200	345
South Pier	656719	296
South Abutment	350250	276

Rotational Stiffness

Location	Stiffness (kN-m/rad)
North Abutment	5796
North Pier	17558
South Pier	8327
South Abutment	2576

Shear Stiffness

Location	Shear Strain (%)	K1 (kN/m)
North Abut.	0.31	3320
North Pier	0.39	5690
South Pier	0.31	2920
South Abut.	0.28	1100

Notes:

Fu= Maximum shear force at the maximum shear strain
K1= Initial stiffness
K2= Post-yielding stiffness
Qd= Characteristic Strength

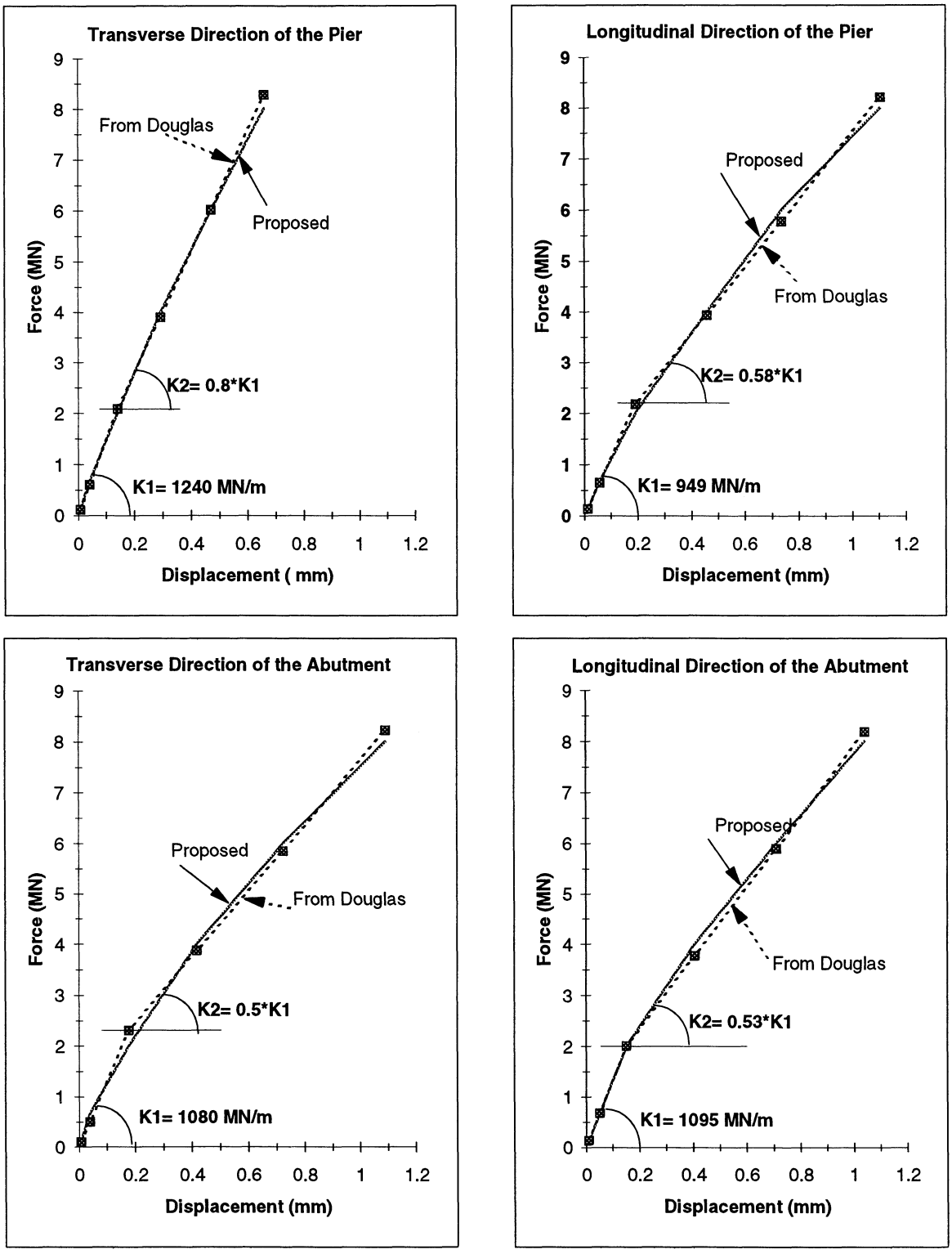

FIGURE 6-1 Non-Linear Soil Properties by Douglas et al., (1994)

bridge, it was assumed that the bearings behaved in a linear fashion. Thus it was not necessary to define a "post-yield" stiffness. As for the Southbound bridge, the shear stiffness was extracted from the results of the system identification procedure which were illustrated in figure 5-5 and presented in table 6-1 with the rotational and axial properties extracted from the component tests. A frame element in the 3D model and a spring element in the DRAIN-2DX model were used to represent the bearings.

The damping values used for the predictions were computed according to the type of model (3D or 2D) and the kind of analysis (linear or non-linear). For the 3D linear analysis of the Southbound bridge where the analysis was done using a secant shear stiffness, the level of equivalent viscous damping used was assigned using an approach suggested by Skinner (1993). The properties of the bearings control the lower modes, whereas the structural characteristics control the higher modes. Following this notion it was decided to initially set the damping corresponding to the frequencies of 1.96 Hz and 3.13 Hz equal to 20% which is the value obtained from the AASHTO equation (5-33). For the third identified transverse mode which can be considered a higher mode (14.03 Hz), and for the known vertical modes, the damping used was extracted from the Fourier spectra using the half power method. All of these values were reported in figure 5-17. All other modes for which the damping was unknown was assumed equal to 5% of the critical. With these initial values of damping, the time histories were computed and compared with the experimental results. It was found that for a better fit it was necessary to increase the damping of the lower modes, from 20% to 23% of the critical value. The other damping values did not require any change.

For the 2D non-linear model of the Southbound bridge, two kinds of damping were considered, viscous and hysteretic. The viscous damping is specified as an input to the DRAIN-2DX program through the definition of the value of the mass proportional factor a_0 and the stiffness proportional factor a_1. To find these values it is necessary first to define the expected damping for two different frequencies. After these factors are computed, the damping for any other frequency are fixed. From figure 5-17 and depending on the method used it can be assumed that a value of 8% of critical is a good initial estimate for a frequency around 1.9 Hz.

For the frequency of 14 Hz, the half power method and the time domain predict an average damping value of 1.35% of the critical value. With these two approximate damping values and for the corresponding frequencies, the proportional factors can be computed using the expression given by Clough (1975):

$$\begin{bmatrix} \xi_1 \\ \xi_2 \end{bmatrix} = \frac{1}{2} \begin{bmatrix} \frac{1}{\omega_1} & \omega_1 \\ \frac{1}{\omega_2} & \omega_2 \end{bmatrix} \begin{bmatrix} a_0 \\ a_1 \end{bmatrix} \qquad \textbf{(6-1)}$$

where ξ_1 = computed damping for mode 1, ξ_2 = computed damping for mode 2, ω_1 = frequency of mode 1, ω_2 = frequency of mode 2, a_0 = mass proportional factor and a_1 = stiffness proportional factor.

With the initial proportional factor, the time histories were obtained and compared with the experimental result, and minor adjustments were made to obtain a better fit. The resulting final values were a_0 = 1.59 and a_1 = 0.0000444. These values correspond to damping factors of 6.5% for the 1.96 Hz frequency and 1.1% for the 14.03 Hz frequency. The hysteretic damping was included in the program through the definition of the bilinear properties of the bearings.

For the Northbound bridge where the structure was assume to behave linearly, the damping used in the 3D model was extracted from the time domain curve fitting method, and from the Fourier spectra a value of 10% of critical was used for the frequency of 1.86 Hz and 12 % of critical for 2.88 Hz. For the remaining known modes the half power values reported in figure 5-18 were used. For the unknown modes a value of 5% of critical was used. In the DRAIN-2DX model an approach similar to that described for the south bound bridge was used. The final values were a_0 = 1.75 and a_1 = 0.000047, which correspond to damping factors of 7.5% and 1.2% of critical for the 1.86 Hz and 14 Hz frequencies, respectively.

6.3 Experimental and Analytical Results of the Post-Retrofitted Test

Figures 6-2 to 6-5 compare the frequencies and vertical mode shapes obtained experimentally with the analytical predictions using the 3D SAP90 model for the Southbound bridge. Similarly, figures 6-6 to 6-10 compare the experimental vs analytical predictions using the 3D SAP90 model for the Northbound bridge. The modes and frequencies were extracted from the ambient vibration tests performed over the bridge using the same methodology as that described for the pre-retrofitted bridges. As expressed by Gates (1982) the use of this technique produces results which are affected by several factors (vehicle mass, level of excitation, etc.) The mode shapes and the frequencies obtained as the average of certain number of tests, however, are considered to be a good estimate of the "true" values.

Figure 6-11 compares the transverse frequencies and mode shapes of the Southbound bridge, extracted from the elastic portion of the experimental results, with the predicted values using the 3D SAP90 and 2D DRAIN-2DX models. Good agreement is evident between the experimental and analytical predictions. The modes clearly show that there no major contributions to the deck response from the piers and abutments. The results also show that the first and second modes correspond closely to rigid body translation of the deck, whereas the third transverse mode looks much like a mode corresponding to a free-free long bent beam.

Figure 6-12 compares for the Northbound bridge the experimental results versus the predictions made using the 3D and 2D FEM models. The characteristic of the first mode, which shows a larger displacement in the south than in the north abutment, is associated with the effect of the asymmetric distribution of the bearing stiffnesses which progressively increase from south to north. The second and third transverse modes resemble the second and third modes observed in the Southbound bridge. The comparison with the Southbound bridge which is structurally similar (but 2.41 m longer and 2.06 m wider using 7 girders instead of 6 girders) shows that the higher modes are not affected by the characteristics of the bearing stiffness. This figure shows that for the lower modes, the deck of the Northbound bridge also behaved essentially as a rigid body.

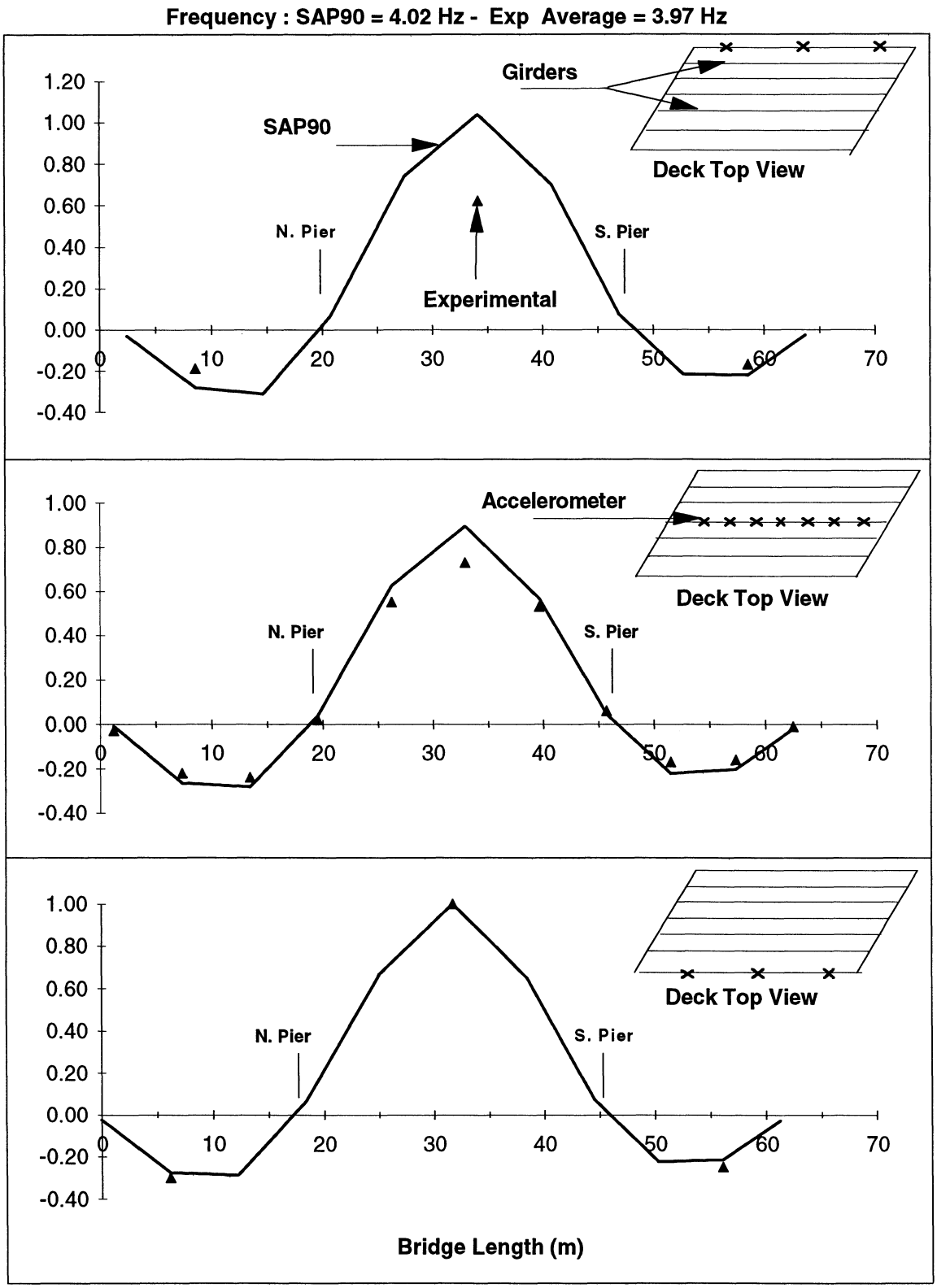

FIGURE 6-2 Southbound Bridge - First Vertical Mode

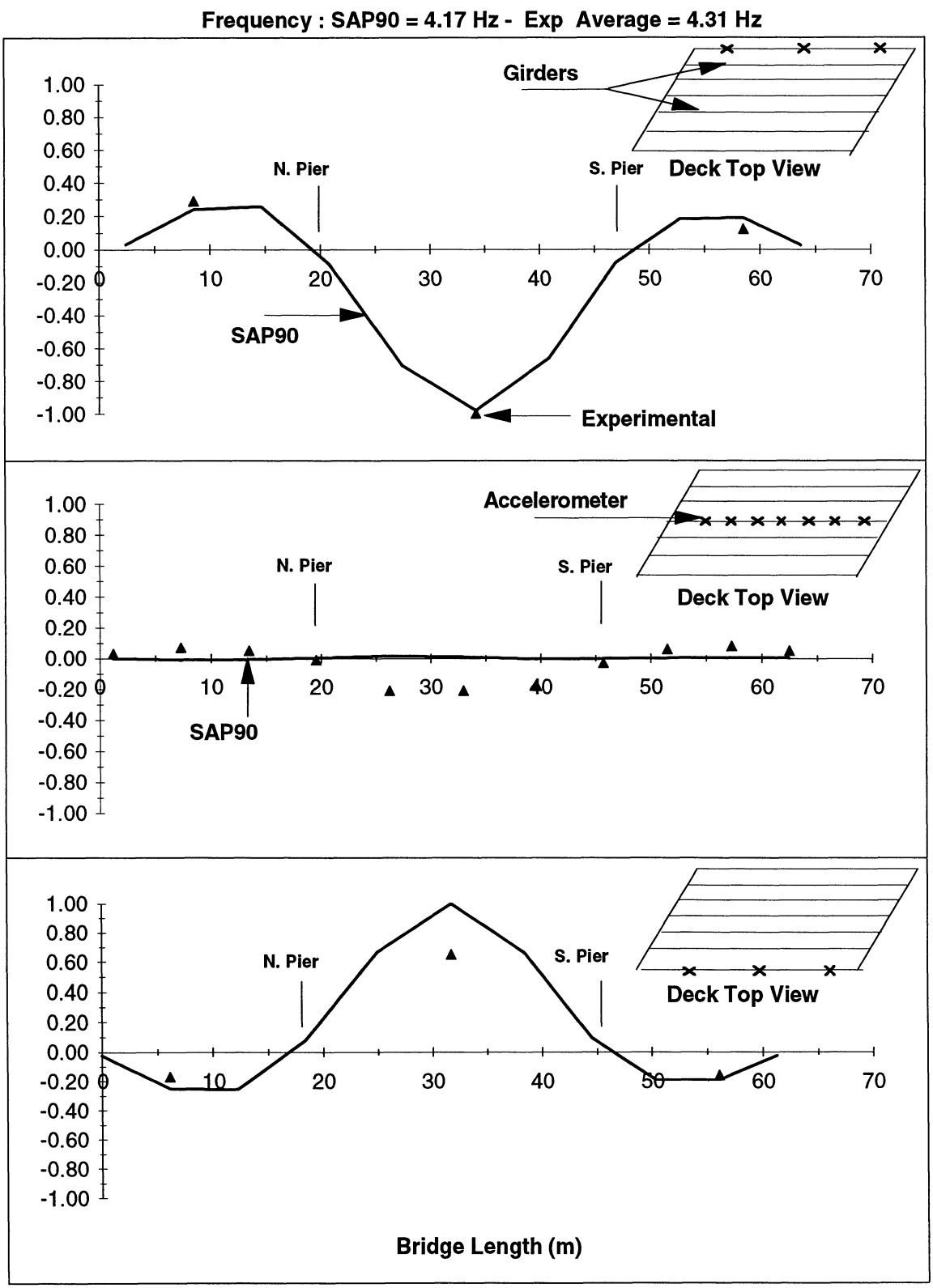

FIGURE 6-3 Southbound Bridge - Second Vertical Mode

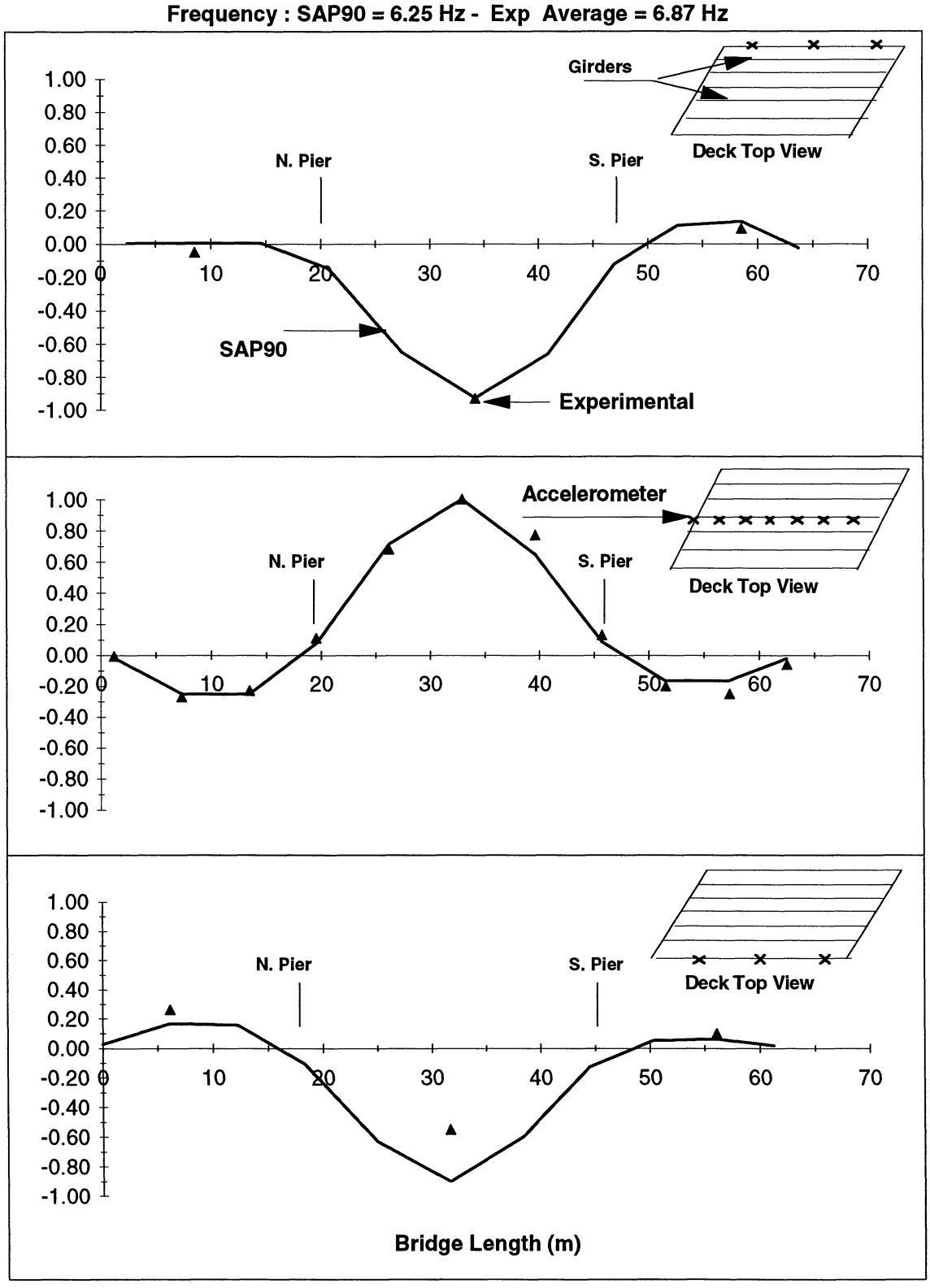

FIGURE 6-4 Southbound Bridge - Third Vertical Mode

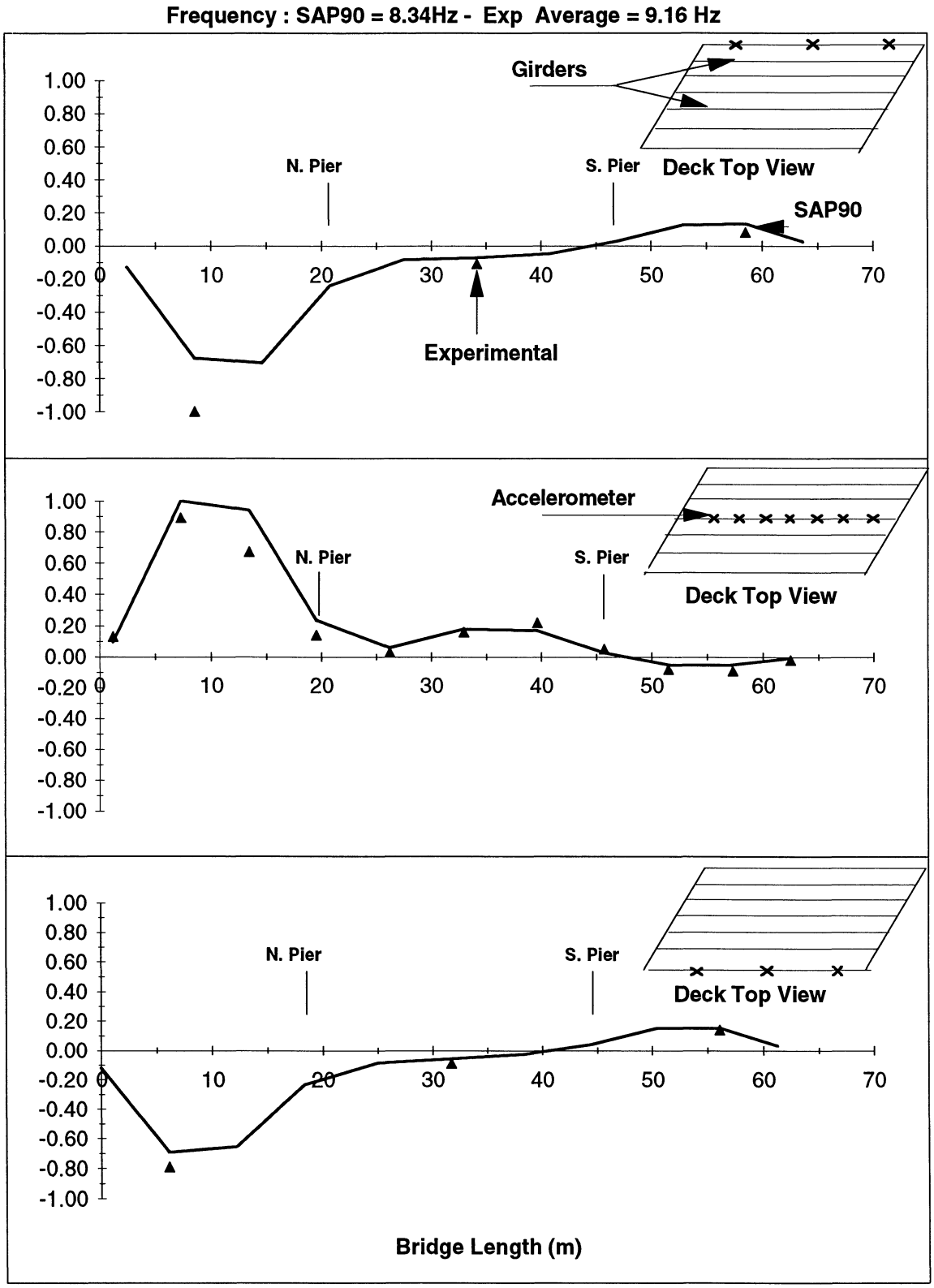

FIGURE 6-5 Southbound Bridge - Fourth Vertical Mode

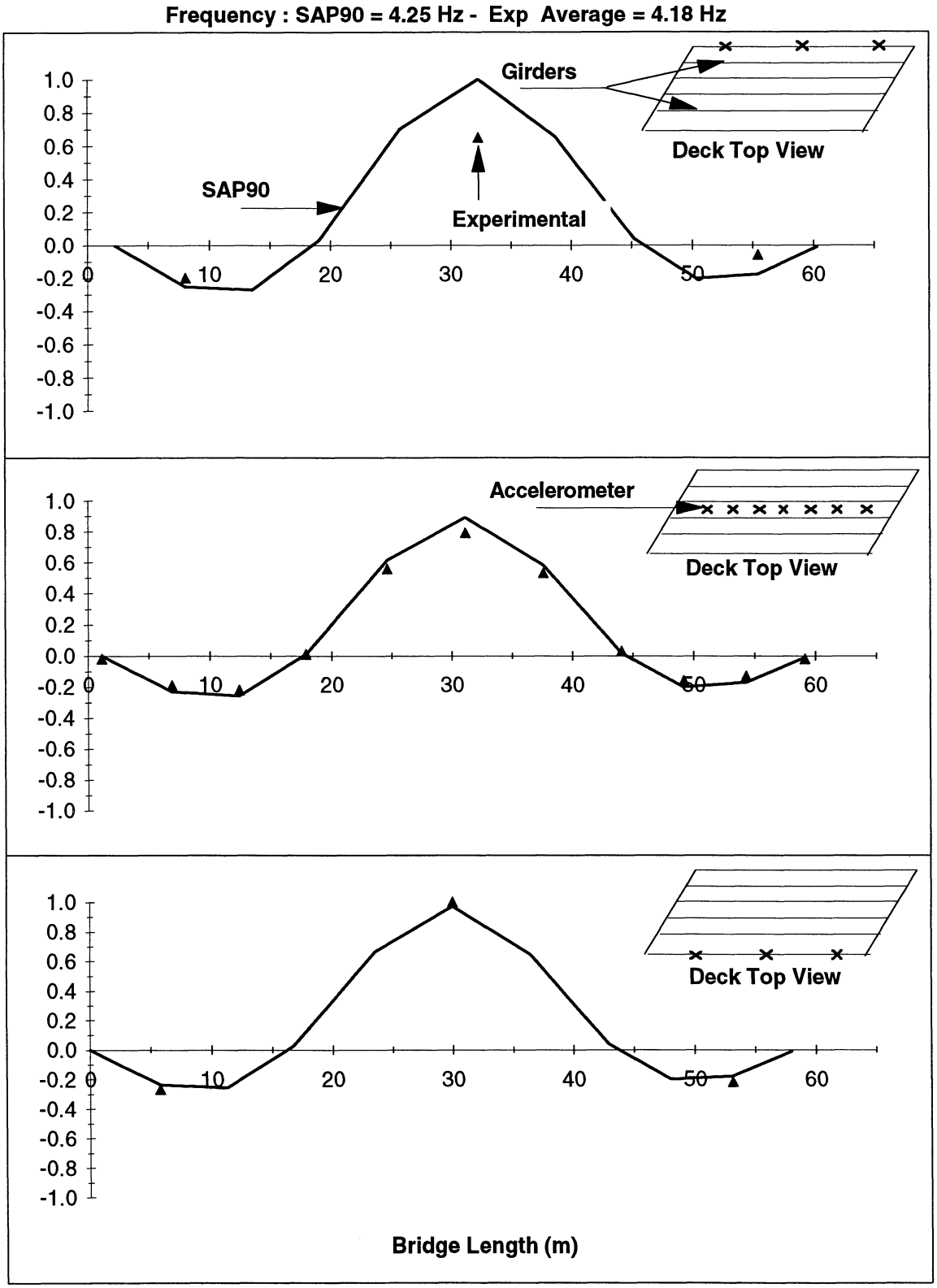

FIGURE 6-6 Northbound Bridge - First Vertical Mode

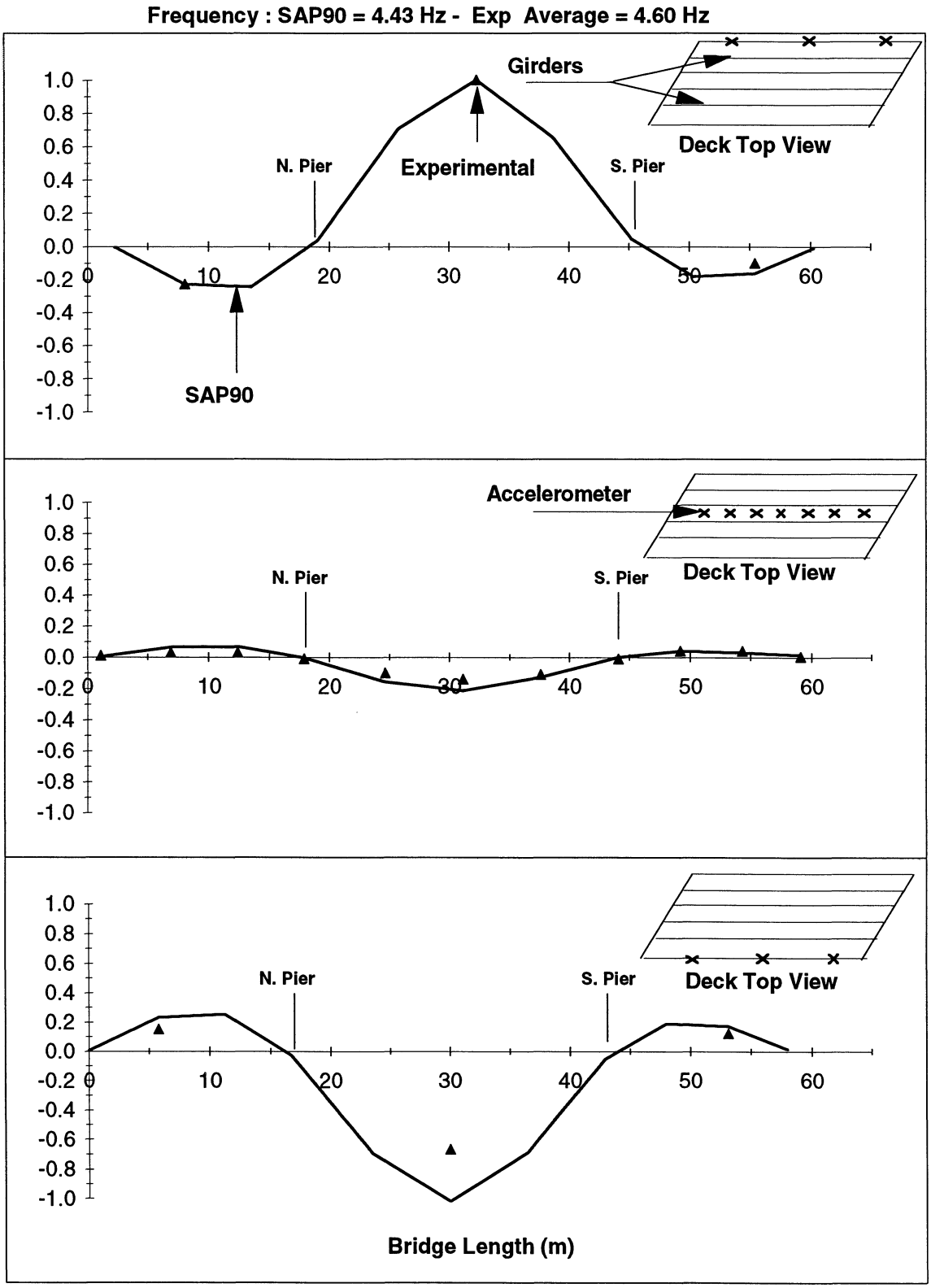

FIGURE 6-7 Northbound Bridge - Second Vertical Mode

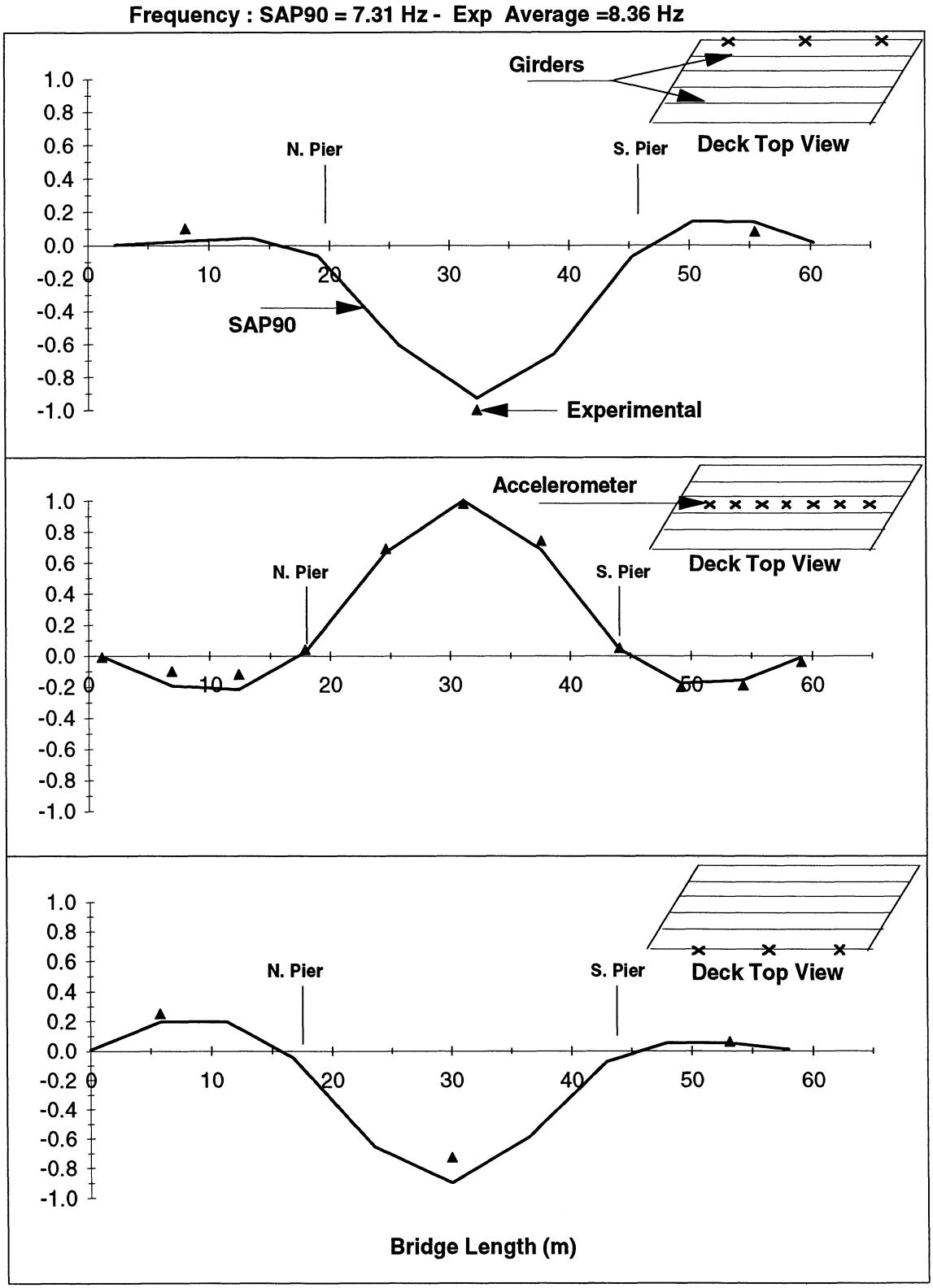

FIGURE 6-8 Northbound Bridge - Third Vertical Mode

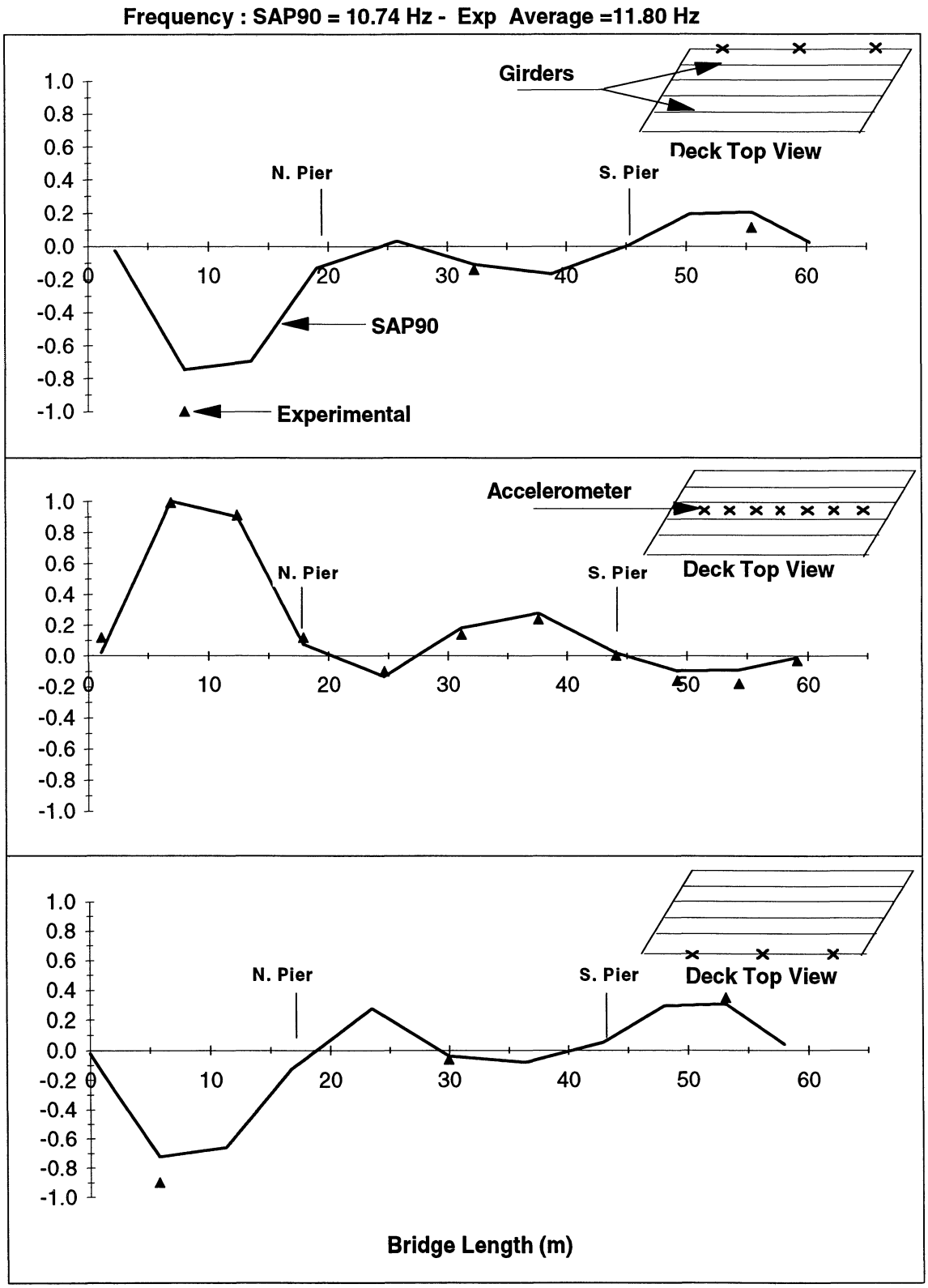

FIGURE 6-9 Northbound Bridge - Fourth Vertical Mode

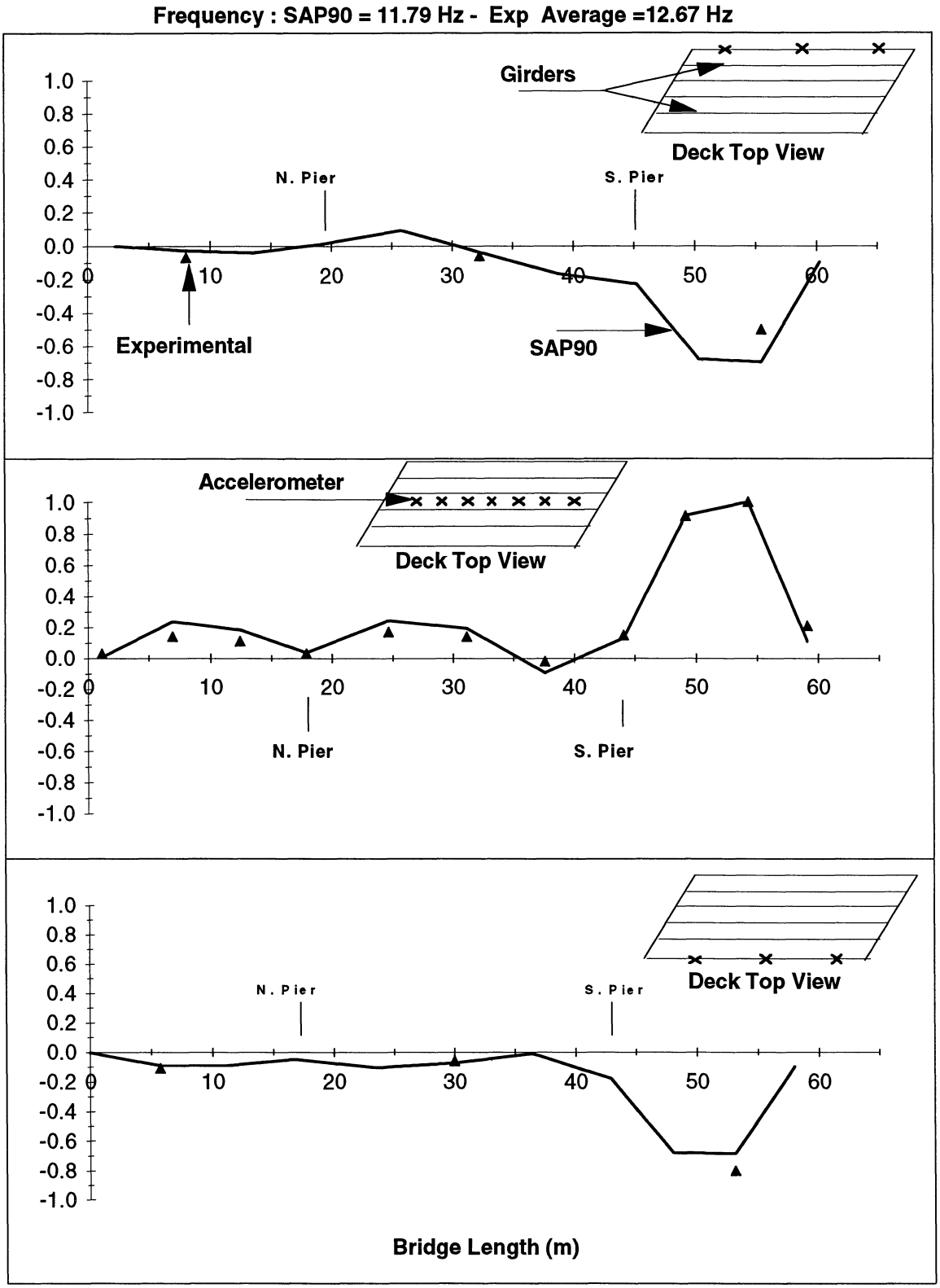

FIGURE 6-10 Northbound Bridge - Fifth Vertical Mode

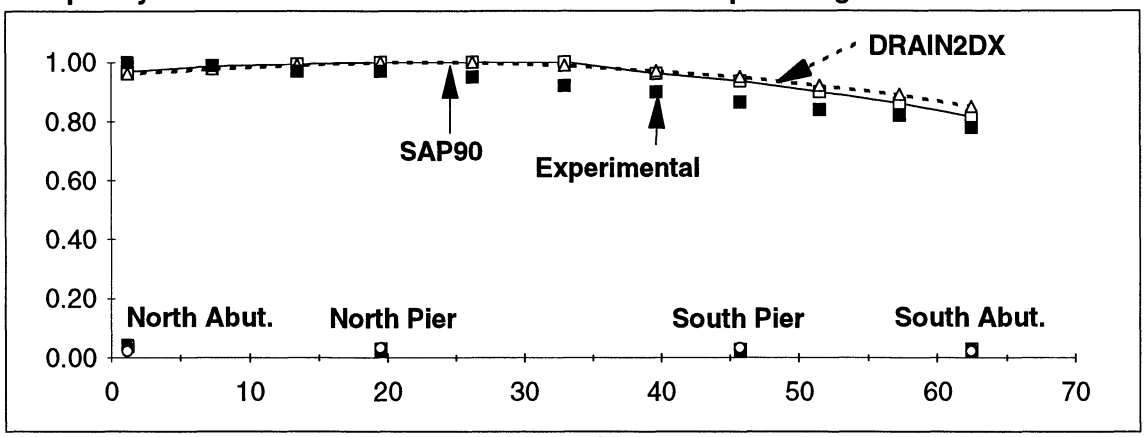

(a)

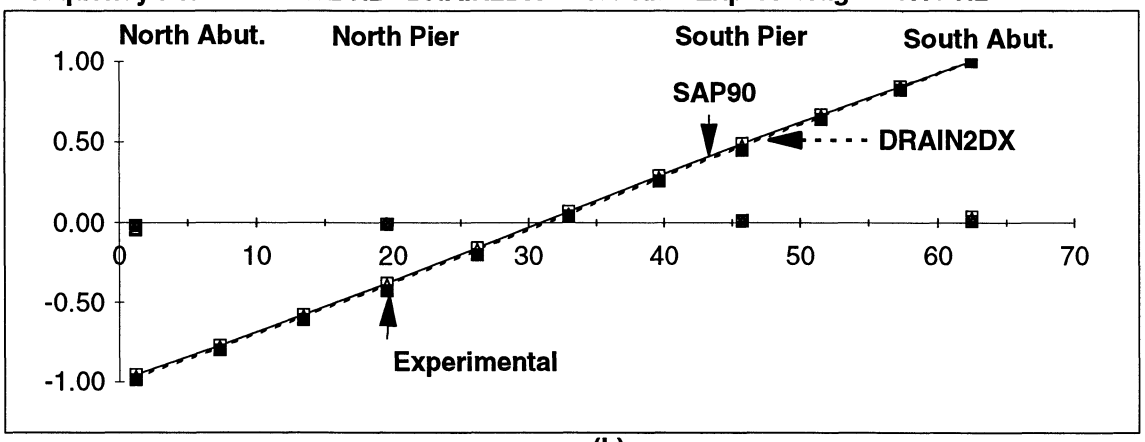

(b)

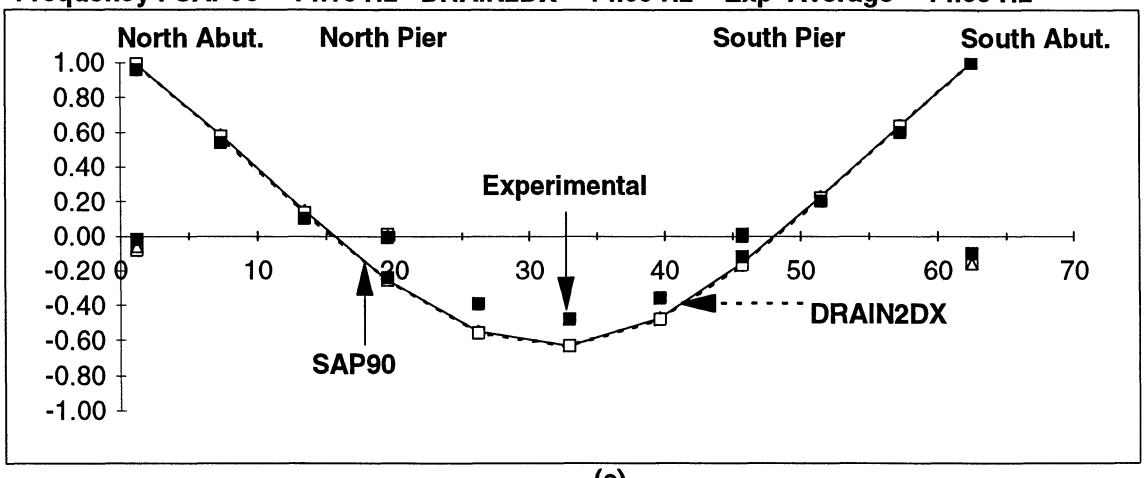

(c)

FIGURE 6-11 Post-Retrofitted Southbound Bridge - Transverse Modes

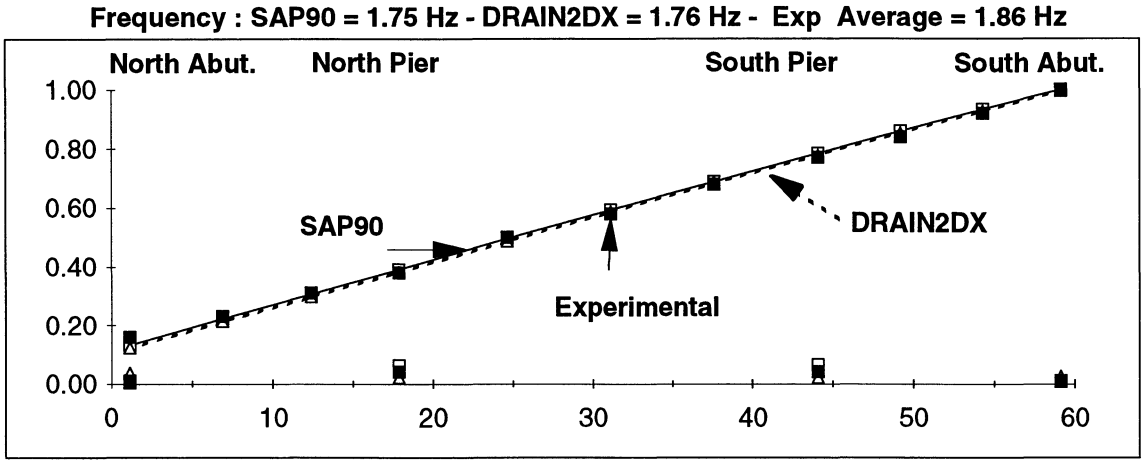

(a)

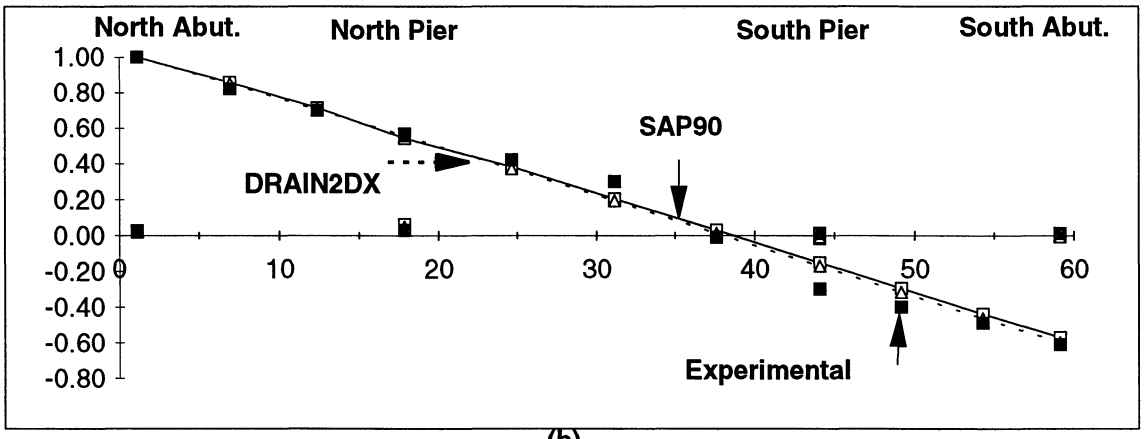

(b)

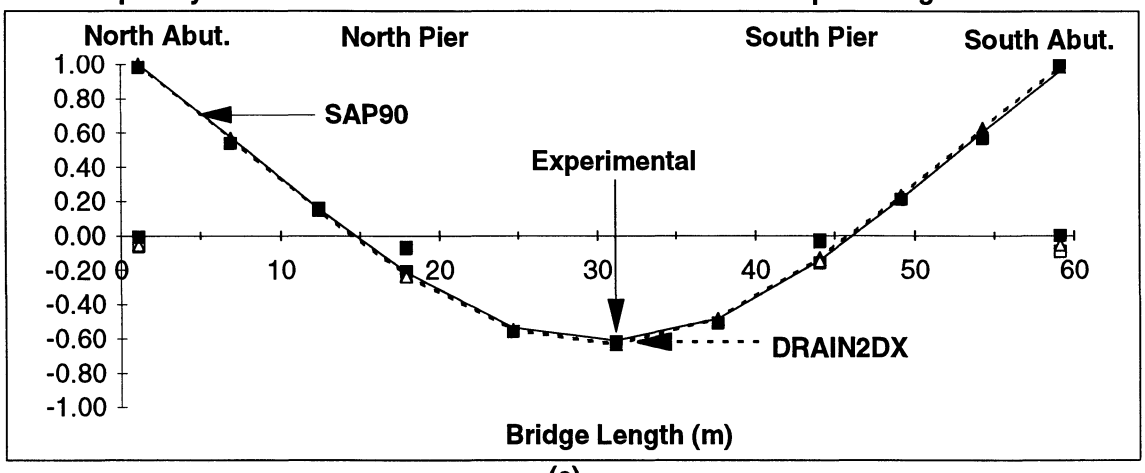

(c)

FIGURE 6-12 Post-Retrofitted Northbound Bridge - Transverse Modes

The agreement of the experimental frequencies and mode shapes with the predicted values using the proposed models shows the accuracy of these models for structures that behave linearly but does not provide information about the ability of the models to reproduce non-linear behavior. To make an overall evaluation of the model including the non-linear behavior it was decided to do a comparison between the experimental time history of selected instruments and the predicted time history for the same instrument's location, using the load time history recorded during the test as an input load.

Figure 6-13a shows the load time history of one of the quick-release tests of the Southbound bridge and figure 6-13b presents one for the Northbound bridge. All of the records were augmented with a fictitious initial loading portion as shown.

Figure 6-14 compares the experimental acceleration time history with the predicted time history using the 3D SAP90 model, and figure 6-15 shows the displacements. From the graph it is evident that the use of the equivalent stiffness approach can predict well the maximum peak acceleration but makes a poor reproduction of the remaining portion of the time history. The same situation can be concluded from the observation of the displacement time history.

Figure 6-16 compares the experimental acceleration time history of three accelerometers located in the deck of the Southbound bridge with the analytical prediction using the nonlinear 2D model and the load time history of figure 6-13a as an applied load. Figure 6-17 shows the experimental vs analytical displacement time history of two points located in the deck at the pier locations and one at the top of the girder at the south abutment. The comparison shows a good agreement between the experimental and analytical predictions. The model is also able to predict quite well the displacement time history. From these predictions it is clear that the behavior of the bridge is controlled basically by the nonlinear properties of the bearings.

It is thus evident that a model that cannot replicate bearing behavior may produce only approximate predictions, independent of the complexity of the overall computational model itself. On the other hand, due to the large differences in stiffness between the bearings and the other

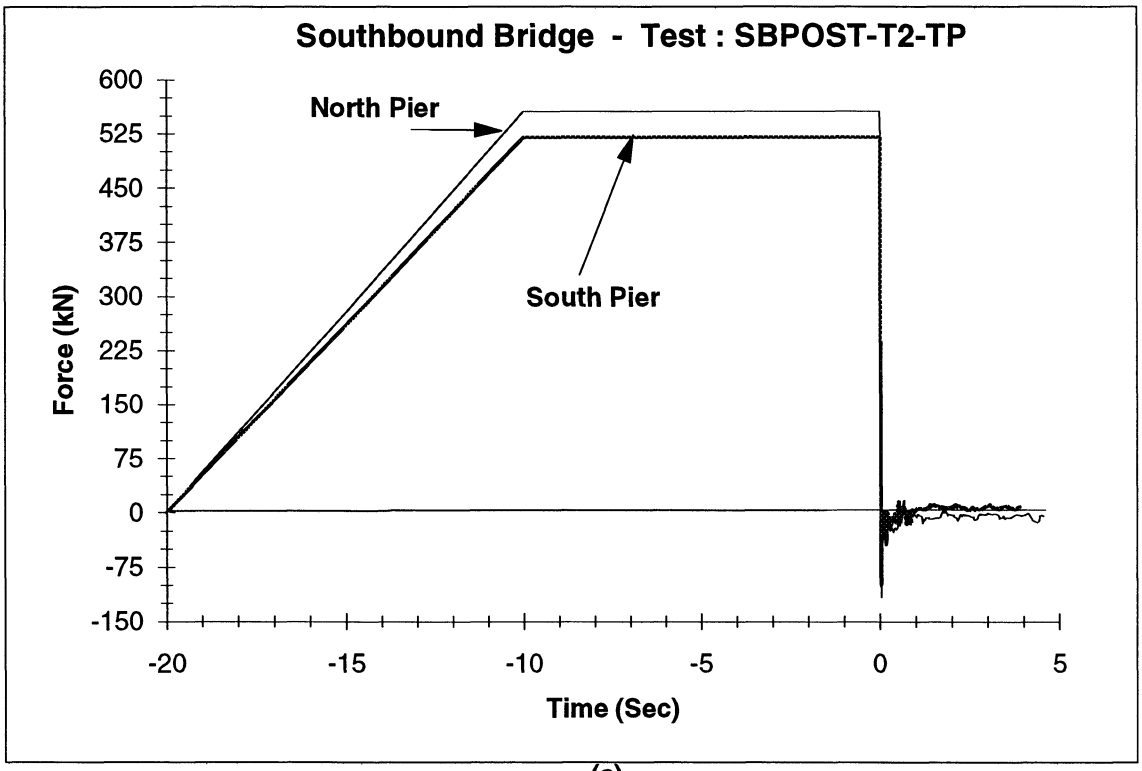

(a)

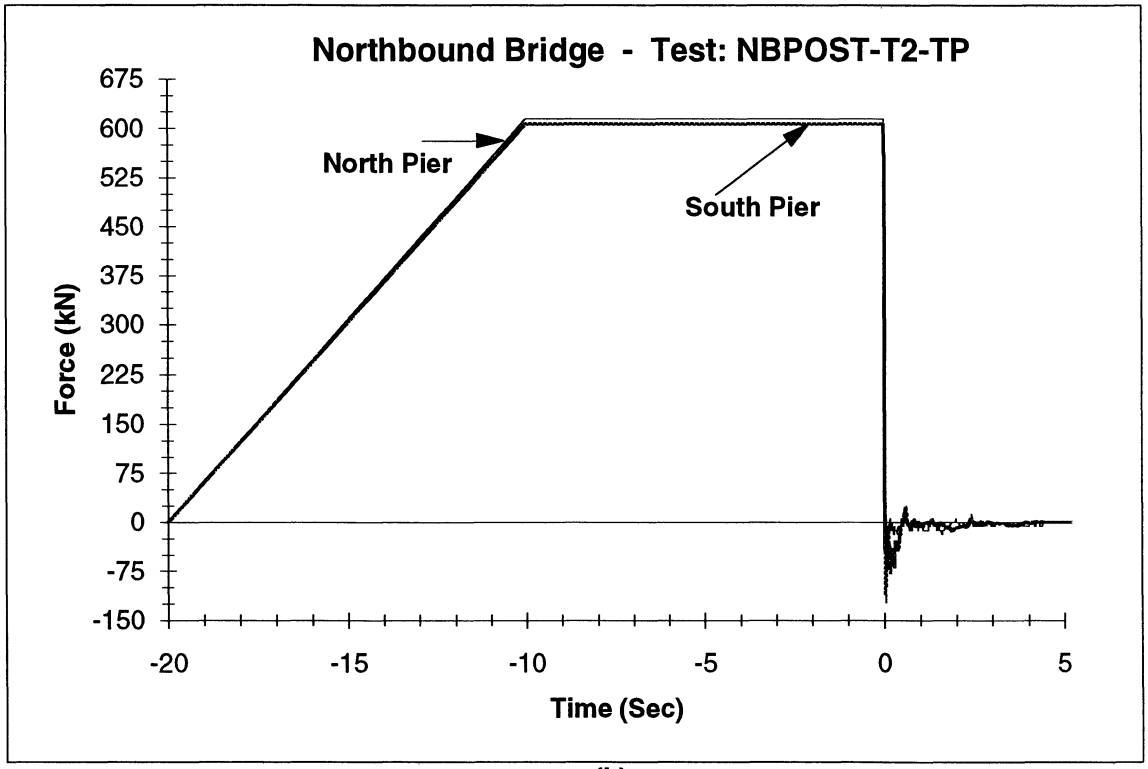

(b)

FIGURE 6-13 Load Time History

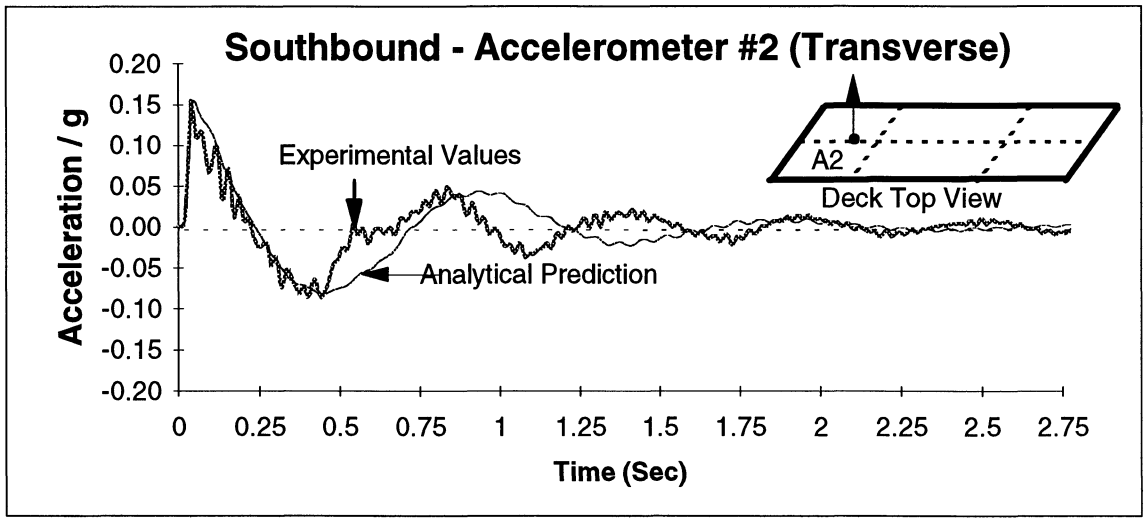

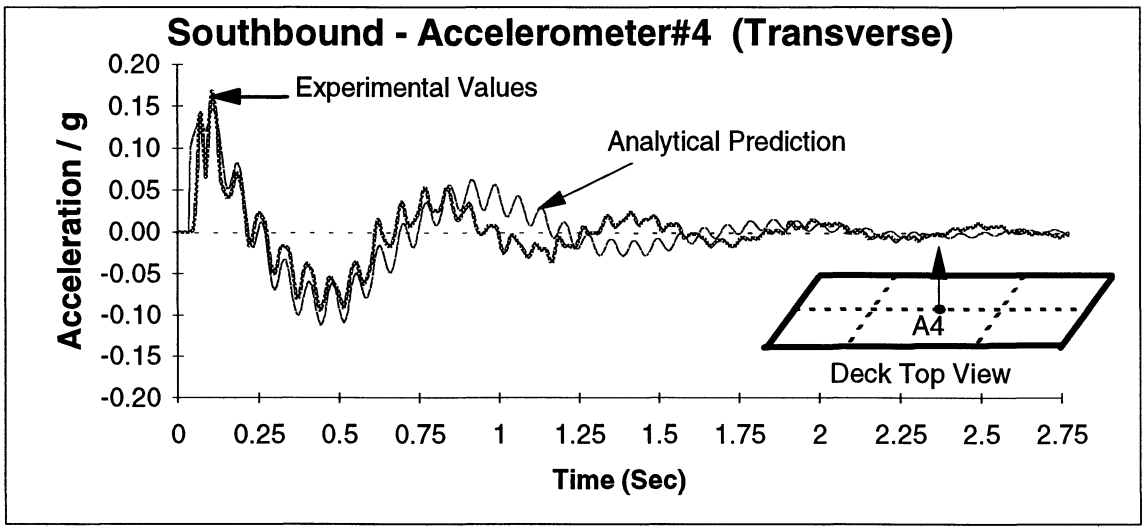

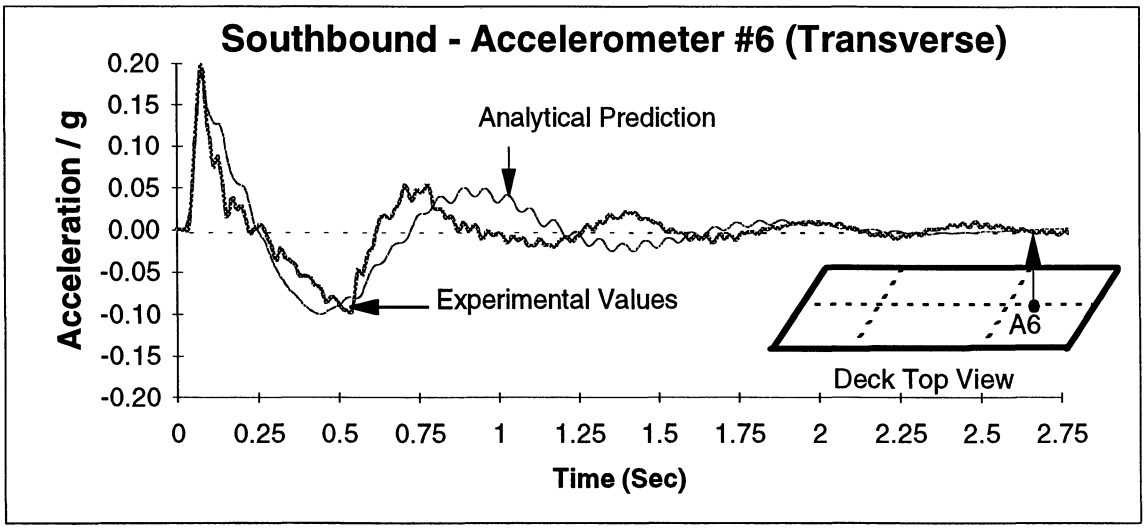

FIGURE 6-14 Analytical SAP90 Acceleration vs Experimental-SBPOST-T2-TP

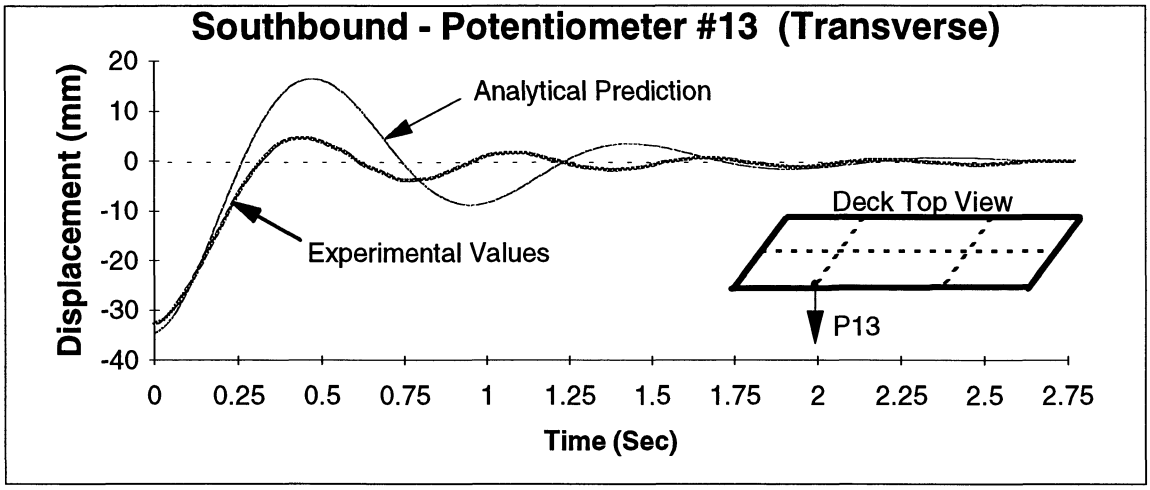

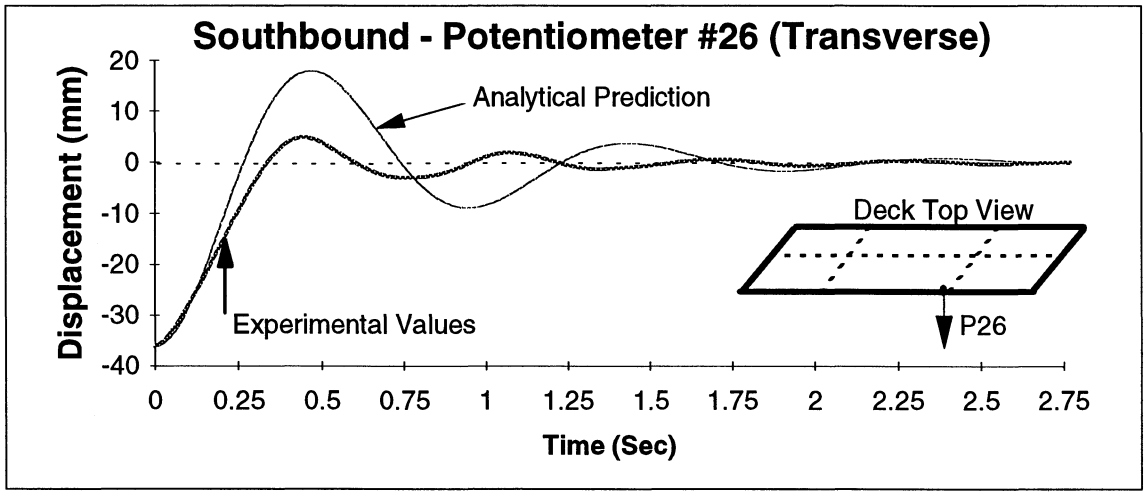

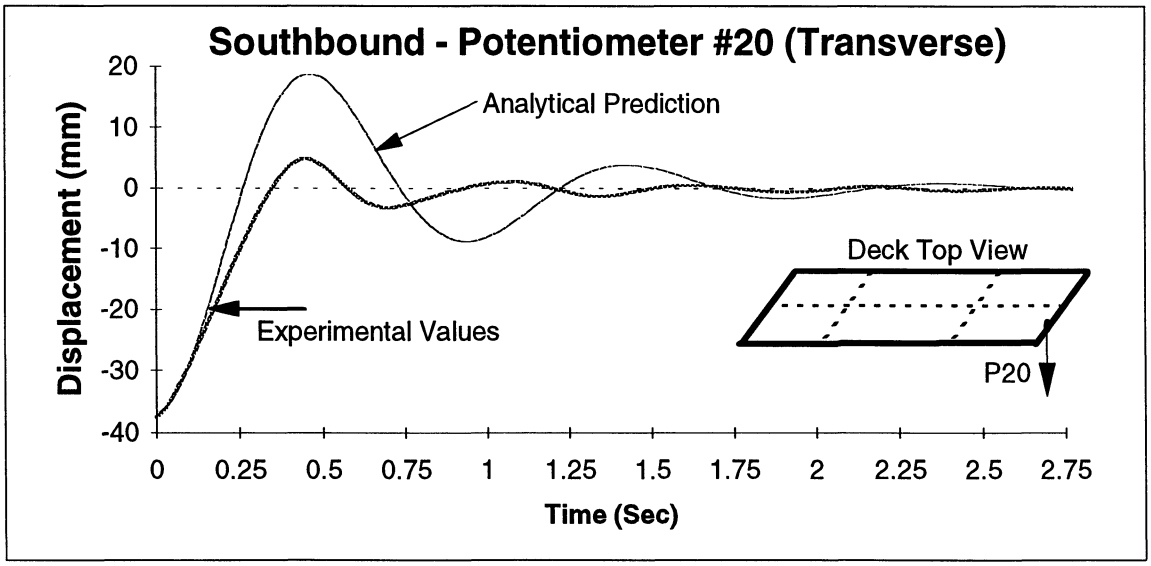

FIGURE 6-15 Analytical SAP90 Displacement vs Experimental-SBPOST-T2-TP

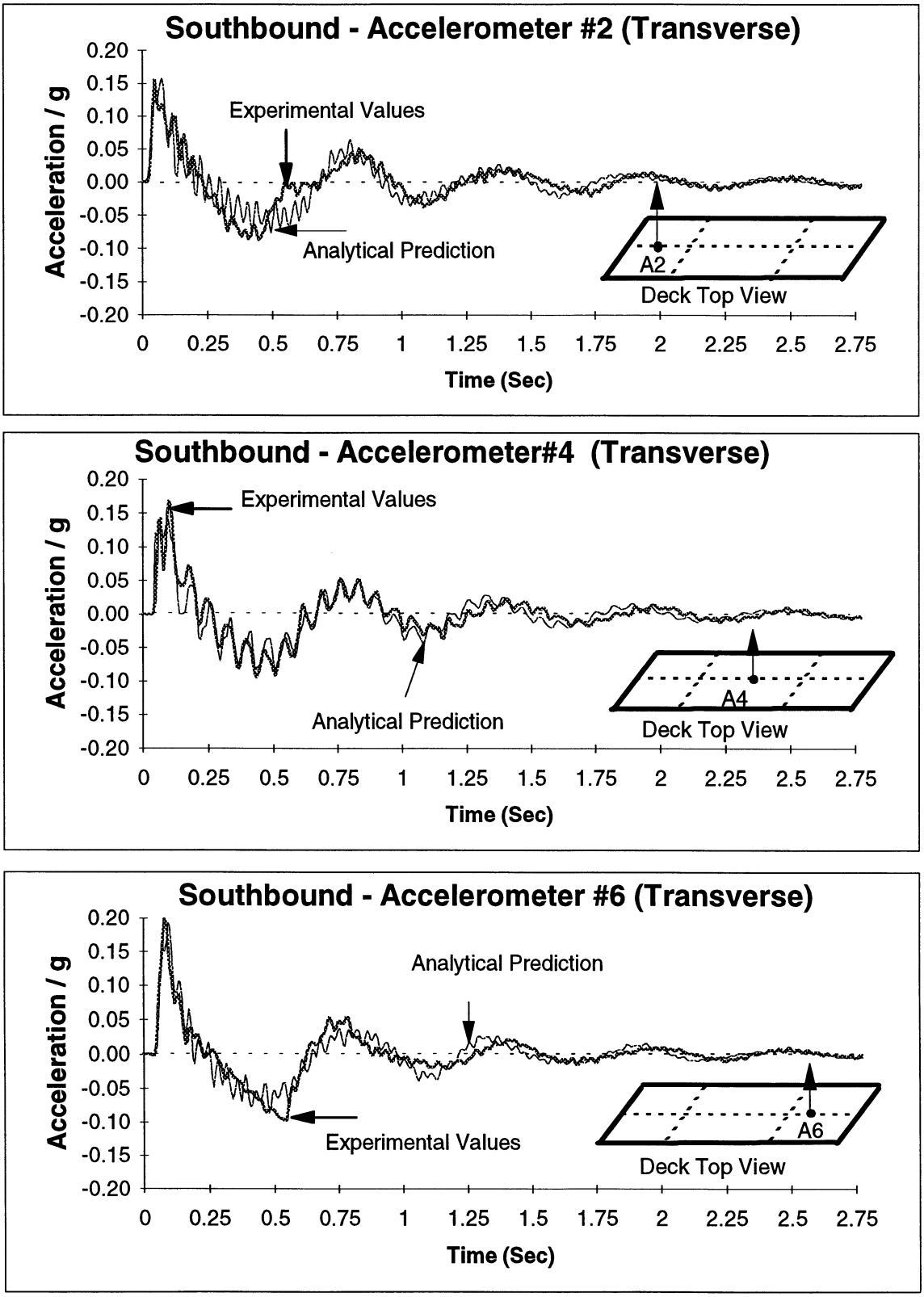

FIGURE 6-16 Analytical DRAIN2D Acceleration vs Experimental-SBPOST-T2-TP

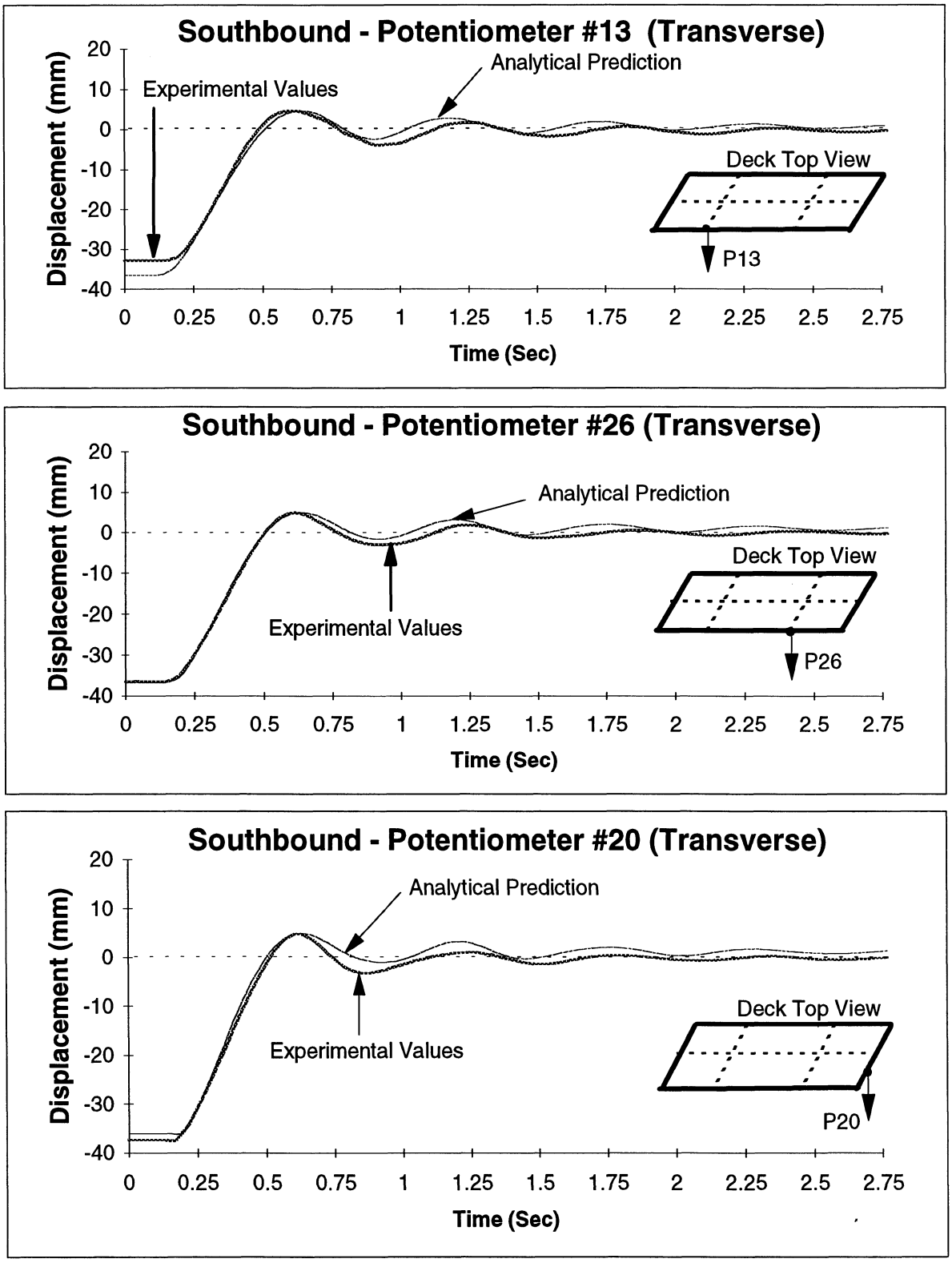

FIGURE 6-17 Analytical DRAIN2DX Displacement vs Experimental-SBPOST-T2-TP

components of the structure, a simpler model that can replicate the bearing behavior well may be able to produce better agreement between the observed and predicted behavior. It is also important to observe the existence of a higher mode in the acceleration time histories. The frequency of this made (which is around 14 Hz) is not related to the bearing properties but rather to the deck-structure characteristics and resembles the bending of a free-ended beam.

Figure 6-18 compares selected experimental acceleration time history vs the analytical prediction of the 3D FEM of the Northbound bridge, while figure 6-19 compares selected displacement time histories. The figures show there is good agreement in acceleration and displacement, specially in the first portion of the record. However, there are significant amplitude differences at the end of the record. Such differences are related to the increase of the shear stiffness that occur at low levels of deformation in the bearings. Although this difference is due to the modeling assumption that the bearings behave linearly and the hysteretic energy dissipated can be represented by equivalent viscous damping, it does not introduce a significant level of error, and a reasonable agreement between experiments and predictions is made.

The predictions made using the 2D model of the Northbound bridge are compared with the experimental acceleration in figure 6-20 and with the experimental displacement in figure 6-21. The 2D model produces results that shows good agreement with the experimental values. The model can reconstruct the main characteristics of the acceleration time histories, but it cannot show the same accuracy that the 3D model in the reconstruction of the effect of the higher modes. In the displacement time history , the predictions of the 2D and 3D model do not exhibit major differences. In this bridge it is also possible to see in the acceleration time histories the same effect of the higher modes as described for the Southbound bridge.

6.4 Post-Retrofitted Model Simplification

From the experimental results and predictions represented up to this point, it is clear that the fundamental modes correspond closely to rigid body motions of the deck. These modes are mainly influenced by the bearings' properties. On the other hand, the higher modes are related

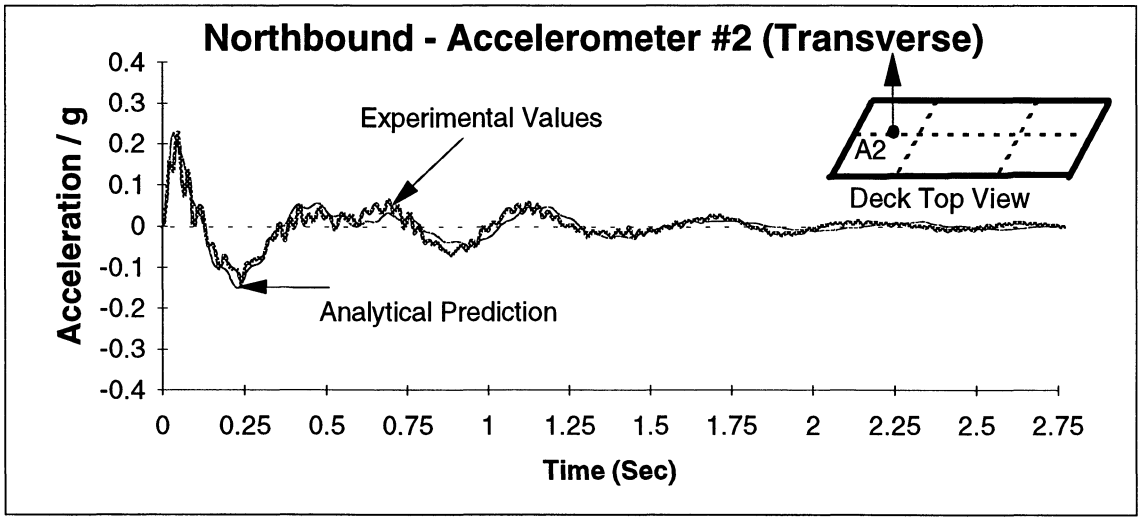

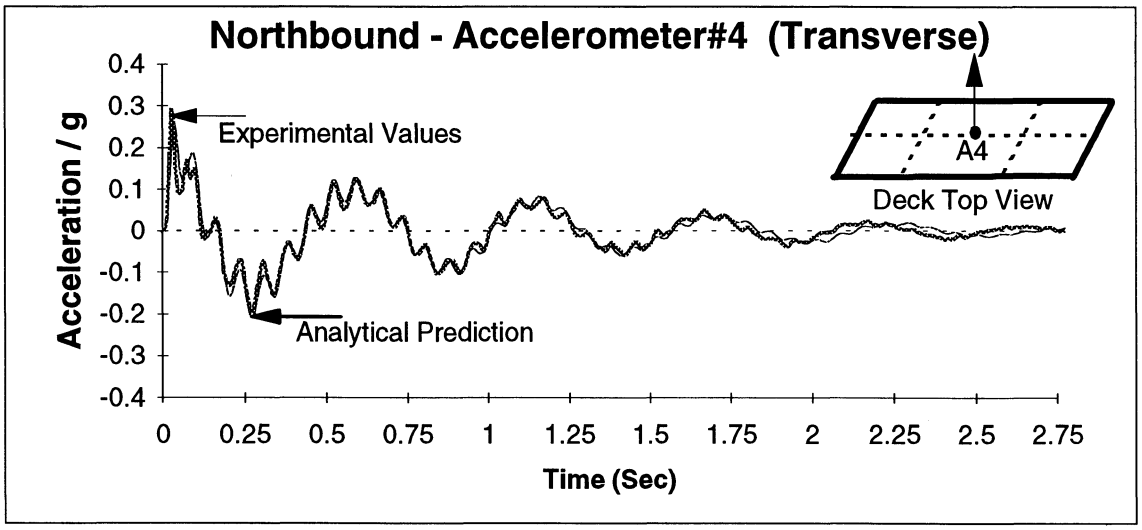

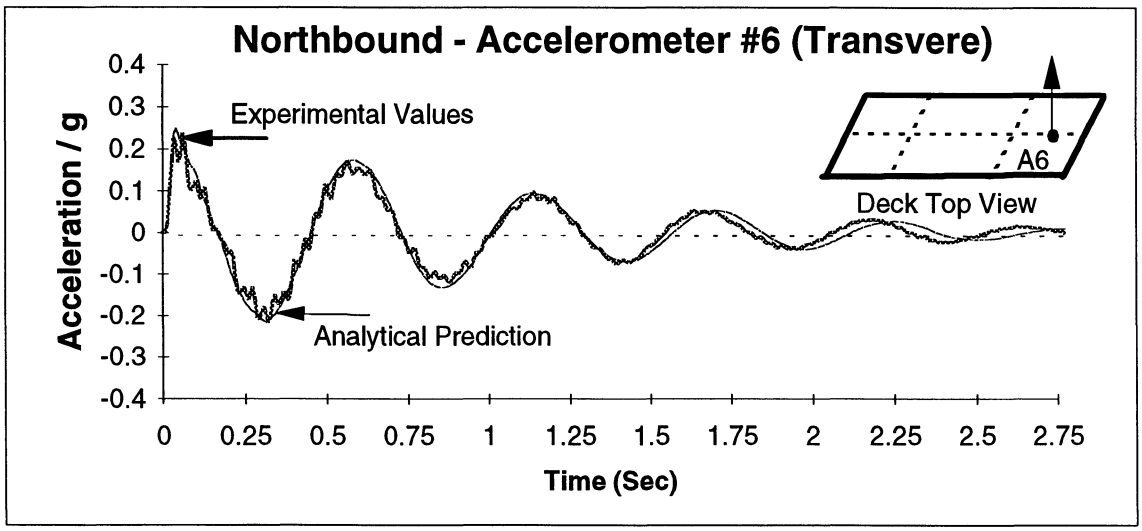

FIGURE 6-18 Analytical SAP90 Acceleration vs Experimental-NBPOST-T2-TP

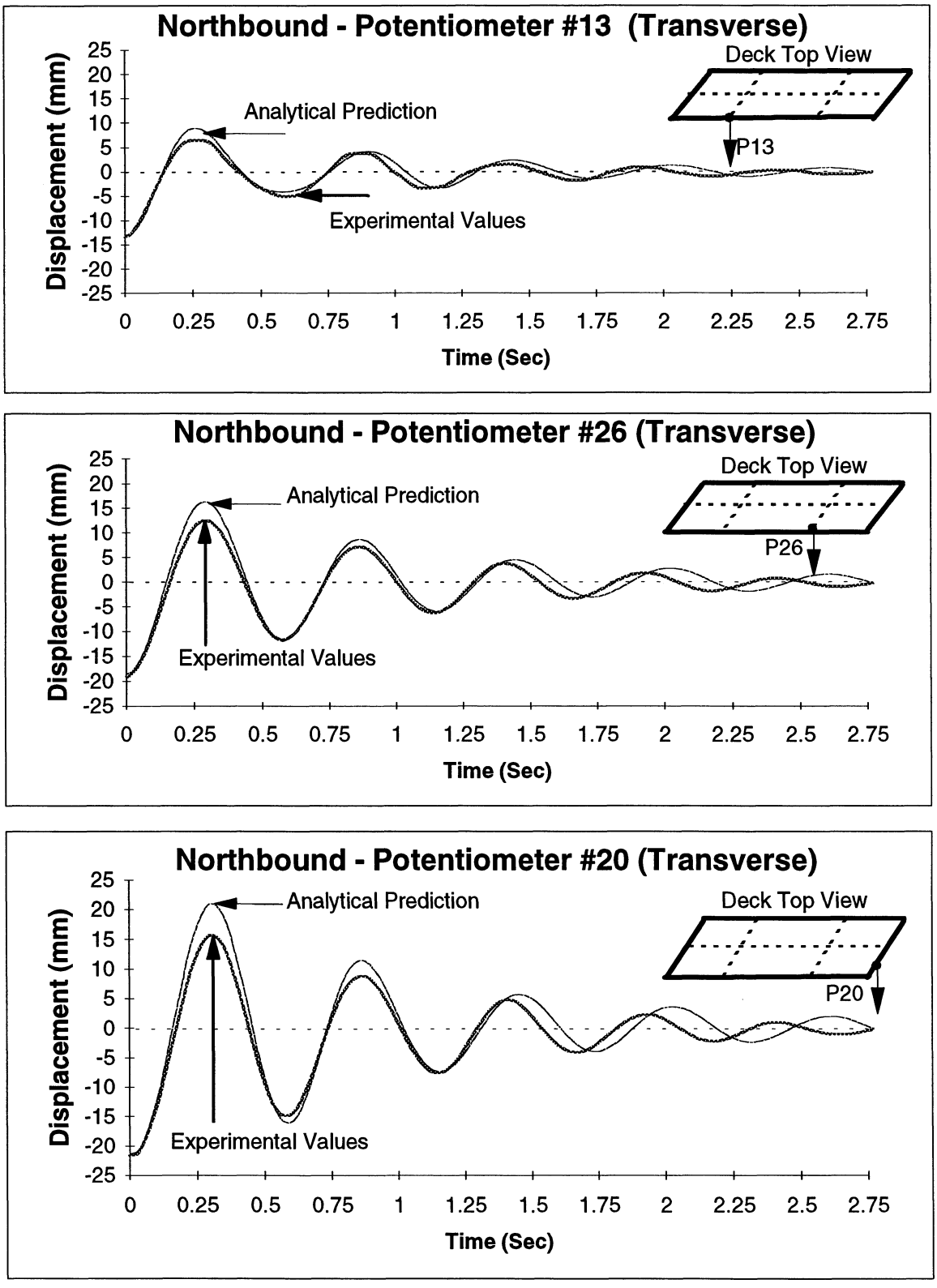

FIGURE 6-19 Analytical SAP90 Displacement vs Experimental-NBPOST-T2-TP

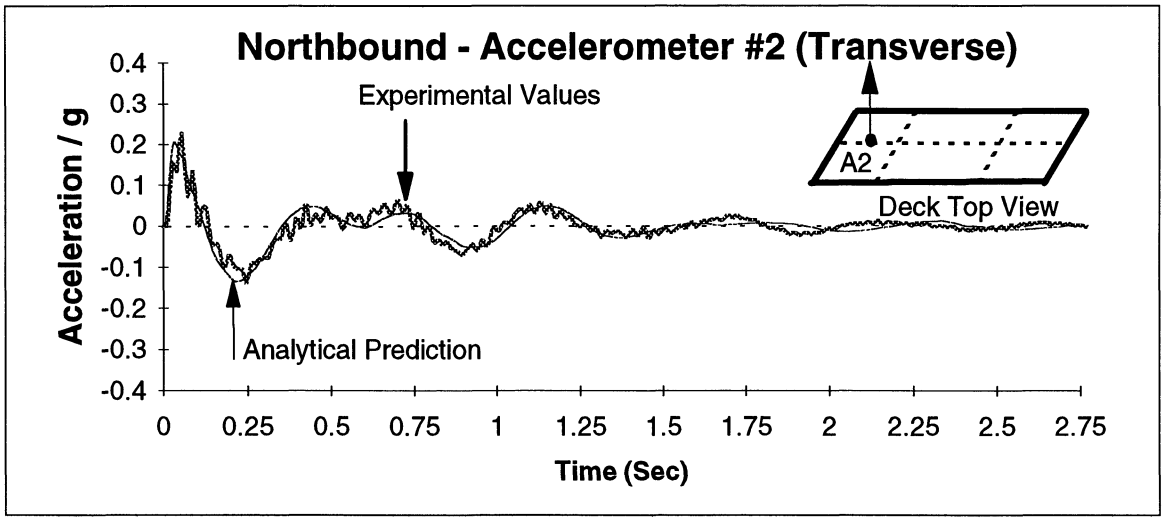

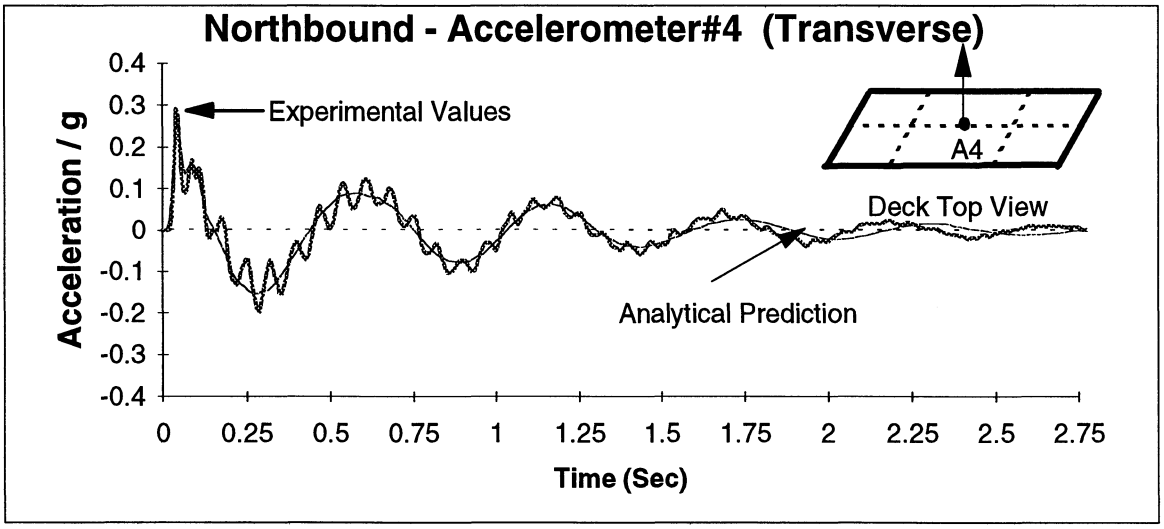

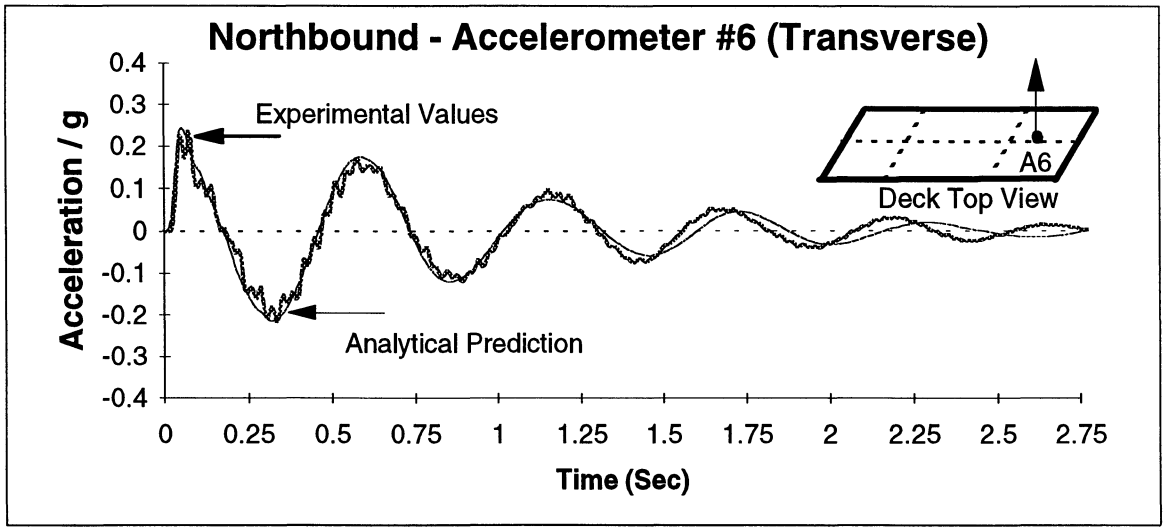

FIGURE 6-20 Analytical DRAIN2D Acceleration vs Experimental SBPOST-T2-TP

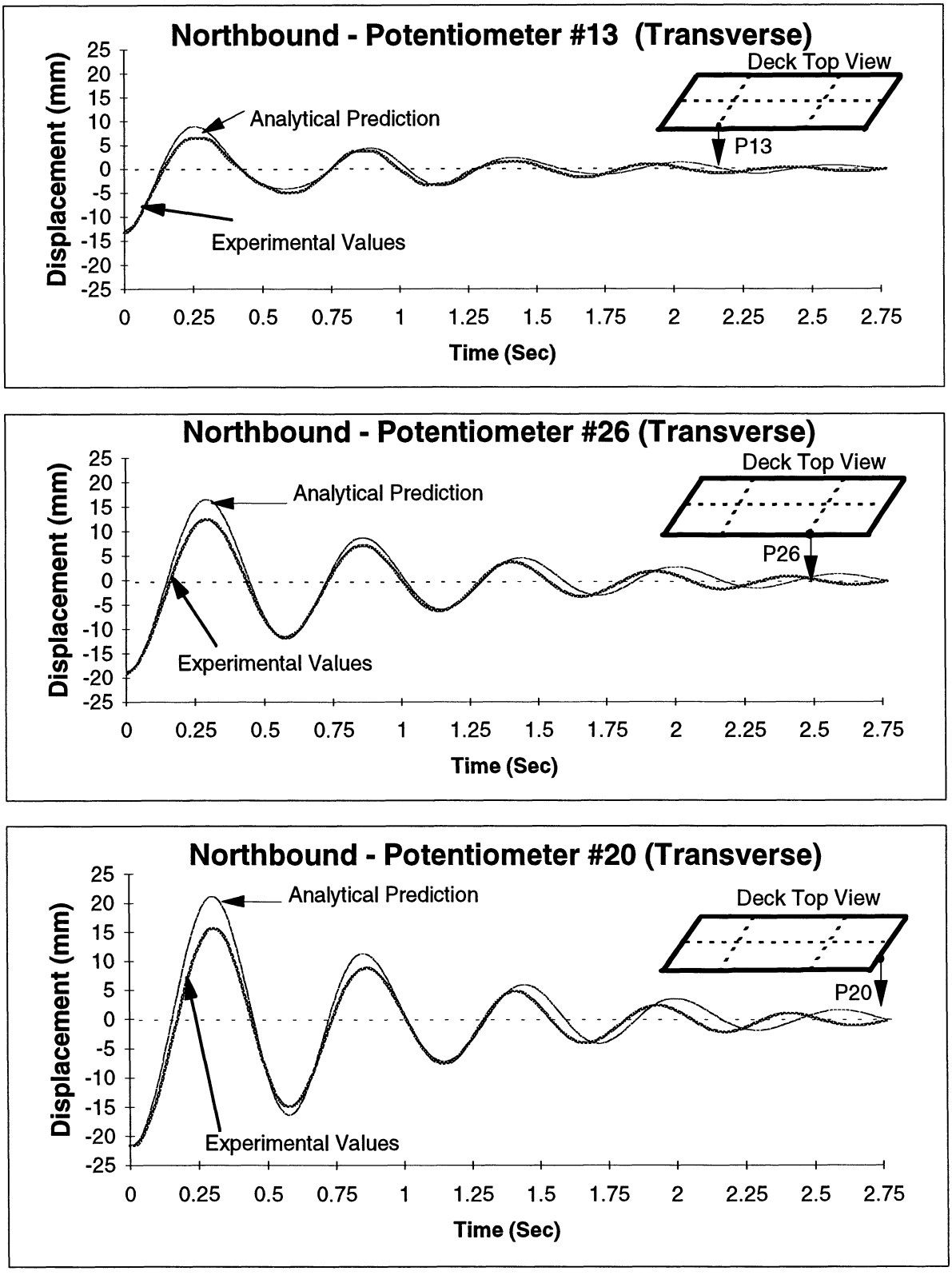

FIGURE 6-21 Analytical DRAIN2DX Displacement vs Experimental NBPOST-T2-TP

to the mass and stiffness properties of the structure and are not greatly influenced by the bearings' properties. With this consideration and from a practical point of view, it is possible with the use of basic concepts of structural dynamics to obtain the frequencies and the mode shapes. The problem can be stated as follows:

From the free body diagram shown in figures 6-22 and 6-23 with the positive values of the motion variables indicated translation and rotation indicated, the force equilibrium equation in the vertical direction can be written as:

$$M\ddot{x} = -K_1(x - L_1\theta) - K_2(x - L_2\theta) - K_3(x + L_3\theta) - K_4(x + L_4\theta) \tag{6-2}$$

The moment equation about the CG can be expressed as:

$$J_0\ddot{\theta} = K_1(x - L_1\theta)L_1 + K_2(x - L_2\theta)L_2 - K_3(x + L_3\theta)L_3 - K_4(x + L_4\theta)L_4 \tag{6-3}$$

$$\begin{bmatrix} M & 0 \\ 0 & J_0 \end{bmatrix} \begin{Bmatrix} \ddot{x} \\ \ddot{\theta} \end{Bmatrix} + \begin{bmatrix} (K_1 + K_2 + K_3 + K_4) & -(K_1L_1 + K_2L_2) + (K_3L_3 + K_4L_4) \\ -(K_1L_1 + K_2L_2) + (K_3L_3 + K_4L_4) & (K_1L_1^2 + K_2L_2^2 + K_3L_3^2 + K_4L_4^2) \end{bmatrix} \begin{Bmatrix} x \\ \theta \end{Bmatrix} = \begin{Bmatrix} 0 \\ 0 \end{Bmatrix} \tag{6-4}$$

Equations (6-1) and (6-2) can be rearranged and written in matrix form as:

$$\begin{bmatrix} M & 0 \\ 0 & J \end{bmatrix} \begin{Bmatrix} \ddot{x} \\ \ddot{\theta} \end{Bmatrix} + \begin{bmatrix} K_{xx} & K_{x\theta} \\ K_{x\theta} & K_{\theta\theta} \end{bmatrix} \begin{Bmatrix} x \\ \theta \end{Bmatrix} = \begin{Bmatrix} 0 \\ 0 \end{Bmatrix} \tag{6-5}$$

or

$$\begin{bmatrix} (-\lambda M + K_{xx}) & K_{x\theta} \\ K_{x\theta} & (-J\lambda + K_{\theta\theta}) \end{bmatrix} \begin{Bmatrix} x \\ \theta \end{Bmatrix} = \begin{Bmatrix} 0 \\ 0 \end{Bmatrix} \tag{6-6}$$

By letting $\lambda = \omega^2$ the eigenvalue problem can be expressed and the characteristic equation as:

$$\lambda^2 MJ - \lambda(MK_{\theta\theta} + J_0K_{xx}) + K_{xx}K_\theta\theta - K_{x\theta}^2 = 0 = A\lambda^2 - B\lambda + C \tag{6-7}$$

Then by solving the quadratic equation:

$$\omega_{1,2}^2 = \frac{-B \pm \sqrt{B^2 - 4AC}}{2A} = \lambda_{1,2} \tag{6-8}$$

Using equation (6-5), the ratio of amplitudes can be found as:

$$\frac{x}{\theta} = \frac{-K_{x\theta}}{(-\lambda M + K_{xx})} \tag{6-9}$$

An estimation of the higher modes can be found using the equation for a beam with both ends free. In order to consider the shear deformation and cracking in slab 80% of the inertia is suggested. Then:

$$\omega_3 = (4.731)^2 \sqrt{\frac{0.81E}{ML^4}} \tag{6-10}$$

and the mode shape (Paz, 1991):

$$\phi_n(x) = \cosh(a_n x) + \cos(a_n x) - \sigma_n \left(\sin h(a_n x) + \sin(a_n x)\right) \tag{6-11}$$

where for ω_3, $a_n L = 4.731$ and $\sigma_n = .982502$.

Figures 6-22 and 6-23 present the results of the suggested approach. the simplified rigid body approach compares closely with both the detailed SAP90 model for elastic and equivalent secant stiffness and with the experimental results.

6.5 Results Summary

Presented above are the modifications made to the models of the pre-retrofitted bridges and the comparison between the experimental results and the predictions made with these models. In this portion are highlighted the most important findings which are subsequently applied to the simplification of the mathematical models.

1. Regarding the dynamic properties of the structure in the vertical direction, it was seen in Section 4 that several vertical modes and frequencies were obtained using the excitation produced by the ambient vibration. These results were

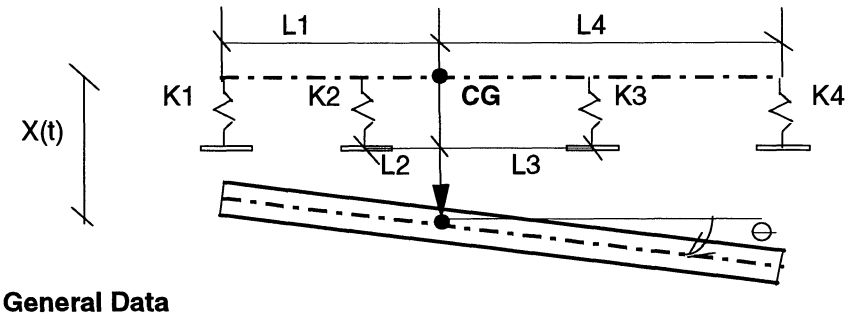

General Data

		Elastic Stiffness	Eq. Secant Stiffness
m= 11.11			
M= 689	**Length (m)**	**Stiffness(kN/m)**	**Stiffness(kN/m)**
Jo= 233257	**L1=** 31	**K1=** 43785	**K1=** 10828
Ltotal= 62	**L2=** 12	**K2=** 5516	**K2=** 5516
E= 30441577	**L3=** 14	**K3=** 5516	**K3=** 5516
I= 106	**L4=** 31	**K4=** 46704	**K4=** 9807
		Frequencies(Hz)	**Frequencies(Hz)**
		SAP90 Rig. Body	SAP90 Rig. Body
		1.88 1.93	1.08 1.07
		3.12 3.11	1.55 1.52
		Free-Free Beam	Free-Free Beam
		14.16 14.12	13.79 14.01

Note: There are 7 bearings at each abut. or pier
K1(Elastic) = 6255*7=43785 kN/m

Experimental vs Rigid Body Mode Shapes (Equivalent Elastic Stiffness)

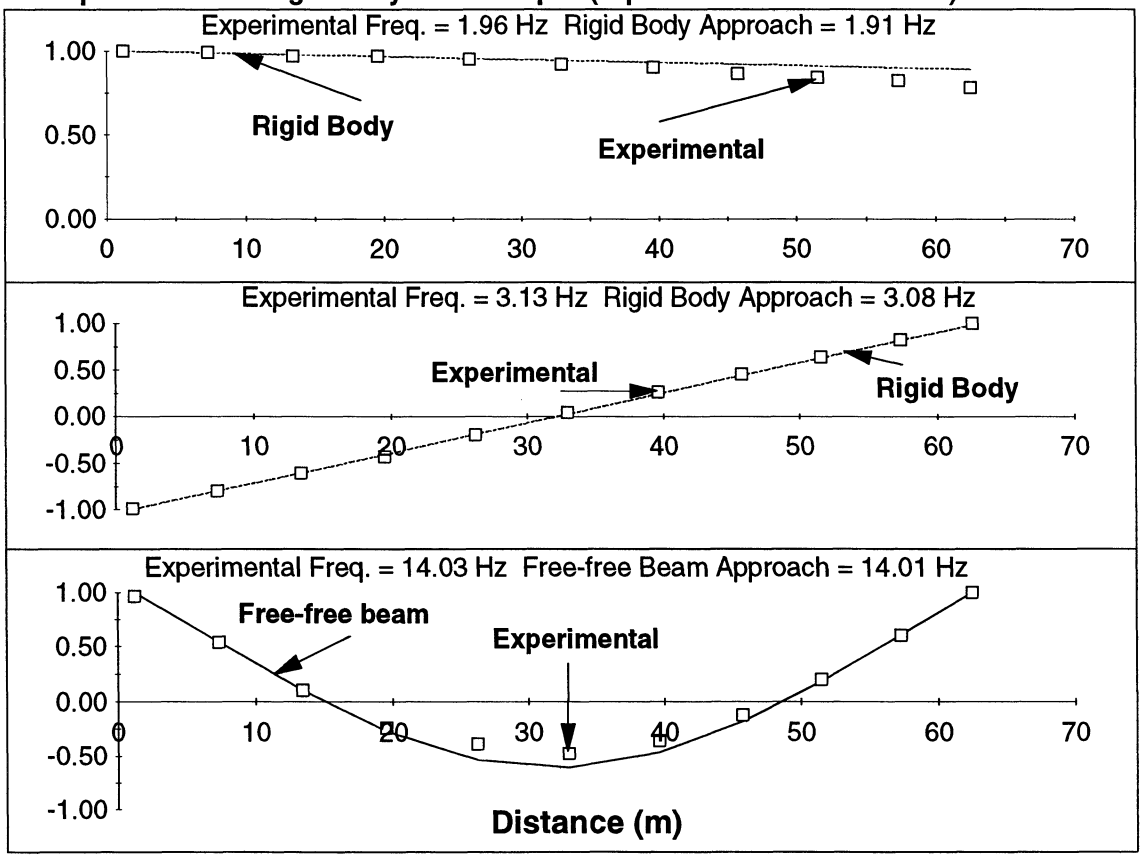

FIGURE 6-22 Experimental vs Simplified Approach for the Southbound Bridge

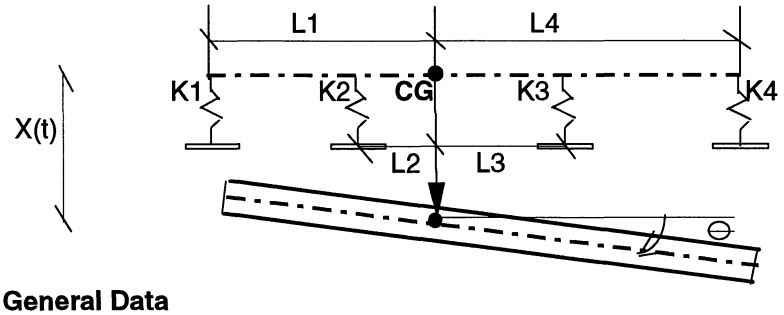

General Data

m= 9.57		Elastic Stiffness	Frequencies(Hz)	
M= 555	Length (m)	Stiffness(kN/m)	SAP90	Rig. Body
Jo= 163346	L1= 29	K1= 24949	1.75	1.70
Ltotal= 58	L2= 12	K2= 34140	2.57	2.60
E= 30441577	L3= 14	K3= 17520	Free-Free Beam	
I= 69	L4= 29	K4= 8910	14.01	14.03

Note: There are 6 bearings at each abutment
or pier
K1 and K4 Include the Expansion
Joint Contribution

Experimental Vs Rigid body Mode Shapes

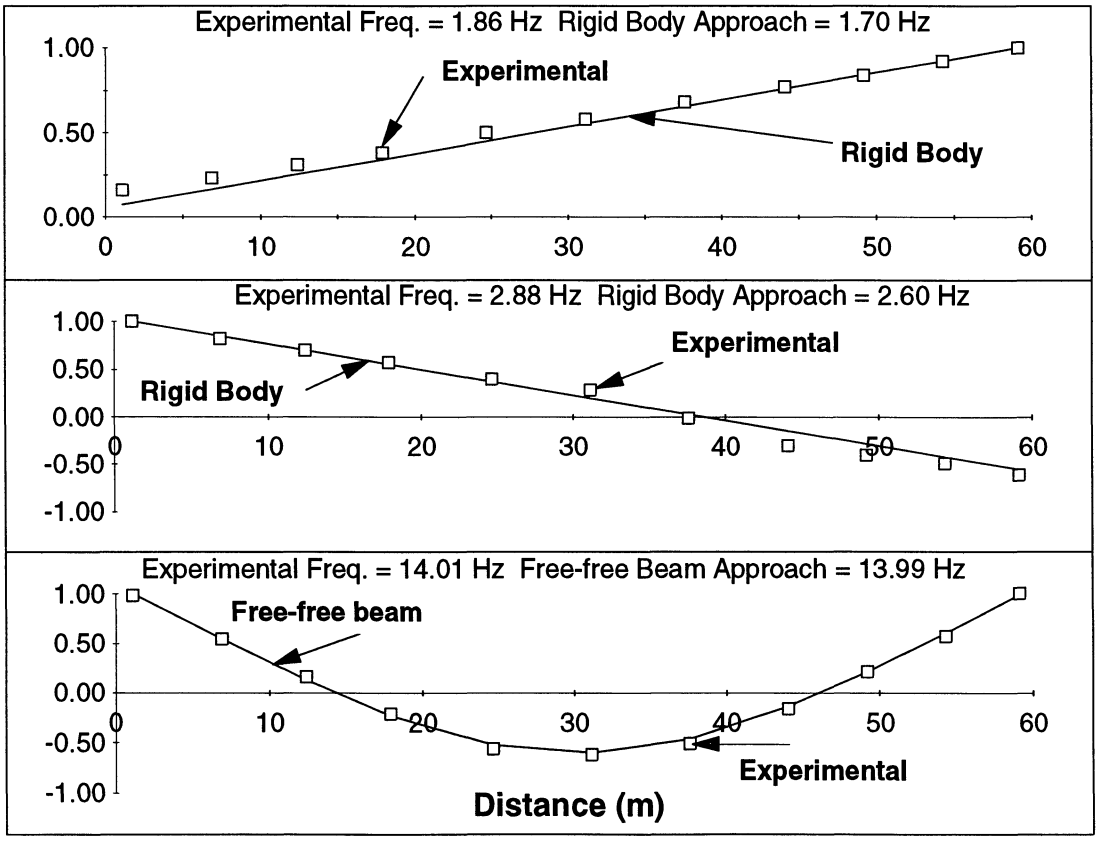

FIGURE 6-23 Northbound Bridge - Experimental vs Simplified Approach

corroborated later with the results of the snap-back tests. There were two vertical modes at around 4 and 4.5 Hz, respectively. These modes were similar in shape to the mode shapes obtained in the Northbound bridge at slightly higher frequencies. Also, the computed damping for the models detected at 4 and 4.5 Hz was less than 1.7% of critical and no more than 3.5% of critical for the others. The replacement of the bearings in both bridges did not produce any substantial change in the dynamic behavior of the bridge in the vertical direction. In general, the vertical frequencies changed no more than 5% and even less than that in the lower modes. The damping in the vertical direction of the post-retrofitted bridges increases for certain modes (figures 3-7 and 5-17) compared to the pre-retrofitted bridges.

2. In the transverse direction of the pre-retrofitted bridges, it was shown that the two modes observed at 5.4 Hz and 6.2 Hz were coupled with longitudinal modes forcing the piers to displace in the longitudinal direction of the bridge, which is the weak direction of the pier bent. The abutments for these modes accompany the rest of the structure in the transverse displacement. The results of the post-retrofitted bridges showed a different bridge behavior. Independent of the type of bearings used (lead-rubber or elastomeric), the piers and abutments essentially do not participate in the transverse movement of the deck at the lower modes. The deck moves as a rigid body, basically without deformation and the piers and abutments remain in place.

3. The comparison between the acceleration time histories of instruments located in different locations help to infer important conclusions. Comparing the two accelerometers located in the same vertical plane, one at the deck level (AP16) and the other at the top of the pier (A10) shows that the peak acceleration at the deck was around five times larger than at the top of the pier. In other words, the piers do not strongly accompany the movement of the deck because they are "isolated" from the rest of the structure. The same conclusion can be reached for

the abutments. The acceleration time histories of both post-retrofitted bridges, showed a situation not observed in the pre-retrofitted bridges; the participation of the higher modes. Particularly noteworthy is the mode found at around 14 Hz. This mode resembles the mode of a free-free beam and is related basically to the characteristics of the deck; it is not affected substantially by the stiffness of other structural elements (bearings, piers, etc.). The mode was also predicted by the three different models (figures 4-34) used in the pre-retrofitted bridges at a frequency around 13.5 Hz, which reinforce the idea that this mode is governed by the deck properties. Although this mode does not have a high participating mass value, it could become more important if the structure has a more flexible deck system.

4. Another point of interest observed in the post-retrofitted results is related to the damping values. In the pre-retrofitted bridges, the damping observed in the different modes was less than 7% of the critical for the lower modes, and increase for the higher. In these bridges and due to the high stiffness of the system, the structure interacts with the soil and part of the energy is dissipated through this medium. The inclusion of a good model of the soil behavior in the overall model is mandatory if reliable results are to be obtained. In the post-retrofitted bridges most of the energy was dissipated through the hysteretic behavior of the bearings. This energy is basically concentrated in the "bearings' modes" or lower modes, so for higher modes the damping decreases. For practical applications and for the case of most programs where the damping values are considered through the definition of the parameters a_0 and a_1, the experimental results of the pre-retrofitted bridge show that the damping is small at the lower mode and increases for the higher. In terms of modeling,a_1 (stiffness factor) this is more important than a_0 (mass factor). The opposite occurs for the post-retrofitted bridges. The opposite situation occurs for the post-retrofitted bridges.

SECTION 7
SUMMARY, CONCLUSIONS AND RECOMMENDATIONS

7.1 EXECUTIVE SUMMARY

Objectives

This report presents the results of an investigation of the lateral dynamic response behavior of two bridges before and after the replacement of the original steel bearings with either laminated rubber isolation bearings or neoprene elastomeric bearings.

The paucity of information related to the field performance of prototype bridges under dynamic loading conditions has been the primary motivation behind this research. Specifically, the field performance of elastomeric bearings and the comparison of these results with the results obtained from the same bridges under different support conditions has been considered. The experimental work done on the two slab-on-girder bridges, both before and after replacement of the original steel bearings, not only provides information to expand the existing sparse data base, but also provides an improved understanding of bridge behavior.

The Bridges

The transverse dynamic performance of two three-span slab-on-girder bridges seated initially on steel bearing sand later rehabilitated with elastomeric bearings, were investigated both experimentally and analytically in this study. The Southbound bridge is a three-lane, 14.8 m wide, 61.2 m long bridge that was rehabilitated using lead-rubber isolation bearings at the abutments and laminated rubber bearings at the piers. The Northbound bridge is a two-lane, 13 m wide, 58 m long bridge that is rehabilitated with elastomeric bearings. The New York State Department of Transportation (NYSDOT) used different bearings in the sister structures in order to compare the relative merits of each type of bering. It should be noted that although this study has considered the expected seismic performance of the two bridges, the NYSDOT did not

intend the Northbound bridge to be a seismic retrofit but rather a routine rehabilitation that included the replacement of the original steel bearings.

The Experiments

The snap-back testing technique advanced in this research has been employed in the field on bridges before and after rehabilitating the steel bearings and complemented by ambient vibration tests. Ambient and post-snap recording resulting from the free-vibration response were examined to infer in-situ frequencies, mode shapes, damping ratios and higher mode effects. Static (pre-snap) data has also provided insight into in-situ bearing stiffnesses, as well as pier and diaphragm flexibility; this information is subsequently being used in the validation of various analytical modeling techniques.

The large force-displacement snap-back field quick-release experiments were complemented by laboratory tests (for steel bearing behavior see Mander et al. 1996; and for elastomeric bearing behavior, see Kim et al., 1996) performed on actual bearings from the bridges (both old steel bearings salvaged from the bridges prior to rehabilitation and new bearings used to rehabilitate both bridges.

System Identification

Several system identification techniques were evaluated for this study, and a simple technical in the time domain was proposed in order to complement the widely-used "peak picking" frequency domain approach. The proposed dual approach was validated using an analytical example and a snap-back test performed on a three-story scaled reinforced concrete building. For the Southbound bridge seated on the seismic isolation bearings, the dual time domain-frequency domain approach was used to identify the initial non-linear pre-yield portion for the linear elastic (small amplitude) portion of the time histories. This initial portion of the post-snap behavior was complemented with the measured pre-snap quasi-static jack force-displacement response measured during the lateral loading of the bridge. From the two

approaches, overall bearing behavior in terms of initial stiffness, yield level and post-yield stiffness, could be inferred.

For the Northbound bridge seated on the neoprene elastomeric beings, the assumption of elastic behavior allowed the use of a modified version of the time domain method proposed for the bridges seated on the steel bearings. In all of the cases, a good agreement between identified and experimental values was found.

Structural Modeling and Validation

During this study, different levels of model complexity and detail were investigated. A full 3D elastic model that included the details of the deck, girders, stiffness, diaphragms, beings, tapered piers, foundation and soil system was constructed and validated. The no-linear soil-structure interaction was included in the model using the soil stiffness values provided by a companion study (Douglas et al., 1994). The model was able to reconstruct most of the field identified frequencies and corresponding modes. It was also possible to reconstruct the time history of different points of the structure suing as "applied load" the time history for the load obtained from the load cell bars during the field experiments. Due to the lack of advanced 3D programs that possess non-linear time history analysis capabilities and include the effect of gaps, friction models and softening force-deformation behavior it was necessary to develop a 2D model that emulated 3D behavior. The predictions using the simplified 2D model showed good agreement with the experimental results for the Southbound bridge seated on lead rubber bearings — the structural configuration where the most non-linear behavior was observed. With this rigorous non-liner model validated, it then serves as the basis to investigate the seismic performance of the two bridge with the different bearing conditions; that is, with (i) steel bearings, (ii) conventional elastomeric/neoprene bearings, and (iii) seismic isolation bearings.

7.2 CONCLUSIONS

The following conclusions are subdivided into experimental methodology, mathematical/structural modeling, and general observations. The first deals with important aspects of the field work, while the second deals with characteristics of the mathematical modeling techniques and their predictions. The third presents general conclusions that arise from comparative analyses and physical observations and summarizes important conclusions derived from the results of analytical predictions for different earthquake conditions.

7.2.1 Experimental Methodology

1) The use of the snap-back technique for full scale bridge experiments is evidently a good method of dynamic excitation to provide experimental mode shapes, frequencies and damping factors. However, the efficiency of this technique is related to the rate of force release. If a quick release (instantaneous snap) cannot be achieved, adequate results may not be obtained. However, in order to obtain nonlinear dynamic response, the release time with respect to the fundamental period of the structure needs to be very small.

2) The use of a hydraulic system that puts the structure in free vibration through the release of the in-line pressure should be used with caution. A hydraulic jack tends to act as a large viscous damper, adding extra damping to the initial portion of the time record and reducing the maximum peak post snap response acceleration.

3) As a minimum, it is essential to install an in-line load cell with the loading system. It is also recommended that quick release devices be included in the experimental setup such as breakable fuse-bars or mechanical fuses, as used in this study. Note, however, that only one fuse-bar can be used at a time, whereas several mechanical fuses can be coordinated electronically via solenoid releases.

4) In order to enhance system identification capabilities, it is recommended that for certain strategic locations displacement transducers be installed in conjunction with accelerometers. The former instruments help in the determination of the initial stiffnesses of the system and also obviate the need to doubly integrate the recorded accelerations to infer displacements.

5) Although in this study it was not possible to install accelerometers close to the foundation level due to the fact that there was more than 2 m of soil and waterway rip-rap over the pile cap, it is recommended that such instruments be included whenever possible. This should ensure improved modeling and identification of soil-structure interaction effects.

6) When analyzing the non-linear experimental behavior of bridges seated on lead-rubber bearings, it is important that this task be done in conjunction with rigorous non-linear analysis — particularly when capturing linear vs. non-linear behavior of the bearing.s By separating the free vibration response after the quick release in an initial non-linear portion followed by liner behavior, it is possible to solve the "assumed" bi-linear relation of the bearings in two well-defined steps. Valuable information to solve the non-linear portion can be obtained by solving the linear portion first — this procedure reduces the number of parameters to be identified in each step.

7.2.2 Mathematical/Structural Modeling

1) In order to assure that all of the parameters that govern the structural behavior are captured in a predictive mathematical model, it was considered important that a sophisticated linear elastic 3D structural model be built first in this study. From this, simplified models could be generated. The use of simplified models can produce good estimates if the correct geometry is chosen. For this study it was found that the transformed section approach to model the entire deck-girder system worked well. When the bridges were seated on steel bearings making the structure very stiff, the inclusion

of the diaphragms' and bearings' flexibility in the model were essential to adequately capture the transverse behavior of the superstructure of the bridge.

2) The properties of the steel bearings play an important role in the overall stiffness of the bridge system. This is especially so if the first longitudinal and transverse modes are close to each other as coupling conditions can be expected. The adequate identification of these modes is very important if one is to achieve accurate fitting between the experimental and analytical results.

3) When initially modeling a bridge structure, there is a temptation to assume that the foundation system is strong and stiff thereby assuming full fixity at the pile cap (column base) level. However, the inclusion of equivalent soil springs and masses in order to model soil-structure the interaction is highly recommended. The inclusion of these springs allow one to consider the flexibility of the structure at the foundation level. The use of a fixed-base system not only ignores such flexibility, but also requires a decrease in other structural stiffness properties in order to fit the results. This may end up being an unrealistic representation.

4) There is also a temptation to assume that steel expansion bearings do indeed expand. Thus an analyst will commonly model such bearings as a roller support. Based on this and companion field and laboratory studies (Mander et al., 1993; Mahmoodzadegan, 1996; and Mander et al., 1996), this is clearly a faulty assumption. Steel bearings possess a significant amount of frictional resistance that until broken (at high force levels) should be modeled by assuming fully fixed supports with only a release of longitudinal moments — that is, a pin support. This is perhaps the most important lesson that engineers should learn from this research — steel bearings are near-rigid until the frictional resistance is broken under high levels of loading. Thus some form of non-linear structural modeling is essential in studying the limits of bridge behavior when seated on steel bearings.

5) From the above three points it is clear that for the construction of a reliable simplified elastic model of a slab-on-girder bridge, special emphasis should be given to determining the contribution of the diaphragm, bearings (especially the degree of bearing fixity), and soil-structure interaction. The analytical models proposed for this project were constructed following this approach and in each case were able to predict with a reasonable agreement the experimental dynamic response.

6) For bridges with flexible seismic isolation bearings, the overall response is governed by the bearings themselves. Therefore the major focus in modeling should be a reliable mechanical model of bearing behavior based on large deformation laboratory tests.

7) It was found that for the bridges seated on the steel bearings, the damping in the vertical direction was much less than in the transverse direction. It was also seen that in the transverse direction the damping increased with the higher modes. This observation showed that if a Rayleigh damping model is used, then for these bridges the damping is apparently more stiffness' than mass' dependent. The opposite trends were observed for the bridges seated on the elastomeric bearings, where the lower modes were heavily damped in comparison to the higher modes.

8) The experimental results of the post-retrofitted Southbound bridge seated on the seismic isolation bearings showed that an adequate prediction can be made of the initial displacement and peak response acceleration using linearized elastic modeling in which an equivalent stiffness and damping approach is used to model the lead rubber bearings. However, the overall time history was poorly modeled. On the other hand, a non-linear model using the laboratory identified properties of the bearings was able to reconstruct with a good agreement the experimental results. For the Northbound bridge, where the elastomeric bearings do not exhibit a substantial hysteretic behavior, the use of an elastic model with damping in the order of 9% of critical for the lower modes was sufficient to reconstruct the experimental behavior.

9) The flexibility of the elastomeric bearings in comparison with the stiff slab-on-girder deck system makes it possible to idealize the bridge as a two degree-degree-of-freedom model possessing only a rotational and translational spring-mass system. Such a simplified model can predict with reasonable accuracy the lower frequencies and mode shapes which are of major interest.

7.2.3 Some Further General Observations

1) Although the use of the snap-back testing technique was used for the purpose of finding the transverse frequencies and mode shapes, the results obtained from the vertically oriented accelerometers showed a good agreement with the results obtained from the ambient vibration tests. Both test techniques were used to identify vertical modes, frequencies and damping factors with good agreement. However, due to the low level of excitation induced by traffic, it was not possible to use the ambient vibration technique to determine longitudinal and/or transverse mode shapes and frequencies. Only vertical modes could be found successfully.

2) The comparison between the results from the ambient vibration test before and after retrofitting showed that the replacement of the steel bearings by elastomeric bearings do not produce significant changes in the vertical frequencies and mode shapes. The damping in some of these vertical modes increased slightly after bearing replacement, but not in such a way to justify the replacement of bearing for this purpose alone.

3) Due to the presence of a mild (10°) skew of the bridge, as well as the 16° angle of inclination of the tension bars in the snap-back testing set-up, it was possible to excite the bridge in all directions. Thus in addition to the predominantly transverse response, longitudinal, vertical, and torsional (plane) response was observed. From this behavior, it was possible to determine global experimental mode shapes, frequencies and damping ratios.

4) The replacement of the original steel bearings with elastomeric isolation bearings produced a significant change in the transverse dynamic characteristics of the bridge. The initial transverse frequency of the Southbound bridge was around 5.5 Hz. This dropped to less than 2 Hz (an upper bound based on the initial elastic stiffness) and frequencies as low as 1.08 Hz were observed due to nonlinear seismic response. This latter result was obtained with a deformation of 38 mm or around 33% of the maximum bearing displacement. Even lower frequencies can be expected for higher deformations that would be expected under seismic loading conditions.

5) For the Northbound bridge the first transverse frequency dropped from a value of 5.8 Hz for the steel bearings to less than 1.8 Hz for the neoprene bearings. For all of the tests performed on the post-retrofitted bridges, it was possible to see the participation of higher modes, especially a mode with a frequency of around 14 Hz with a mode shape resembling the shape of free-end beam bending. This mode is independent of the bearing properties and is basically dependent on the mass and in-plane stiffness characteristics of the slab-on-girder superstructure.

6) After the bearings were replaced, a considerable increase in damping was observed in the important lower transverse modes of the Southbound bridge. From the initial values of around 6.5% for the lower transverse modes, the equivalent viscous damping increased to around 22% of critical. For the Northbound bridge the increase in the damping value was not as substantial, rising from around 6% for the steel bearings to 9% of critical for neoprene bearings. In both bridges, the free-end beam bending mode detected at a frequency around 14 Hz had a damping ratio of around 1.4%.

7) Bearing properties from the field experiments showed good agreement with companion laboratory component tests. Predictions based on laboratory values gave good agreement with the field observations.

8) New rubber expansion joints were installed a few weeks before the test on the retrofitted bridges. These joints provide a noticeable contribution to the overall transverse stiffness of the retrofitted bridges. When modeling the bridge behavior, the results were particularly sensitive to the expansion joint contribution at the south abutment of the Northbound bridge. At this location, the stiffness of the bearings is low compared to the shear stiffness of the rubber joint seal used. For modeling purposes, the joint was considered as a spring acting parallel with the abutment.

9) For the Southbound bridge, the presence of the deck joint seal at the abutment expansion joint increased the overall abutment stiffness by approximately 10% of the total lead-rubber bearing stiffness at the abutment. However, for the Northbound bridge, the increase was more, reaching values of around 20% for the north abutment and 38% for the south abutment with respect to the total bearing stiffnesses at those locations.

10) The present work has also shown that the use of linearized elastic model s to analyze isolated structures may provide a good estimation of the maximum displacement amplitudes if the structure behaviors in fundamental model. However, if the structure has a torsional imbalance, either a more sophisticated multi-mode spectral or transient analysis needs to be undertaken in order to predict the maximum displacement in the bearings resulting from combined torsional and translational response.

7.3 Recommendations for Future Research

Experimental Studies

1) It is recommended that studies be continued on bridges not designed for earthquake resistance. Such studies should include full-scale field experiments, as well as companion tests on critical components such as bearings, non-ductile periods and foundations. Such studies will enhance the present sparse data base of experimental

evidence. This data base is really the only means to validate theoretical models that form the basis of future code provisions.

2) The ultimate strength capacity of different steel bearing types mounted in real structures should be investigated — particularly the class of steel bearings used to seat large bridge spans. Such tests can provide improved insights of real bridge behavior, but also provide valuable information as to how the new generation of steel bearings for large bridges should be designed.

3) There is not clear guidance on the determination of the maximum capacity of elastomeric bearings. Most of the designs are presently based on arbitrary strain limitations. However, experimental results would provide a better understanding of the bearing behavior at the maximum deformation. These studies should be done considering the changes in properties that bearings can suffer with time and whether the bearings are doweled or bolted down.

Theoretical Studies

1) Closely spaced frequencies, high damping and non-linear behavior of the structure make system identification of experimental results a very difficult task. Most current solutions tend to be ad hoc and problem specific. Research should be continued in the area of highly damped, non-linear structures to provide more generic and robust system identification tools.

2) It was shown in this study that it is important to include the effect of the soil-structure interaction to obtain proper results. There is not clear guide when this effect could be important in base isolated structures. Future research could provide some important information to help with the non-linear modeling process.

3) The predictions obtained herein have shown that for simples bridges, a 2D linear model can provide a good estimation of the real behavior. However, more detailed studies such as this one, should be conducted for bridges that are more flexible and where the brittle failure of the bolts could produce a catastrophic collapse.

4) This study focused on the transverse behavior of the two bridges — principally because the experiments were designed to obtain the dynamic characteristics in tat direction. Additional experiments and more rigorous analysis need to be undertaken in the longitudinal direction to investigate the non-linear response of the structure-soil-pavement system and the dynamic effect of pounding between the three.

5) The rigorous analysis presented herein was, of necessity,performed using 2D non-linear models that we constructed so that 3D behavior could be emulated. Naturally, some simplifying assumption were necessary, the major disadvantage being that vertical motion effects could not be concurrently studied. It is therefore recommended that the development of 3D computational models that can handle the highly non-linear cyclic gap, sliding, and post-failure softening characteristics of steel beings be pursued with vigor.

SECTION 8

REFERENCES

AASHTO (1992), "Standard Specifications for Highway Bridges, 15th edition," American Association of State Highway and Transportation Officials, Washington, D.C.

AASHTO (1991), "Guide Specifications for Seismic Isolation Design," American Association of State Highway and Transportation Officials, Washington, D.C.

Abdel-Ghaffar, A.M., and Housner, G.W. (1978) "Ambient Vibration Tests of Suspension Bridge," *Journal of Engineering Mechanics Division*, Proceedings of the American Society of Civil Engineers, ASCE, Vol. 104: EM5, October.

ACI 318-95, (1995) Building Code Requirements for Reinforced Concrete, American Concrete Institute, Detroit, Michigan.

Aktan, A.E., Zwick, M., Miller, R., and Shahrooz, B. (1992) "Nondestructive and Destructive Testing of Decommissioned Reinforced Concrete Slab Highway Bridge and Associated Analytical Studies," Transportation Research Record 1371, pp. 142-153.

Allemang, R.J. (1983) "Experimental Modal Analysis, Modal Testing and Model Refinement", The Winter Annual Meeting of the American Society of Mechanical Engineers, Boston, Massachusetts, November 13-18 1983, pp. 1-23.

Aoki, M. (1971) *Introduction to Optimization Techniques: Fundamentals and Applications of Nonlinear Programming*, MacMillan Press, New York.

ATC (1983), "Seismic Retrofitting Guidelines for Highway Bridges (ATC 6-2)," Applied Technology Council, Palo Alto, California.

Beck, J.V. (1978) "Determining Models of Structures from Earthquake Records," Earthquake Engineering Research Laboratory, EERL 78-01, California Institute of Technology, Pasadena, CA.

Brown, D.L., Allemang, R.J., Zimmerman, R. and Mergeay, M. (1976) "Parameter Estimation Techniques for Modal Analysis," SAE Paper Number 790221, *SAE Transactions*, Vol. 88, pp. 828-846.

Buckland, P.G., Hooley, R., Morgenstern, B.D., Rainer, JH., and Van Selst (1979) "Suspension Bridge Vibrations: Computed and Measured," *Journal of the Structural Division*, Proceedings of the American Society of Civil Engineers, ASCE, Vol. 105: ST5, pp. 859-875, May.

Buckle, I.G. and Mayes, R.L. (1990) "Seismic Isolation: History, Application and Performance -A World View," *Earthquake Spectra*, Vol. 6: 2, pp. 161-201, May.

Buckle, I.G., and Lui, H. (1993) "Stability of Elastomeric Seismic Isolation Systems," *Proceedings* of Seminar on Seismic Isolation, Passive Energy Dissipation and Active Control, San Francisco, CA, Vol. 1: ATC17-1, pp. 293-305.

Buckle, I.G., Douglas, B.M., Saiidi, M., Richardson, J.A. and Butterworth, J.W. (1986) "Field Tests of a Curved Box Girder Bridge Using Simulated Earthquake Loads," *Proceedings*, Eighth European Conference of Earthquake Engineering, Lisbon, Portugal, September.

Chen, M-C., and Penzien, J. (1975) "Analytical Investigations of Seismic Response of Short, Single, or Multiple-Span Highway Bridges," Report No. EERC 754, Earthquake Engineering Research Center, University of California, Berkeley, CA, January.

Chen, S.S., Mander, J.B., MacEwan, D.S. and Mahmoodzadegan, B. (1993) "Quick-Release Behavior of Two Eastern U.S. Highway Bridges", *Proceedings* of the 10th International Bridge Conference, Pittsburgh, Pa., June.

Cifuentes, A.O. (1984) "System Identification of Hysteretic Structures", Report No. EERL 84-04, California Institute of Technology.

Cofer, W.F., McLean D.I. and McGuire, J.W. (1994), "Analytical Modeling of Foundations for Seismic Analysis of Bridges," Report No. WA-RD 328.2, Washington State Department of Transportation, Olympia, Washington, February.

Constantinou, M.C., Symans, M.D., Tsopelas, P., and Taylor, D. P. (1993), "Fluid Viscous Dampers in Applications of Seismic Energy Dissipation and Seismic Isolation," Applied Technology Council, *Proceedings* of Seminar on Seismic Isolation, Passive Energy Dissipation, and Active Control, Vol. 2, pp. 581-593.

Cooley, J.W. and Tukey, J.W. (1965) "An Algorithm for Machine Calculation of Complex Fourier Series", *Math Computation*, Vol. 19, April, pp. 297-301.

Coppolino, R.N. (1981) "A Simultaneous Frequency Domain Technique for Estimation of Modal Parameters from Measured Data," Paper No. 811046, *SAE Aerospace Congress and Exposition*, October.

DADISP (1994), DSP Development Corporation User Guide, Cambridge, MA, USA, 1994 Version 3.01D.

Dicleli, M. and Bruneau, M. (1995) "Seismic Performance of Multispan Simple Supported Slab-on-Girder Steel Highway Bridges," *Engineering Structures*, Vol. 17, No 1, pp. 1-14.

DiJulio, R.M. and Hart G.C. (1994) "Torsional Response and Design of High-Rise Buildings," Full Scale Laboratory, Earthquake and Wind Engineering, UCLA, School of Engineering and Applied Science, University of California, Los Angeles, CA, Report No. UCLA-ENG-7373, EWE 74-01, June.

Distefano, N. and Rath, A. (1974) "Modeling and Identification in Nonlinear Structural Dynamics," Report EERC, University of California, Berkeley.

Douglas, B.M. (1976) "Quick Release Pullback Testing and Analytical Seismic Analysis of a Six Span Composite Girder Bridge," Final Report for the Federal Highway Administration, University of Nevada, Reno, USA, August, Report RD-76-173.

Douglas, B.M., Maragakis, E. and Feng, S. (1994) "Stiffness Evaluation of Pile Foundation of Cazenovia Creek Overpass," Report No. CCEER-94-2, University of Nevada, Reno, April.

Douglas, B.M., Maragakis, E.A. and Nath, B. (1990) "Static Deformations of Bridges from Quick-Release Dynamic Experiments," *Journal of Structural Engineering,* Proceedings of the American Society of Civil Engineers, ASCE, Vol. 116, No. 8 pp. 2201-2213.

Douglas, B.M. and Reid, W.H. (1982) "Dynamic Tests and System Identification of Bridges," *Journal of the Structural Division*, Proceedings of the American Society of Civil Engineers, ASCE, Vol. 108, No. ST10, pp. 2295-2312, October.

Eberhard, M.O., Marsh, M.L., O'Donovan, T. and Hjartarson G. (1992) "Lateral-Load Tests of Reinforced Concrete Bridge," Transportation Research Record 1371, pp. 92-100.

Elliott, A.L. and Nagai, I. (1973) *Earthquake Damage to Freeway Bridges*, U.S. Department of Commerce Report on the San Fernando, California Earthquake of February 9, 1971, Vol. II.

Ewins, D.J. (1984) *Modal Testing: Theory and Practice*, 2nd Edition, Research Studies Press Ltd., England.

Fung, G. (1971) "Field Investigation of Bridge Damage in San Fernando Earthquake," Bridge Department, Division of Highways, California Department of Transportation, Sacramento, CA, Report #FHWA/CA/SD-82/07.

Gates, J.H. and Smith, M.J. (1982) "Verification of Dynamic Modeling Methods by Prototype Excitation," Office of Structures Design, California Department of Transportation, Sacramento, CA.

Ghali, A., and Neville, A., (1989) "Structural Analysis —A Unified Classical and Matrix Approach," Third Edition, Chapman and Hall.

Ghanem, R., Gavin, H., and Shinozuka, M. (1991) "Experimental Verification of a Number of Structural System Identification Algorithms", Technical Report, NCEER 91-0024, National Center for Earthquake Engineering Research, State University of New York at Buffalo.

Guyan, R.J. (1965) "Reduction of Stiffness and Mass Matrix", *Journal AIAA, No. 3*, pp. 380.

Harris, F.J. (1978) "On the Use of Windows for Harmonic Analysis with the Discrete Fourier Transform," *Proceedings* of the IEEE, Vol. 66, No. 1, pp. 51-83, January.

Hasegawa, K., Shikauchi, S., Osaki, H. and Fujiwara, Y. (1994) "Design of a long prestressed concrete continuous Girder Bridge Using Base Isolators", Third US-Japan Workshop on Earthquake Protective System for Bridges, Technical Report NCEER-94-0009, National Center for Earthquake Engineering Research, State University of New York at Buffalo, Part 5, pp. 37-53.

Ibrahim, S.R. and Mikulcik, E.C. (1976) "The Experimental Determination of Vibration Parameters from Time Domain Responses," *Shock and Vibration Bulletin*, No. 47, 1976, pp. 187-196.

Imbsen, R.A. and Penzien, J. (1984) "Evaluation of Energy Absorption Characteristics of Highway Bridges Under Seismic Conditions," Report No. UCB/EERC-84/17, College of Engineering, University of California, Berkeley, CA, September.

Jennings, P.C. (Ed.) (1971) "Engineering Features of the San Fernando Earthquake," Report N° EERL 71-02, California Institute of Technology, California, Pasadena, CA.

Kakinuma, T., Kawakami, K., Kumakura, K., Tani, H. and Abe, N. (1994) "Vibration Test of a Menshin Designed Multi-Span Continuous Prestressed Concrete Bridge," Third US-Japan Workshop on Earthquake Protective System for Bridges, Technical Report NCEER-94-0009, National Center for Earthquake Engineering Research, State University of New York at Buffalo, Part 5, pp. 3-20.

Kelly, J.M., Buckle, I.G., and Tsai, H.C. (1985) "Earthquake Simulator Testing of a Base-Isolated Bridge Deck," Report of the National Science Foundation, Earthquake Engineering Research Center, University of California, Berkeley, CA, Report No. UCB/EERC-85/09, January.

Kelly, J.M. and Hodder, S.B. (1981) "Experimental Study of Lead and Elastomeric Dampers for Base Isolation Systems," Report of the National Science Foundation, Earthquake Engineering Research Center, University of California, Berkeley, CA, Report No. UCB/EERC-81/16.

Kennedy, C.C. and Pancu, C.D.P. (1947) "Use of Vectors in Vibration Measurement and Analysis," *Journal of Aeronautical Sciences*, Vol. 14, No. 11, pp. 603-625.

Kim, D.K., Mander, J.B., and Chen, S.S., (1996), "Experimental Study and Thermo-Visco-Elasto-Plastic Modeling of Elastomeric Seismic Isolation Bearings," Technical Report NCEER-96-xxxx, National Center for Earthquake Engineering Research, State University of New York at Buffalo.

Klosterman, A. (1971) "On the Experimental Determination and Use of Modal Representations of Dynamic Characteristics", Ph.D. Dissertation, University of Cincinnati, Mechanical Engineering Department.

Labtech Notebook, Laboratory Technologies Corporation User Guide, Massachusetts 1989, Version 6.

Lam, I. and Martin, G.R. (1986) "Seismic Design of Highway Bridge Foundations, Vol. II. Design Procedures and Guidelines," Federal Highway Administration, FHWA Technical Report, No. 35A1062, June.

Lam, V.K.M. (1990) "The System Identification of a Nonlinearly Responding Base Isolated Bridge," Doctoral Dissertation, Department of Civil Engineering, University of Auckland, New Zealand, February.

Mahmoodzadegan, B., (1995) "Experimental Evaluation of the Seismic Resistance of a Slab-On-Girder Highway Bridge," doctoral dissertation, University of New York at Buffalo, January.

Mander, J.B., Kim, J-H. and Chen, S.S. (1993) "Experimental Performance and Modeling of a 30 Year Old Bridge with Steel Bearings", Transportation Research Record #1393, pp. 65-74.

Mander, J.B., Kim, D-K., Chen, S.S,. and Premus, A.J., (1996), "Response of Steel Bridge Bearings to Reversed Cyclic Loading," Technical Report NCEER-96-xxxx, National Center for Earthquake Engineering Research, State University of New York at Buffalo.

Mander, J.B., Priestley, M.J.N., and Park, R., (1984), "Seismic Design of Bridge Piers," Departmennt of Civil Engineering, University of Canterbury, Report 84-2, February 1984.

Maragakis, E. (1985) "A Model for the Rigid Body Motions of Skew Bridges," California Institute of Technology, Earthquake Engineering Research Laboratory, Report No. EERL 85-02, Pasadena, CA, January.

Maragakis, E.A., Douglas, B.M., and Abdel-Ghaffar, S.M. (1992) "Equivalent Linear Finite Element Modeling of Pile Foundations," *Proceedings* of the 8th US-Japan Bridge Engineering Workshop, Chicago, IL, USA, May 11-12 1992, pp. 531-543.

McCallen, D.B. and Romstad, K.M. (1994) "Dynamic Analysis of a Skewed Short-Span, Box-Girder Overpass," *Earthquake Spectra*, Vol. 10, No. 4, pp. 729-755.

McVerry, G.H. (1979) "Frequency Domain Identification of Structural Models from Earthquake Records," California Institute of Technology, Earthquake Engineering Research Laboratory, Report No. EERL 79-02, Pasadena, CA, October.

Masri, S.F., and Werner S.D. (1985) "An Evaluation of a Class of Practical Optimization Techniques For Structural Dynamics Applications," National Science Foundation, Grant No. CEE-8111964, Agbabian Associates, El Segundo, CA, March, Report R8222-5817.

NYSDOT (1964) Soil Report for Aurora Expressway, South Bound Lane at Cazenovia Creek Overpass, Bureau of Soil Mechanics, State of New York, Departments of Public Works.

Penzien, J., Imbsen, R., Liu, W. (1981) "NEABS-Nonlinear Earthquake Analysis of Bridge Systems", EERC University of California at Berkeley.

Pappa, R.S. and Juang, J.N. (1984) "An Eigensystem Realization Algorithm, (ERA) for Modal Parameter Identification," JPL Workshop on Identification and Control of Flexible Space Structures, Pasadena, CA, June.

Pappa, R.S. and Juang, J.N. (1984) "Galileo Spacecraft Modal Identification Using and Eigensystem Realization Algorithm," paper presented at the AIAA Dynamics Specialists Conference, Palm Springs, CA, May 1984, pp. 373-389.

Paz, M. (1991) Structural Dynamics Theory and Computation, 3rd Edition,Van Nostrand: Reinhold.

Pekcan, G., Mander, J.B. and Chen, S.S (1995) "The Seismic Response of a 1:3 Scale Model R.C. Structure with Elastomeric Spring Dampers," Technical Report NCEER-95-0010, National Center for Earthquake Engineering Research, State University of New York at Buffalo, May 1995.

Pekcan, G., Mander, J.B. and Chen, S.S (1995) "The Seismic Response of a 1:3 Scale Model R.C. Structure with Elastomeric Spring Dampers," Earthquake Spectra, Vol. 11, N°. 2, May.

Pender, M.J. (1993) "Aseismic Pile Foundation Design Analysis," Bulletin of New Zealand Society for Earthquake Engineering, Vol. 26, N°. 1, New Zealand, March.

Peng, C-Y. and Iwan, W.D. (1992) "An Identification Methodology for a Class of Hysteretic Structures," *Earthquake Engineering and Structural Dynamics*, Vol. 21, pp. 695-712.

Penzien, J., Iwasaki, T. and Clough, R. (1972) "Literature Survey-Seismic Effects on Highway Bridges," Report EERC 72-11, Earthquake Engineering Research Center, University of California, Berkeley, CA, November.

Prakash, V., Powell, G.H. and Filippou, F.C. (1992) "DRAIN2-DX," Report No. UCB/SEMM-92/29, Department of Civil Engineering, University of California, Berkeley, California, December.

Priestley, M.J.N., Seible, F., and Chai, Y.H., (1992) "Design Guidelines for Assessment Retrofit and Repair of Bridges for Seismic Performance," Report N°SSRP_92/01, Department of Applied Mechanics and Engineering Sciences, University of California, San Diego.

Raghavendrachar, M. and Aktan, A. (1992) "Flexibility by Multi-reference Impact Testing for Bridge Diagnostics", *Journal of Structural Engineering, ASCE, No. 8*, August, pp. 2186-2203.

Ramirez, W.R. (1984) *The FFT Fundamentals and Concepts*, Englewood-Cliffs, N.J: Prentice Hall.

Richardson, M. (1975) "Modal Analysis Using Digital Test Systems," Seminar on Understanding Digital Control and Analysis in Vibration Systems, The Shock and Vibration Information Center, Naval Research Laboratory, Washington D.C., May.

Richardson, J.A. (1988) "Dynamic Response Analysis of the Dominion Road Bridge Test Data," Doctoral Dissertation, Department of Civil Engineering, University of Nevada, Reno, December.

Richardson, M. and Potter, R. (1974) "Identification of the Modal Properties of an Elastic Structure from Measured Transfer Function Data", Instrument Society of America, ISA ASI 74250, pp. 239-246.

Roy, R. and Craig, J.F. (1981) *Structural Dynamics and Introduction to Computer Methods*, New York: John Wiley.

Salawu, O.S. and Williams, C. (1995) "Review of Full-Scale Dynamic Testing of Bridge Structures," *Engineering Structures*, Vol. 17, No. 2, pp. 113-121.

SAP90 (1992) *Computers and Structures*, Berkeley, CA, User Guide, May.

Skinner, R.I., Robinson, W.H. and McVerry, G.H. (1993) "An Introduction to Seismic Isolation," *DSIR Physical Sciences*, Wellington, New Zealand.

Somaprasad, H.R., Toksoy, T., Yoshiyuki, H., and Aktan, A.E. (1991) "Closed-Loop Modal Testing of a 27-Story Reinforced Concrete Flat Plate-Core Building,", Technical Report NCEER-91-0016, National Center for Earthquake Engineering Research, State University of New York at Buffalo, July.

Stroud, R.C. (1985) "Excitation, Measurement, and Analysis Methods for Modal Testing", Combined Experimental Analytical Modeling of Dynamic Structural System, The Joint ASCE/ASME, Mechanics Conference, Albuquerque, New Mexico, pp. 49-75, June 14-16.

Trifunac, M.D. (1970) "Ambient Vibration Tests of a Thirty-Nine Story Steel Frame Building," Report on Research Conducted Under a Grant from the National Science Foundation, Report No. EERL 70-02, California Institute of Technology, Earthquake Engineering Research Laboratory, Pasadena, CA.

Trifunac, M.D. (1970) "Wind and Microtremor Induced Vibrations of a Twenty-Two Story Steel Frame Building," California Institute of Technology, Earthquake Engineering Research Laboratory, Report No. EERL 70-01, Pasadena, CA.

Tsai, H-C. and Kelly, J.M. (1988) "Non-Classical Damping in Dynamic Analysis of Base-Isolated Structures with Internal Equipment," *Earthquake Engineering and Structural Dynamics*, Vol. 16, pp. 29-43.

Tsai, H-C. and Kelly, J.M. (1993) "Seismic Response of Heavily Damped Base Isolation Systems," *Earthquake Engineering and Structural Dynamics*, Vol. 22, pp. 633-645.

Tsopelas, P., Okamoto, S., Constantinou, M., Ozaki, D., and Fujii, S. (1994) "Experimental and Analytical Study of System Consisting of Sliding Bearings, Rubber Restoring Force Device and Fluid Dampers," Technical Report NCEER-94-0002, National Center for Earthquake Engineering Research, State University of New York at Buffalo.

Tyler, R. and Robinson, W. (1984) "High-Strain Test on Lead-Rubber Bearings For Earthquake Loading," Bulletin of the New Zealand Society for Earthquake Engineering, Vol. 17, No. 2, June, pp. 90-105.

Veletsos, A.S. and Ventura, C.E. (1985) "Dynamic Analysis of Structures by the DFT Method," *Journal of Structural Engineering*, Proceedings of the American Society of Civil Engineers, ASCE, Vol. 111, No. 12, pp. 2625-2643, December.

Vold, H., and Rocklin, G.E. (1982) "The Numeric Implementation of a Multi-Input Modal Estimation Method for Minicomputers," *Proceedings* of the 1st International Modal Analysis Conference, Orlando, Florida, pp. 542-548.

Wilson, J.C. (1984) "Analysis of the Observed Earthquake Response of a Multiple Span Bridge," Report No. EERL 84-01, California Institute of Technology, Pasadena, CA, May.

Winterkorn, H.F. and Fang, H-Y. (1993) *Foundation Engineering Handbook*, Van Nostrand Reinhold Company, 2nd Edition.

Wood, J.H. and Jennings, P.C. (1971) "Damage to Freeway Structures in the San Fernando Earthquake," *Bulletin of the New Zealand Society for Earthquake Engineering*, Vol. 4, No. 3, pp. 347-376, December.

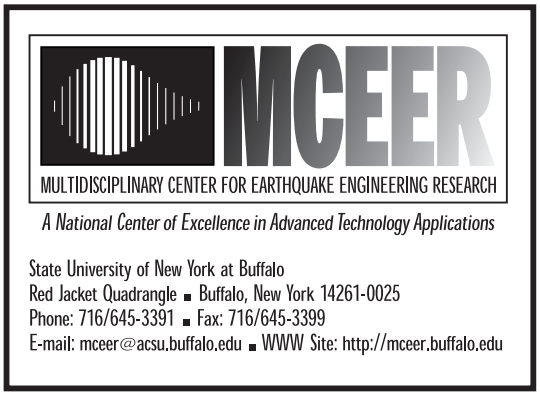

ISSN 1520-295X